

**RESPONSE STUDY OF DIFFERENT PARAMETERS OF LONG  
BRIDGES DUE TO ASYNCHRONOUS INPUT MOTION IN  
DIFFERENT PIERS**

By

Md. Mehedi Hasan

Roll: 0409042342

A Thesis Submitted to the Department of Civil Engineering, Bangladesh University of Engineering and Technology, Dhaka, in Partial Fulfilment of the Requirement for the Degree of Masters of Science in Civil Engineering.

Supervised by

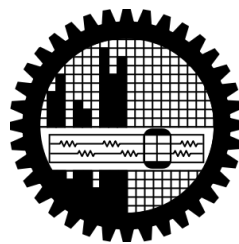
**Dr. Raquib Ahsan**

Professor

Department of Civil Engineering

Bangladesh University of Engineering and Technology

Dhaka



**Department of Civil Engineering**

**Bangladesh University of Engineering and Technology**

**Dhaka, Bangladesh**

**December 2015**

## BOARD OF EXAMINERS

This thesis titled “**Response Study of Different Parameters of Long Bridges Due to Asynchronous Input Motion in Different Piers**”, submitted by Md. Mehedi Hasan, Roll No. 0409042342, Session: April 2009, has been accepted as satisfactory in partial fulfilment of the requirement for the degree of **Master of Science in Civil Engineering (Structural)** on December 19, 2015.



---

Dr. Raquib Ahsan  
Professor  
Department of Civil Engineering  
BUET, Dhaka

Chairman  
(Supervisor)



---

Dr. Abdul Muqtadir  
Professor and Head  
Department of Civil Engineering  
BUET, Dhaka

Member  
(Ex-Officio)



---

Dr. Ishtiaque Ahmed  
Professor  
Department of Civil Engineering  
BUET, Dhaka

Member



---

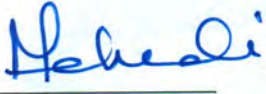
Dr. Sharmin Reza Chowdhury  
Professor  
Department of Civil Engineering  
Ahsanullah University of Science and Technology (AUST), Dhaka

Member  
(External)

## DECLARATION

It is hereby declared that except for the contents where specific references have been made to the work of others, the studies contained in this thesis is the result of investigation carried out by the author. No part of this thesis has been submitted to any other University or other educational establishment for a Degree, Diploma or other qualification (except for publication)

Signature of the Candidate



Md. Mehedi Hasan

## **ACKNOWLEDGEMENT**

The author wishes to convey his profound gratitude to Almighty Allah for His graciousness, unlimited kindness and for allowing him to complete the thesis.

It is the author's great pleasure and privilege to record his deepest sense of gratitude, indebtedness and thankful acknowledgement to Dr. Raquib Ahsan, Professor, Department of Civil Engineering, Bangladesh University of Engineering and Technology, for his continuous support, invaluable ideas, excellent comments, feedback and most importantly his encouragement to carry out this work. His knowledge, guidance and cooperation have provided the author as the basis and inspiration to work.

The author wishes to express his deep regard and profound love to his parents, family members who always motivated him to go ahead.

## ABSTRACT

Based on observed damage patterns from previous earthquakes and a rich history of analytical studies, asynchronous input motion has been identified as a major source of unfavourable response for long span structures, such as bridges. Frequently long span bridges provide deep valley crossings, which require special consideration due to the possibility of local amplification of the ground motion as a consequence of topographical irregularities and local soil conditions. This does in fact cause locally enhanced seismic input with the possibility for the bridge piers to respond asynchronously. This introduces special design requirements so that possible out of phase ground displacements and the associated large relative displacements of adjacent piers can be accommodated without excessive damage. Assessment of the local variability of the ground motion due to local lateral heterogeneities and to attenuation properties is thus crucial toward the realistic definition of the asynchronous motion at the base of the bridge piers.

Normally the bridges are designed with synchronous earthquake (same earthquake time-history input to all piers). But this assumption is not fully correct when a bridge has more than one pier and the spans are not very small. When the earthquake reaches at the first pier, then at the same time there is no earthquake at other piers. The earthquake reaches at other piers after some time lag from first pier. So the bridges are required to be designed according to asynchronous earthquake data.

The main objective of the present work is to study the response of box girder bridges due to time differences in dynamic motions at different piers and to study the response of box girder bridges due to variations of soil conditions at different piers. For this, a detailed finite element model of a straight concrete box girder bridge consisting of long spans (695.625 metre length for first bridge and 845.625 metre length for second bridge) has been developed and has been subjected to synchronous earthquake data and asynchronous earthquake data of 0.01 second time lag, asynchronous earthquake data 0.10 second time lag, asynchronous earthquake data 0.10 second time lag with 45 degree angle, asynchronous earthquake data 0.10 second time lag with 90 degree angle, asynchronous earthquake data 0.5 second time lag and asynchronous earthquake generated for different types of soil layers beneath the piers.

Analyses have been carried out to determine displacement variation due to synchronous and asynchronous motions with time lags of 0.01 second, 0.10 second and 0.5 second. Z-0 degree and 45-degree incident angles were considered for the case of 0.1 second time lag motion. In addition, the effect of different sub soil conditions at two portions of the bridge was also investigated.

For this box girder bridge, the finite element analysis shows that there is significant effect on the response of the bridge in case of 0.01 second or longer time delays. Similar effects can be observed due to asynchronous motion caused by different soil profiles at different portions of the bridge. Thus, asynchronous earthquake input should be considered for bridge design for earthquakes with long epicentral distance.

## TABLE OF CONTENTS

<b>DECLARATION</b> .....	<b>III</b>
<b>ACKNOWLEDGEMENT</b> .....	<b>IV</b>
<b>ABSTRACT</b> .....	<b>V</b>
<b>CHAPTER 1</b> .....	<b>1</b>
<b>1. INTRODUCTION</b> .....	<b>1</b>
1.1    GENERAL.....	1
1.2    OBJECTIVES OF THE STUDY .....	2
1.3    SCOPE OF THE STUDY .....	2
<b>CHAPTER 2</b> .....	<b>3</b>
<b>2. LITERATURE REVIEW</b> .....	<b>3</b>
2.1    BOX GIRDER BRIDGE .....	3
2.2    FINITE ELEMENT ANALYSIS OF BRIDGE.....	3
2.3    ASYNCHRONOUS EARTHQUAKE .....	4
2.3.1    Sources of Asynchronous Motion.....	4
2.3.2    Observations from Previous Earthquakes .....	4
2.3.3    Previous Studies .....	5
<b>CHAPTER 3</b> .....	<b>7</b>
<b>3. FINITE ELEMENT ANALYSIS</b> .....	<b>7</b>
3.1    GENERAL.....	7
3.2    BRIDGE DESCRIPTION .....	7
3.3    FINITE ELEMENT MODELING OF THE BRIDGE .....	8
3.4    MODELING ELEMENTS & PARAMETERS.....	8
3.4.1    Frame Elements.....	8
3.4.2    Shell Elements .....	9
3.4.3    Link Elements .....	11
3.4.4    Tendon Elements .....	12
3.4.5    Solid Elements .....	12
3.5    MODEL VERIFICATION.....	13
3.6    MATLAB PROGRAM FOR ESTIMATION SURFACE DISPLACEMENT FROM THE INPUT ACCELERATION.....	13

<b>CHAPTER 4.....</b>	<b>14</b>
<b>4. RESULTS.....</b>	<b>14</b>
4.1 DISPLACEMENT VARIATION FOR SYNCHRONOUS AND ASYNCHRONOUS EARTHQUAKE .....	14
4.2 SYNCHRONOUS AND ASYNCHRONOUS EFFECT FOR 100 M MODEL .....	24
4.3 SOIL EFFECT ON TWO BRIDGES: .....	34
4.4 COMPARISON BETWEEN RATIO OF SYNCHRONOUS AND ASYNCHRONOUS EARTHQUAKE .....	40
4.5 AXIAL FORCE, SHEAR FORCE & MOMENT ANALYSIS .....	45
4.6 MODAL ANALYSIS.....	52
<b>CHAPTER 5.....</b>	<b>66</b>
<b>5. CONCLUSIONS AND RECOMMENDATIONS .....</b>	<b>66</b>
5.1 GENERAL.....	66
5.2 CONCLUSIONS.....	67
5.3 FUTURE RECOMMENDATIONS.....	67
<b>REFERENCES .....</b>	<b>68</b>
<b>APPENDIX A.....</b>	<b>70</b>
<b>FINITE ELEMENT MODELING OF THE BRIDGE.....</b>	<b>70</b>
<b>APPENDIX B.....</b>	<b>91</b>
<b>MATLAB PROGRAM FOR ESTIMATION SURFACE DISPLACEMENT FROM THE INPUT ACCELERATION.....</b>	<b>91</b>
<b>APPENDIX C.....</b>	<b>106</b>
<b>DISPLACEMENT VARIATION FOR SYNCHRONOUS AND ASYNCHRONOUS EARTHQUAKE.....</b>	<b>106</b>
<b>APPENDIX D.....</b>	<b>135</b>
<b>SOIL EFFECT ON TWO BRIDGES.....</b>	<b>135</b>

# List of Figures

FIGURE 3.1: PIER SECTION AT MODEL .....	9
FIGURE 4.1: DISPLACEMENT VARIATION AT FIRST ABUTMENT ALONG X-AXIS .....	15
FIGURE 4.2: DISPLACEMENT VARIATION AT FIRST PIER ALONG X-AXIS .....	15
FIGURE 4.3: DISPLACEMENT VARIATION AT MIDDLE OF FIRST PIER AND SECOND PIER ALONG X-AXIS .....	16
FIGURE 4.4: DISPLACEMENT VARIATION AT MIDDLE OF THIRD PIER AND FOURTH PIER ALONG X-AXIS .....	16
FIGURE 4.5: DISPLACEMENT VARIATION AT FIFTH PIER ALONG X-AXIS .....	17
FIGURE 4.6: DISPLACEMENT VARIATION AT END ABUTMENT ALONG X-AXIS.....	17
FIGURE 4.7: DISPLACEMENT VARIATION AT FIRST PIER ALONG Y-AXIS .....	18
FIGURE 4.8: DISPLACEMENT VARIATION AT SECOND PIER ALONG Y-AXIS .....	18
FIGURE 4.9: DISPLACEMENT VARIATION AT MIDDLE OF THIRD PIER AND FOURTH PIER ALONG Y-AXIS .....	19
FIGURE 4.10: DISPLACEMENT VARIATION AT MIDDLE OF FOURTH PIER AND FIFTH PIER ALONG Y-AXIS.....	19
FIGURE 4.11: DISPLACEMENT VARIATION AT MIDDLE OF SIXTH PIER AND SEVENTH PIER ALONG Y-AXIS ..	20
FIGURE 4.12: DISPLACEMENT VARIATION AT END ABUTMENT ALONG Y-AXIS.....	20
FIGURE 4.13: DISPLACEMENT VARIATION AT FIRST ABUTMENT ALONG Z-AXIS .....	21
FIGURE 4.14: DISPLACEMENT VARIATION AT SECOND PIER ALONG Z-AXIS.....	21
FIGURE 4.15: DISPLACEMENT VARIATION AT MIDDLE OF SECOND PIER AND THIRD PIER ALONG Z-AXIS ....	22
FIGURE 4.16: DISPLACEMENT VARIATION AT FOURTH PIER ALONG Z-AXIS.....	22
FIGURE 4.17: DISPLACEMENT VARIATION AT MIDDLE OF FIFTH PIER AND SIXTH PIER ALONG Z-AXIS.....	23
FIGURE 4.18: DISPLACEMENT VARIATION AT END ABUTMENT ALONG Z-AXIS .....	23
FIGURE 4.19: DISPLACEMENT VARIATION FOR FOURTH PIER ALONG X-AXIS .....	24
FIGURE 4.20: DISPLACEMENT VARIATION FOR MIDDLE OF FIFTH & SIXTH PIER ALONG X-AXIS .....	24
FIGURE 4.21: DISPLACEMENT VARIATION FOR END ABUTMENT ALONG X-AXIS.....	25
FIGURE 4.22: DISPLACEMENT VARIATION FOR FOURTH PIER ALONG Y-AXIS .....	25
FIGURE 4.23: DISPLACEMENT VARIATION FOR MIDDLE OF FIFTH & SIXTH PIER ALONG Y-AXIS .....	26
FIGURE 4.24: DISPLACEMENT VARIATION FOR END ABUTMENT ALONG Y-AXIS.....	26
FIGURE 4.25: DISPLACEMENT VARIATION FOR FOURTH PIER ALONG Z-AXIS.....	27
FIGURE 4.26: DISPLACEMENT VARIATION FOR MIDDLE OF FIFTH & SIXTH PIER ALONG Z-AXIS.....	27
FIGURE 4.27: DISPLACEMENT VARIATION FOR END ABUTMENT ALONG Z-AXIS .....	28
FIGURE 4.28: DISPLACEMENT VARIATION FOR FOURTH PIER ALONG X-AXIS .....	28
FIGURE 4.29: DISPLACEMENT VARIATION FOR MIDDLE OF FIFTH & SIXTH PIER ALONG X-AXIS .....	29
FIGURE 4.30: DISPLACEMENT VARIATION FOR SEVENTH PIER ALONG X-AXIS.....	29
FIGURE 4.31: DISPLACEMENT VARIATION FOR END ABUTMENT ALONG X-AXIS.....	30
FIGURE 4.32: DISPLACEMENT VARIATION FOR FOURTH PIER ALONG Y-AXIS .....	30
FIGURE 4.33: DISPLACEMENT VARIATION FOR MIDDLE OF FIFTH & SIXTH PIER ALONG Y-AXIS .....	31
FIGURE 4.34: DISPLACEMENT VARIATION FOR END ABUTMENT ALONG Y-AXIS.....	31
FIGURE 4.35: DISPLACEMENT VARIATION FOR FOURTH PIER ALONG Z-AXIS.....	32
FIGURE 4.36: DISPLACEMENT VARIATION FOR MIDDLE OF FIFTH & SIXTH PIER ALONG Z-AXIS.....	32
FIGURE 4.37: DISPLACEMENT VARIATION FOR END ABUTMENT ALONG Z-AXIS .....	33
FIGURE 4.38: DISPLACEMENT VARIATION FOR FOURTH PIER ALONG X-AXIS .....	34
FIGURE 4.39: DISPLACEMENT VARIATION FOR MIDDLE OF FIFTH & SIXTH PIER ALONG X-AXIS .....	34
FIGURE 4.40: DISPLACEMENT VARIATION FOR FOURTH PIER ALONG Y-AXIS .....	35
FIGURE 4.41: DISPLACEMENT VARIATION FOR MIDDLE OF FIFTH & SIXTH PIER ALONG Y-AXIS .....	35
FIGURE 4.42: DISPLACEMENT VARIATION FOR FOURTH PIER ALONG Z-AXIS.....	36
FIGURE 4.43: DISPLACEMENT VARIATION FOR MIDDLE OF FIFTH & SIXTH PIER ALONG Z-AXIS.....	36
FIGURE 4.44: DISPLACEMENT VARIATION FOR FOURTH PIER ALONG X-AXIS .....	37
FIGURE 4.45: DISPLACEMENT VARIATION FOR MIDDLE OF FIFTH & SIXTH PIER ALONG X-AXIS .....	37
FIGURE 4.46: DISPLACEMENT VARIATION FOR FOURTH PIER ALONG Y-AXIS .....	38



FIGURE 4.47: DISPLACEMENT VARIATION FOR MIDDLE OF FIFTH & SIXTH PIER ALONG Y-AXIS .....	38
FIGURE 4.48: DISPLACEMENT VARIATION FOR FOURTH PIER ALONG Z-AXIS .....	39
FIGURE 4.49: DISPLACEMENT VARIATION FOR MIDDLE OF FIFTH & SIXTH PIER ALONG Z-AXIS.....	39
FIGURE 4.50: COMPARISON OF DISPLACEMENT RATIO BETWEEN ASYNC 0.01S LAG & SYNC ALONG LENGTH OF THE BRIDGE .....	40
FIGURE 4.51: COMPARISON OF DISPLACEMENT RATIO BETWEEN ASYNC 0.01S LAG & SYNC ALONG WIDTH OF THE BRIDGE .....	41
FIGURE 4.52: COMPARISON OF DISPLACEMENT RATIO BETWEEN ASYNC 0.01S LAG & SYNC ALONG VERTICAL DIRECTION OF THE BRIDGE .....	41
FIGURE 4.53: COMPARISON OF DISPLACEMENT RATIO BETWEEN ASYNC 0.1S LAG & SYNC ALONG LENGTH OF THE BRIDGE .....	42
FIGURE 4.54: COMPARISON OF DISPLACEMENT RATIO BETWEEN ASYNC 0.1S LAG & SYNC ALONG WIDTH OF THE BRIDGE .....	42
FIGURE 4.55: COMPARISON OF DISPLACEMENT RATIO BETWEEN ASYNC 0.1S LAG & SYNC ALONG VERTICAL DIRECTION OF THE BRIDGE .....	43
FIGURE 4.56: COMPARISON OF DISPLACEMENT RATIO BETWEEN ASYNC-SOIL & SYNC ALONG LENGTH OF THE BRIDGE .....	43
FIGURE 4.57: COMPARISON OF DISPLACEMENT RATIO BETWEEN ASYNC-SOIL & SYNC ALONG WIDTH OF THE BRIDGE .....	44
FIGURE 4.58: COMPARISON OF DISPLACEMENT RATIO BETWEEN ASYNC-SOIL & SYNC ALONG VERTICAL DIRECTION OF THE BRIDGE .....	44
FIGURE 4.59: VARIATION OF AXIAL FORCE (100 M SPAN BRIDGE) .....	45
FIGURE 4.60: VARIATION OF SHEAR FORCE ALONG MAJOR AXIS (100 M SPAN BRIDGE).....	46
FIGURE 4.61: VARIATION OF SHEAR FORCE ALONG MINOR AXIS (100 M SPAN BRIDGE).....	46
FIGURE 4.62: VARIATION OF MOMENT ALONG MAJOR AXIS (100 M SPAN BRIDGE) .....	47
FIGURE 4.63: VARIATION OF MOMENT ALONG MINOR AXIS (100 M SPAN BRIDGE) .....	47
FIGURE 4.64: VARIATION OF TORSIONAL MOMENT (100 M SPAN BRIDGE) .....	48
FIGURE 4.65: VARIATION OF AXIAL FORCE (125 M SPAN BRIDGE) .....	49
FIGURE 4.66: VARIATION OF SHEAR FORCE ALONG MAJOR AXIS (125 M SPAN BRIDGE).....	49
FIGURE 4.67: VARIATION OF SHEAR FORCE ALONG MINOR AXIS (125 M SPAN BRIDGE).....	50
FIGURE 4.68: VARIATION OF MOMENT ALONG MAJOR AXIS (125 M SPAN BRIDGE) .....	50
FIGURE 4.69: VARIATION OF MOMENT ALONG MINOR AXIS (125 M SPAN BRIDGE) .....	51
FIGURE 4.70: VARIATION OF TORSIONAL MOMENT (125 M SPAN BRIDGE) .....	51
FIGURE 4.71: 3D VIEW OF MODE SHAPE 1 FOR FIRST MODEL (T=0.93).....	53
FIGURE 4.72: 3D VIEW OF MODE SHAPE 2 FOR FIRST MODEL (T=0.89).....	54
FIGURE 4.73: 3D VIEW OF MODE SHAPE 3 FOR FIRST MODEL (T=0.85).....	54
FIGURE 4.74: 3D VIEW OF MODE SHAPE 4 FOR FIRST MODEL (T=0.76).....	55
FIGURE 4.75: 3D VIEW OF MODE SHAPE 5 FOR FIRST MODEL (T=0.72).....	55
FIGURE 4.76: 3D VIEW OF MODE SHAPE 6 FOR FIRST MODEL (T=0.69).....	56
FIGURE 4.77: 3D VIEW OF MODE SHAPE 7 FOR FIRST MODEL (T=0.67).....	56
FIGURE 4.78: 3D VIEW OF MODE SHAPE 8 FOR FIRST MODEL (T=0.63).....	57
FIGURE 4.79: 3D VIEW OF MODE SHAPE 9 FOR FIRST MODEL (T=0.59).....	57
FIGURE 4.80: 3D VIEW OF MODE SHAPE 10 FOR FIRST MODEL (T=0.57).....	58
FIGURE 4.81: 3D VIEW OF MODE SHAPE 11 FOR FIRST MODEL (T=0.54).....	58
FIGURE 4.82: 3D VIEW OF MODE SHAPE 12 FOR FIRST MODEL (T=0.50).....	59
FIGURE 4.83: 3D VIEW OF MODE SHAPE 1 FOR SECOND MODEL (T=1.36) .....	59
FIGURE 4.84: 3D VIEW OF MODE SHAPE 2 FOR SECOND MODEL (T=1.24) .....	60
FIGURE 4.85: 3D VIEW OF MODE SHAPE 3 FOR SECOND MODEL (T=1.10) .....	60
FIGURE 4.86: 3D VIEW OF MODE SHAPE 4 FOR SECOND MODEL (T=0.96) .....	61

FIGURE 4.87: 3D VIEW OF MODE SHAPE 5 FOR SECOND MODEL (T=0.90) .....	61
FIGURE 4.88: 3D VIEW OF MODE SHAPE 6 FOR SECOND MODEL (T=0.86) .....	62
FIGURE 4.89: 3D VIEW OF MODE SHAPE 7 FOR SECOND MODEL (T=0.83) .....	62
FIGURE 4.90: 3D VIEW OF MODE SHAPE 8 FOR SECOND MODEL (T=0.79) .....	63
FIGURE 4.91: 3D VIEW OF MODE SHAPE 9 FOR SECOND MODEL (T=0.77) .....	63
FIGURE 4.92: 3D VIEW OF MODE SHAPE 10 FOR SECOND MODEL (T=0.74) .....	64
FIGURE 4.93: 3D VIEW OF MODE SHAPE 11 FOR SECOND MODEL (T=0.70) .....	64
FIGURE 4.94: 3D VIEW OF MODE SHAPE 12 FOR SECOND MODEL (T=0.65) .....	65
FIGURE A.1: BRIDGE LAYOUT LINE FORM .....	70
FIGURE A.2: DECK SECTION DATA FORM .....	71
FIGURE A.3: CONCRETE PROPERTY .....	72
FIGURE A.4: REBAR PROPERTY .....	73
FIGURE A.5: STEEL PROPERTY .....	74
FIGURE A.6: DIAPHRAGM PROPERTY .....	75
FIGURE A.7: BEARING PROPERTIES .....	75
FIGURE A.8: ABUTMENT PROPERTIES.....	76
FIGURE A.9: BENT PROPERTIES .....	76
FIGURE A.10: BRIDGE OBJECT FORM .....	77
FIGURE A.11: BRIDGE OBJECT SPAN ASSIGNMENT FORM.....	78
FIGURE A.12: BRIDGE OBJECT DISCRETIZATION POINTS ASSIGNMENTS FORM.....	78
FIGURE A.13: BRIDGE OBJECT ABUTMENT ASSIGNMENT FORM .....	79
FIGURE A.14: BRIDGE OBJECT BENT ASSIGNMENTS FORM.....	79
FIGURE A.15: BRIDGE OBJECT CROSS DIAPHRAGM ASSIGNMENTS ASSIGNMENT FORM.....	80
FIGURE A.16: BRIDGE CONSTRUCTION GROUP DEFINITION FORM.....	80
FIGURE A.17: BRIDGE PARAMETRIC VARIATIONS DEFINITION FORM .....	81
FIGURE A.18: BRIDGE PARAMETRIC VARIATIONS DEFINITION FORM_2 .....	81
FIGURE A.19: TENDON LAYOUT PLAN AND TENDON DETAILS FOR FIRST BRIDGE.....	82
FIGURE A.20: BRIDGE TENDON ASSIGNMENT .....	82
FIGURE A.21: STATIC LOAD PATTERN DEFINITION FORM.....	83
FIGURE A.22: TIME VS DISPLACEMENT FIGURE (DHAKA).....	83
FIGURE A.23: STATIC LOAD CASE DEFINITION FORM .....	84
FIGURE A.24: LOAD CASE ASSIGNMENT-SYNCHRONOUS .....	85
FIGURE A.25: LOAD CASE ASSIGNMENT-ASYNCHRONOUS WITH 0.01 SEC TIME LAG.....	85
FIGURE A.26: LOAD CASE ASSIGNMENT-ASYNCHRONOUS WITH 0.1 SEC TIME LAG.....	86
FIGURE A.27: LOAD CASE ASSIGNMENT-ASYNCHRONOUS WITH 0.1 SEC TIME LAG (45 DEGREE).....	86
FIGURE A.28: LOAD CASE ASSIGNMENT-ASYNCHRONOUS WITH 0.1 SEC TIME LAG (90 DEGREE).....	87
FIGURE A.29: LOAD CASE ASSIGNMENT-ASYNCHRONOUS WITH 0.5 SEC TIME LAG.....	87
FIGURE A.30: LOAD CASE ASSIGNMENT-ASYNCHRONOUS WITH SOIL VARIATION.....	88
FIGURE A.31: LOAD ASSIGNMENT AT PIER .....	89
FIGURE A.32: 3D VIEW OF FIRST MODEL (EACH SPAN 100 METRE) .....	90
FIGURE A.33: 3D VIEW OF SECOND MODEL (EACH SPAN 125 METRE) .....	90
FIGURE C.1: DISPLACEMENT VARIATION AT FIRST ABUTMENT ALONG X-AXIS.....	106
FIGURE C.2: DISPLACEMENT VARIATION AT FIRST PIER ALONG X-AXIS.....	107
FIGURE C.3: DISPLACEMENT VARIATION AT SECOND PIER ALONG X-AXIS.....	107
FIGURE C.4: DISPLACEMENT VARIATION AT FIFTH PIER ALONG X-AXIS.....	108
FIGURE C.5: DISPLACEMENT VARIATION AT END ABUTMENT ALONG X-AXIS.....	109
FIGURE C.6: DISPLACEMENT VARIATION AT FIRST PIER ALONG Y-AXIS.....	109

FIGURE C.7: DISPLACEMENT VARIATION AT MIDDLE OF SECOND PIER AND THIRD PIER ALONG Y-AXIS ...	110
FIGURE C.8: DISPLACEMENT VARIATION AT MIDDLE OF THIRD PIER AND FOURTH PIER ALONG Y-AXIS ...	110
FIGURE C.9: DISPLACEMENT VARIATION AT MIDDLE OF SIXTH PIER AND SEVENTH PIER ALONG Y-AXIS..	111
FIGURE C.10: DISPLACEMENT VARIATION AT END ABUTMENT ALONG Y-AXIS .....	111
FIGURE C.11: DISPLACEMENT VARIATION AT FIRST PIER ALONG Z-AXIS .....	112
FIGURE C.12: DISPLACEMENT VARIATION AT MIDDLE OF FIRST PIER AND SECOND PIER ALONG Z-AXIS...	112
FIGURE C.13: DISPLACEMENT VARIATION AT SECOND PIER ALONG Z-AXIS .....	113
FIGURE C.14: DISPLACEMENT VARIATION AT FIFTH PIER ALONG Z-AXIS .....	113
FIGURE C.15: DISPLACEMENT VARIATION AT MIDDLE OF SIXTH PIER AND SEVENTH PIER ALONG Z-AXIS	114
FIGURE C.16: DISPLACEMENT VARIATION AT RIGHT SIDE TOP OF MIDDLE OF SECOND & THIRD PIER ALONG X-AXIS.....	115
FIGURE C.17: DISPLACEMENT VARIATION AT MIDDLE TOP OF MIDDLE OF SECOND & THIRD PIER ALONG X- AXIS.....	115
FIGURE C.18: DISPLACEMENT VARIATION AT LEFT SIDE TOP OF MIDDLE OF SECOND & THIRD PIER ALONG X- AXIS.....	116
FIGURE C.19: DISPLACEMENT VARIATION AT RIGHT SIDE BOTTOM OF MIDDLE OF SECOND & THIRD PIER ALONG X-AXIS.....	116
FIGURE C.20: DISPLACEMENT VARIATION AT MIDDLE BOTTOM OF MIDDLE OF SECOND & THIRD PIER ALONG X-AXIS.....	117
FIGURE C.21: DISPLACEMENT VARIATION AT LEFT SIDE BOTTOM OF MIDDLE OF SECOND & THIRD PIER ALONG X-AXIS.....	117
FIGURE C.22: DISPLACEMENT VARIATION FOR MIDDLE OF SECOND & THIRD PIER ALONG X-AXIS .....	118
FIGURE C.23: DISPLACEMENT VARIATION FOR FOURTH PIER ALONG X-AXIS.....	118
FIGURE C.24: DISPLACEMENT VARIATION FOR MIDDLE OF FIFTH & SIXTH PIER ALONG X-AXIS .....	119
FIGURE C.25: DISPLACEMENT VARIATION FOR SEVENTH PIER ALONG X-AXIS .....	119
FIGURE C.26: DISPLACEMENT VARIATION FOR END ABUTMENT ALONG X-AXIS .....	120
FIGURE C.27: DISPLACEMENT VARIATION FOR FOURTH PIER ALONG Y-AXIS.....	121
FIGURE C.28: DISPLACEMENT VARIATION FOR MIDDLE OF FIFTH & SIXTH PIER ALONG Y-AXIS .....	121
FIGURE C.29: DISPLACEMENT VARIATION FOR END ABUTMENT ALONG Y-AXIS .....	122
FIGURE C.30: DISPLACEMENT VARIATION FOR FOURTH PIER ALONG Z-AXIS .....	123
FIGURE C.31: DISPLACEMENT VARIATION FOR MIDDLE OF FIFTH & SIXTH PIER ALONG Z-AXIS .....	123
FIGURE C.32: DISPLACEMENT VARIATION FOR END ABUTMENT ALONG Z-AXIS .....	124
FIGURE C.33: DISPLACEMENT VARIATION AT RIGHT SIDE TOP OF MIDDLE OF SECOND & THIRD PIER ALONG X-AXIS.....	125
FIGURE C.34: DISPLACEMENT VARIATION AT MIDDLE TOP OF MIDDLE OF SECOND & THIRD PIER ALONG X- AXIS.....	125
FIGURE C.35: DISPLACEMENT VARIATION AT LEFT SIDE TOP OF MIDDLE OF SECOND & THIRD PIER ALONG X- AXIS.....	126
FIGURE C.36: DISPLACEMENT VARIATION AT RIGHT SIDE BOTTOM OF MIDDLE OF SECOND & THIRD PIER ALONG X-AXIS.....	126
FIGURE C.37: DISPLACEMENT VARIATION AT MIDDLE BOTTOM OF MIDDLE OF SECOND & THIRD PIER ALONG X-AXIS.....	127
FIGURE C.38: DISPLACEMENT VARIATION AT LEFT SIDE BOTTOM OF MIDDLE OF SECOND & THIRD PIER ALONG X-AXIS.....	127
FIGURE C.39: DISPLACEMENT VARIATION FOR MIDDLE OF SECOND & THIRD PIER ALONG X-AXIS .....	128
FIGURE C.40: DISPLACEMENT VARIATION FOR FOURTH PIER ALONG X-AXIS.....	128
FIGURE C.41: DISPLACEMENT VARIATION FOR MIDDLE OF FIFTH & SIXTH PIER ALONG X-AXIS .....	129
FIGURE C.42: DISPLACEMENT VARIATION FOR SEVENTH PIER ALONG X-AXIS.....	129
FIGURE C.43: DISPLACEMENT VARIATION FOR END ABUTMENT ALONG X-AXIS .....	130
FIGURE C.44: DISPLACEMENT VARIATION FOR FOURTH PIER ALONG Y-AXIS.....	131

FIGURE C.45: DISPLACEMENT VARIATION FOR MIDDLE OF FIFTH & SIXTH PIER ALONG Y-AXIS .....	131
FIGURE C.46: DISPLACEMENT VARIATION FOR END ABUTMENT ALONG Y-AXIS .....	132
FIGURE C.47: DISPLACEMENT VARIATION FOR FOURTH PIER ALONG Z-AXIS .....	133
FIGURE C.48: DISPLACEMENT VARIATION FOR MIDDLE OF FIFTH & SIXTH PIER ALONG Z-AXIS .....	133
FIGURE C.49: DISPLACEMENT VARIATION FOR END ABUTMENT ALONG Z-AXIS .....	134
FIGURE D.1: DISPLACEMENT VARIATION AT RIGHT SIDE TOP OF FOURTH PIER ALONG X-AXIS .....	135
FIGURE D.2: DISPLACEMENT VARIATION AT MIDDLE TOP OF FOURTH PIER ALONG X-AXIS .....	135
FIGURE D.3: DISPLACEMENT VARIATION AT LEFT SIDE TOP OF FOURTH PIER ALONG X-AXIS .....	136
FIGURE D.4: DISPLACEMENT VARIATION AT RIGHT SIDE BOTTOM OF FOURTH PIER ALONG X-AXIS .....	136
FIGURE D.5: DISPLACEMENT VARIATION AT MIDDLE BOTTOM OF FOURTH PIER ALONG X-AXIS .....	137
FIGURE D.6: DISPLACEMENT VARIATION AT LEFT SIDE BOTTOM OF FOURTH PIER ALONG X-AXIS .....	137
FIGURE D.7: DISPLACEMENT VARIATION FOR FOURTH PIER ALONG X-AXIS .....	138
FIGURE D.8: DISPLACEMENT VARIATION FOR MIDDLE OF FIFTH & SIXTH PIER ALONG X-AXIS .....	138
FIGURE D.9: DISPLACEMENT VARIATION FOR SEVENTH PIER ALONG X-AXIS .....	139
FIGURE D.10: DISPLACEMENT VARIATION FOR END ABUTMENT ALONG X-AXIS .....	139
FIGURE D.11: DISPLACEMENT VARIATION FOR FOURTH PIER ALONG Y-AXIS .....	140
FIGURE D.12: DISPLACEMENT VARIATION FOR MIDDLE OF FIFTH & SIXTH PIER ALONG Y-AXIS .....	140
FIGURE D.13: DISPLACEMENT VARIATION FOR END ABUTMENT ALONG Y-AXIS .....	141
FIGURE D.14: DISPLACEMENT VARIATION FOR FOURTH PIER ALONG Z-AXIS .....	141
FIGURE D.15: DISPLACEMENT VARIATION FOR MIDDLE OF FIFTH & SIXTH PIER ALONG Z-AXIS .....	142
FIGURE D.16: DISPLACEMENT VARIATION FOR END ABUTMENT ALONG Z-AXIS .....	142
FIGURE D.17: DISPLACEMENT VARIATION AT RIGHT SIDE TOP OF FOURTH PIER ALONG X-AXIS .....	143
FIGURE D.18: DISPLACEMENT VARIATION AT MIDDLE TOP OF FOURTH PIER ALONG X-AXIS .....	143
FIGURE D.19: DISPLACEMENT VARIATION AT LEFT SIDE TOP OF FOURTH PIER ALONG X-AXIS .....	144
FIGURE D.20: DISPLACEMENT VARIATION AT RIGHT SIDE BOTTOM OF FOURTH PIER ALONG X-AXIS .....	144
FIGURE D.21: DISPLACEMENT VARIATION AT MIDDLE BOTTOM OF FOURTH PIER ALONG X-AXIS .....	145
FIGURE D.22: DISPLACEMENT VARIATION AT LEFT SIDE BOTTOM OF FOURTH PIER ALONG X-AXIS .....	145
FIGURE D.23: DISPLACEMENT VARIATION FOR FOURTH PIER ALONG X-AXIS .....	146
FIGURE D.24: DISPLACEMENT VARIATION FOR MIDDLE OF FIFTH & SIXTH PIER ALONG X-AXIS .....	146
FIGURE D.25: DISPLACEMENT VARIATION FOR END ABUTMENT ALONG X-AXIS .....	147
FIGURE D.26: DISPLACEMENT VARIATION FOR FOURTH PIER ALONG Y-AXIS .....	147
FIGURE D.27: DISPLACEMENT VARIATION FOR MIDDLE OF FIFTH & SIXTH PIER ALONG Y-AXIS .....	148
FIGURE D.28: DISPLACEMENT VARIATION FOR END ABUTMENT ALONG Y-AXIS .....	148
FIGURE D.29: DISPLACEMENT VARIATION FOR FOURTH PIER ALONG Z-AXIS .....	149
FIGURE D.30: DISPLACEMENT VARIATION FOR MIDDLE OF FIFTH & SIXTH PIER ALONG Z-AXIS .....	149
FIGURE D.31: DISPLACEMENT VARIATION FOR END ABUTMENT ALONG Z-AXIS .....	150

## List of Tables

TABLE 3.1: SALIENT FEATURES OF TWO BRIDGE .....	7
TABLE 4.1: MODAL PERIOD AND FREQUENCY OF FIRST BRIDGE .....	52
TABLE 4.2: MODAL PERIOD AND FREQUENCY OF SECOND BRIDGE .....	52

## LIST OF ABBREVIATIONS

FE	Finite Element
FEM	Finite Element Model
UK	United Kingdom
NASA	National Aeronautics and Space Administration

# CHAPTER 1

## 1. INTRODUCTION

---

### 1.1 GENERAL

Bangladesh is one of the most disaster-prone countries in the world. Although it is vulnerable to a wide variety of natural hazards, viz. flood, cyclone and storm surge, drought, riverbank erosion and earthquake, most of the recent disasters have been caused by floods and cyclones. The low incidence of severe earthquakes during this century has led to a situation where most of the populations do not perceive seismic risks to be important. However, due to increasing number of bridges, buildings and industrial structures being built during the last two decades, assessment of seismicity in different regions in the country received considerable attention of engineers and scientists. There is lack of awareness not only among the public but also among the decision makers about the earthquake hazard in the country. A review of the available data shows that considerable seismic hazard exists for major parts of the country (Ansary & Sharfuddin, 2002).

Because irregular elevated transportation structures are becoming a common solution to complex transportation problems, it is important that a commensurate breadth and depth of research are invested in understanding these complex structures. Natural disasters of the past few decades have provided numerous examples of bridge damage and collapse for bridges that were designed for seismic forces (Elnashai *et al.*, 1999). To better protect bridges from future earthquakes, researchers must aid bridge designers by utilizing field observations and expanding on past investigations to include representative bridges of all types and alignments, striving to make inelastic dynamic analyses as realistic as possible. With advances in computing power, structural and seismological features previously simplified can be fully included in analysis.

It is well accepted that one of the most important factors influencing the space variability of the ground motion is the site response. Due to the insurgence of local surface waves and local resonance, the local amplification or de-amplification effects can dominate the ground shaking whenever lateral heterogeneities, such as topographical features or soft-sedimentary basins, are present in the vicinity of a site. If a built structure has dimensions greater than the main wavelengths of the ground motion, different parts of its foundation can vibrate out of phase due to the non-synchronous seismic input. The presence of relevant differential motions makes the structure move in an incoherent way with respect to surrounding ground.

Dynamic response during earthquake is a very important factor for both the serviceability and safety of bridge structures. The controlling parameters that govern dynamic response of a bridge depend on different structural attributes of a particular bridge. Conventional structural design methods neglect the asynchronous earthquake effects. The effect of asynchronous earthquake may be prominent for heavy structures like bridges, resting on relatively soft soils. Damage sustained in recent earthquakes have also highlighted that the seismic behaviour of a structure is highly influenced not only by the response of superstructure, but also by the response of the foundation and ground as well.

Utilizing advanced analysis tools, this study seeks to include the complicating factor not often considered in seismic analysis: spatially varied seismic input with a range of incoherence cases. The factor is included due to increased understanding of the seismological characteristics of earthquakes and the higher displacement demand possible from asynchronous input, demonstrated in recent studies (Sextos *et al.*, 2004, Lupoi *et al.*, 2005).

## **1.2 OBJECTIVES OF THE STUDY**

The behaviour of bridge under the influence of seismic load has been a major point of interest for engineers over a long period of time. The 1971 San Fernando earthquake was a major turning point in the development of seismic design criteria for bridges. Although significant advances have been achieved since that time in the design and construction of an earthquake resistant bridge, numerous gaps still remain in the understanding of the seismic behaviour of bridges. In this study, we have used acceleration, velocity and displacement data recorded on the Jamuna Multi-Purpose bridge pile cap (horizontal direction) on June 16, 2004. The principal objectives of the present study are:

- (i). To study the response of box girder bridges due to time differences in dynamic motions at different piers.
- (ii). To study the response of box girder bridges to variations of soil conditions at different piers.

## **1.3 SCOPE OF THE STUDY**

The research work involves the seismic response of a box girder bridge considering the earthquake effect. The following are the scopes of the study.

- The structural behaviour of the bridge is assumed to be linear ignoring material and other non-linearity.
- The horizontal and vertical curvatures of the bridge have not been considered.
- This design is only for concrete box Girder Bridge.
- The bridge is straight.
- The number of span of the bridge is only eight (6+2 end span).
- Time-history analysis is performed.
- The mathematical modelling of the bridge has not been formulated for studying the response of the bridge.

## CHAPTER 2

### 2. LITERATURE REVIEW

---

#### 2.1 BOX GIRDER BRIDGE

A box girder bridge is a bridge in which the main beams comprise girders in the shape of a hollow box. The box girder normally comprises either prestressed concrete, structural steel, or a composite of steel and reinforced concrete. The box is typically rectangular or trapezoidal in cross-section. Box girder bridges are commonly used for highway flyovers and for modern elevated structures of light rail transport. Although normally the box girder bridge is a form of Beam Bridge, box girders may also be used on cable-stayed bridges and other forms.

The box girder bridge was a popular choice during the road building expansion of the 1960s and many new bridge projects were in progress simultaneously. A serious blow to this use was a sequence of three serious disasters, when new bridges collapsed in 1970 (West Gate Bridge and Cleddau Bridge) and 1971 (Koblenz Bridge). Fifty-one people were killed in these failures, leading in the UK to the formation of the Merrison Committee and considerable investment in new research into steel box girder behaviour.

Most of the bridges still under construction at this time were delayed for investigation of the basic design principle. Some were abandoned rebuilt as a different form of bridge altogether. Most of those that remained as box girder bridges, such as Erskine Bridge were either redesigned or had additional stiffening added later. Some bridges were strengthened a few years after opening and then further strengthened years later, although this was often due to increased traffic load as much as better design standards. The Irwell Valley Bridge of 1970 was strengthened in 1970 and again in 2000.

#### 2.2 FINITE ELEMENT ANALYSIS OF BRIDGE

The finite element analysis from the mathematical side was first developed in 1943 by Richard Courant, who used the Ritz method of numerical analysis and minimization of variation calculus to obtain approximate solutions to vibration systems. From the engineering side, the finite element analysis originated as the displacement method of the matrix structural analysis, which emerged over the course of several decades mainly in British aerospace research as a variant suitable for computers. By late 1950s, the key concepts of stiffness matrix and element assembly existed essentially in the form used today and NASA issued request for proposals for the development of the finite element software NASTRAN in 1965.

The finite element method (FEM) is used for finding approximate solutions of partial differential equations (PDE) as well as of integral equations such as the heat transport



equation. The solution approach is based either on eliminating the differential equation completely (steady state problems), or rendering the PDE into an approximating system of ordinary differential equations, which are then solved using standard techniques such as finite differences, Runge-Kutta, etc.

In solving partial differential equations, the primary challenge is to create an equation that approximates the equation to be studied, but is numerically stable, meaning that errors in the input data and intermediate calculations do not accumulate and cause the resulting output to be meaningless. There are many ways of doing this, all with advantages and disadvantages. The finite element method is a good choice for solving partial differential equations over complex domains (like cars and oil pipelines), when the domain changes (as during a solid state reaction with a moving boundary), when the desired precision varies over the entire domain, or when the solution lacks smoothness.

## **2.3 ASYNCHRONOUS EARTHQUAKE**

### **2.3.1 Sources of Asynchronous Motion**

Consideration of spatially varied seismic input motion is challenging due to its complexity. Wave travel speed, reflection and refraction, and heterogeneous soil conditions all cause deviations from synchronous excitation for distributed foundation structures such as bridges. For simplification, asynchronous motion is commonly divided into three components: (i) a wave passage effect, (ii) geometric incoherence of the input and (iii) local site conditions. The first component is due to the finite travel speed of seismic waves, resulting in progressive excitation of each support point as a wave front passes. The second component accounts for the reflection and refraction of seismic waves as they pass through the ground, changing their signal content between support points. The final component accounts for situations where structures are founded on different soil types, such as a bridge that spans a geologic divide. Though the asynchronous motion observed during earthquakes is a complex interaction of all three components, for analytical simplicity, researchers have divided the phenomenon into these three sources.

### **2.3.2 Observations from Previous Earthquakes**

In recent earthquakes there are numerous examples of bridge failures that may have been caused or aided by differential support motion. During the Northridge earthquake of 1994, a number of spans of the Gavin Canyon undercrossing fell off of their supports, resulting in the total collapse of substantial portions of the structure (Tzanetos *et al.*, 2000). The spans became unseated and collapsed, despite being retrofitted with restraining devices following the San Fernando earthquake. While shifting and pounding of deck slabs from synchronous motion could cause unseating, differential support motion is a more likely cause of the large displacements resulting in failure of this retrofitted structure.

The Kobe earthquake of 1995 provides further examples of deck unseating where differential support movement was likely involved. The city of Kobe has many kilometres

of elevated highways where single spans supported on Rollers Bridge the gaps between piers. Many of these single spans fell off of their supports at expansion joints during this earthquake because of large longitudinal displacements between piers (Elnashai *et al.*, 1995). Again, it is difficult to fully attribute these failures to asynchronous earthquake motion, but such motion is known to cause large differential movement of neighbouring supports. As discussed in greater detail below, several studies have shown that spatially varied ground motion can exact higher demands on a bridge structure than synchronous motion.

### 2.3.3 Previous Studies

Studies on the response of extended foundation structures to differential support excitation began over 40 years ago with a study by Bodganoff *et al.* (1965) on the effect of ground transmission time on long structures. This and other early studies, such as Dumanoglu, *et al.* (1987) and Leger *et al.* (1990), focused on long bridges subjected to wave passage effects only. These studies identified isolated cases of response amplification due to asynchronous motion, but their conclusions were limited due to their simplicity. Significant advances in computing power in the early 1990s allowed larger, more involved studies to be performed. The advent of “spatial” models of asynchronous motion allowed geometric incoherence to be incorporated into studies using a stochastic field based on random vibration theory.

The majority of studies including both the wave passage effect and geometric incoherence terms use synthetic ground motion based on the Luco and Wong coherency function (Luco and Wong, 1986). This function provides a mathematical representation of coherence and consists of two terms, one which quantifies the severity of the wave passage effect, and another which represents the level of geometric incoherence. While other coherence functions have been suggested (see Oliveira *et al.*, 1991 and Der Kiureghian *et al.*, 1992, among others), the function proposed by Luco and Wong has gained the widest use for its simplicity and clarity.

One of the first studies based on the random vibration theory approach was done by Zerva (1990). In this study the structural response of beams with varied lengths were evaluated for seismic input with different degrees of incoherence, including totally synchronous excitation. The results showed that asynchronous response is very complex and a clear trend is hard to define, with incoherence either increasing or decreasing the structural response, depending on many parameters.

The first major study to include inelastic dynamic analysis was by Monti *et al.*, (1996) and involved the inelastic response of a simple, symmetric, 6-span reinforced concrete bridge to asynchronous motion. The results showed that in cases of severe incoherence, the bridge responds almost entirely pseudo statically, though the response is still less than the synchronous case. Because the simplicity of this study structure limited the scope of the results, future researchers often introduced irregularities into simple bridge structures. Tzanetos *et al.*, (2000) varied the pier heights of a straight bridge which was analysed using inelastic asynchronous analysis. For this irregular bridge, asynchronous motion was shown to significantly increase response for many cases, especially in the transverse

direction. Tzanetos *et al.*, (2000) identified suppression of the fundamental mode and dominance of higher-mode response as a hallmark of asynchronous excitation, a finding supported in future studies.

Two recent asynchronous inelastic bridge analyses including structural irregularities are by Sextos *et al.*, (2003) and Lupoi *et al.*, (2005). The first study involved a broad parametric study of 20 bridges with different geometric and dynamic characteristics (though all straight). Results from this study showed that relative pier displacements are strongly tied to the overall length of the bridge, with these displacements increasing logarithmically for the study range (up to 600m) and exceeding synchronous displacements frequently above 400 meters. The second study by Lupoi *et al.*, (2005) involved the analysis of a straight, 200m 4-span bridge in the longitudinal direction only, with varied pier heights, deck stiffness, and coherency level of the input motion. This study showed that asynchronous motion can increase the probability of bridge failure for even relatively short structures.

The analytical study most similar to the current investigation of Figured bridges under asynchronous motion is by Sextos *et al.* (2004). The study involved the inelastic response history analysis of a Figured, prestressed concrete bridge in Greece, the Krystallopigi Bridge. The study structure is a 12-span, 638 m, Figured Bridge with varied pier heights. The bridge was analysed with both a natural record recorded near the bridge site, and a suite of synthetic records with varied degrees of correlation. Results of this analysis support the conclusion of previous studies that asynchronous motion can excite higher dynamic modes, and cases of pier displacement demands doubling were noted. This led the authors to propose the 600 m length suggested by Euro code 8 as a threshold for asynchronous analysis be reduced in the case of Figured bridges, although the difficulty in drawing further conclusions for such a complex bridge without further study is acknowledged.

## CHAPTER 3

### 3. FINITE ELEMENT ANALYSIS

---

#### 3.1 GENERAL

Two long span box girder bridge are required for the analysis of the effect of synchronous and asynchronous earthquake on the bridge. In this chapter, steps and assumptions of modelling of the bridge using CSiBridge 2015 are presented.

#### 3.2 BRIDGE DESCRIPTION

The first bridge is straight, about 695 meter long, box girder concrete type and consists of eight spans (first span 73.05 m, second to seven spans 99.375 m and last span 26.325 m). The total width of the bridge deck is 18.5 m. The first bridge is supported by seven 2-pile piers. The bridge consists of two lane roads and footpath.

The second bridge is straight, about 845 meter long, box girder concrete type and consists of eight spans (first span 73.05 m, second to seven spans 124.375 m and last span 26.325 m). The total width of the bridge deck is 18.5 m. The second bridge is also supported by seven 2-pile piers. The bridge consists of two lane roads and footpath.

**Table 3.1: Salient Features of two Bridge**

Length of bridge	695.625 m	845.625 m
Width of bridge	18.5 m	18.5 m
Number of spans	8	8
Length of span	First-73.05 m Second to Seventh-99.375 m Eighth-26.325 m	First-73.05 m Second to Seventh-124.375 m Eighth-26.325 m
Number of lanes	2	2
Number of piers	7	7

### **3.3 FINITE ELEMENT MODELING OF THE BRIDGE**

The following are the important features of the modelling of the bridge-

- The structural behaviour of the bridge was assumed to be linear ignoring material nonlinearity.
- Only nonlinearity of the isolator was considered.

Some steps of modelling using CSiBridge2015 are shown in Appendix A

### **3.4 MODELING ELEMENTS & PARAMETERS**

#### **3.4.1 Frame Elements**

The Frame element is a very powerful element that can be used to model beams, columns, braces and trusses in planar and three-dimensional structures. Nonlinear material behaviour is available through the use of Frame Hinges.

The Frame element uses a general, three-dimensional, beam-column formulation which includes the effects of biaxial bending, torsion, axial deformation and biaxial shear deformations, Bathe and Wilson (1976).

A Frame element is modelled as a straight line connecting two points. In the graphical user interface, it can be divided curved objects into multiple straight objects, subject to requirement.

Each element has its own local coordinate system for defining section properties and loads, and for interpreting output.

The element may be prismatic or non-prismatic. The non-prismatic formulation allows the element length to be divided into any number of segments over which properties may vary. The variation of the bending stiffness may be linear, parabolic or cubic over each segment of length. The axial, shear, torsional, mass and weight properties all vary linearly over each segment.

Insertion points and end offsets are available to account for the finite size of beam and column intersections. The end offsets may be made partially or fully rigid to model the stiffening effect that can occur when the ends of an element are embedded in beam and column intersections. End releases are also available to model different fixity conditions at the ends of the element.

Each Frame element may be loaded by gravity (in any direction), multiple concentrated loads, multiple distributed loads, strain and deformation loads and loads due to temperature change.

Target-force loading is available that iteratively applies deformation load to the element to achieve a desired axial force.

Element internal forces are produced at the ends of each element and at a user specified number of equally spaced output stations along the length of the element.

In this analysis two frame sections, Pier and Cap Beam are used. Concrete strength is assumed 4,000 psi at pier and cap beams and steel strength is assumed 60,000 psi. Pier section is shown at **Figure 3.1**. Cap beam size is 2.5 X 2.0 meter.

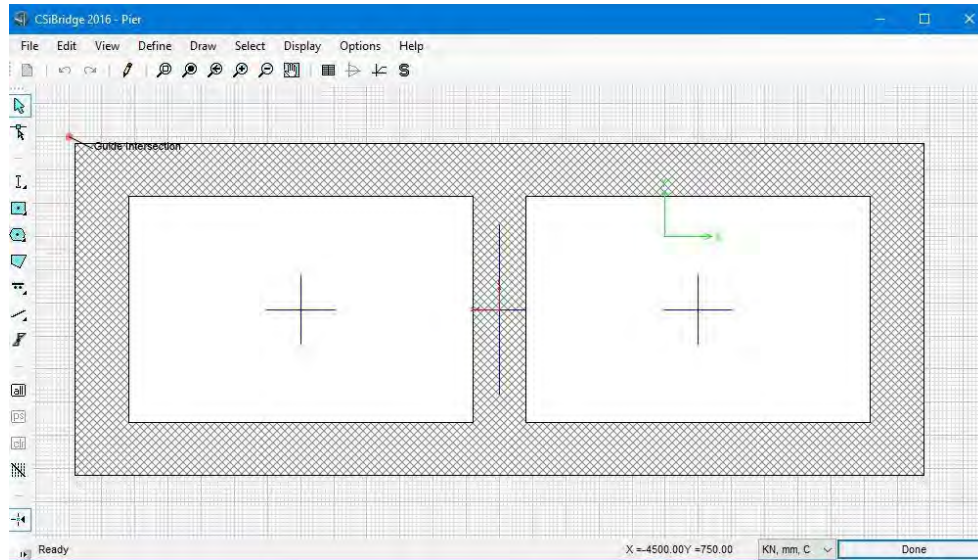


**Figure 3.1: Pier Section at Model**

### 3.4.2 Shell Elements

The Shell element is a type of area object that is used to model membrane, plate and shell behaviour in planar and three-dimensional structures. The shell material may be homogeneous or layered through the thickness. Material nonlinearity can be considered when using the layered shell.

The Shell element is a three- or four-node formulation that combines membrane and plate-bending behaviour. The four-joint element does not have to be planar.

Each Shell element has its own local coordinate system for defining Material properties and loads and for interpreting output. Temperature-dependent, orthotropic material properties are allowed. Each element may be loaded by gravity and uniform loads in any direction; surface pressure on the top, bottom and side faces; and loads due to strain and temperature change.

A four-point numerical integration formulation is used for the Shell stiffness. Stresses and internal forces and moments, in the element local coordinate system, are evaluated at the 2-by-2 Gauss integration points and extrapolated to the joints of the element. An approximate error in the element stresses or internal forces can be estimated from the difference in values calculated from different elements attached to a common joint. This will give an indication of the accuracy of a given finite element approximation and can then be used as the basis for the selection of a new and more accurate finite element mesh.

Structures that can be modelled with this element include:

- Floor systems
- Wall systems
- Bridge decks
- Three-dimensional curved shells, such as tanks and domes
- Detailed models of beams, columns, pipes, and other structural members

Two distinct formulations are available: homogenous and layered.

➤ **Homogeneous**

The homogeneous shell combines independent membrane and plate behaviour. These behaviours become coupled if the element is warped (non-planar.) The membrane behaviour uses an isoperimetric formulation that includes translational in-plane stiffness components and a “drilling” rotational stiffness component in the direction normal to the plane of the element. Taylor and Simo (1985) and Ibrahimbegovic and Wilson (1991). In-plane displacements are quadratic.

Plate-bending behaviour includes two-way, out-of-plane, plate rotational stiffness components and a translational stiffness component in the direction normal to the plane of the element. You may choose a thin-plate (Kirchhoff) formulation that neglects transverse shearing deformation, or a thick-plate (Mindlin/Reissner) formulation which includes the effects of transverse shearing deformation. Out-of-plane displacements are cubic.

For each homogeneous Shell element in the structure, anyone can choose to model pure-membrane, pure-plate, or full-shell behaviour. It is generally recommended to use the full shell behaviour unless the entire structure is planar and is adequately restrained.

➤ **Layered**

The layered shell allows any number of layers to be defined in the thickness direction, each with an independent location, thickness, behaviour and material. Material behaviour may be nonlinear.

Membrane deformation within each layer uses a strain-projection method (Hughes, 2000.) In-plane displacements are quadratic. Unlike for the homogeneous shell, the “drilling” degrees of freedom are not used, and they should not be loaded. These rotations normal to the plane of the element are only loosely tied to the rigid-body rotation of the element to prevent instability.

For bending, a Mindlin/Reissner formulation is used which always includes transverse shear deformations. Out-of-plane displacements are quadratic and are consistent with the in-plane displacements.

The layered Shell usually represents full-shell behaviour, although it can be controlled on a layer-by-layer basis. Unless the layering is fully symmetrical in the thickness direction, membrane and plate behaviour will be coupled.

In this analysis one shell element, Deck is used. Shell – thin is assumed for analysis, thickness is 250 mm for membrane and bending. Concrete strength is also assumed 4,000 psi.

### **3.4.3 Link Elements**

The Link element is used to connect two joints together. The Support element is used to connect one joint to ground. Both element types use the same types of properties. Each Link or Support element may exhibit up to three different types of behaviour: linear, nonlinear, and frequency-dependent, according to the types of properties assigned to that element and the type of analysis being performed.

A Link element is a two-joint connecting link. A Support element is a one-joint grounded spring. Properties for both types of element are defined in the same way. Each element is assumed to be composed of six separate “springs,” one for each of six deformational degrees-of freedom (axial, shear, torsion, and pure bending).

There are two categories of Link/Support properties that can be defined: Linear/Nonlinear, and Frequency-Dependent. A Linear/Nonlinear property set must be assigned to each Link or Support element. The assignment of a Frequency Dependent property set to a Link or Support element is optional.

All Linear/Nonlinear property sets contain linear properties that are used by the element for linear analyses and for other types of analyses if no other properties are defined. Linear/Nonlinear property sets may have nonlinear properties that will be used for all nonlinear analyses, and for linear analyses that continue from nonlinear analyses.

Frequency-dependent property sets contain impedance (stiffness and damping) properties that will be used for all frequency-dependent analyses. If a Frequency Dependent property has not been assigned to a Link/Support element, the linear properties for that element will be used for frequency-dependent analyses.

The types of nonlinear behaviour that can be modelled with this element include:

- Viscoelastic damping
- Gap (compression only) and hook (tension only)
- Multi-linear uniaxial elasticity
- Uniaxial plasticity (Wen model)
- Multi-linear uniaxial plasticity with several types of hysteretic behaviour: kinematic, Takeda and pivot
- Biaxial-plasticity base isolator



- Friction-pendulum base isolator, with or without uplift prevention. This can also be used for modelling gap-friction contact behaviour

Each element has its own local coordinate system for defining the force deformation properties and for interpreting output.

Each Link/Support element may be loaded by gravity (in any direction).

Available output includes the deformation across the element and the internal forces at the joints of the element.

In this analysis two type of link sections (BBRG1 & BFIXSS) are used. Translation at three directions (U1, U2 & U3) are restrained at BBRG1. Translation at three directions and rotation at three directions (U1, U2, U3, R1, R2 & R3) are restrained at BFIXSS.

#### **3.4.4 Tendon Elements**

Tendons are a special type of object that can be embedded inside other objects (frames, shells, planes, asolids and solids) to represent the effect of prestressing and post-tensioning. These tendons attach to the other objects through which they pass and impose load upon them.

It may be specified whether the tendons are to be modelled as independent elements in the analysis or just to act upon the rest of the structure as loads. Modelling as loads is adequate for linear analyses when you know the losses that will be caused by elastic shortening and time-dependent effects.

Tendons should be modelled as elements if anyone want the program to calculate the losses due to elastic shortening and time-dependent effects, if anyone want to consider nonlinearity in the Tendons, or if want to know the forces acting in the Tendons due to other loading on the structure. Tendon objects share some features with Frame elements.

One type of prestressed tendon has been used in analysis. Prestress type is post tension, tendon area 3447.7 mm<sup>2</sup>, tendon load is 3711 kN.

#### **3.4.5 Solid Elements**

The Solid element is an eight-node element for modelling three-dimensional structures and solids. It is based upon an isoperimetric formulation that includes nine optional incompatible bending modes.

The incompatible bending modes significantly improve the bending behaviour of the element if the element geometry is of a rectangular form. Improved behaviour is exhibited even with non-rectangular geometry.

Each Solid element has its own local coordinate system for defining Material properties and loads, and for interpreting output. Temperature-dependent, anisotropic material properties are allowed. Each element may be loaded by gravity (in any direction); surface

pressure on the faces; pore pressure within the element; and loads due to temperature change.

A 2 x 2 x 2 numerical integration scheme is used for the Solid. Stresses in the element local coordinate system are evaluated at the integration points and extrapolated to the joints of the element. An approximate error in the stresses can be estimated from the difference in values calculated from different elements attached to a common joint. This will give an indication of the accuracy of the finite element approximation and can then be used as the basis for the selection of a new and more accurate finite element mesh.

In this analysis one solid element, Diaphragm is used. Diaphragm thickness is 2000 mm and depth is 1000 mm.

### **3.5 MODEL VERIFICATION**

One paper was issued on 3<sup>rd</sup> International Earthquake Symposium, Bangladesh, Dhaka on March 5-6, 2010 (R. Ahsan, M. M. Hasan and S. M. Reza, 'Modal analysis of the Jamuna multi-purpose bridge considering soil-structure interaction').

From that thesis, time period has been found 1.3 second at first effective mode. But from this analysis time period of first mode has been found 0.93 second. Because, prestressed tendons have been incorporated at analysis file and for this reason time period is slightly less.

So model has been verified.

### **3.6 MATLAB PROGRAM FOR ESTIMATION SURFACE DISPLACEMENT FROM THE INPUT ACCELERATION**

A Matlab program has been prepared for estimation surface displacement from the input acceleration (Konagai, K & Ahsan, R 2002, 'Simulation of nonlinear soil-structure interaction on a shaking table' Journal of Earthquake Engineering, vol 6, no. 1, pp. 31-51). Detail Matlab program is shown in Appendix B.

## CHAPTER 4

### 4. RESULTS

---

#### 4.1 DISPLACEMENT VARIATION FOR SYNCHRONOUS AND ASYNCHRONOUS EARTHQUAKE

Six points (three points on top and three points on bottom) are selected on First Abutment, Middle of First Abutment and First Pier, First Pier, Middle of First Pier and Second Pier, Second Pier, Middle of Second Pier and Third Pier, Third Pier, Middle of Third Pier and Fourth Pier, Fourth Pier, Middle of Fourth Pier and Fifth Pier, Fifth Pier, Middle of Fifth Pier and Sixth Pier, Sixth Pier, Middle of Sixth Pier and Seventh Pier, Seventh Pier, Middle of Seventh Pier and End Abutment, End Abutment for two models. Here used earthquake types are-

1. Synchronous Motion
2. Asynchronous Motion with 0.01 sec time lag
3. Asynchronous Motion with 0.1 sec time lag
4. Asynchronous Motion with 0.1 sec time lag and 45 degree angle
5. Asynchronous Motion with 0.01 sec time lag and 90 degree angle
6. Asynchronous Motion with 0.5 sec time lag
7. Asynchronous Motion-Soil Effect

Displacements due to these earthquake data for first bridge (100 m span) are shown from Figure 4.1 to Figure 4.6 along X-axis (along length of the bridge), from Figure 4.7 to Figure 4.12 along Y-axis (along width of the bridge) & from Figure 4.13 to Figure 4.18 along Z-axis (along vertical direction of the bridge). Besides, for second bridge (125 m span) those figures are shown in Appendix C.

Six points (three points on top and three points on bottom) are notified as RST, MT, LST, RSB, MB & LSB. Full meaning of these are Right Side Top (RST), Middle Top (MT), Left Side Top (LST), Right Side Bottom (RSB), Middle Bottom (MB) & Left Side Bottom (LSB).

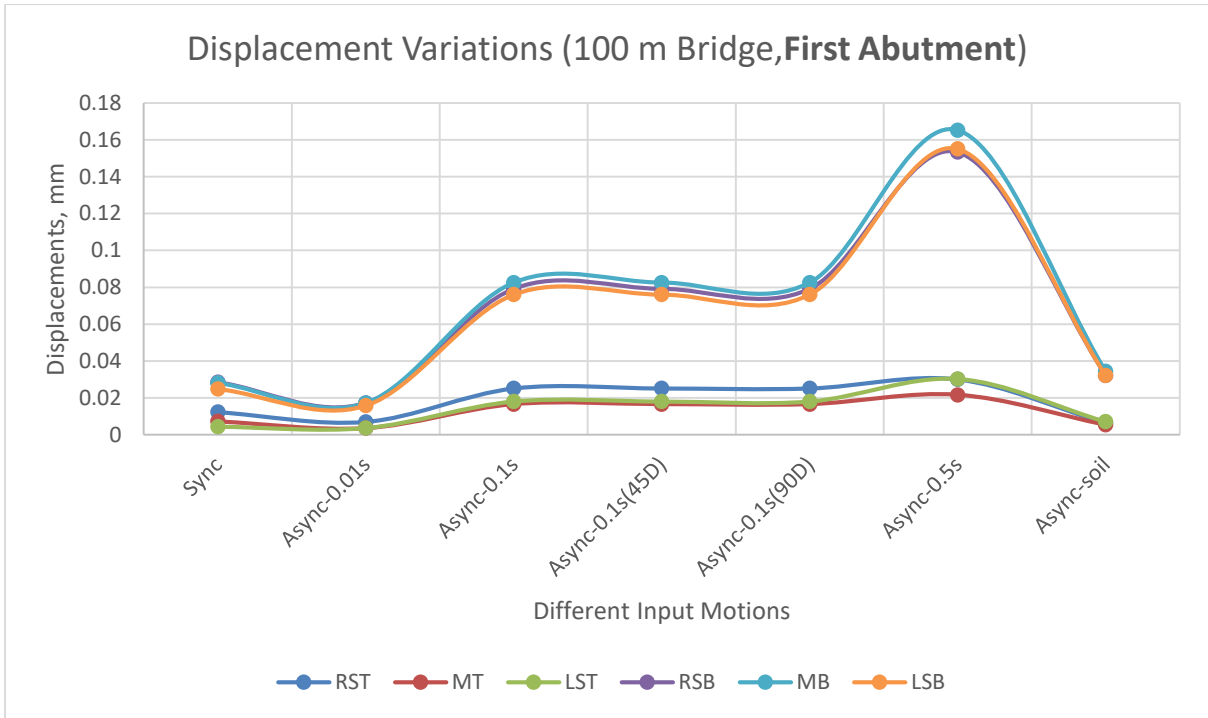


**Figure 4.1: Displacement Variation at First Abutment along X-axis**

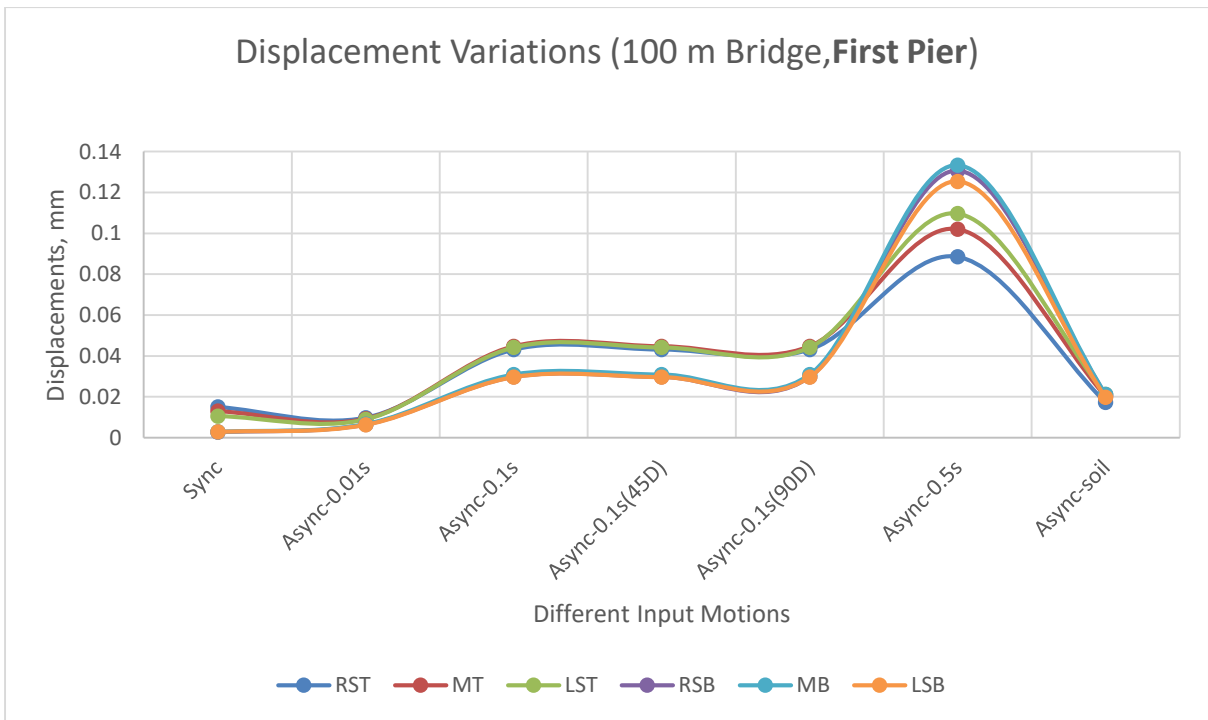


**Figure 4.2: Displacement Variation at First Pier along X-axis**

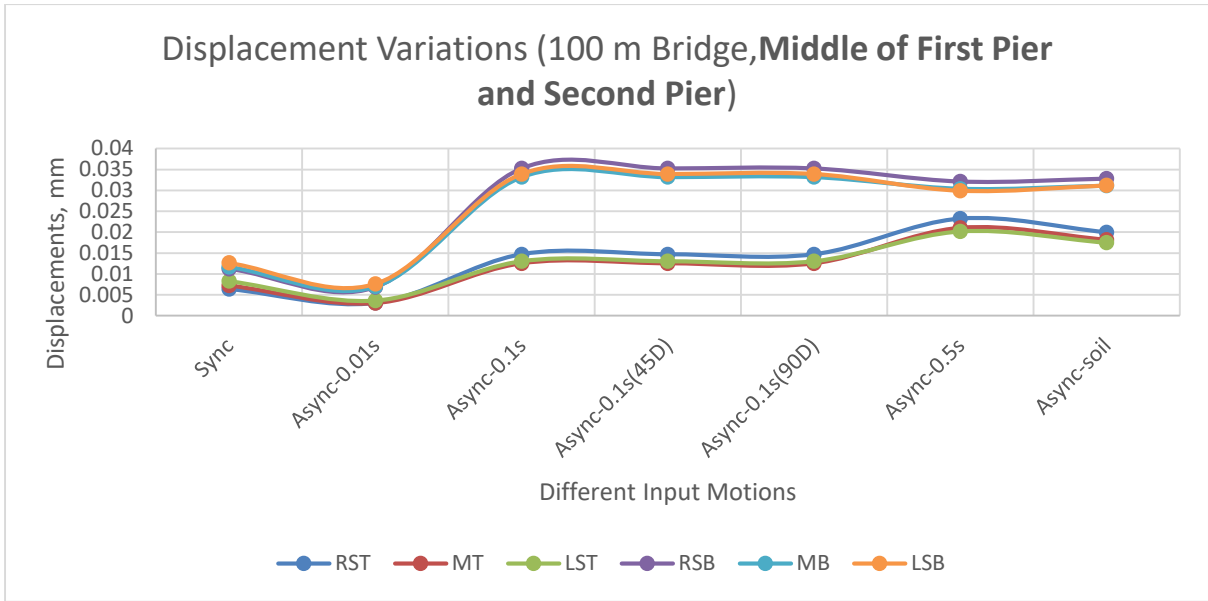


**Figure 4.3: Displacement Variation at Middle of First Pier and Second Pier along X-axis**

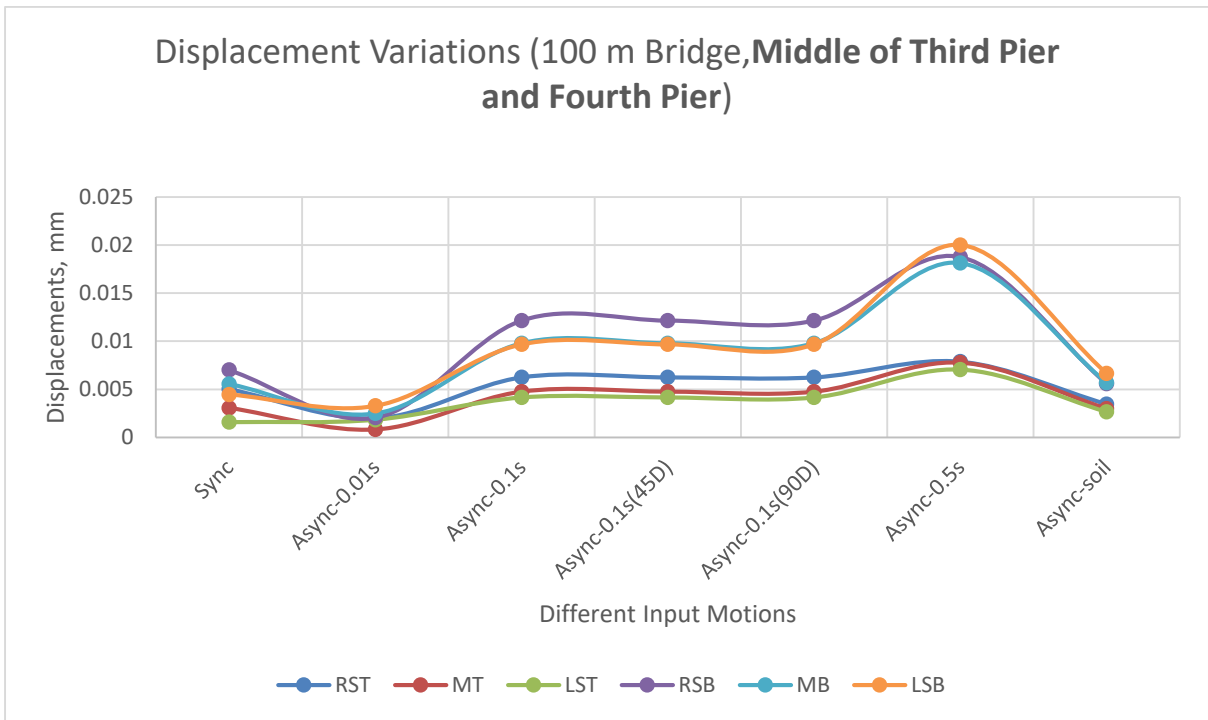


**Figure 4.4: Displacement Variation at Middle of Third Pier and Fourth Pier along X-axis**

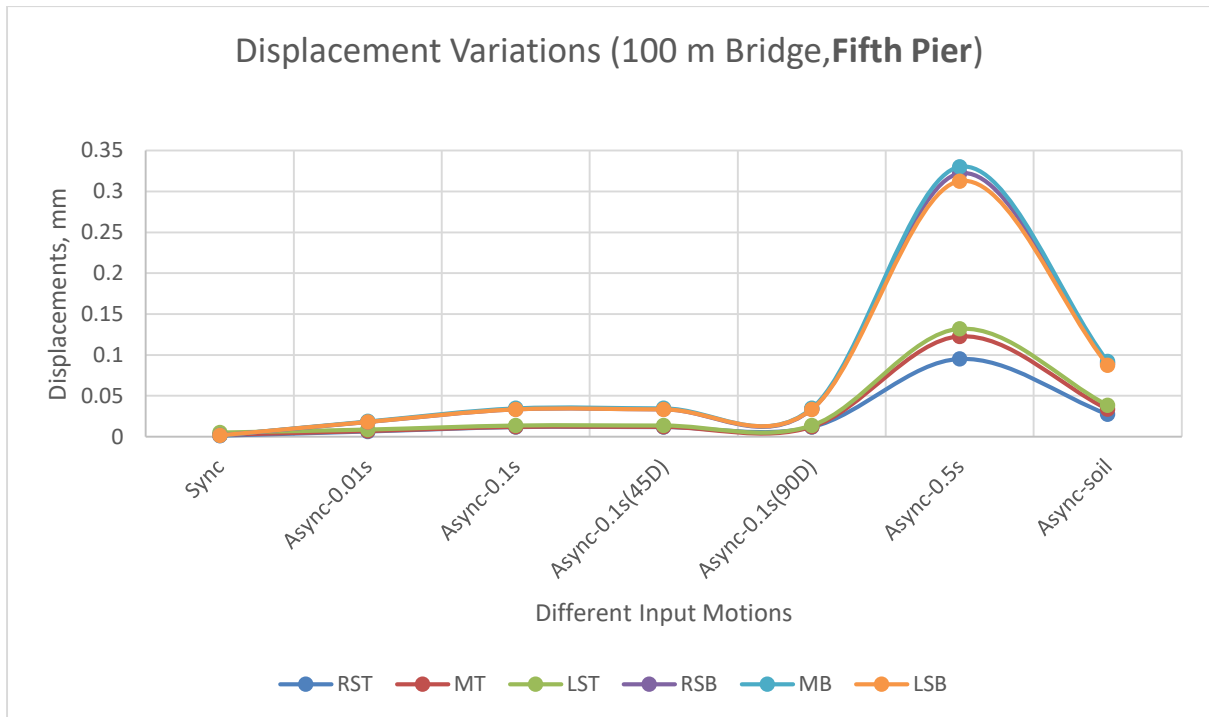


**Figure 4.5: Displacement Variation at Fifth Pier along X-axis**

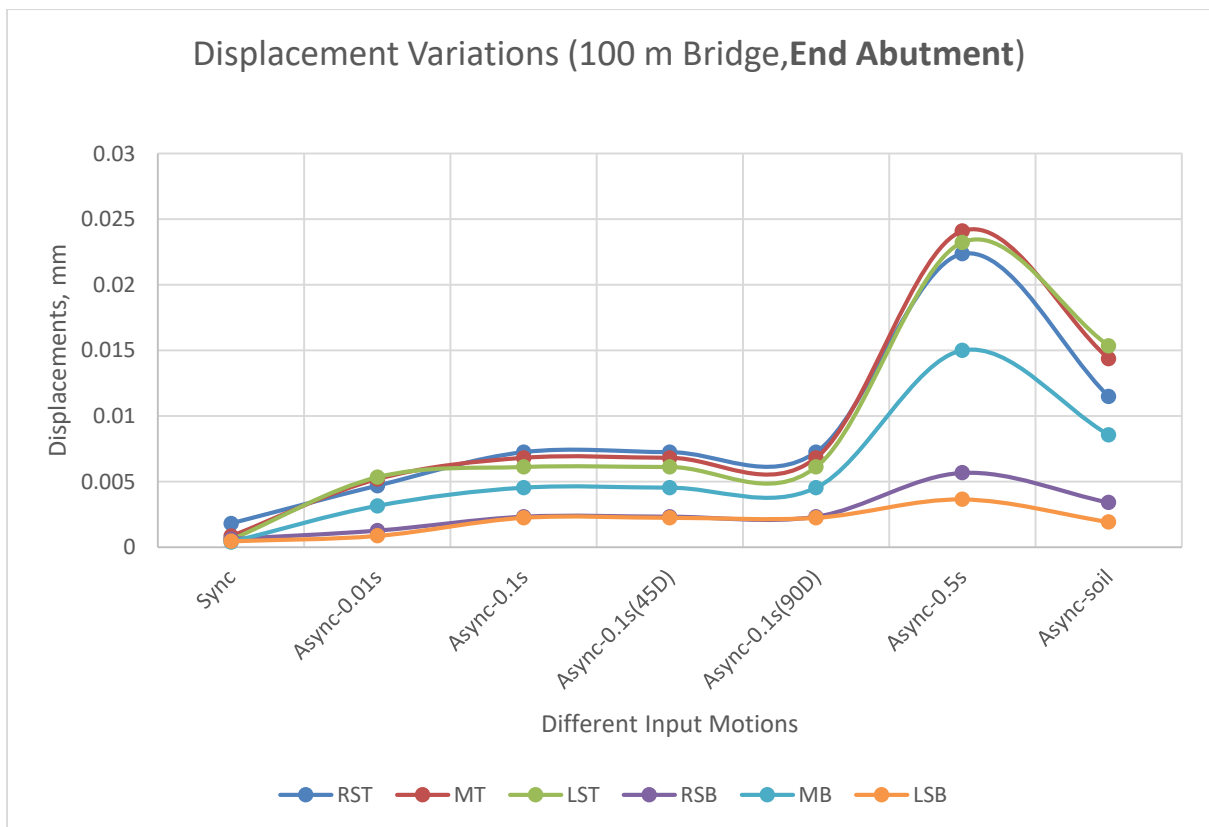


**Figure 4.6: Displacement Variation at End Abutment along X-axis**

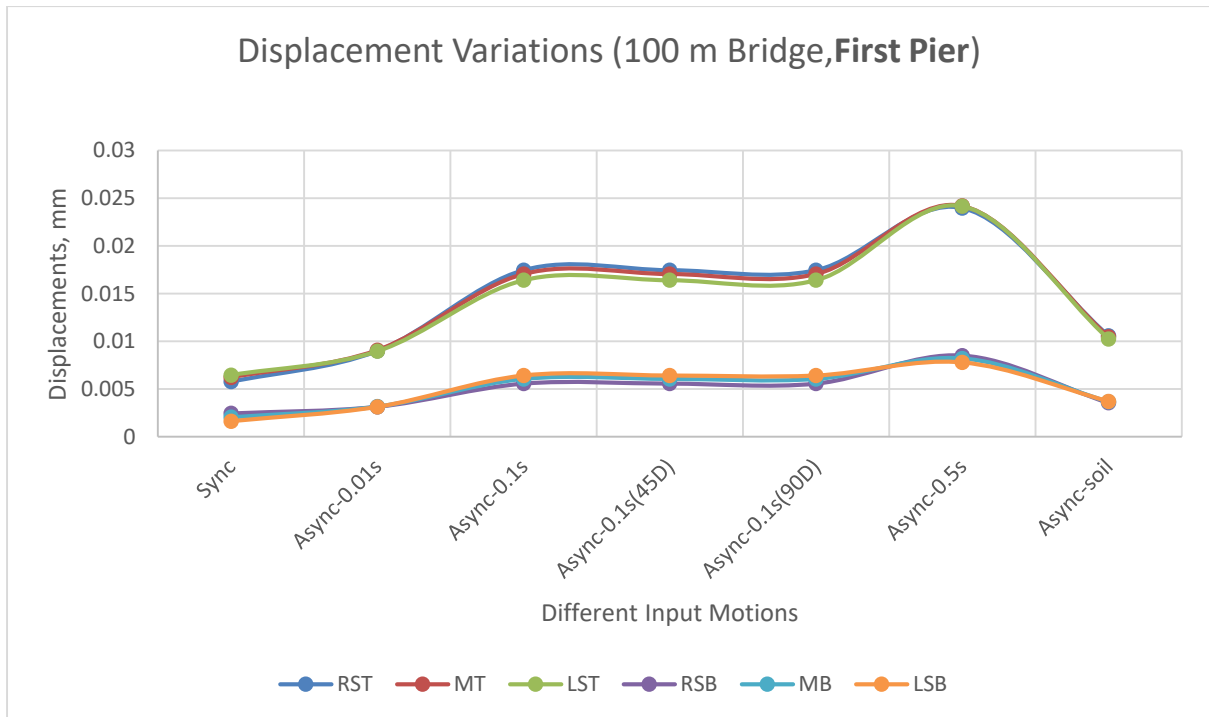


**Figure 4.7: Displacement Variation at First Pier along Y-axis**

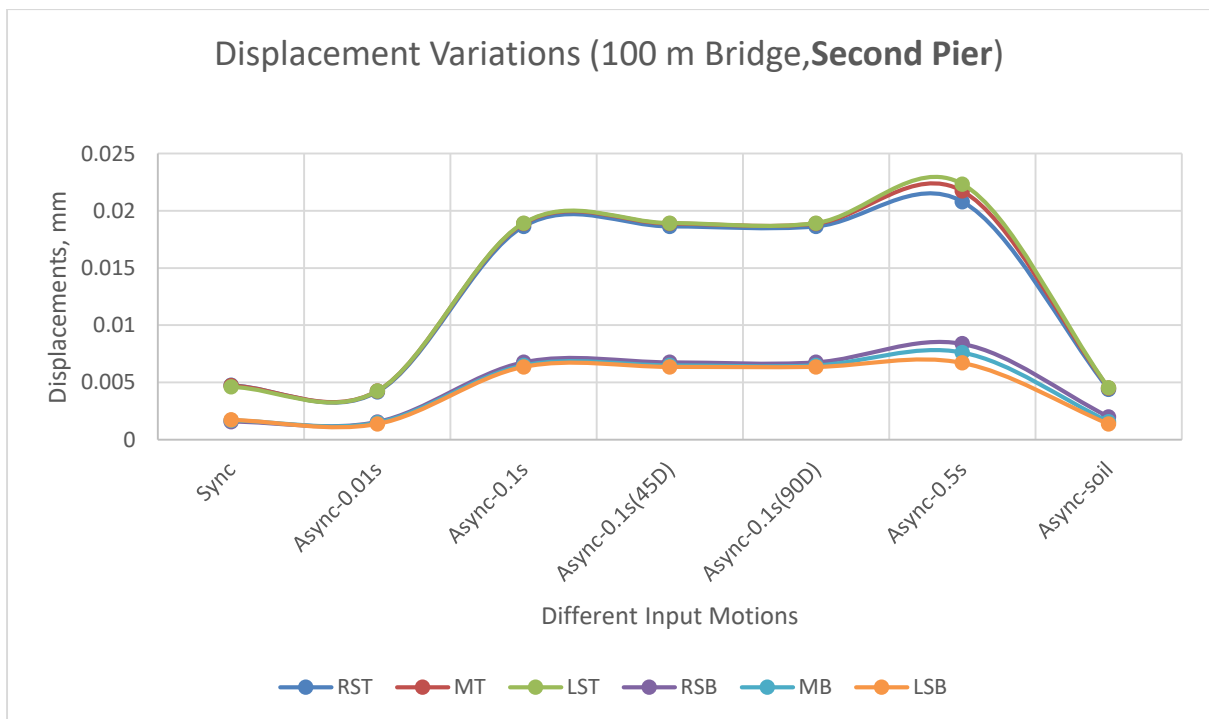


**Figure 4.8: Displacement Variation at Second Pier along Y-axis**

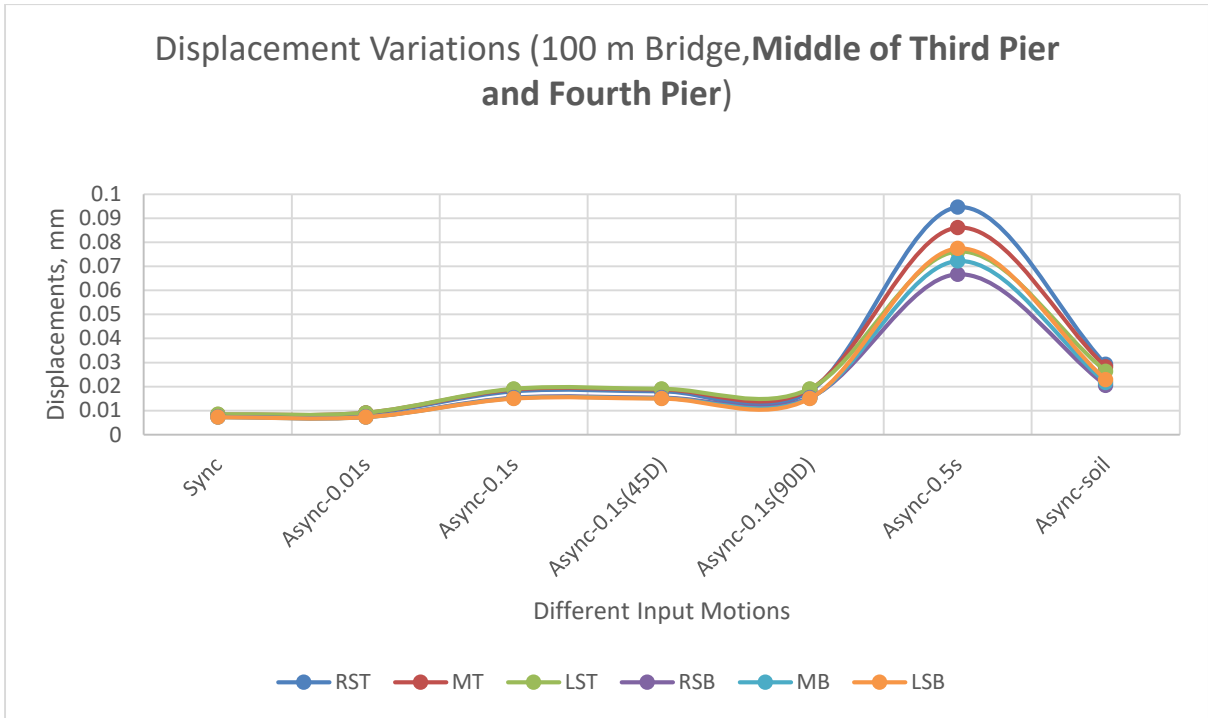


**Figure 4.9: Displacement Variation at Middle of Third Pier and Fourth Pier along Y-axis**

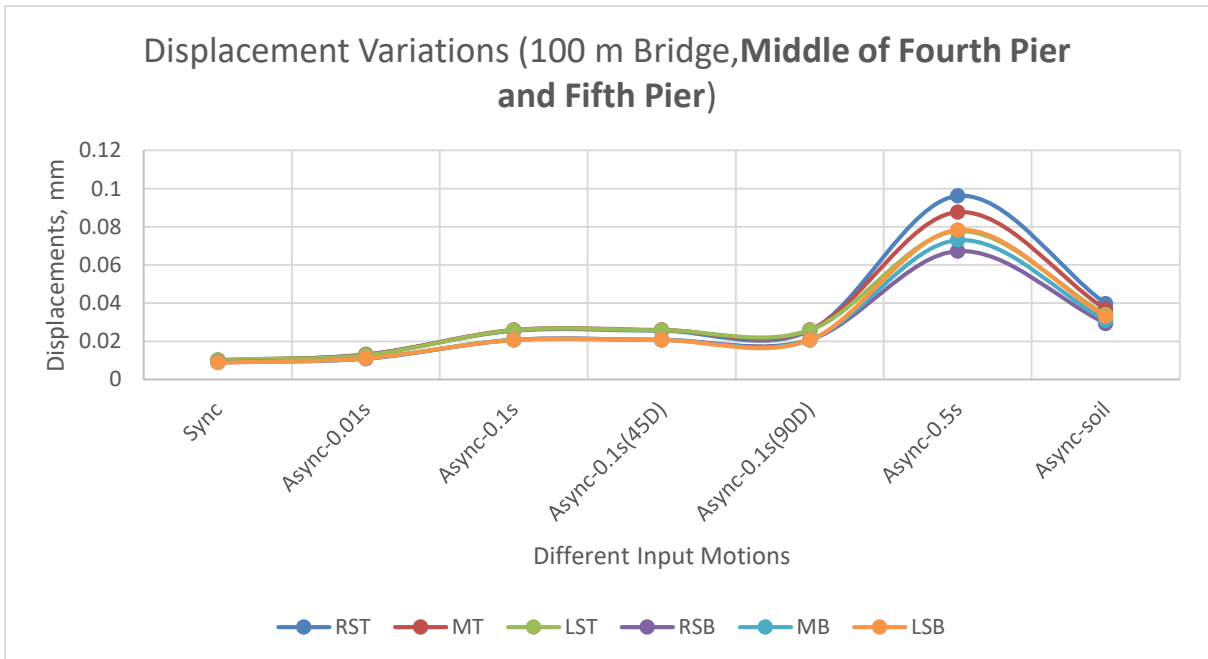


**Figure 4.10: Displacement Variation at Middle of Fourth Pier and Fifth Pier along Y-axis**



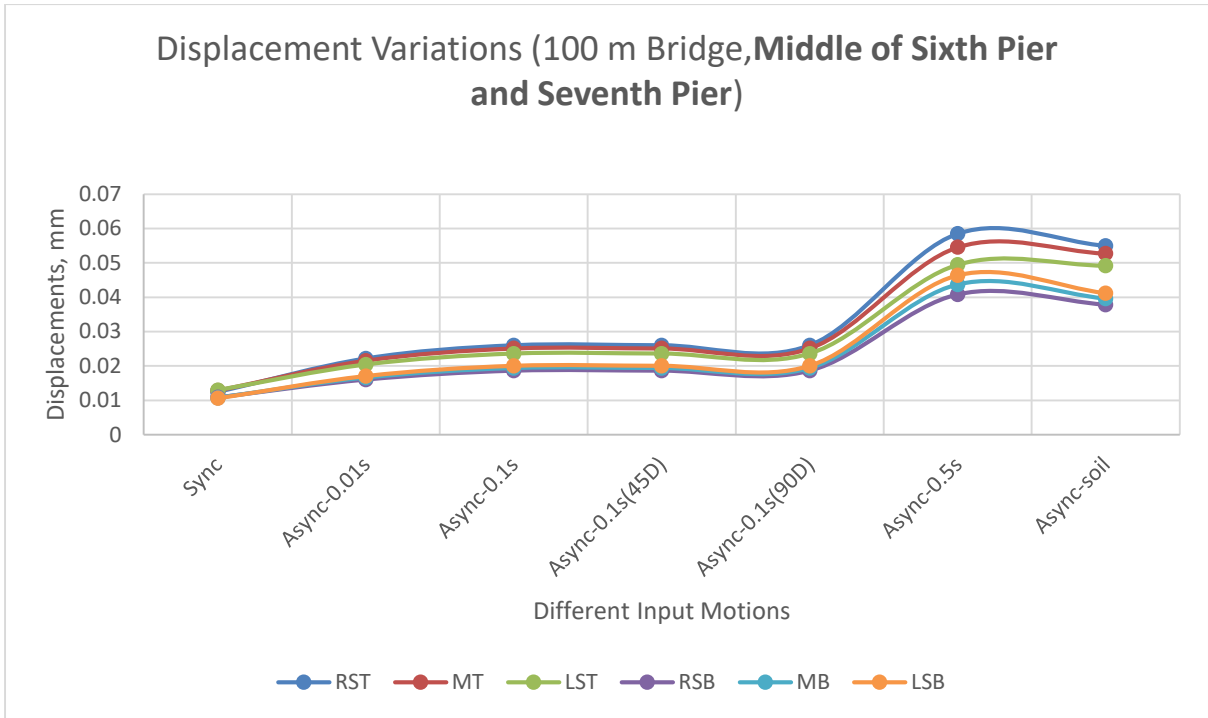


**Figure 4.11: Displacement Variation at Middle of Sixth Pier and Seventh Pier along Y-axis**

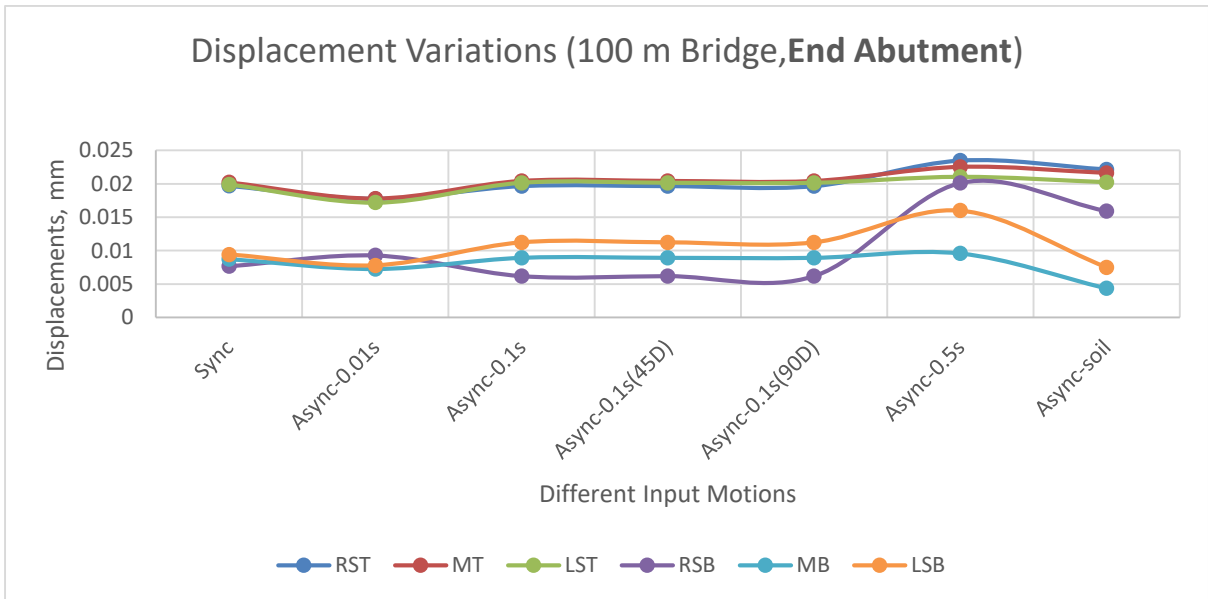


**Figure 4.12: Displacement Variation at End Abutment along Y-axis**

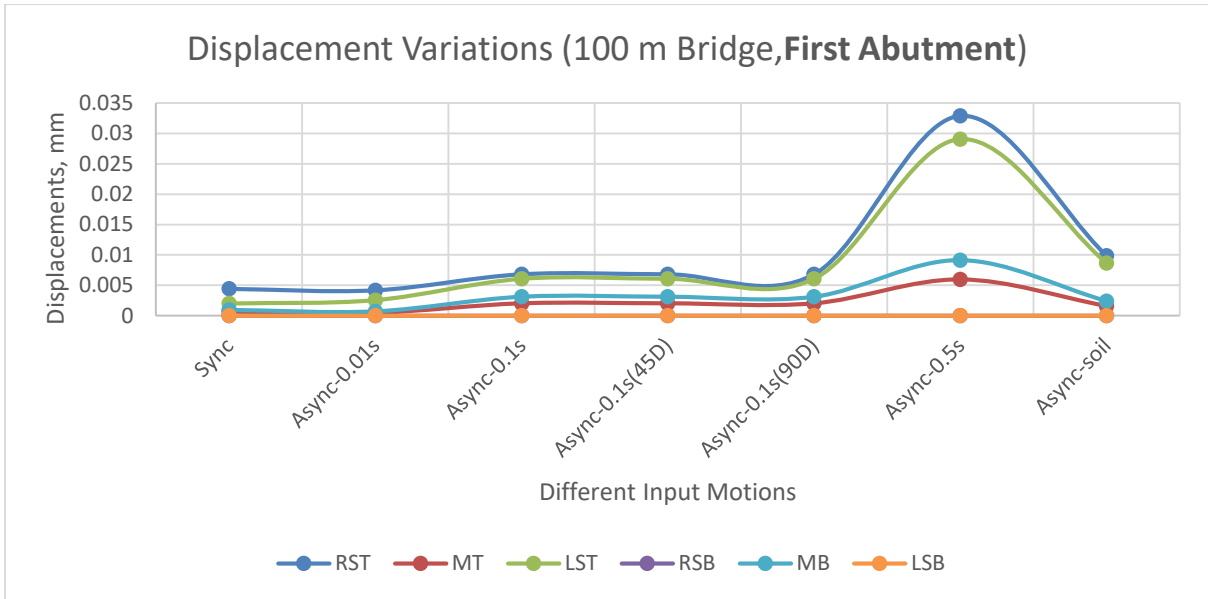


**Figure 4.13: Displacement Variation at First Abutment along Z-axis**

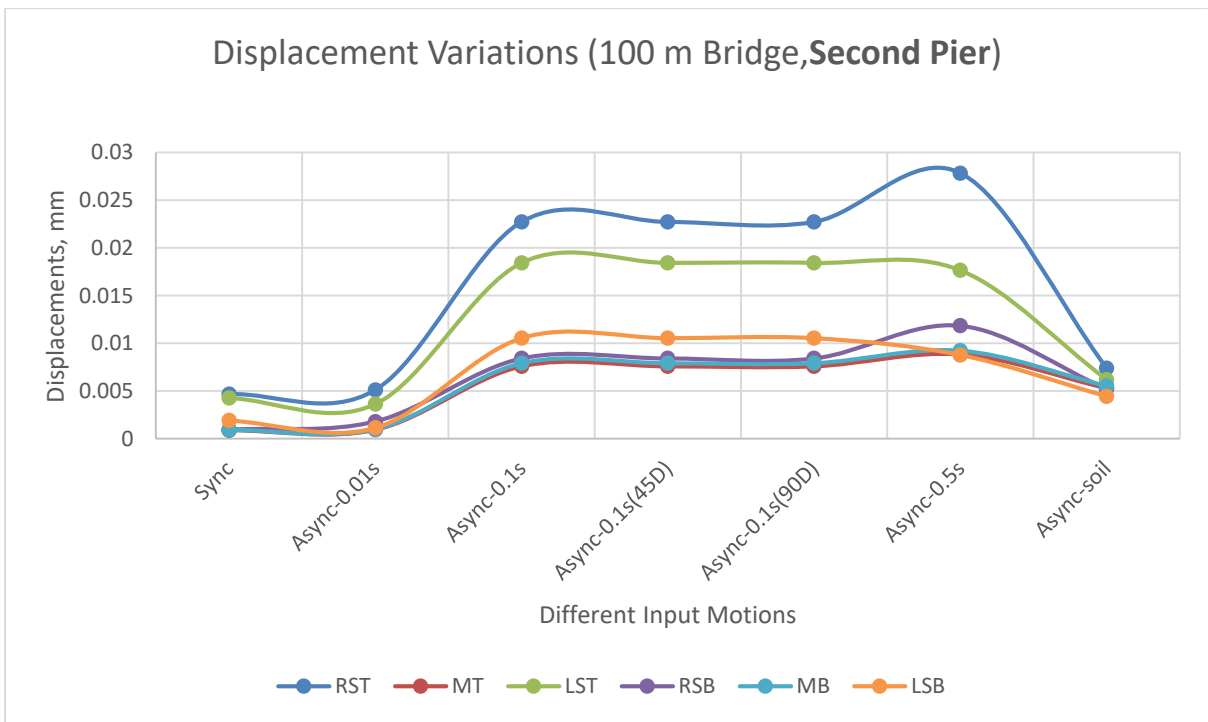


**Figure 4.14: Displacement Variation at Second Pier along Z-axis**

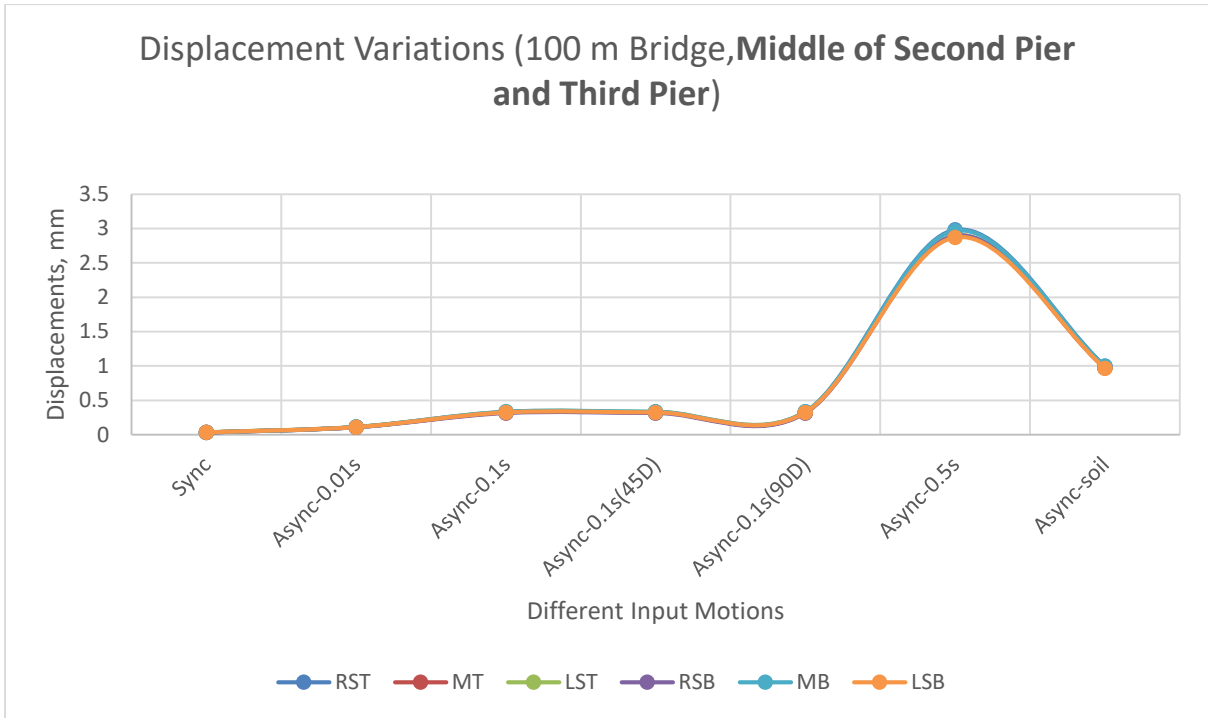


**Figure 4.15: Displacement Variation at Middle of Second Pier and Third Pier along Z-axis**

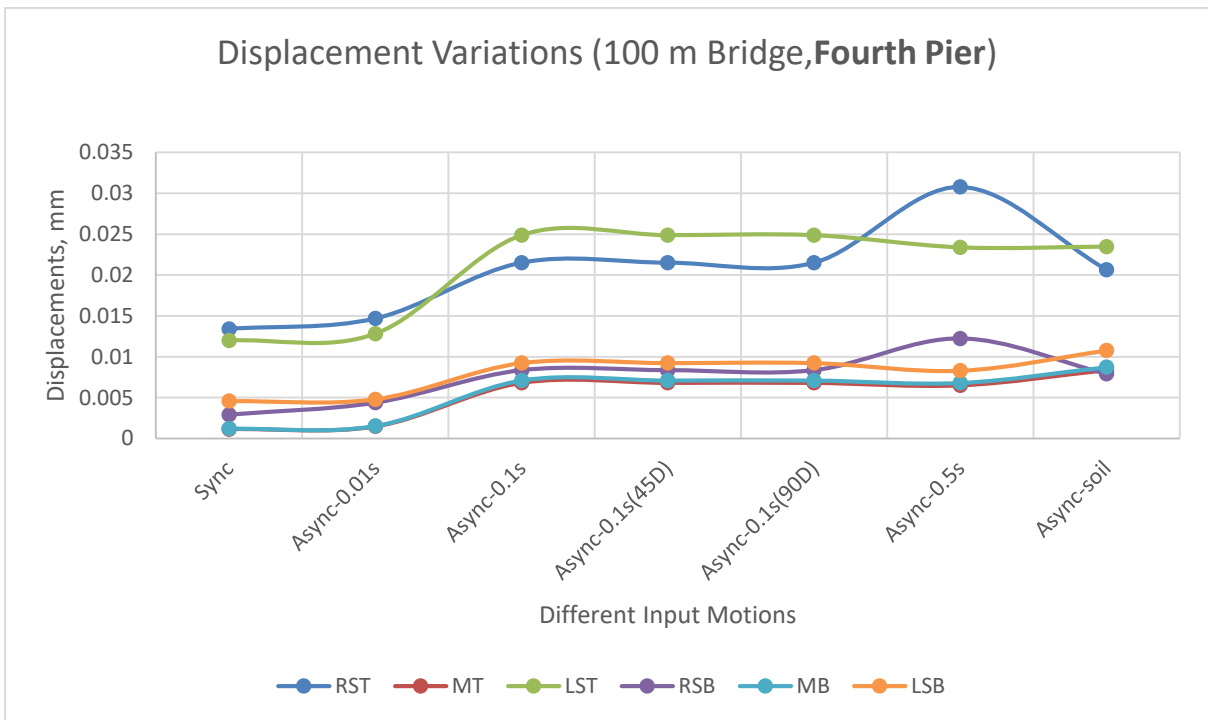


**Figure 4.16: Displacement Variation at Fourth Pier along Z-axis**

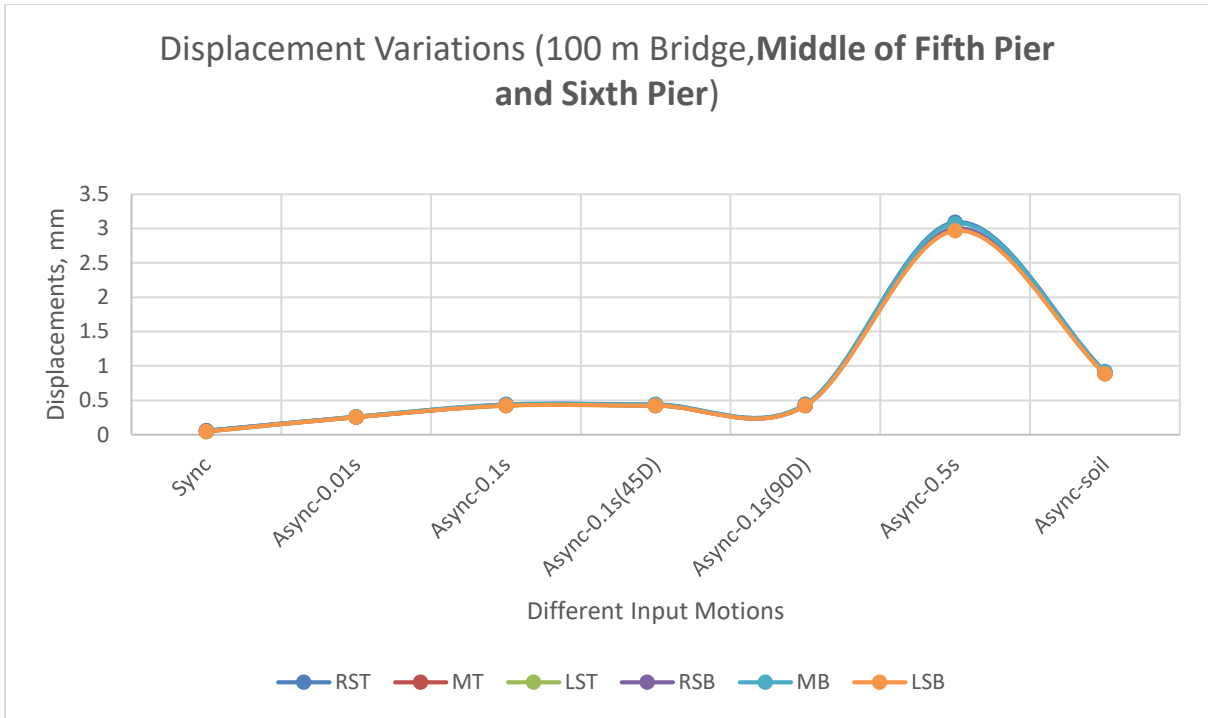


**Figure 4.17: Displacement Variation at Middle of Fifth Pier and Sixth Pier along Z-axis**

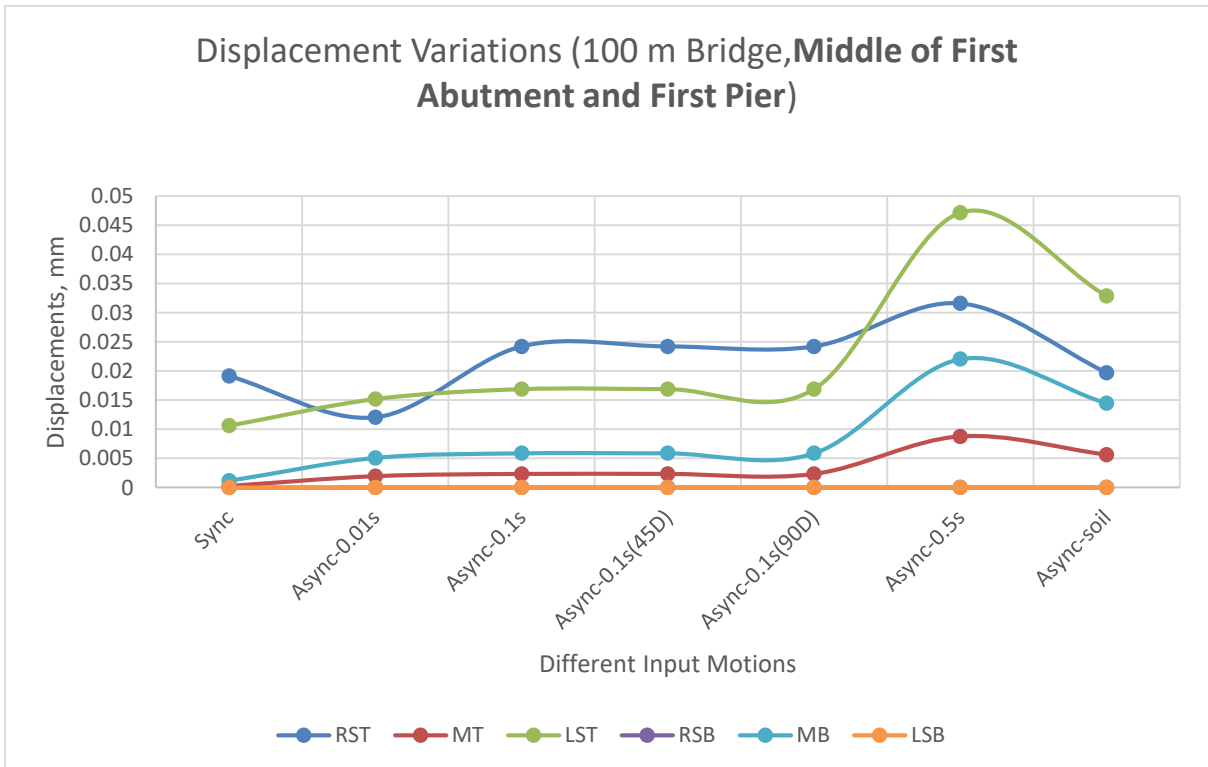


**Figure 4.18: Displacement Variation at End Abutment along Z-axis**

## 4.2 SYNCHRONOUS AND ASYNCHRONOUS EFFECT FOR 100 M MODEL

### 4.2.1 Synchronous and Asynchronous Effect for 100 m Model along X-axis (along Length of the Bridge)

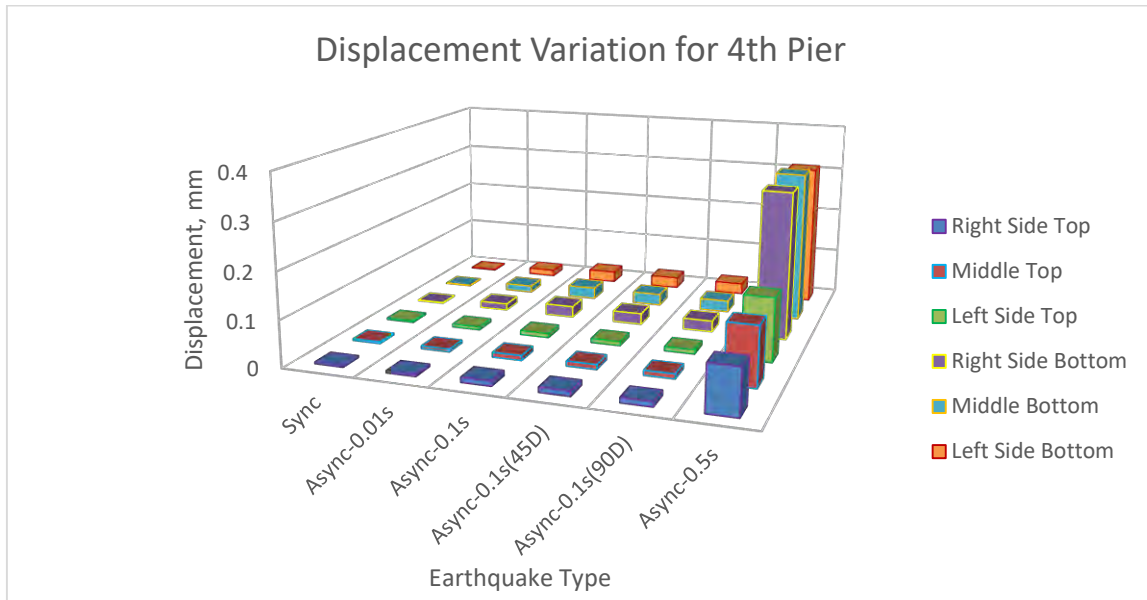


**Figure 4.19: Displacement Variation for Fourth Pier along X-axis**

From above graph, it can be said that at fourth pier, asynchronous effect due to 0.5 second time lag governs at three bottom points.

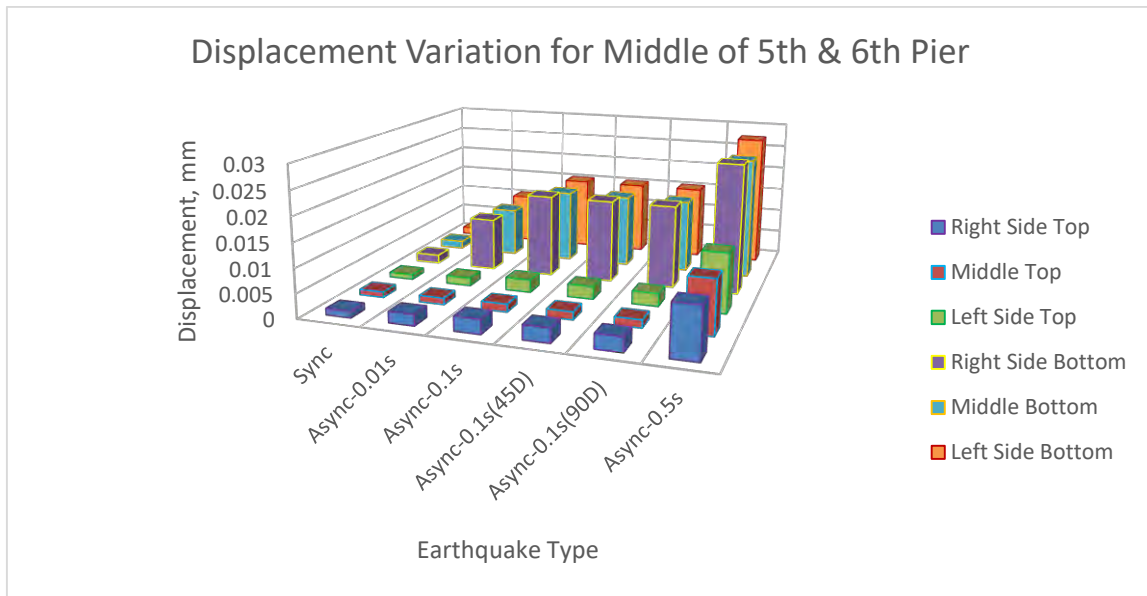


**Figure 4.20: Displacement Variation for middle of fifth & sixth pier along X-axis**

From above graph, it can be said that at middle of 5<sup>th</sup> & 6<sup>th</sup> pier, asynchronous effect due to 0.1 second & 0.5 second time lag govern at three bottom points.

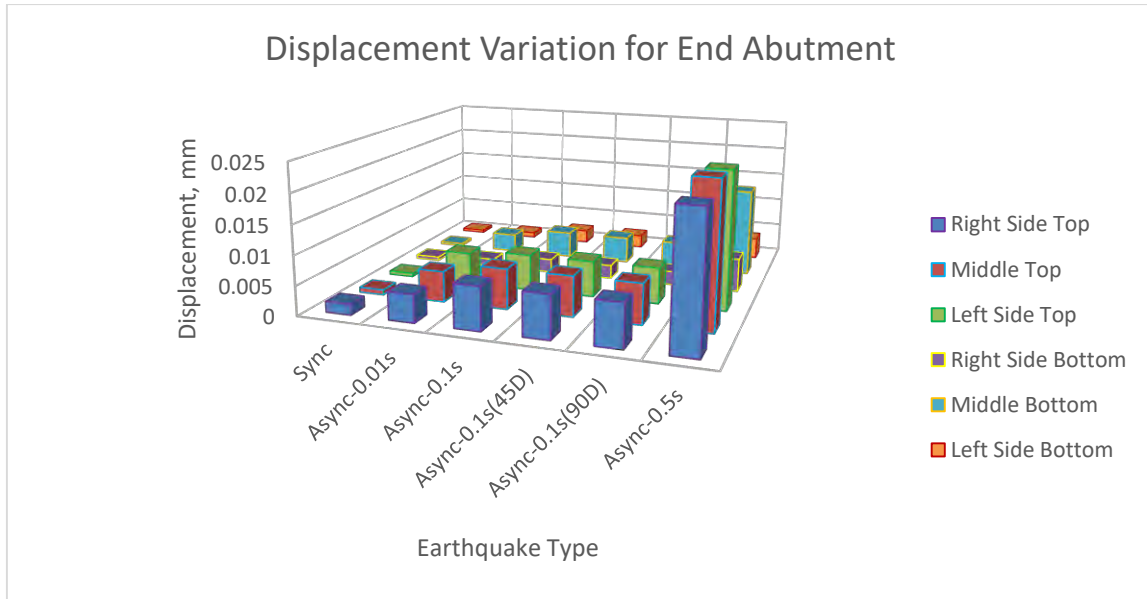


**Figure 4.21: Displacement Variation for end abutment along X-axis**

From above graph, it can be said that at end abutment, asynchronous effect due to 0.5 second time lag govern at three top points.

#### 4.2.2 Synchronous and Asynchronous Effect for 100 m Model along Y-axis (along Width of the Bridge)

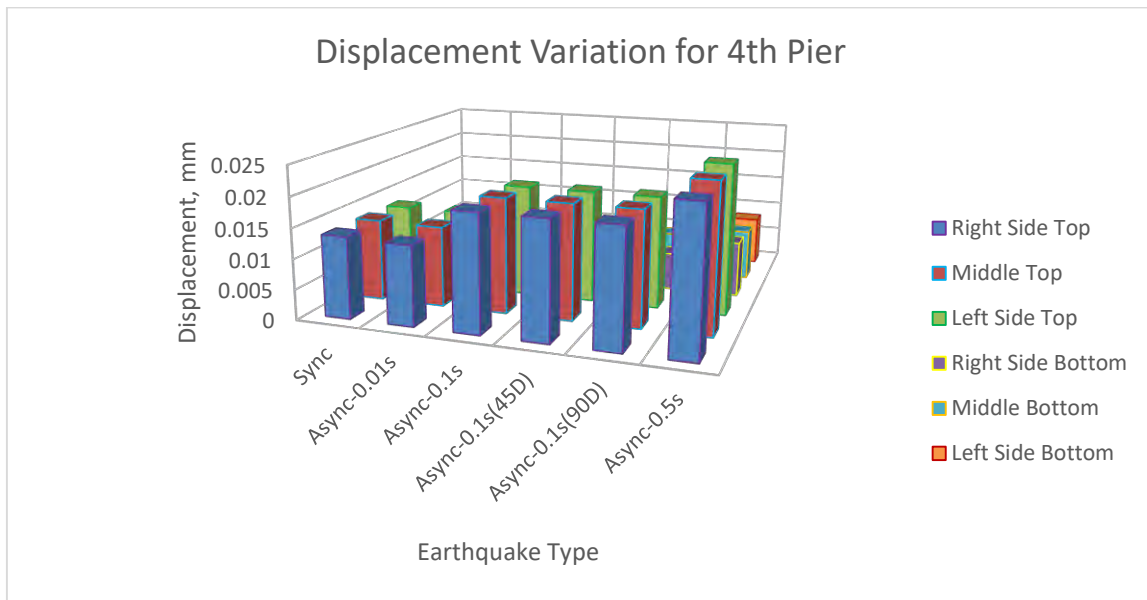


**Figure 4.22: Displacement Variation for Fourth Pier along Y-axis**

From above graph, it can be said that at 4<sup>th</sup> pier, asynchronous effect due to 0.1 second & 0.5 second time lag govern at three top points.

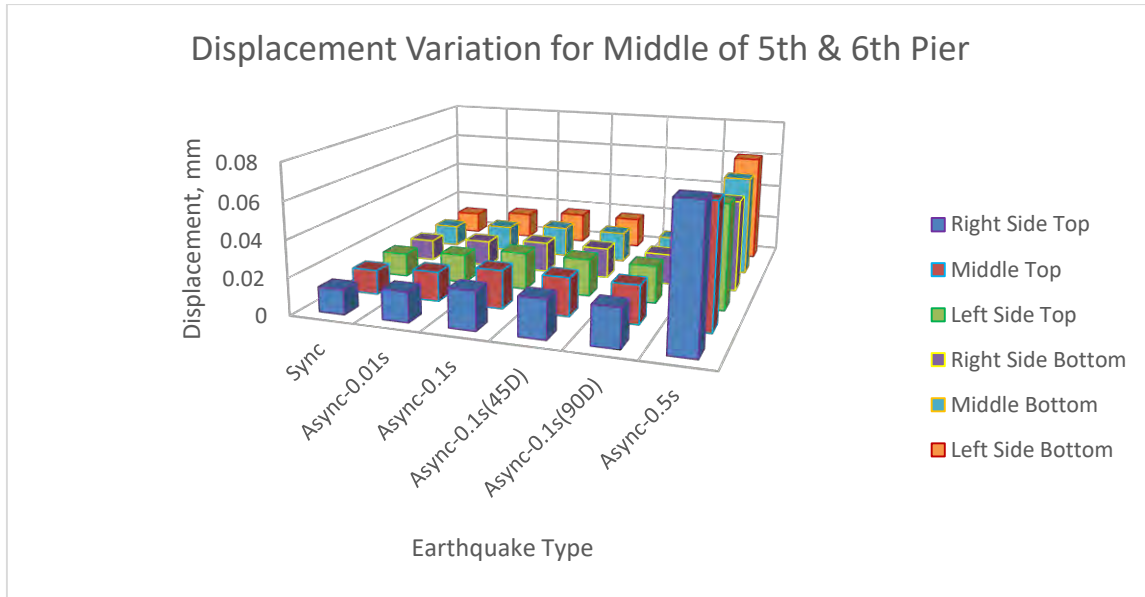


**Figure 4.23: Displacement Variation for middle of fifth & sixth pier along Y-axis**

From above graph, it can be said that at middle of 5<sup>th</sup> & 6<sup>th</sup> pier, asynchronous effect due to 0.5 second time lag govern at all six points.

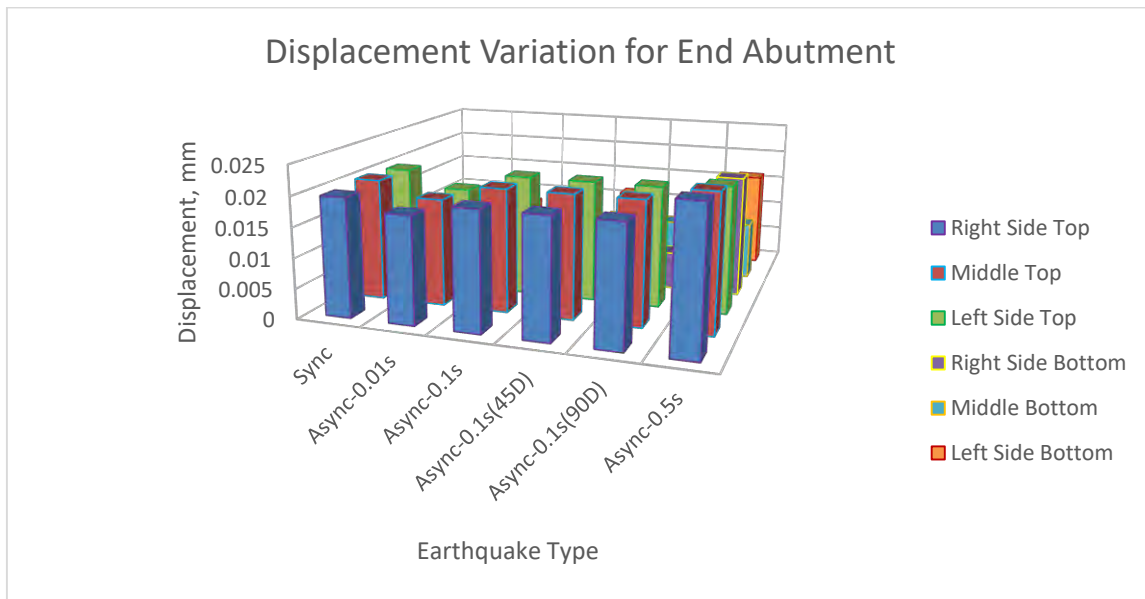


**Figure 4.24: Displacement Variation for end abutment along Y-axis**

From above graph, it can be said that at end abutment, synchronous & asynchronous effect due to 0.01 second, 0.1 second & 0.5 second time lag govern at three top points.

### 4.2.3 Synchronous and Asynchronous Effect for 100 m Model along Z-axis (along Vertical Direction of the Bridge)

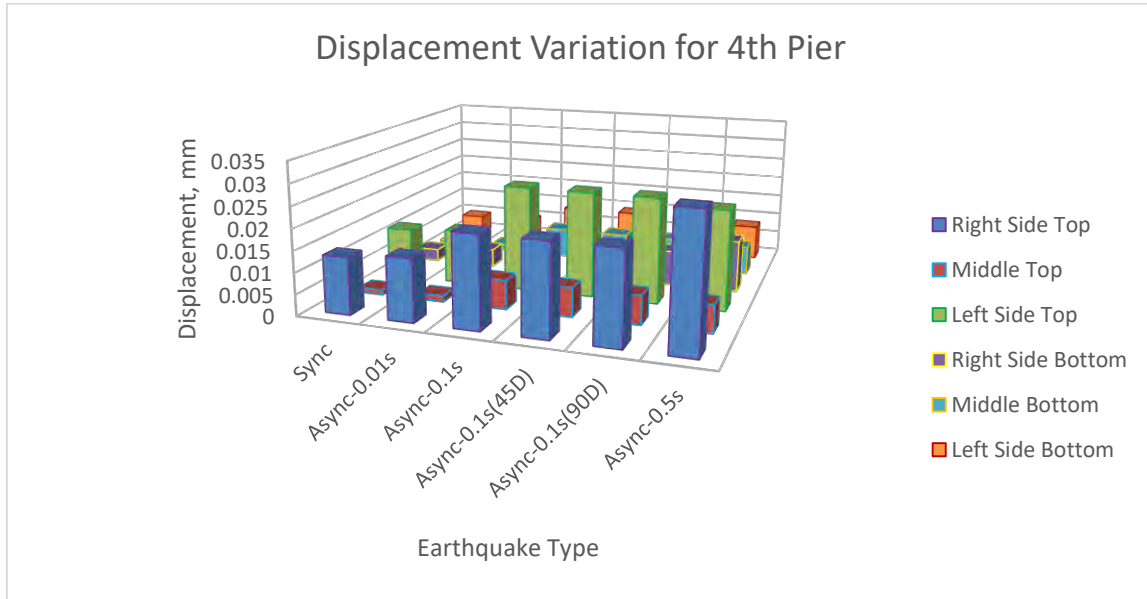


**Figure 4.25: Displacement Variation for Fourth Pier along Z-axis**

From above graph, it can be said that at 4<sup>th</sup> pier, asynchronous effect due to 0.1 second & 0.5 second time lag govern at right side top & left side top points.

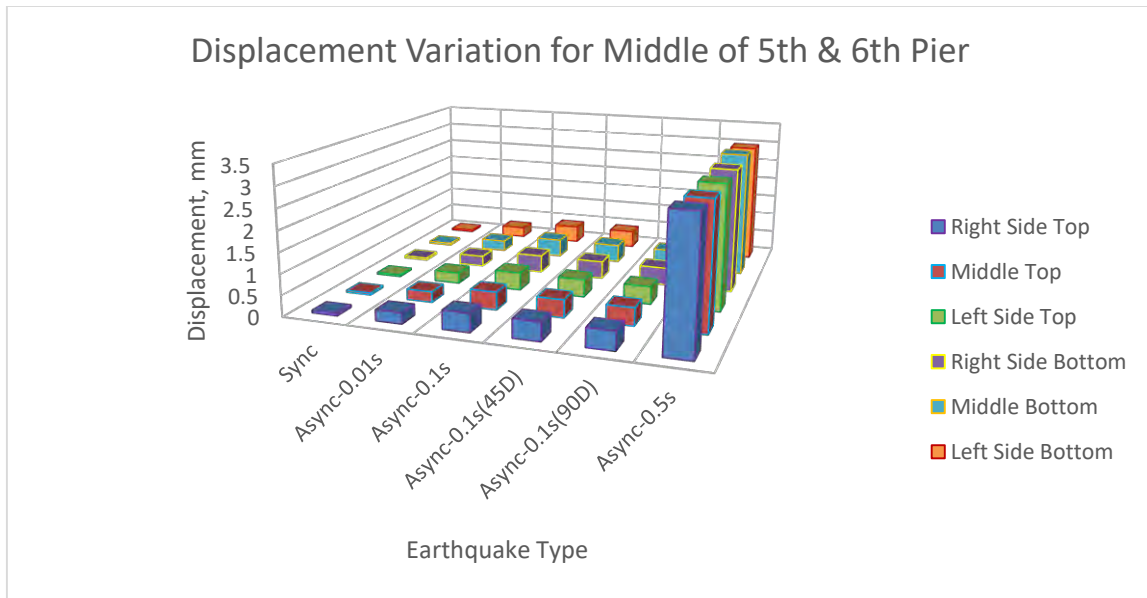


**Figure 4.26: Displacement Variation for middle of fifth & sixth pier along Z-axis**

From above graph, it can be said that at middle of 5<sup>th</sup> & 6<sup>th</sup> pier, asynchronous effect due to 0.5 second time lag govern at all six top & bottom points.



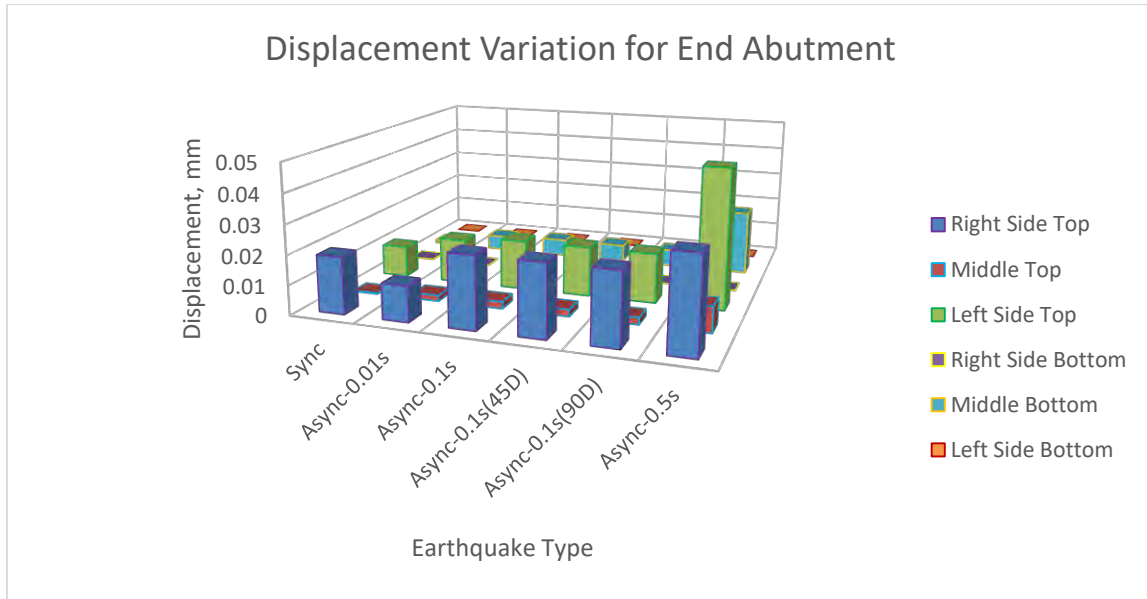


**Figure 4.27: Displacement Variation for end abutment along Z-axis**

From above graph, it can be said that at end abutment, asynchronous effect due to 0.5 second time lag govern at right side top & left side top points.

#### 4.2.4 Synchronous and Asynchronous Effect for 125 m Model along X-axis (along length of the bridge)

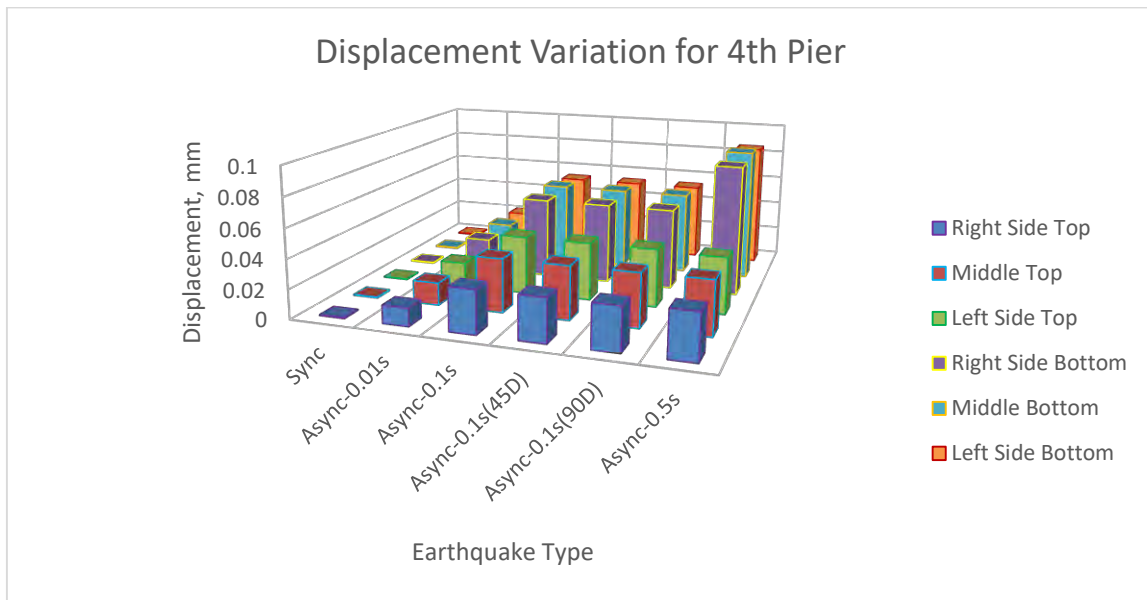


**Figure 4.28: Displacement Variation for Fourth Pier along X-axis**

From above graph, it can be said that at 4<sup>th</sup> pier, asynchronous effect due to 0.5 second time lag govern at three bottom points.

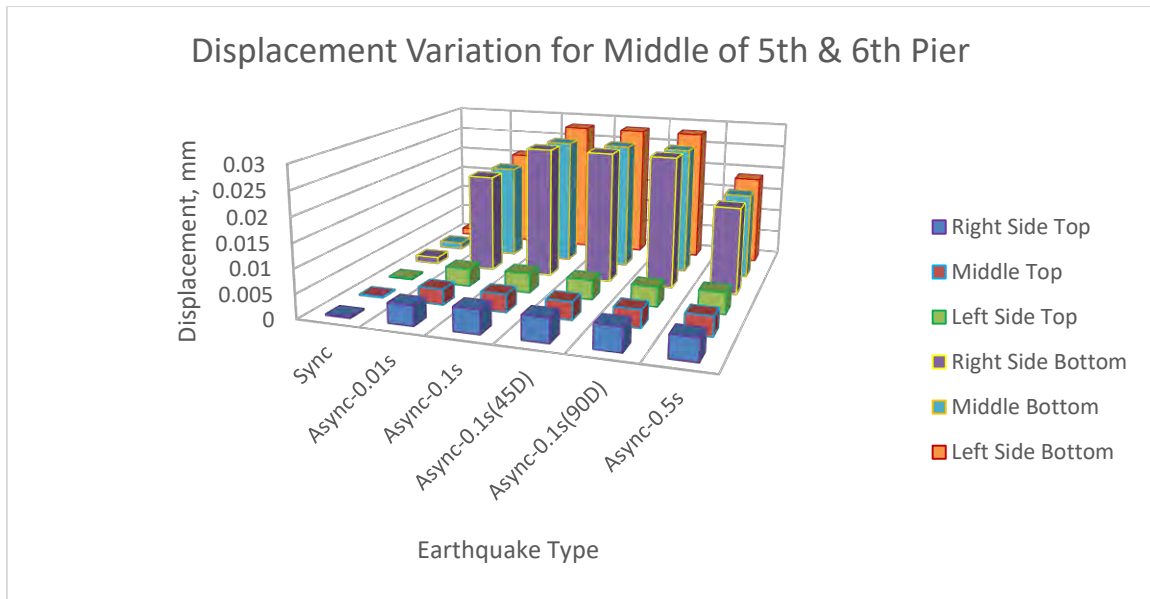


**Figure 4.29: Displacement Variation for middle of fifth & sixth pier along X-axis**

From above graph, it can be said that at middle of 5<sup>th</sup> & 6<sup>th</sup> pier, asynchronous effect due to 0.1 second time lag govern at three bottom points.

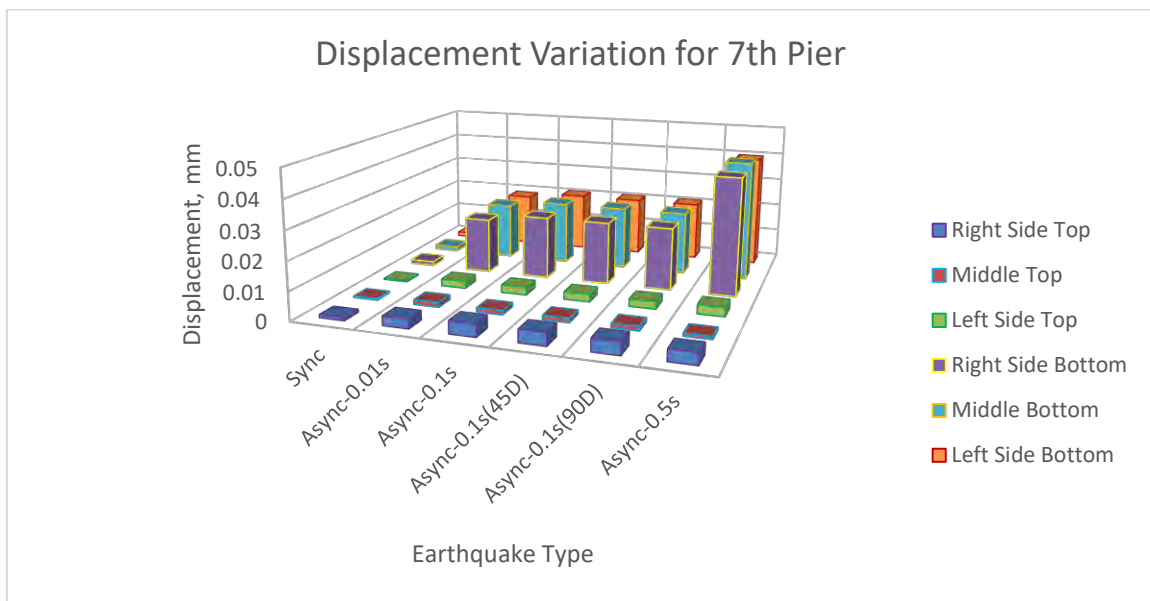


**Figure 4.30: Displacement Variation for Seventh Pier along X-axis**

From above graph, it can be said that at 7<sup>th</sup> pier, asynchronous effect due to 0.5 second time lag govern at three bottom points.

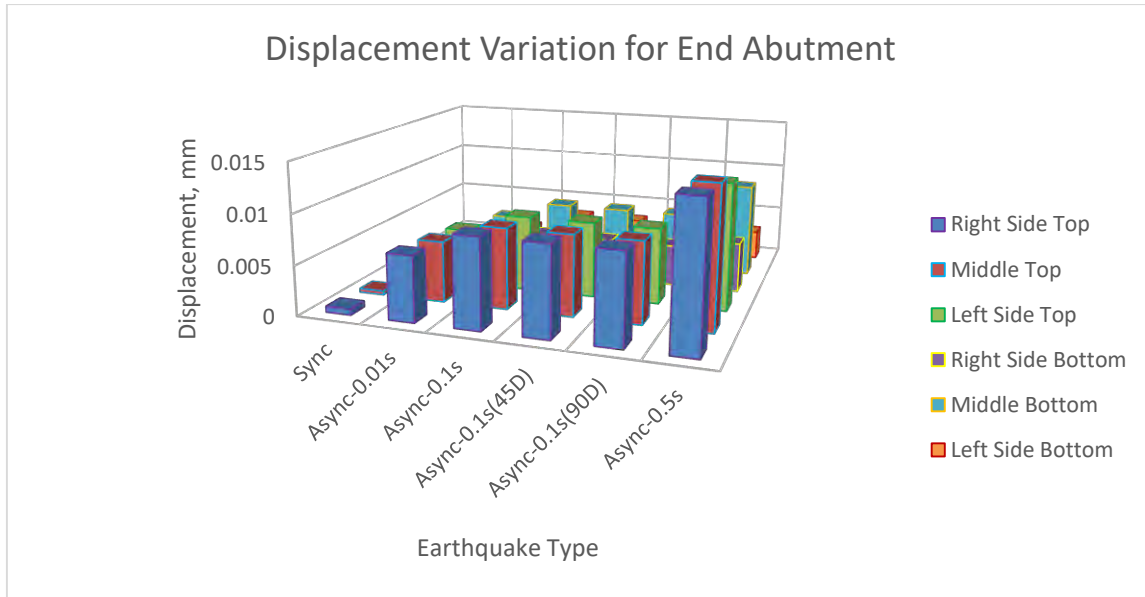


**Figure 4.31: Displacement Variation for end abutment along X-axis**

From above graph, it can be said that at end abutment, asynchronous effect due to 0.5 second time lag govern at three top points.

#### 4.2.5 Synchronous and Asynchronous Effect for 125 m Model along Y-axis (along Width of the Bridge)

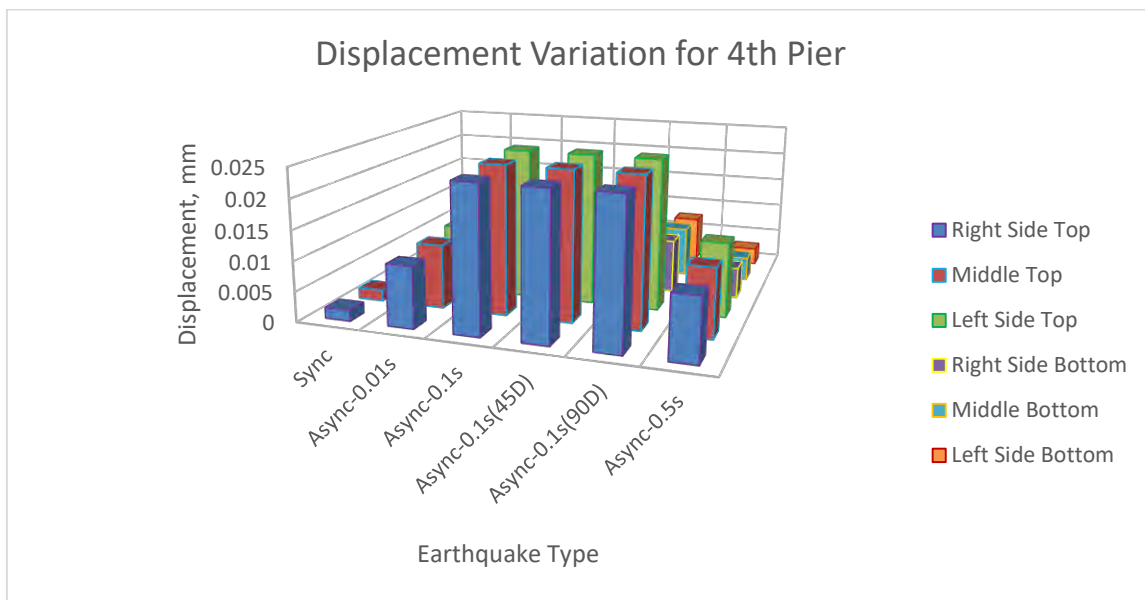


**Figure 4.32: Displacement Variation for Fourth Pier along Y-axis**

From above graph, it can be said that at 4<sup>th</sup> pier, asynchronous effect due to 0.1 second time lag govern at three top points.

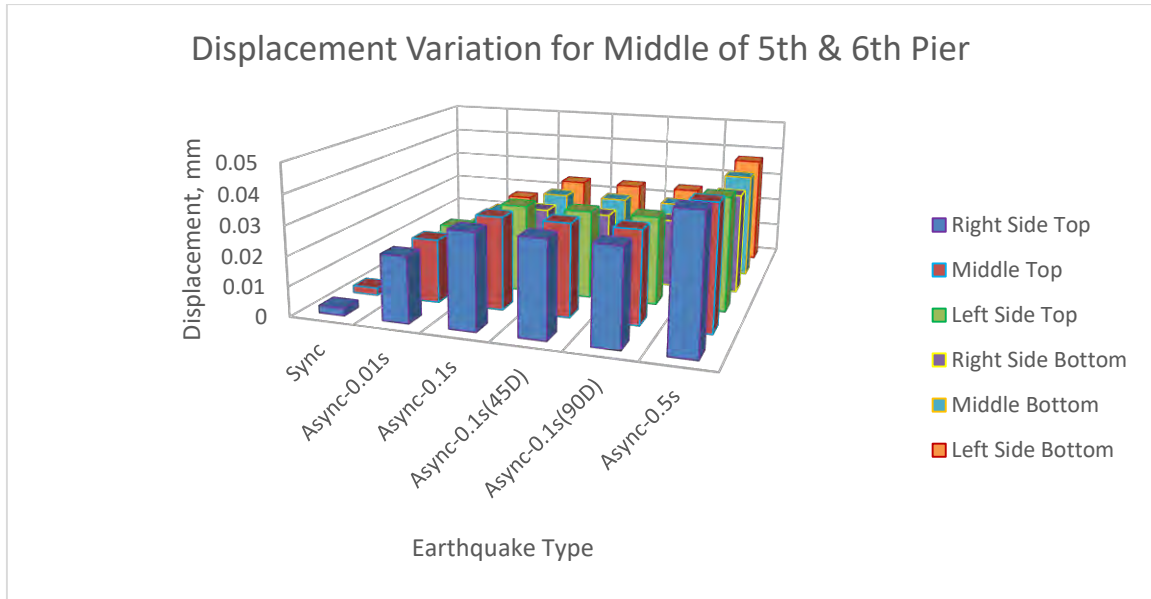


**Figure 4.33: Displacement Variation for middle of fifth & sixth pier along Y-axis**

From above graph, it can be said that at middle of 5<sup>th</sup> & 6<sup>th</sup> pier, asynchronous effect due to 0.1 second & 0.5 second time lag govern at all six points.

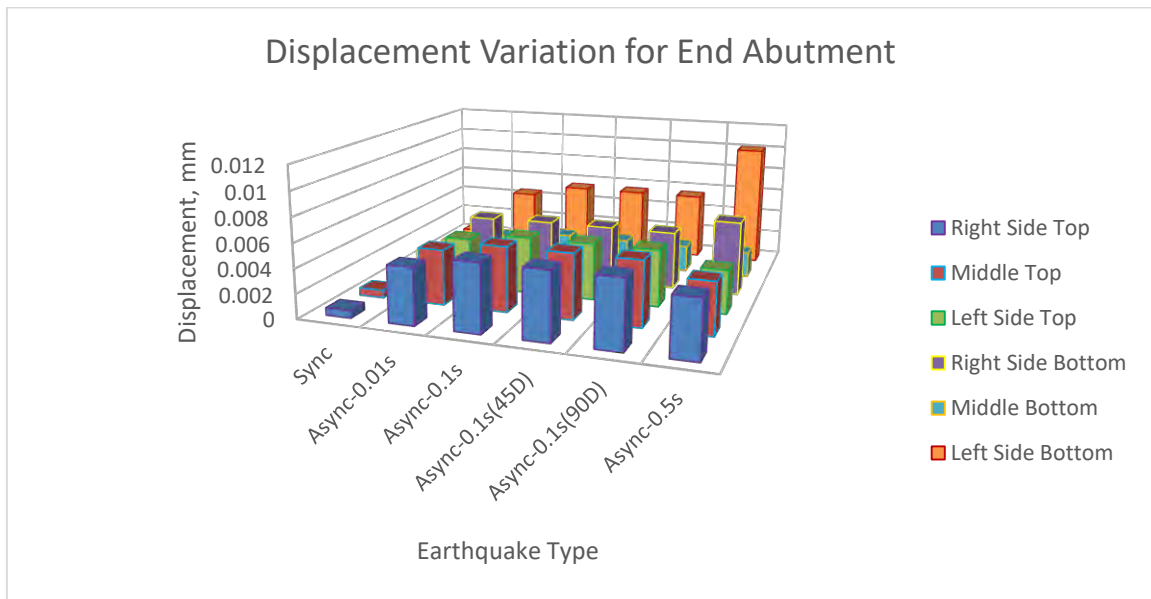


**Figure 4.34: Displacement Variation for end abutment along Y-axis**

From above graph, it can be said that at end abutment, asynchronous effect due to 0.5 second time lag govern at left side bottom point.

#### 4.2.6 Synchronous and Asynchronous Effect for 125 m Model along Z-axis (along Vertical Direction of the Bridge)

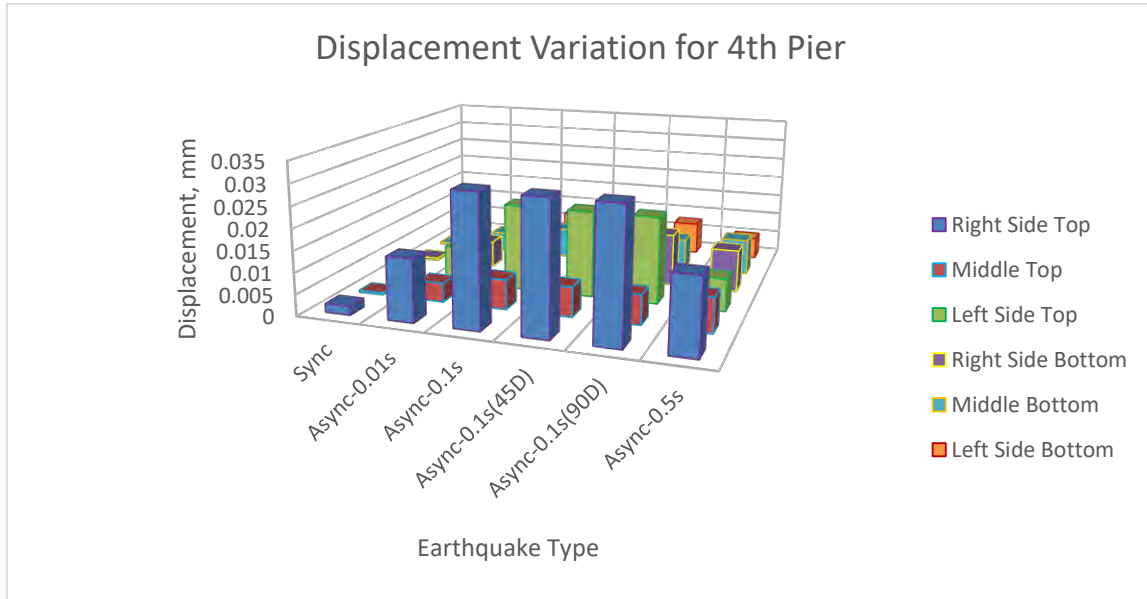


**Figure 4.35: Displacement Variation for Fourth Pier along Z-axis**

From above graph, it can be said that at 4<sup>th</sup> pier, asynchronous effect due to 0.1 second time lag govern at right side top & left side top points.

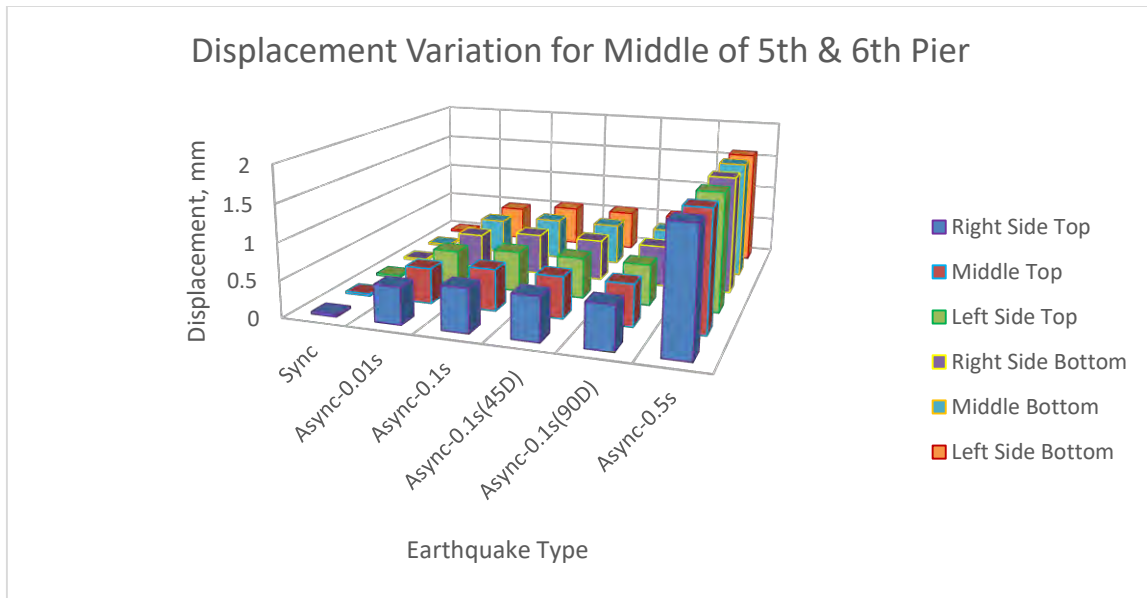


**Figure 4.36: Displacement Variation for middle of fifth & sixth pier along Z-axis**

From above graph, it can be said that at middle of 5<sup>th</sup> & 6<sup>th</sup> pier, asynchronous effect due to 0.5 second time lag govern at all six top & bottom points.

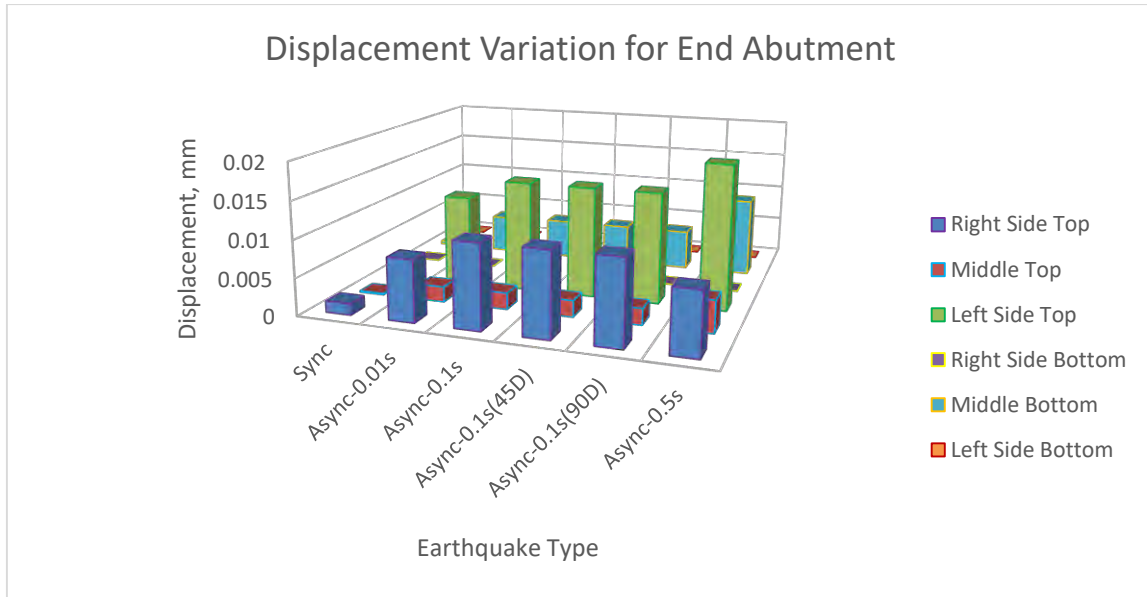


**Figure 4.37: Displacement Variation for end abutment along Z-axis**

From above graph, it can be said that at end abutment, asynchronous effect due to 0.1 second & 0.5 second time lag govern at left side top & right side top points.

### 4.3 SOIL EFFECT ON TWO BRIDGES:

One type of soil is used up to fourth pier and from fourth pier another type of soil due to asynchronous motion is used in two models. Displacement variation due to soil effect (synchronous vs asynchronous-soil) are shown in below Figures.

#### 4.3.1 Soil Effect for 100 m Model along X-axis (along length of the bridge):

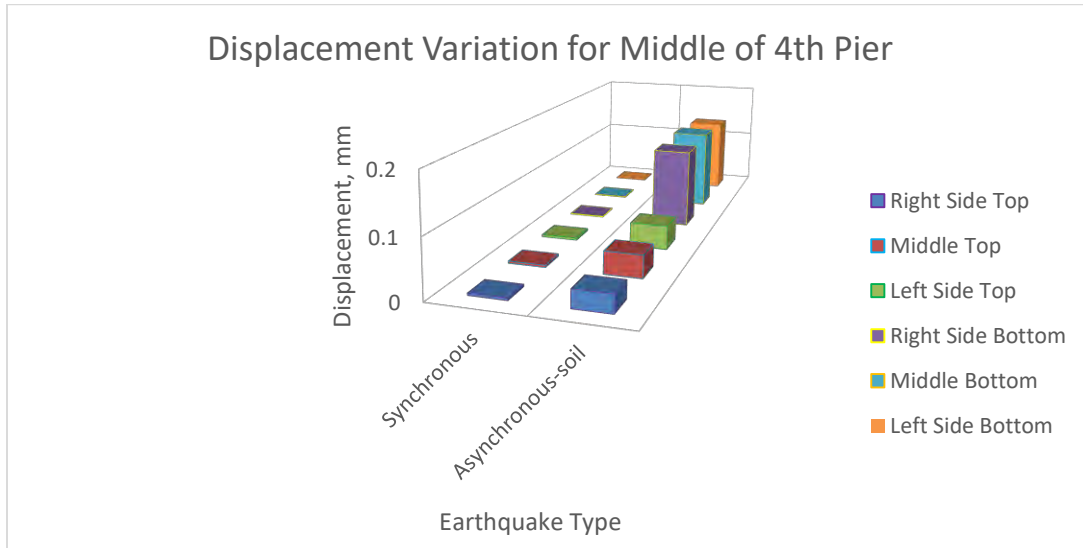


**Figure 4.38: Displacement Variation for Fourth Pier along X-axis**

From above graph between synchronous & asynchronous-soil, it can be said that at 4<sup>th</sup> pier, asynchronous-soil govern at three bottom points.

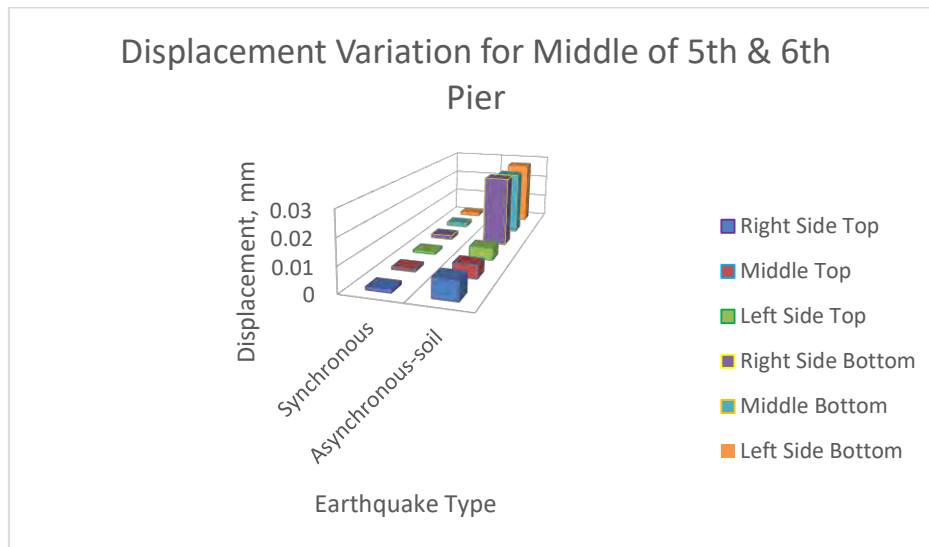


**Figure 4.39: Displacement Variation for middle of fifth & sixth pier along X-axis**

From above graph between synchronous & asynchronous-soil, it can be said that at middle of 5<sup>th</sup> & 6<sup>th</sup> pier, asynchronous-soil govern at three bottom points.

### 4.3.2 Soil Effect for 100 m Model along Y-axis (along Width of the Bridge):

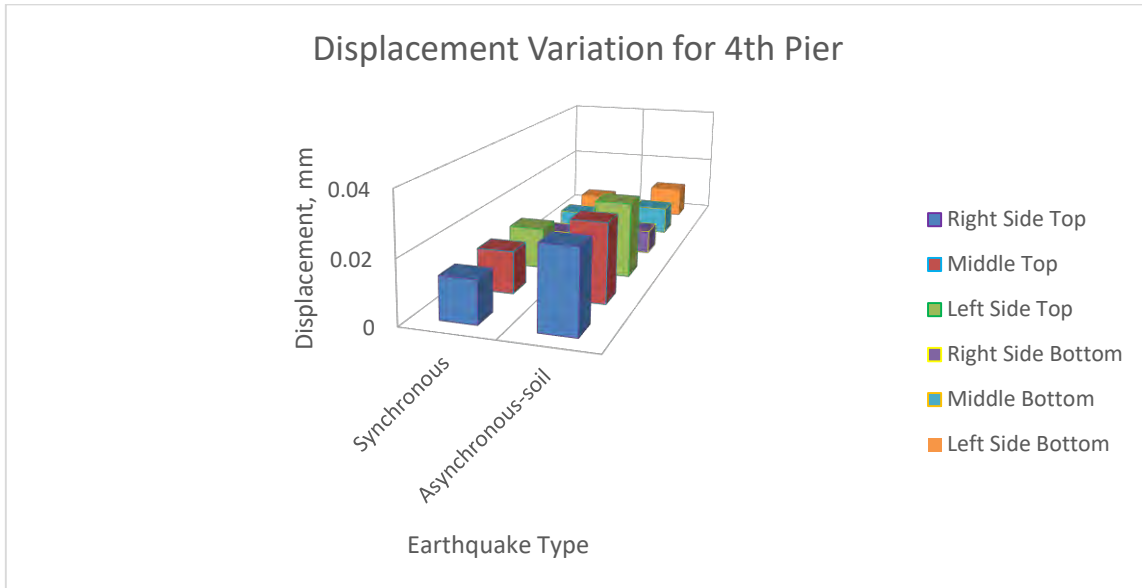


**Figure 4.40: Displacement Variation for Fourth Pier along Y-axis**

From above graph between synchronous & asynchronous-soil, it can be said that at 4<sup>th</sup> pier, asynchronous-soil govern at three top points.

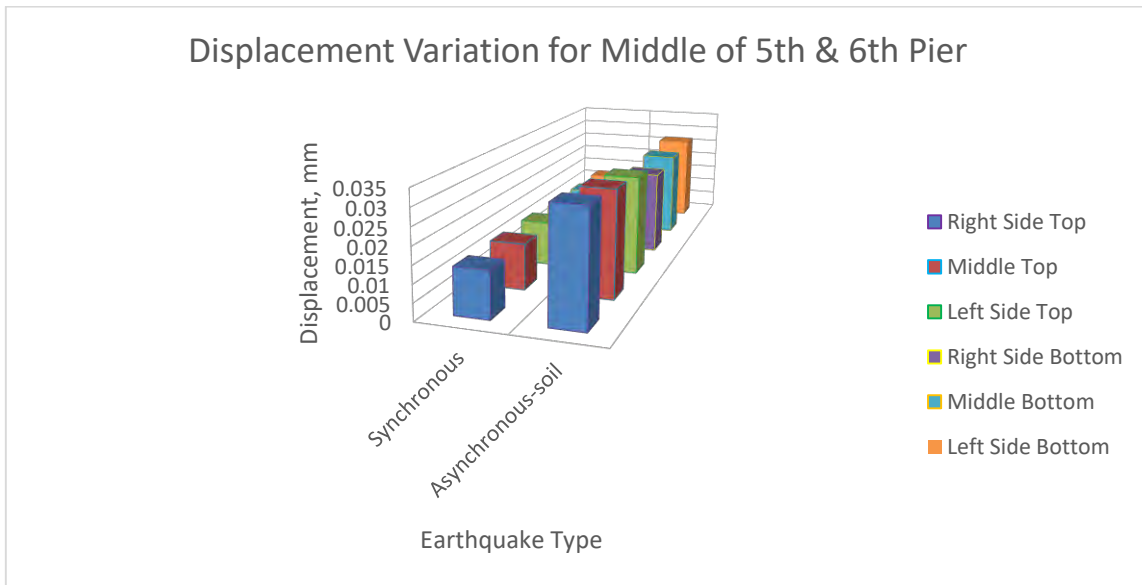


**Figure 4.41: Displacement Variation for middle of fifth & sixth pier along Y-axis**

From above graph between synchronous & asynchronous-soil, it can be said that at middle of 5<sup>th</sup> & 6<sup>th</sup> pier, asynchronous-soil govern at all six top & bottom points.



**4.3.3 Soil Effect for 100 m Model along Z-axis (along Vertical Direction of the Bridge):**

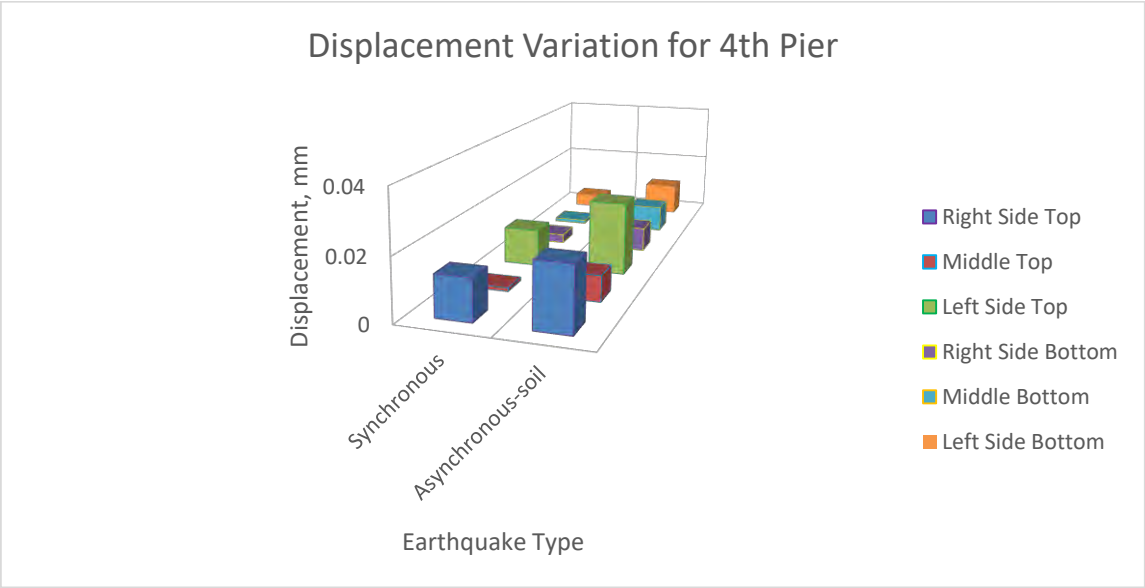


**Figure 4.42: Displacement Variation for Fourth Pier along Z-axis**

From above graph between synchronous & asynchronous-soil, it can be said that at 4<sup>th</sup> pier, asynchronous-soil govern at right side top & left side top points.

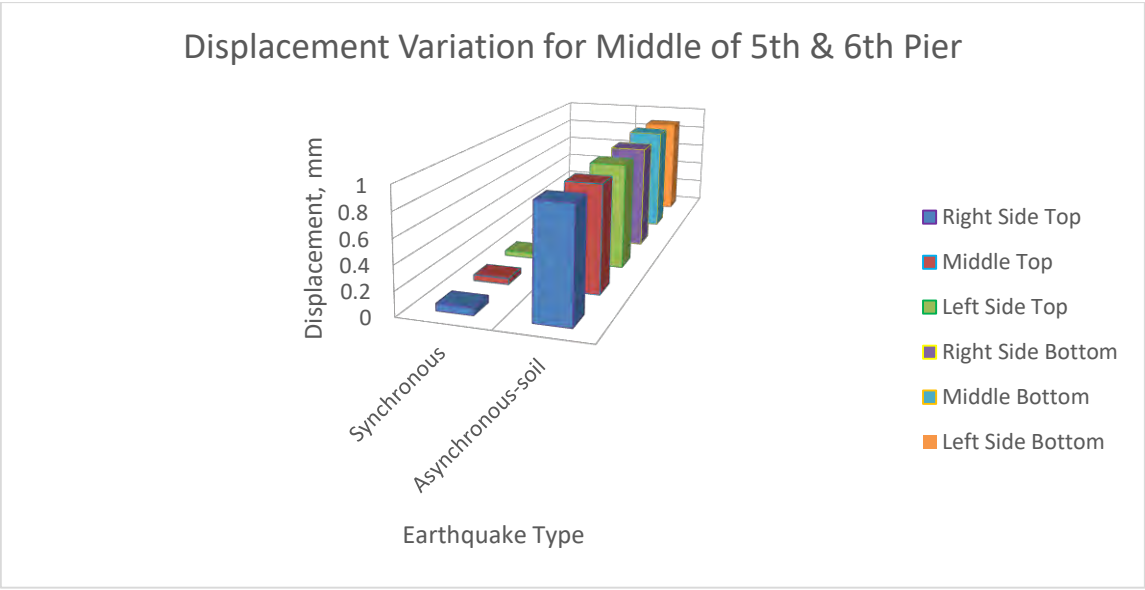


**Figure 4.43: Displacement Variation for middle of fifth & sixth pier along Z-axis**

From above graph between synchronous & asynchronous-soil, it can be said that at middle of 5<sup>th</sup> & 6<sup>th</sup> pier, asynchronous-soil govern at all six top & bottom points.

**4.3.4 Soil Effect for 125 m Model along X-axis (along length of the bridge):**

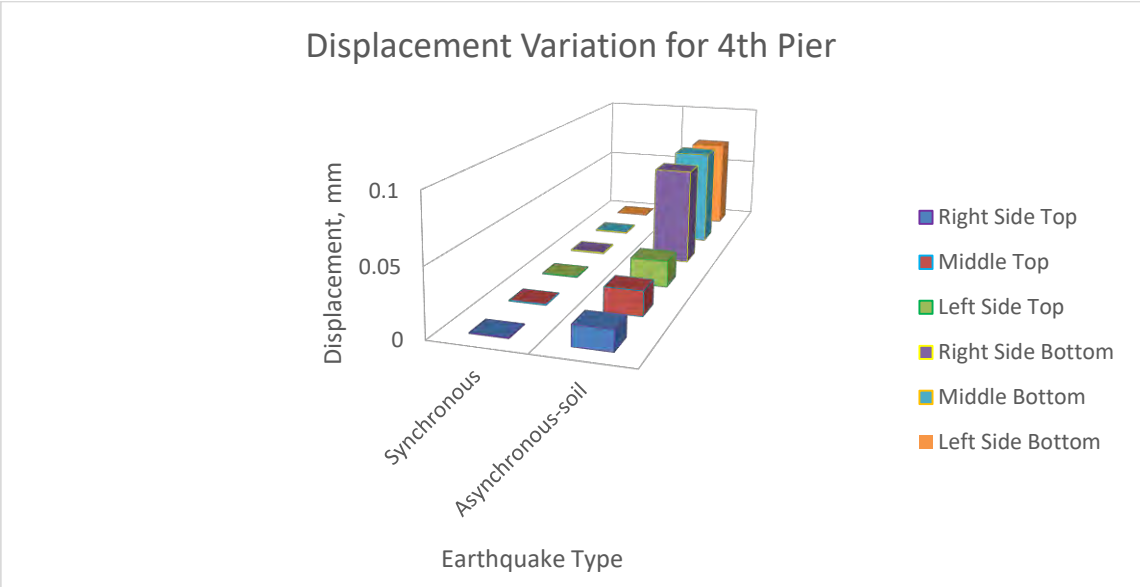


**Figure 4.44: Displacement Variation for Fourth Pier along X-axis**

From above graph between synchronous & asynchronous-soil, it can be said that at 4<sup>th</sup> pier, asynchronous-soil govern at three bottom points.

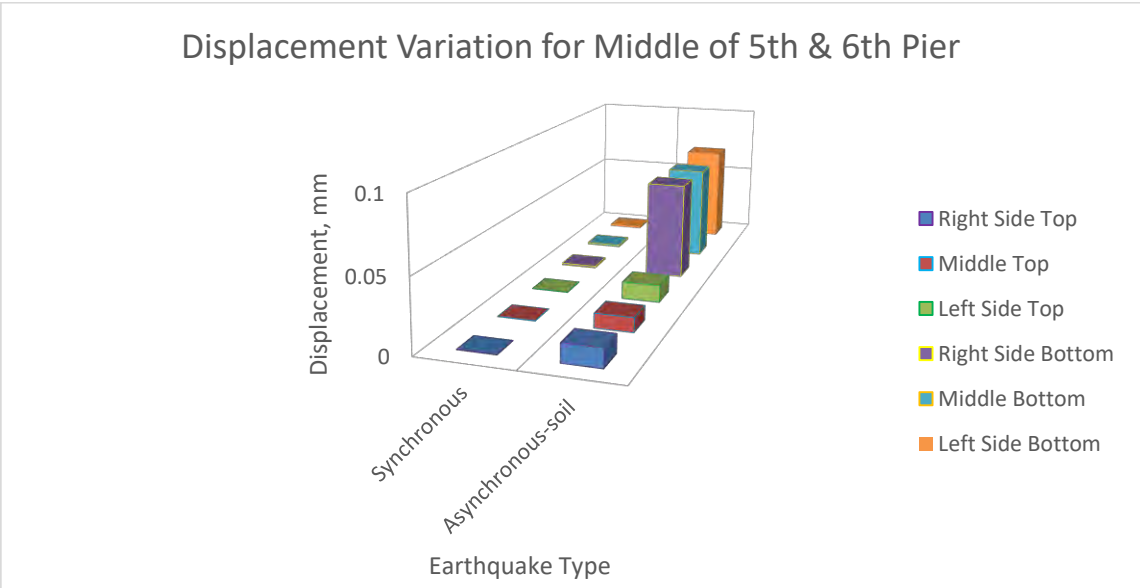


**Figure 4.45: Displacement Variation for middle of fifth & sixth pier along X-axis**

From above graph between synchronous & asynchronous-soil, it can be said that at middle of 5<sup>th</sup> & 6<sup>th</sup> pier, asynchronous-soil govern at three bottom points.

#### 4.3.5 Soil Effect for 125 m Model along Y-axis (along Width of the Bridge):

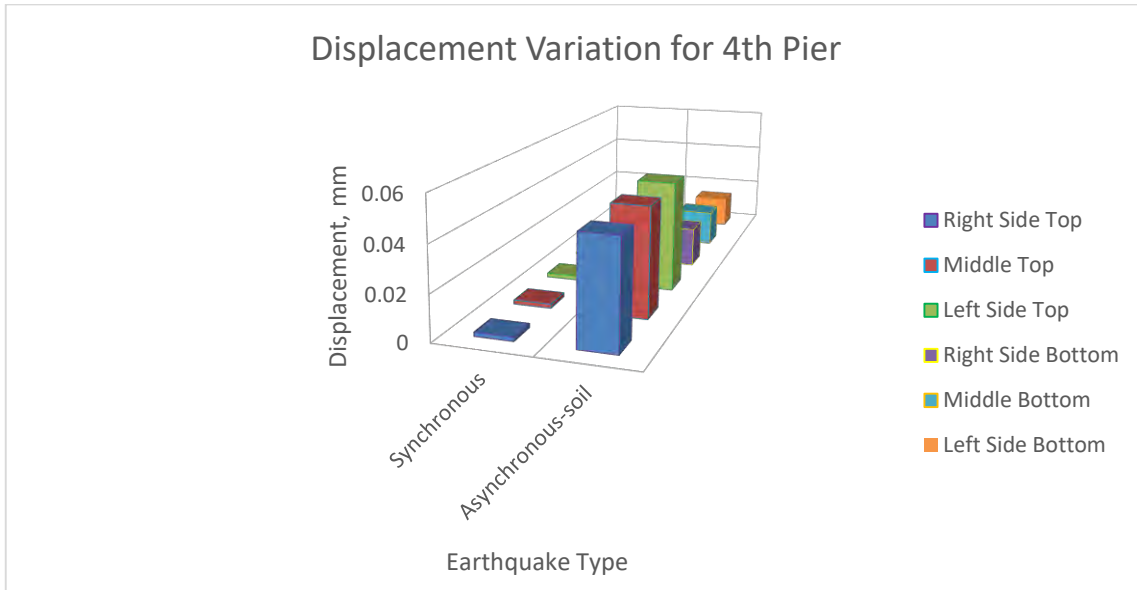


**Figure 4.46: Displacement Variation for Fourth Pier along Y-axis**

From above graph between synchronous & asynchronous-soil, it can be said that at 4<sup>th</sup> pier, asynchronous-soil govern at three top points.

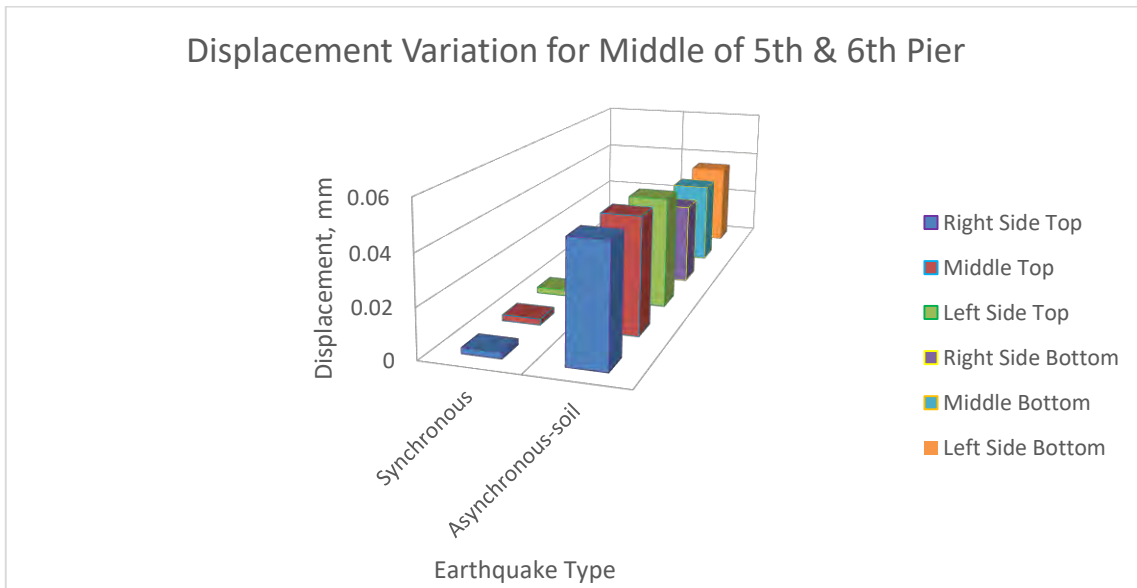


**Figure 4.47: Displacement Variation for middle of fifth & sixth pier along Y-axis**

From above graph between synchronous & asynchronous-soil, it can be said that at middle of 5<sup>th</sup> & 6<sup>th</sup> pier, asynchronous-soil govern at all six top & bottom points.

**4.3.6 Soil Effect for 125 m Model along Z-axis (along Vertical Direction of the Bridge):**

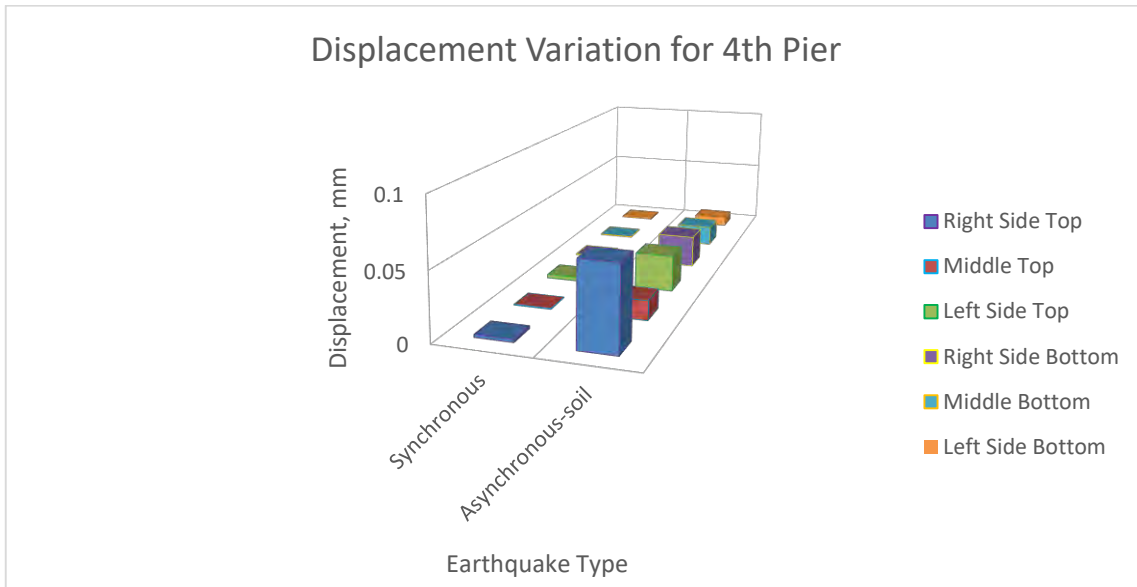


**Figure 4.48: Displacement Variation for Fourth Pier along Z-axis**

From above graph between synchronous & asynchronous-soil, it can be said that at 4<sup>th</sup> pier, asynchronous-soil govern at right side top point.

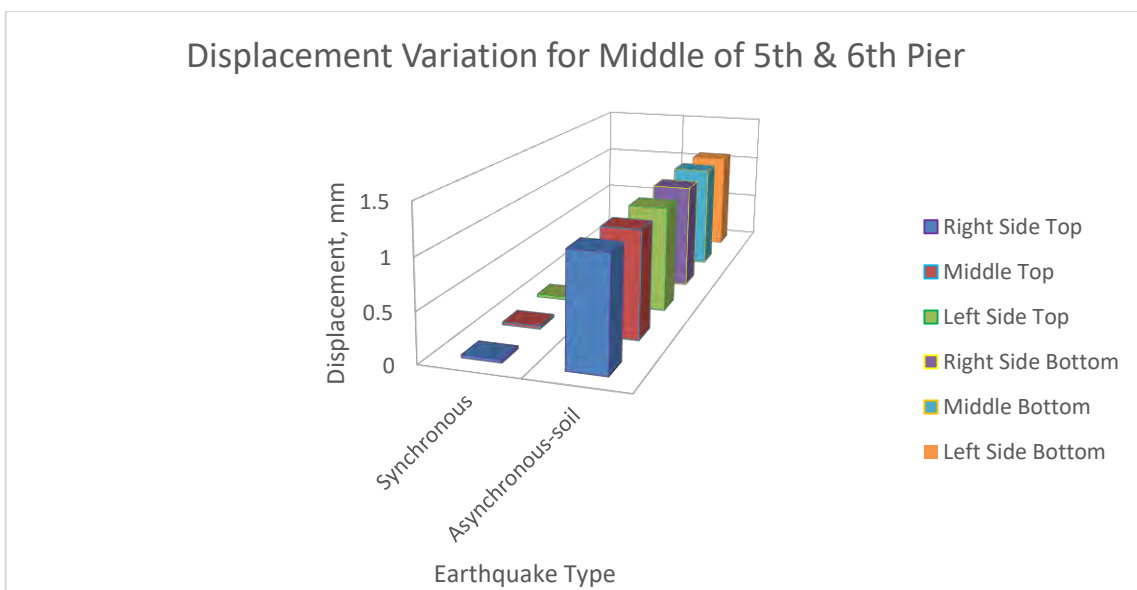


**Figure 4.49: Displacement Variation for middle of fifth & sixth pier along Z-axis**

From above graph between synchronous & asynchronous-soil, it can be said that at middle of 5<sup>th</sup> & 6<sup>th</sup> pier, asynchronous-soil govern at all six top & bottom points.

#### 4.4 COMPARISON BETWEEN RATIO OF SYNCHRONOUS AND ASYNCHRONOUS EARTHQUAKE

Seven points (Mid points of Slab along Span) are selected for this comparison from first model and second model. Displacement at these seven points for synchronous earthquake, asynchronous earthquake with 0.01 second time lag, asynchronous earthquake with 0.1 second time lag and asynchronous-soil at three direction (along length of the bridge, along width of the bridge and along vertical direction of the bridge) are found out from first model and second model. Then ratio of displacement between asynchronous earthquake (0.01 s time lag, 0.1 s time lag & soil effect) and synchronous earthquake are plotted and shown in below.

From Figure 4.50 it is shown that displacement ratio between Asynchronous 0.01s time lag & Synchronous at middle of fifth pier & sixth pier is more than ten times of other parts of 100m span bridge along length of the bridge.

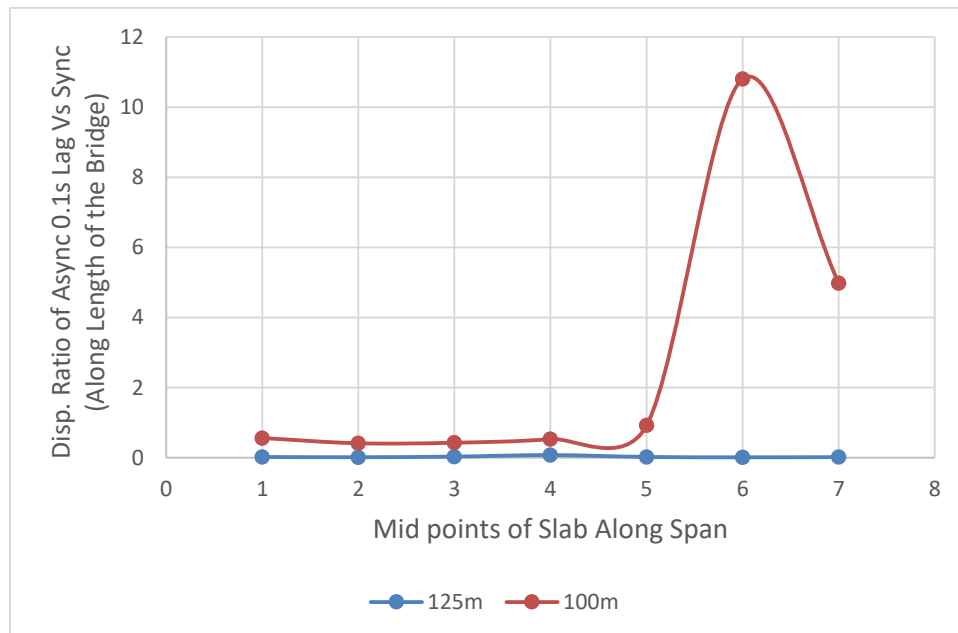


**Figure 4.50: Comparison of Displacement Ratio between Async 0.01s Lag & Sync along Length of the Bridge**

From Figure 4.51 it is shown that displacement ratio between Asynchronous 0.01s time lag & Synchronous at middle of second pier & third pier is more than three times of middle of third pier & fourth pier of 125m span bridge along width of the bridge. Besides, more effect along width of the bridge of Asynchronous 0.01s time lag motion arises with increment of span.

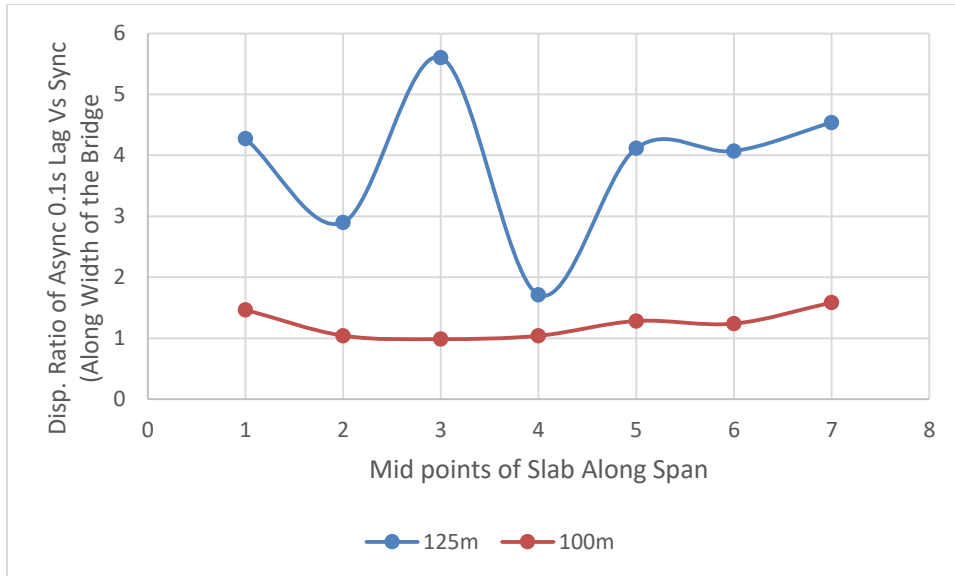


**Figure 4.51: Comparison of Displacement Ratio between Async 0.01s Lag & Sync along Width of the Bridge**

From Figure 4.52 it is shown that displacement ratio between Asynchronous 0.01s time lag & Synchronous at middle of second pier & third pier is more than three times of middle of third pier & fourth pier of 100m span bridge along vertical direction of the bridge. Besides, more effect along vertical direction of the bridge of Asynchronous 0.01s time lag motion has been found at 100m span bridge than 125m span bridge.

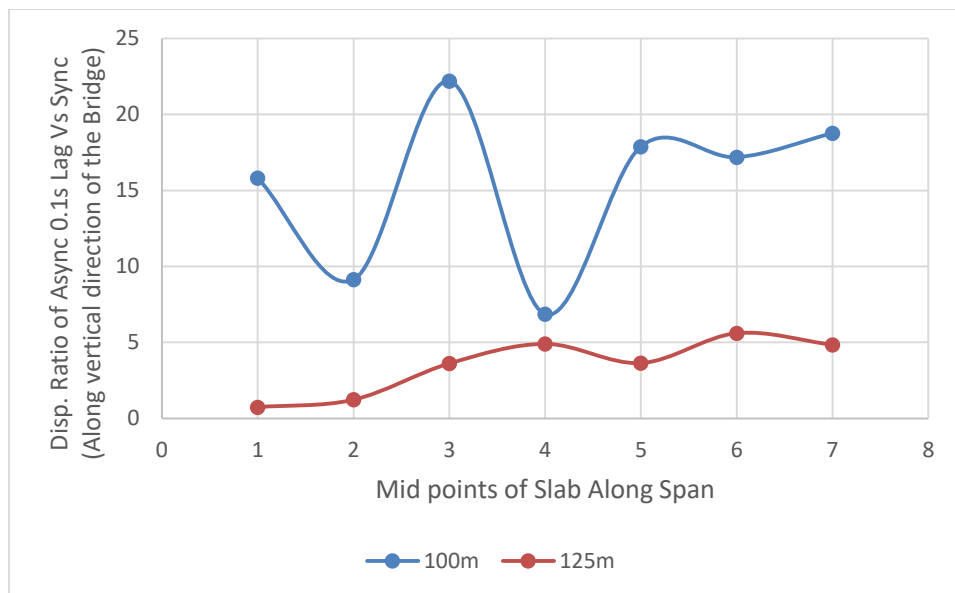


**Figure 4.52: Comparison of Displacement Ratio between Async 0.01s Lag & Sync along Vertical Direction of the Bridge**

From Figure 4.53 it is shown that displacement ratio between Asynchronous 0.1s time lag & Synchronous at middle of fifth pier & sixth pier is more than eight times of other parts of 100m span bridge along length of the bridge.

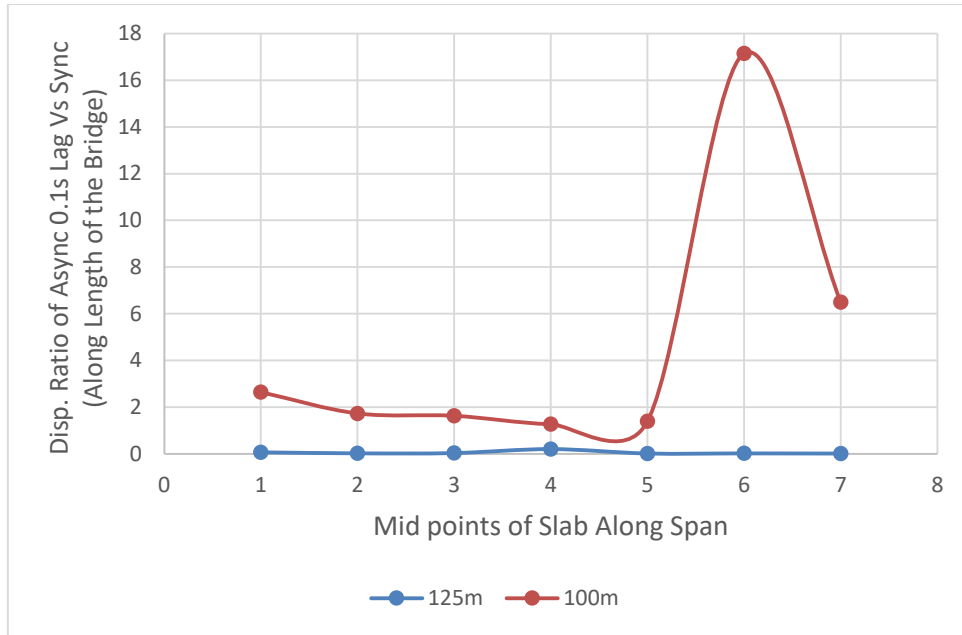


**Figure 4.53: Comparison of Displacement Ratio between Async 0.1s Lag & Sync along Length of the Bridge**

From Figure 4.54 it is shown that displacement ratio between Asynchronous 0.1s time lag & Synchronous at middle of first pier & second pier is more than three times of middle of third pier & fourth pier of 125m span bridge along width of the bridge. Besides, more effect along width of the bridge of Asynchronous 0.1s time lag motion arises with increment of span.

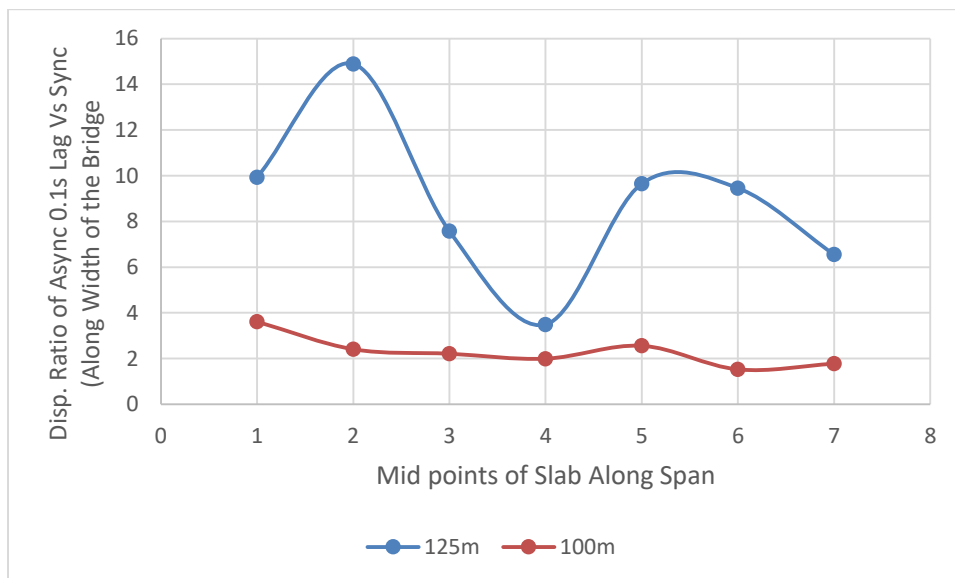


**Figure 4.54: Comparison of Displacement Ratio between Async 0.1s Lag & Sync along Width of the Bridge**

From Figure 4.55 it is shown that displacement ratio between Asynchronous 0.1s time lag & Synchronous at middle of first pier & second pier is more than three times of middle of

third pier & fourth pier of 125m span bridge along vertical direction of the bridge. Besides, more effect along vertical direction of the bridge of Asynchronous 0.1s time lag motion has been found at 125m span bridge than 100m span bridge.

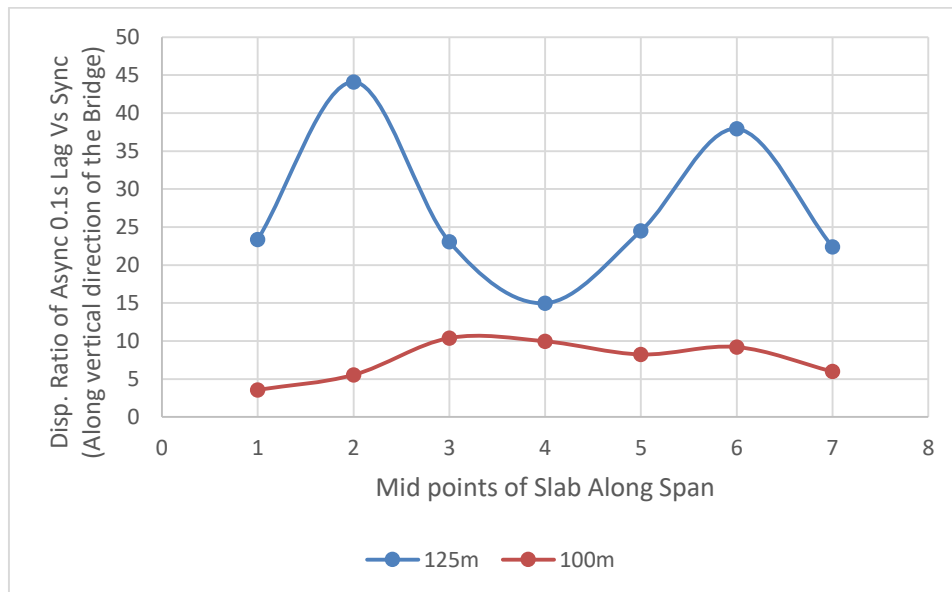


**Figure 4.55: Comparison of Displacement Ratio between Async 0.1s Lag & Sync along Vertical Direction of the Bridge**

From Figure 4.56 it is shown that displacement ratio between Asynchronous-soil & Synchronous at middle of fifth pier & sixth pier is more than seven times of other parts of 100m span bridge along length of the bridge.

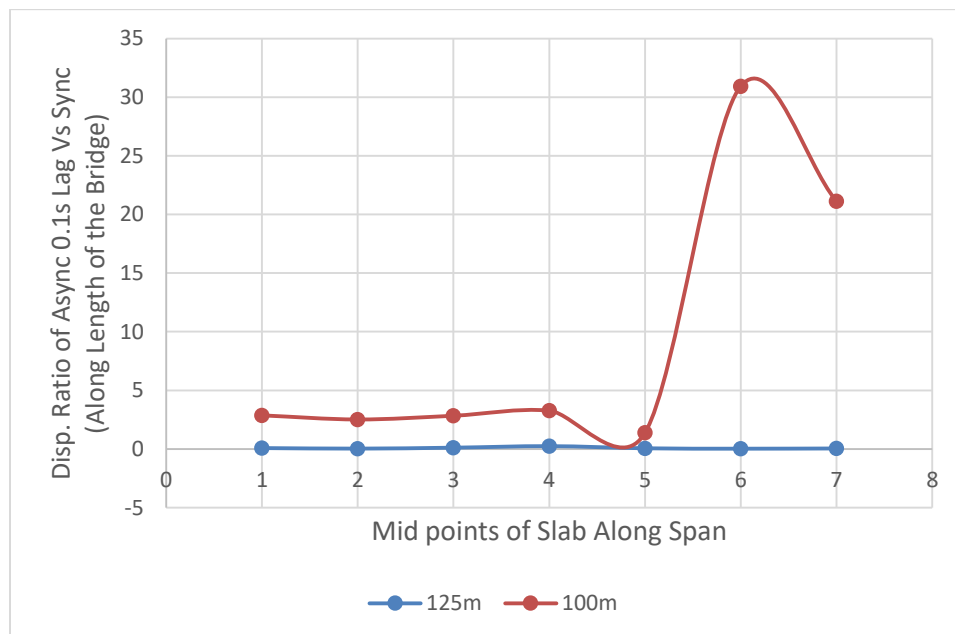


**Figure 4.56: Comparison of Displacement Ratio between Async-Soil & Sync along Length of the Bridge**



From Figure 4.57 it is shown that displacement ratio between Asynchronous-soil & Synchronous at middle of second pier & third pier is more than four times of middle of third pier & fourth pier of 125m span bridge along width of the bridge. Besides, more effect along width of the bridge of Asynchronous-soil arises with increment of span.

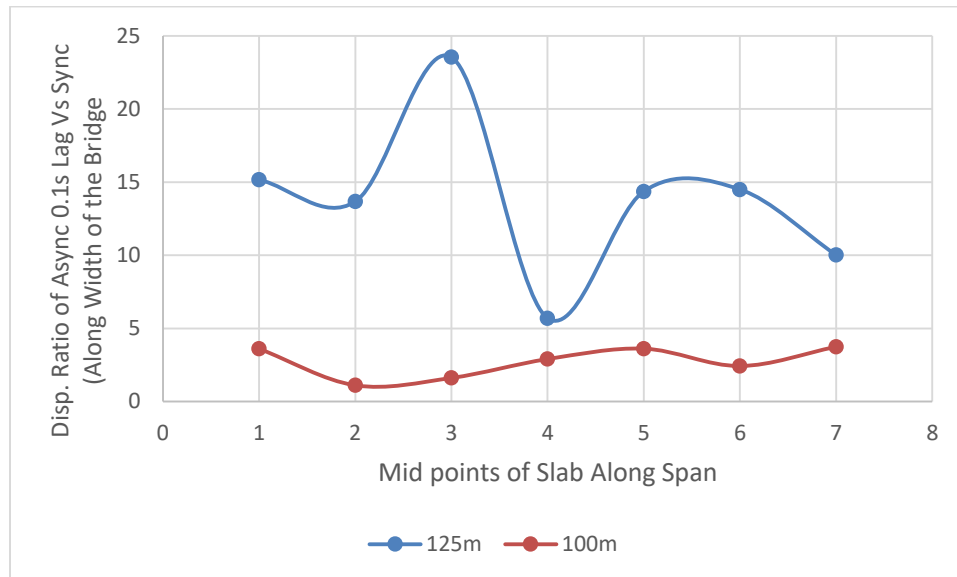


**Figure 4.57: Comparison of Displacement Ratio between Async-Soil & Sync along Width of the Bridge**

From Figure 4.58 it is shown that displacement ratio between Asynchronous-soil & Synchronous at middle of second pier & third pier is more than four times of middle of third pier & fourth pier of 100m span bridge along vertical direction of the bridge. Besides, more effect along vertical direction of the bridge of Asynchronous-soil has been found at 100m span bridge than 125m span bridge.

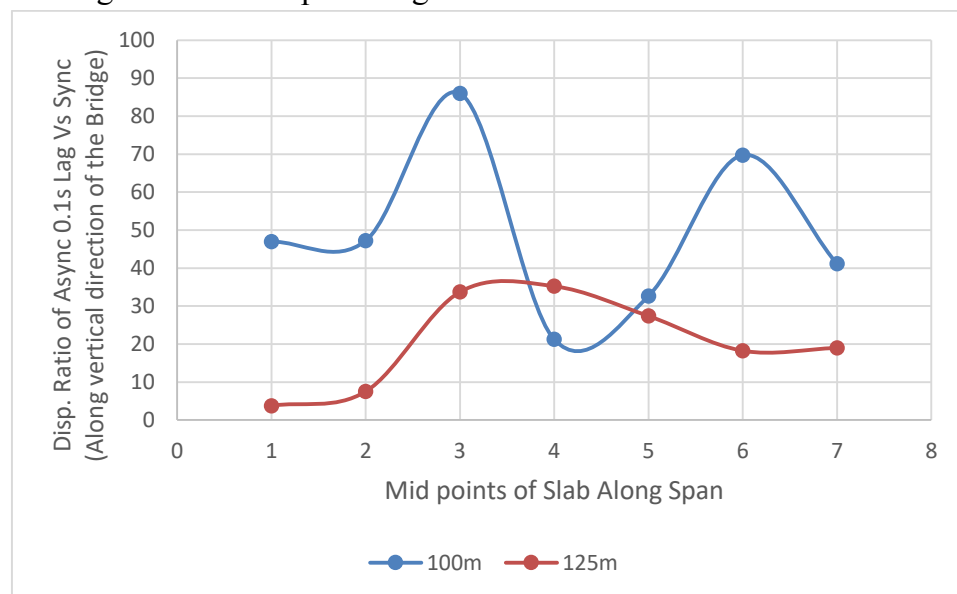


**Figure 4.58: Comparison of Displacement Ratio between Async-Soil & Sync along Vertical Direction of the Bridge**

#### 4.5 AXIAL FORCE, SHEAR FORCE & MOMENT ANALYSIS

This article includes analysis on axial force diagram, shear force diagram along major & minor axis, moment diagram along major & minor axis and torsional moment diagram for two bridges (100 m span and 125 m span).

**Figure 4.59** to **Figure 4.64** show variation of axial force, shear force along major & minor axis, moment along major & minor axis and torsional moment for first bridge and **Figure 4.65** to **Figure 4.70** show variation of axial force, shear force along major & minor axis, moment along major & minor axis and torsional moment for second bridge.

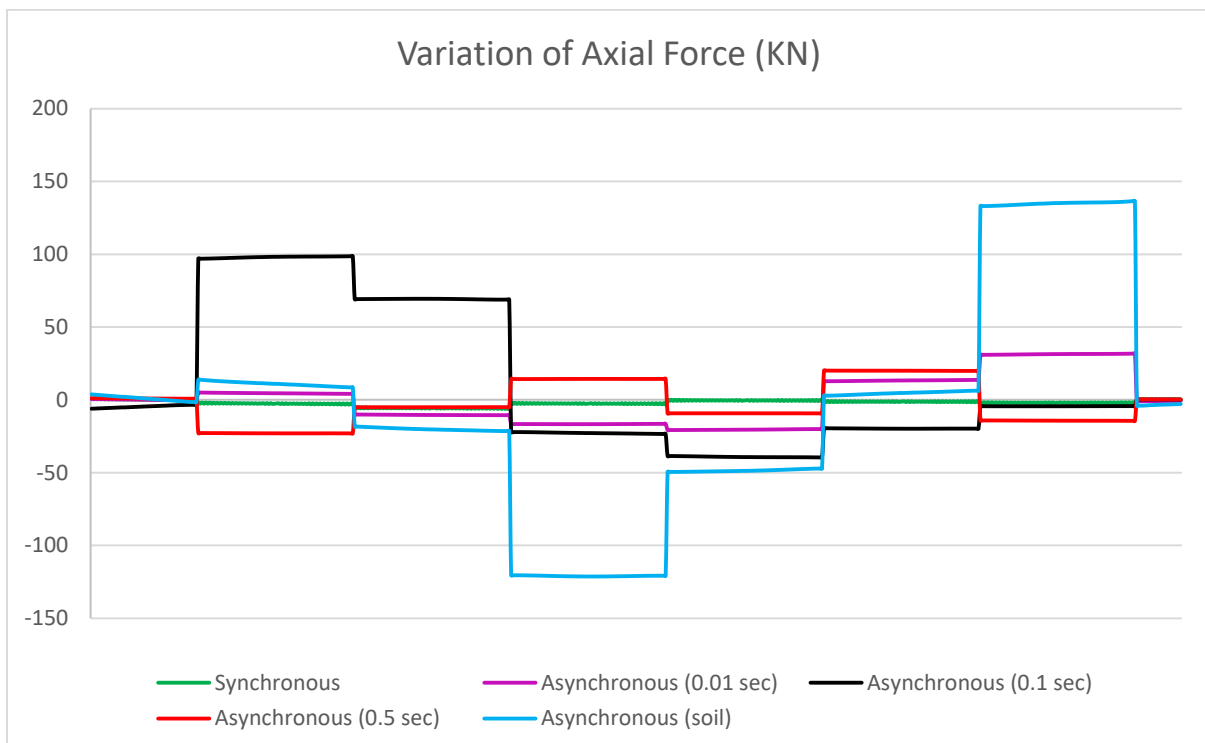


**Figure 4.59: Variation of Axial Force (100 m Span Bridge)**

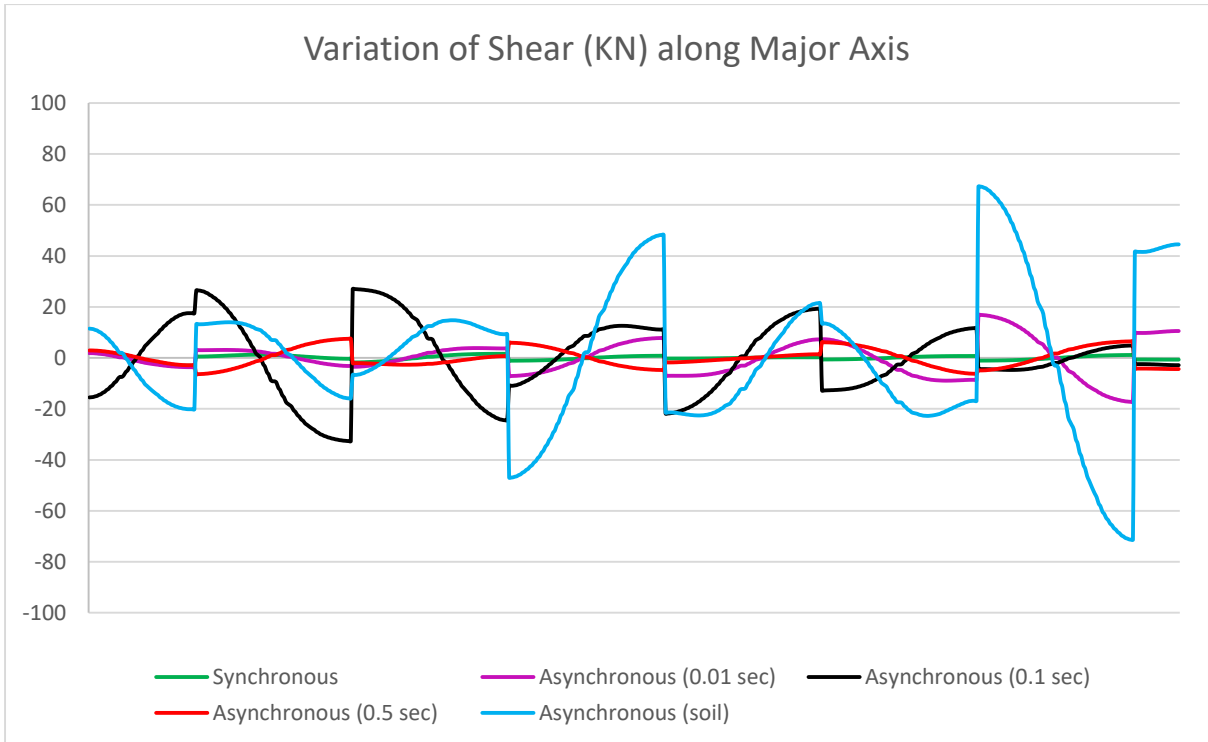


**Figure 4.60: Variation of Shear Force along Major Axis (100 m Span Bridge)**

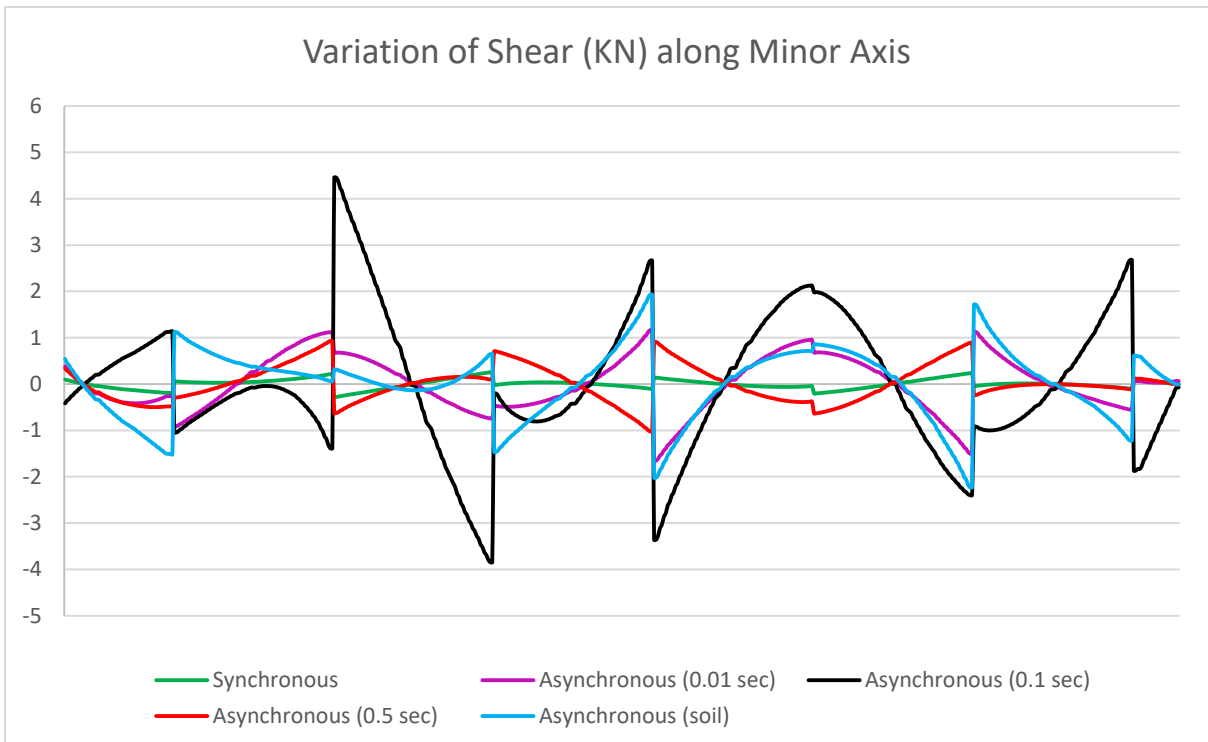


**Figure 4.61: Variation of Shear Force along Minor Axis (100 m Span Bridge)**

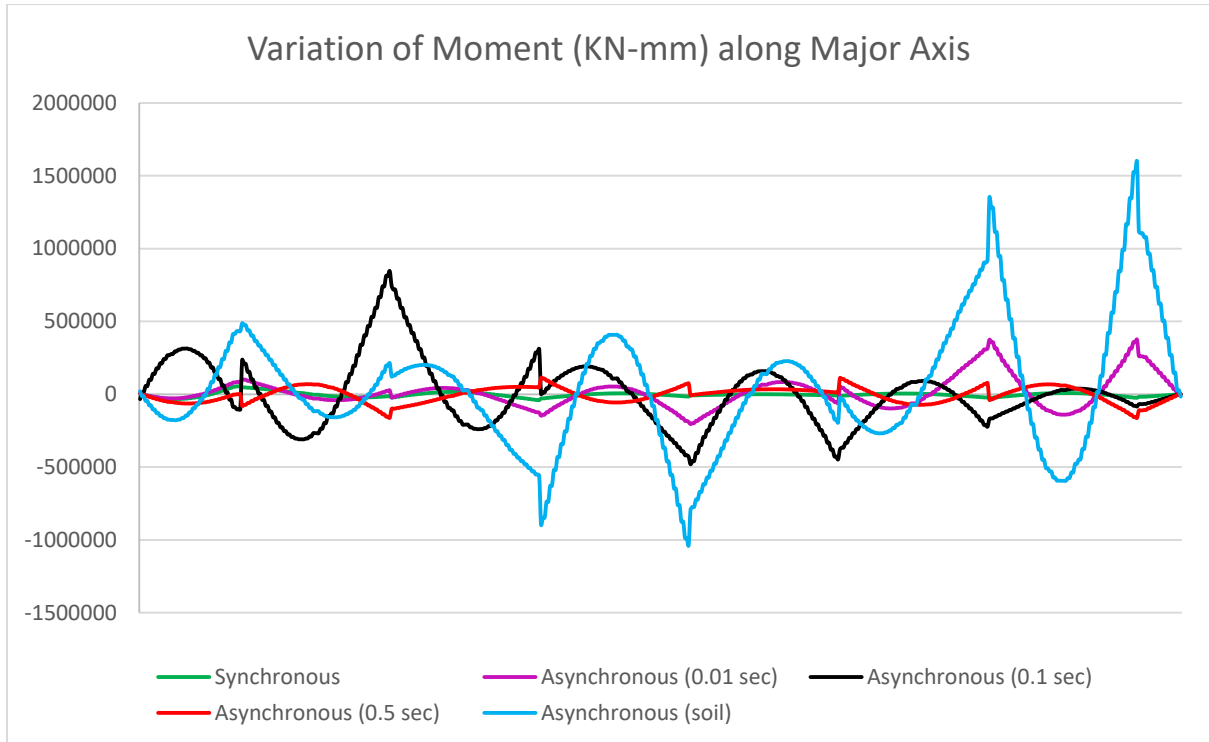


**Figure 4.62: Variation of Moment along Major Axis (100 m Span Bridge)**

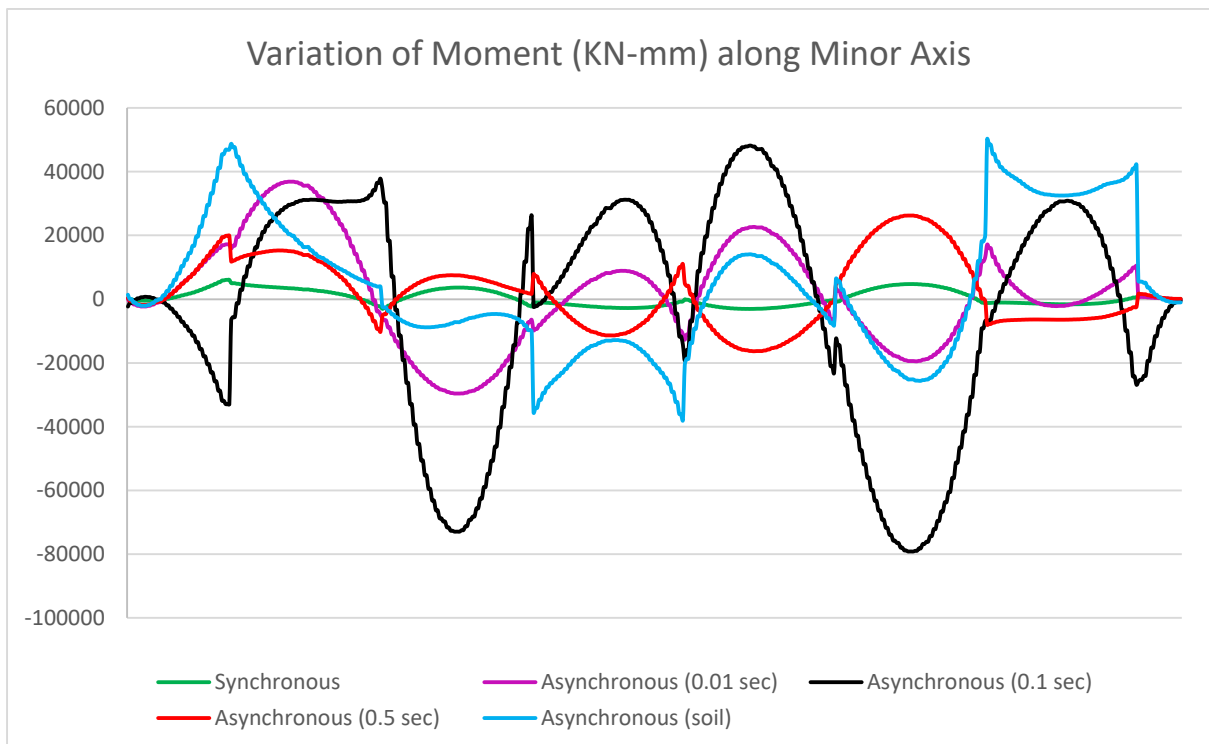


**Figure 4.63: Variation of Moment along Minor Axis (100 m Span Bridge)**

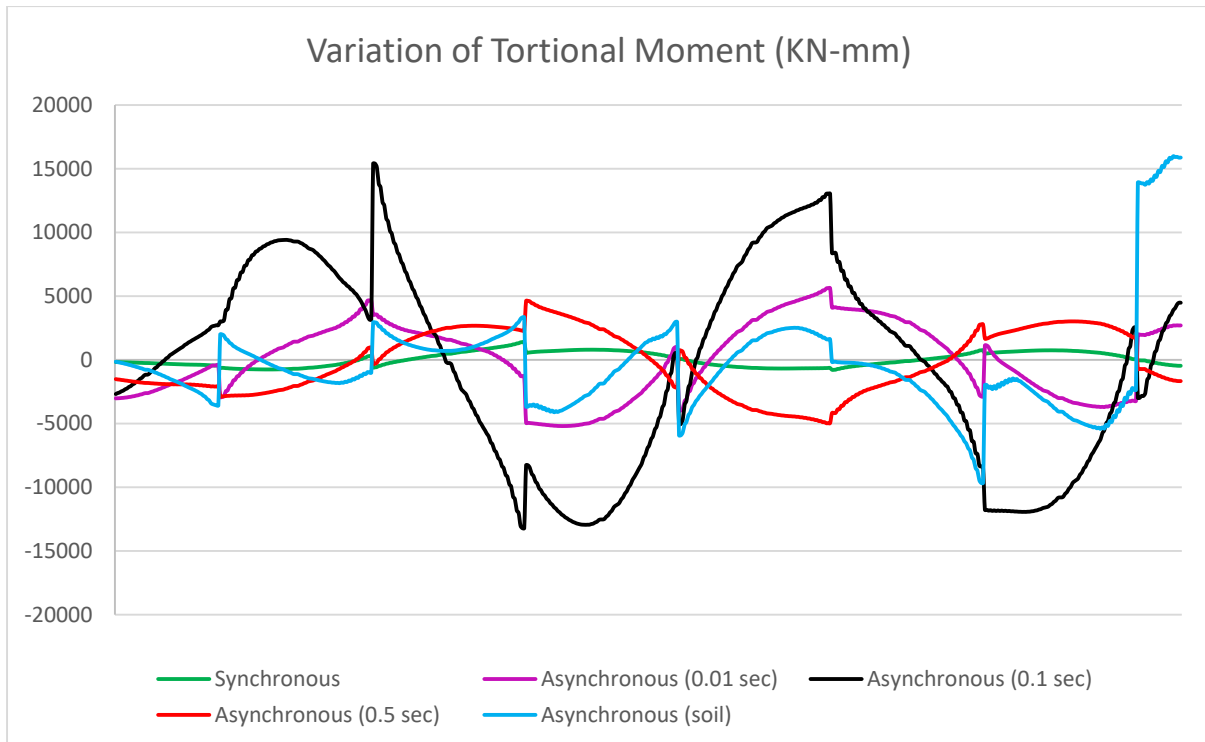


**Figure 4.64: Variation of Torsional Moment (100 m Span Bridge)**

From above axial force, shear force & moment diagram we have found that for 100 m span bridge peak value of axial force, shear force & moment have been found for Asynchronous motion of 0.1 second time lag, somewhere Asynchronous-soil governs.

From below axial force, shear force & moment diagram we have found that for 125 m span bridge peak value of axial force, shear force & moment have been found for Asynchronous motion due to soil effect, somewhere Asynchronous motion of 0.1 second time lag governs.

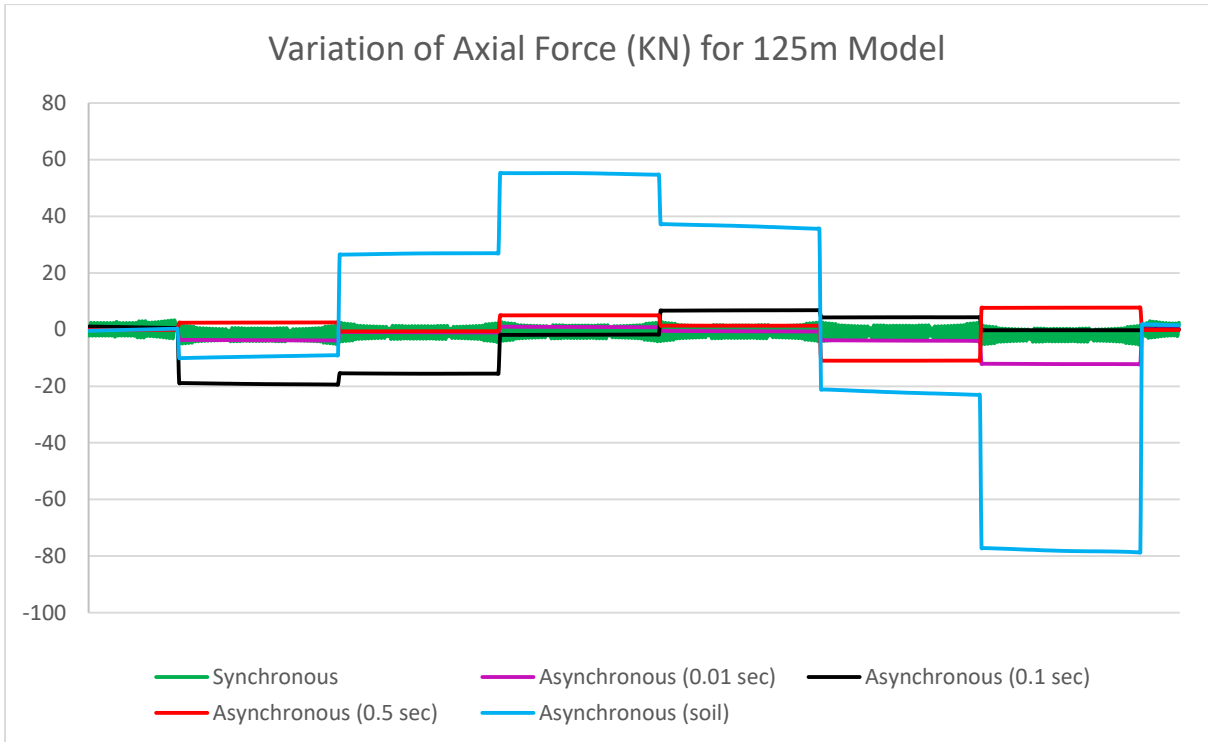


**Figure 4.65: Variation of Axial Force (125 m Span Bridge)**

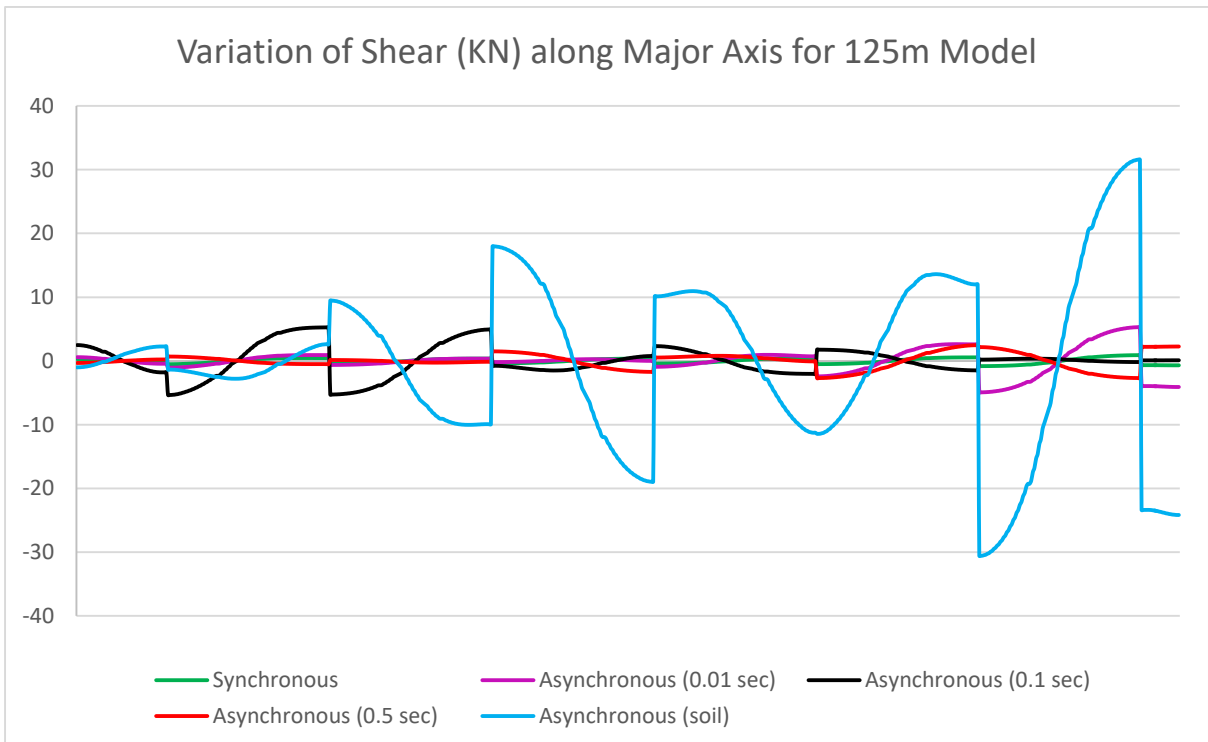


**Figure 4.66: Variation of Shear Force along Major Axis (125 m Span Bridge)**

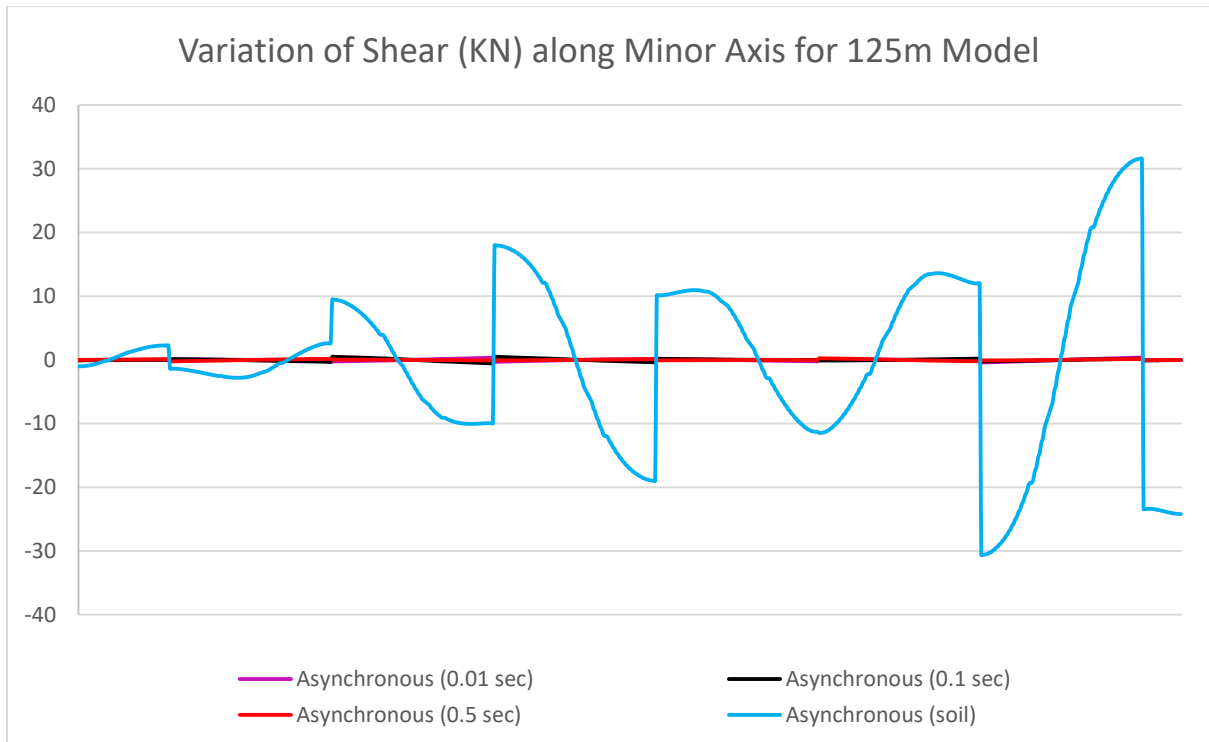


**Figure 4.67: Variation of Shear Force along Minor Axis (125 m Span Bridge)**

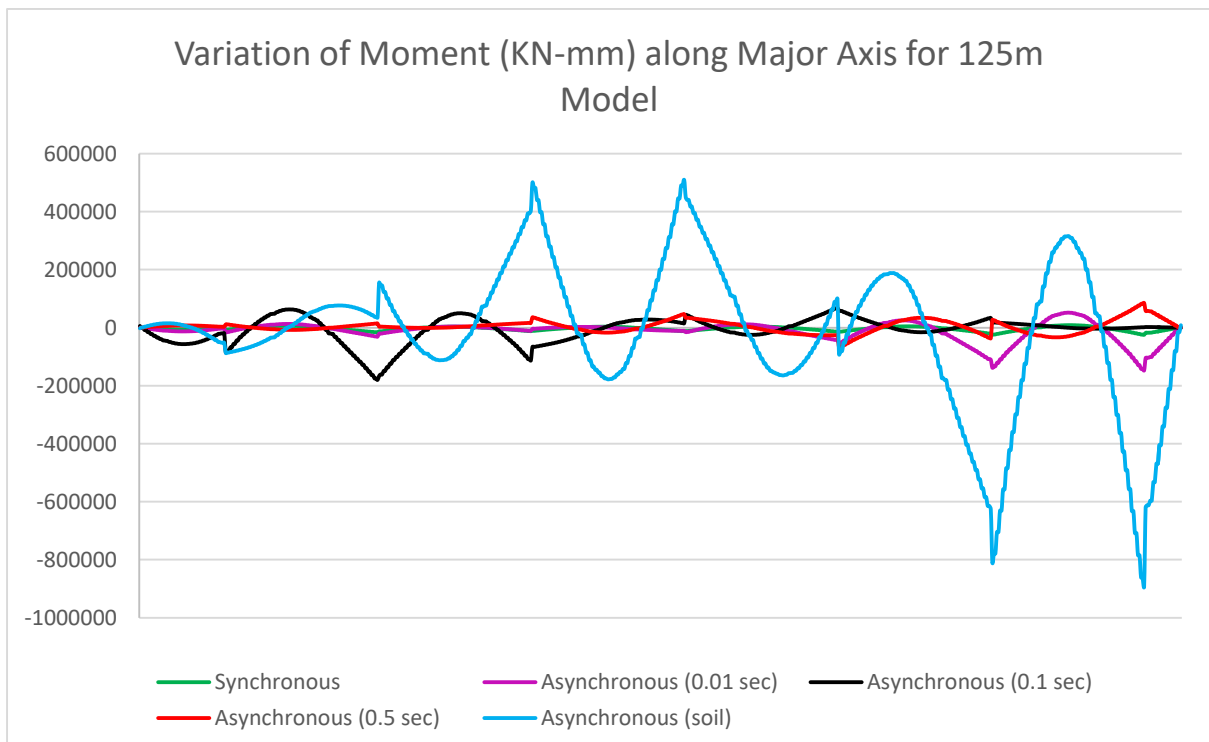


**Figure 4.68: Variation of Moment along Major Axis (125 m Span Bridge)**

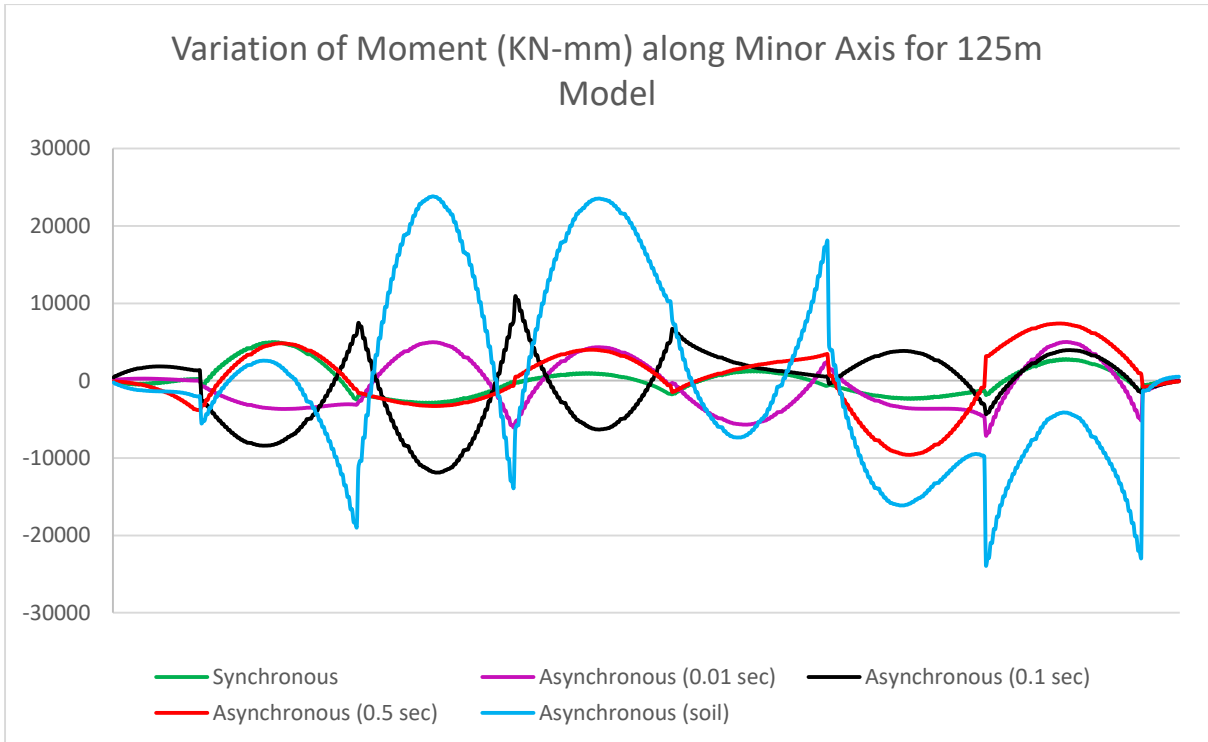


**Figure 4.69: Variation of Moment along Minor Axis (125 m Span Bridge)**

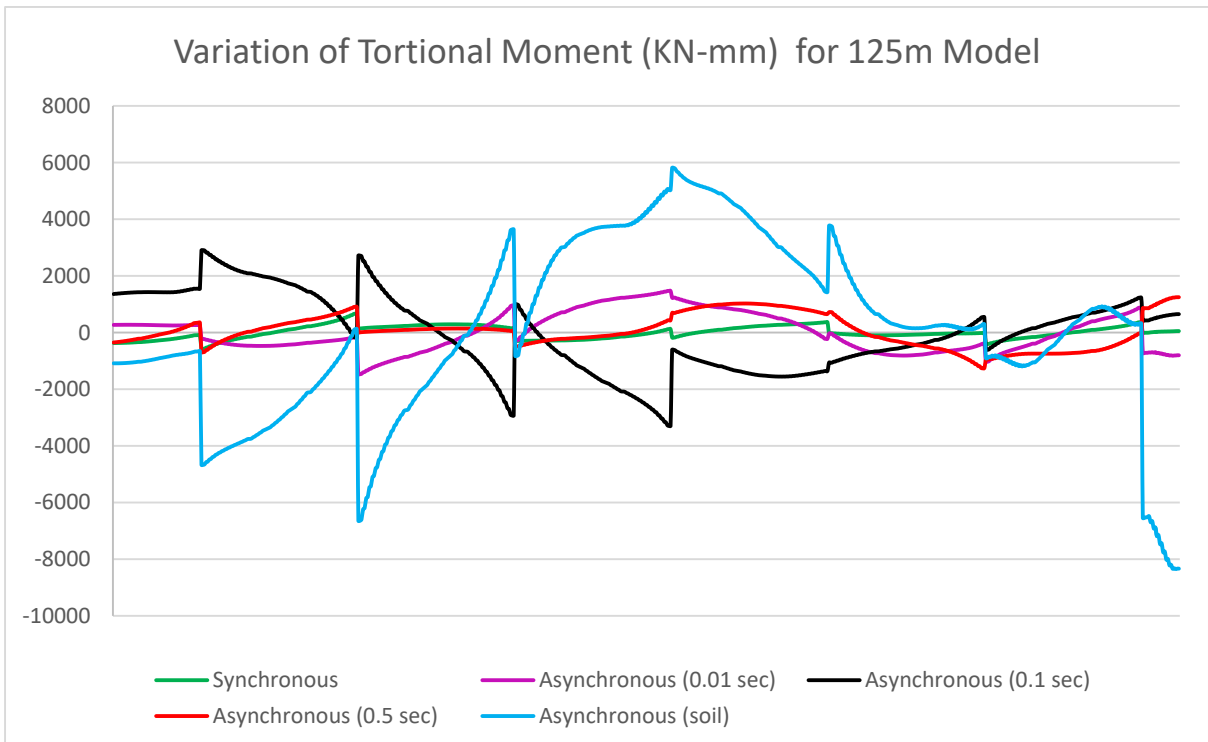


**Figure 4.70: Variation of Torsional Moment (125 m Span Bridge)**



## 4.6 MODAL ANALYSIS

The modal analysis involves determination of natural frequencies and vibration modes of the structure. Modal analysis results for first bridge are presented in Table 4.1 and for second bridge are presented in Table 4.2.

**Table 4.1: Modal Period and Frequency of First Bridge**

Mode	Period (sec)	Frequency (Hz)
1	0.93122	1.07386
2	0.89279	1.12009
3	0.85471	1.16999
4	0.76034	1.31520
5	0.72491	1.37947
6	0.68634	1.45700
7	0.67090	1.49054
8	0.62895	1.58996
9	0.59230	1.68834
10	0.56533	1.76888
11	0.53644	1.86413
12	0.50308	1.98776

**Table 4.2: Modal Period and Frequency of Second Bridge**

Mode	Period (sec)	Frequency (Hz)
1	1.35800	0.73638
2	1.24004	0.80643
3	1.09754	0.91113
4	0.96432	1.03701
5	0.90385	1.10637
6	0.85708	1.16675

7	0.83100	1.20337
8	0.78869	1.26792
9	0.77042	1.29800
10	0.74395	1.34418
11	0.69551	1.43779
12	0.65142	1.53510

The frequency increases with higher modes. If we allow this bridge to vibrate with every modal frequency with their same vibration direction, then the bridge will vibrate with these frequencies in this direction forever. Figure 4.71 to Figure 4.82 show the first twelve mode shapes for first bridge and Figure 4.83 to Figure 4.94 for second bridge.



**Figure 4.71: 3D View of Mode Shape 1 for First Model (T=0.93)**

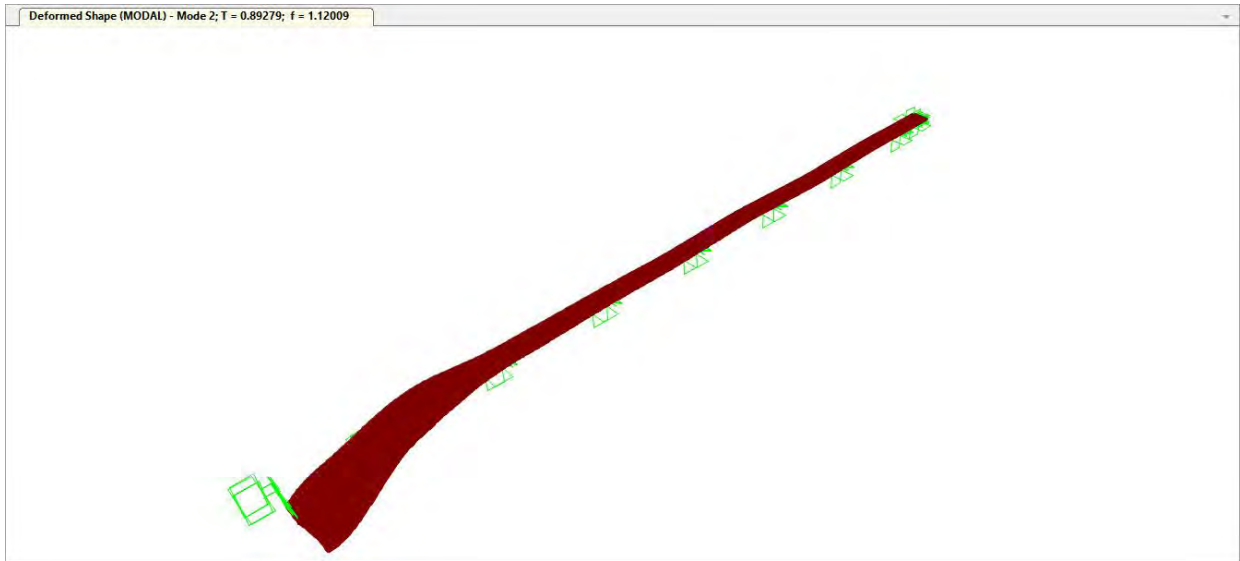


**Figure 4.72: 3D View of Mode Shape 2 for First Model (T=0.89)**

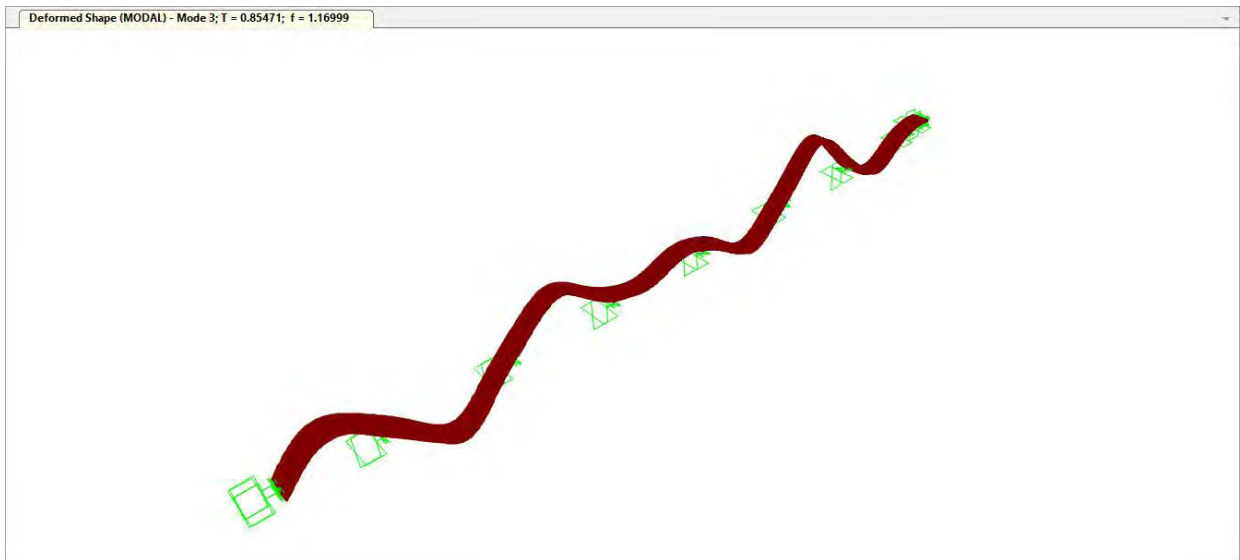


**Figure 4.73: 3D View of Mode Shape 3 for First Model (T=0.85)**



**Figure 4.74: 3D View of Mode Shape 4 for First Model (T=0.76)**

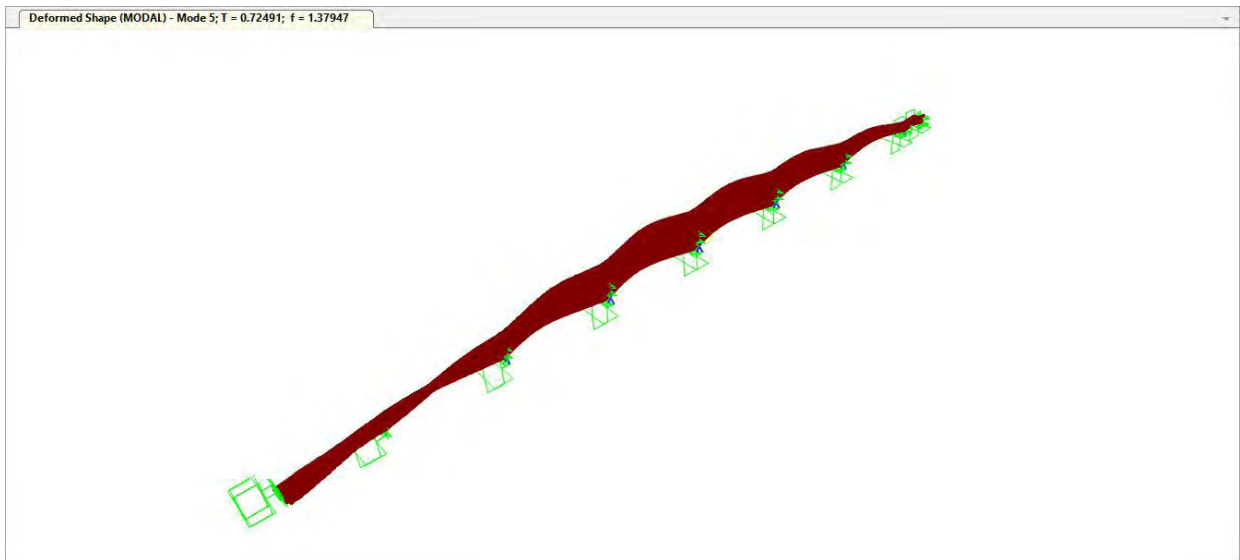


**Figure 4.75: 3D View of Mode Shape 5 for First Model (T=0.72)**

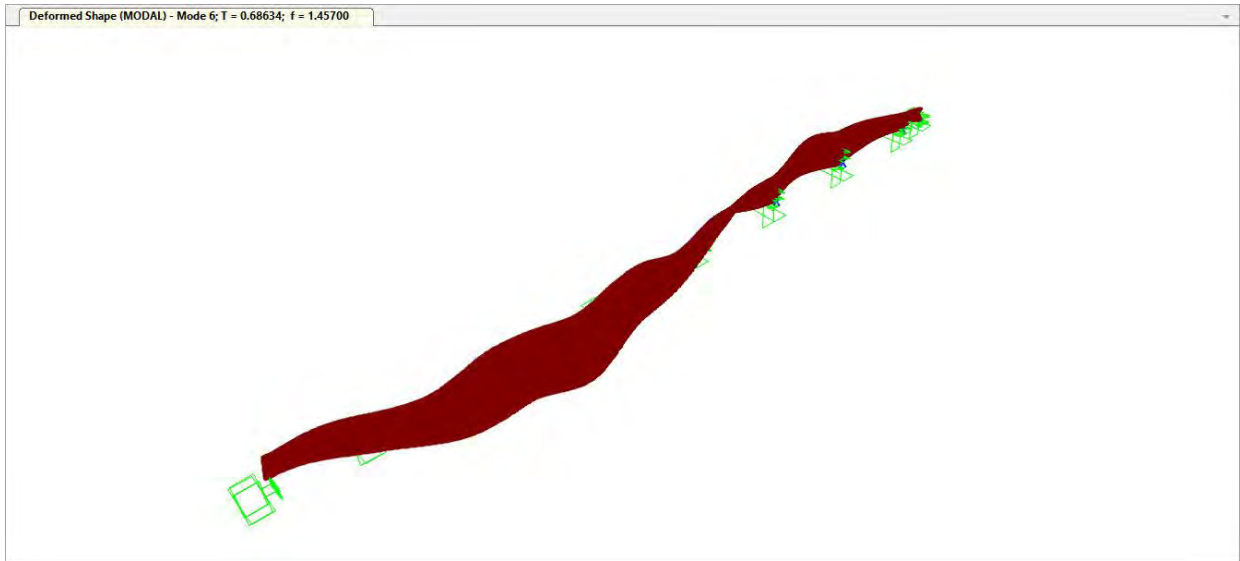


**Figure 4.76: 3D View of Mode Shape 6 for First Model (T=0.69)**

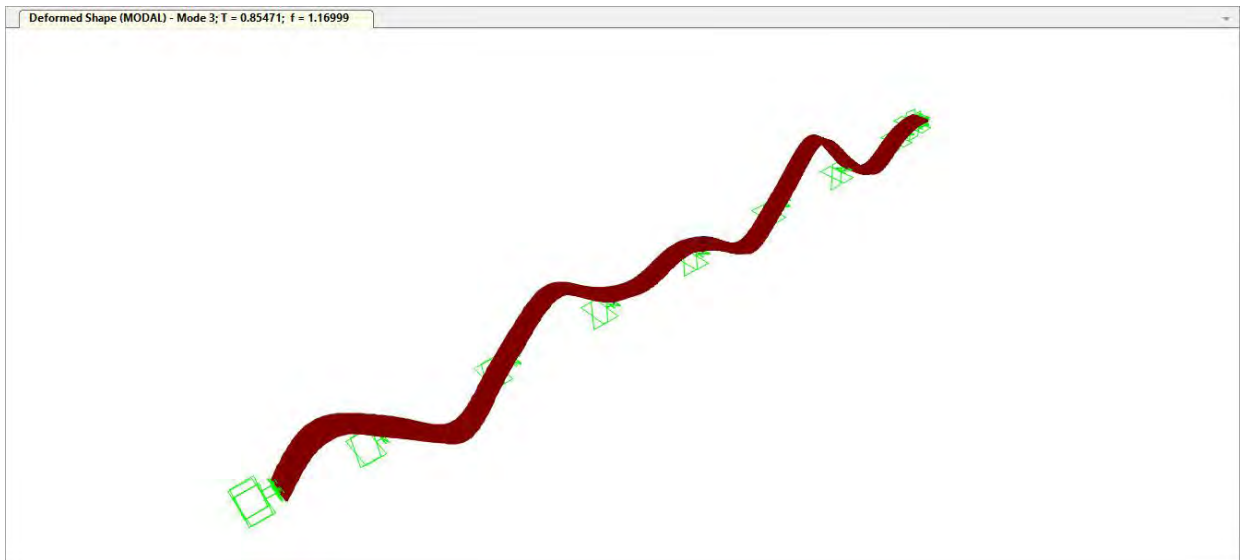


**Figure 4.77: 3D View of Mode Shape 7 for First Model (T=0.67)**

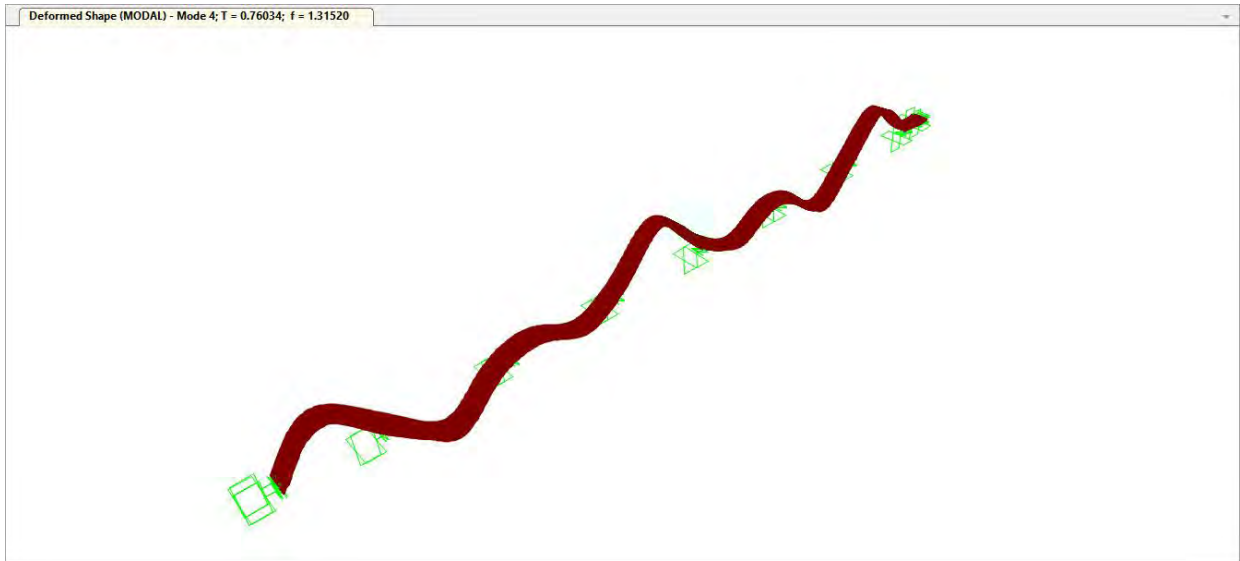


**Figure 4.78: 3D View of Mode Shape 8 for First Model (T=0.63)**

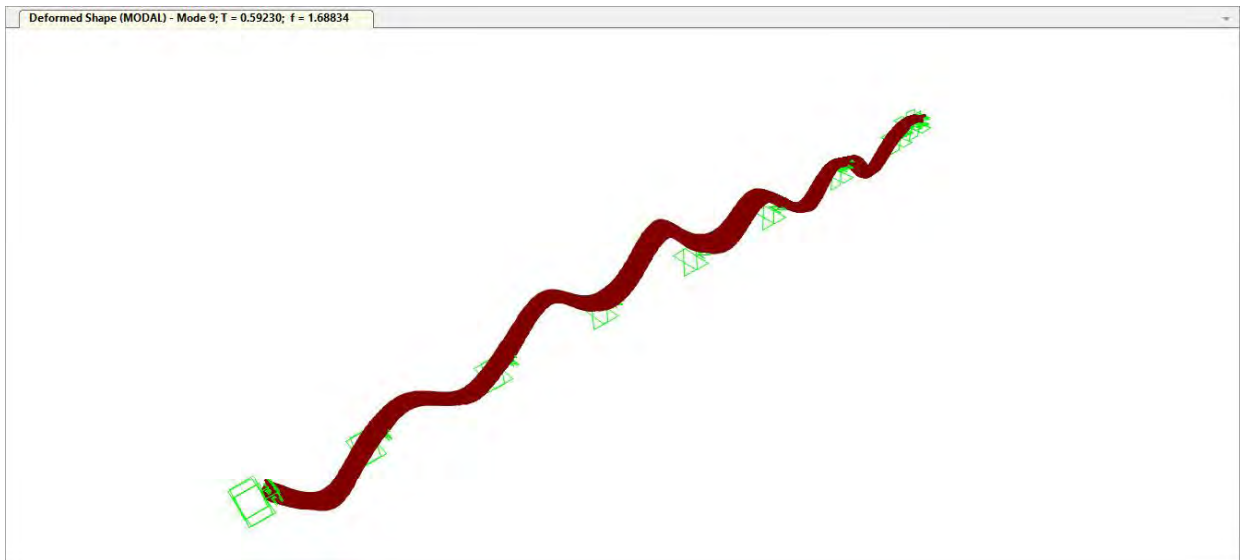


**Figure 4.79: 3D View of Mode Shape 9 for First Model (T=0.59)**

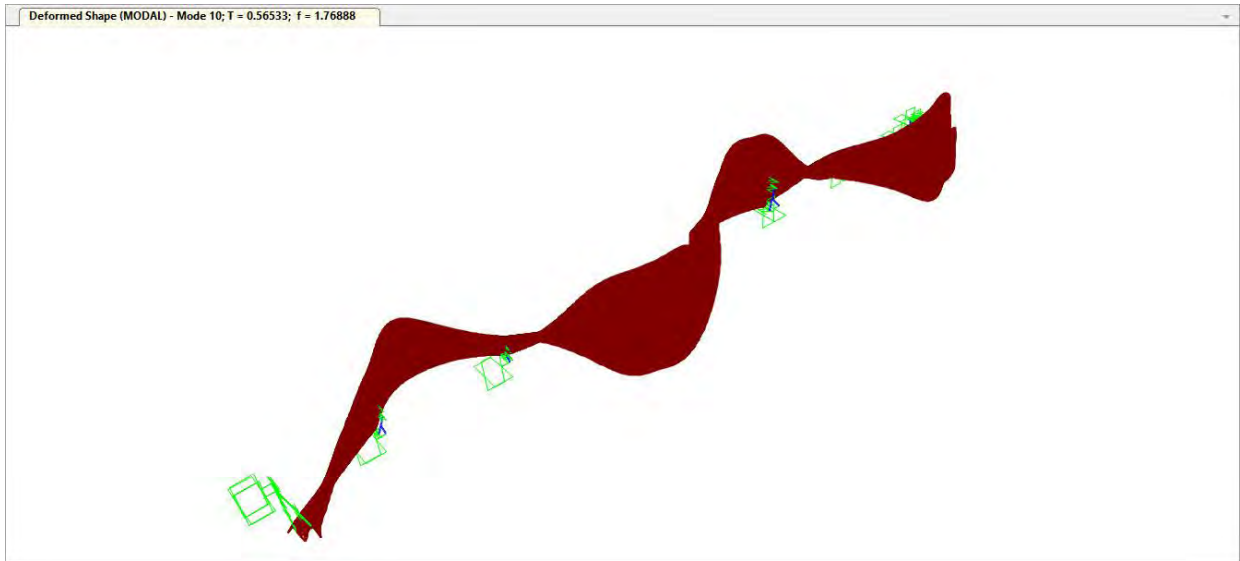


**Figure 4.80: 3D View of Mode Shape 10 for First Model (T=0.57)**

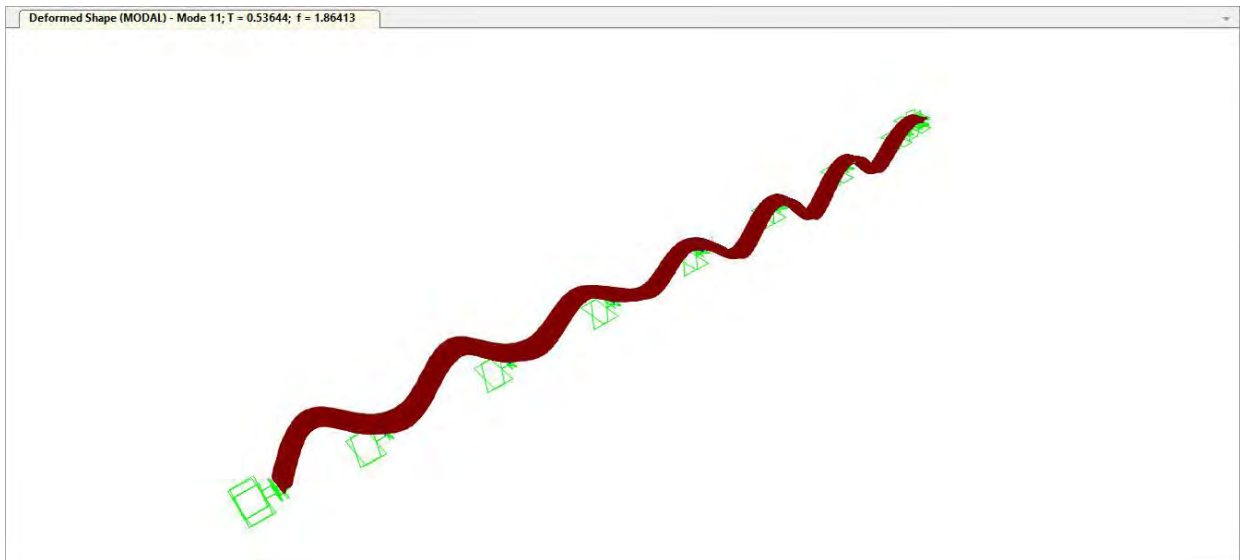


**Figure 4.81: 3D View of Mode Shape 11 for First Model (T=0.54)**

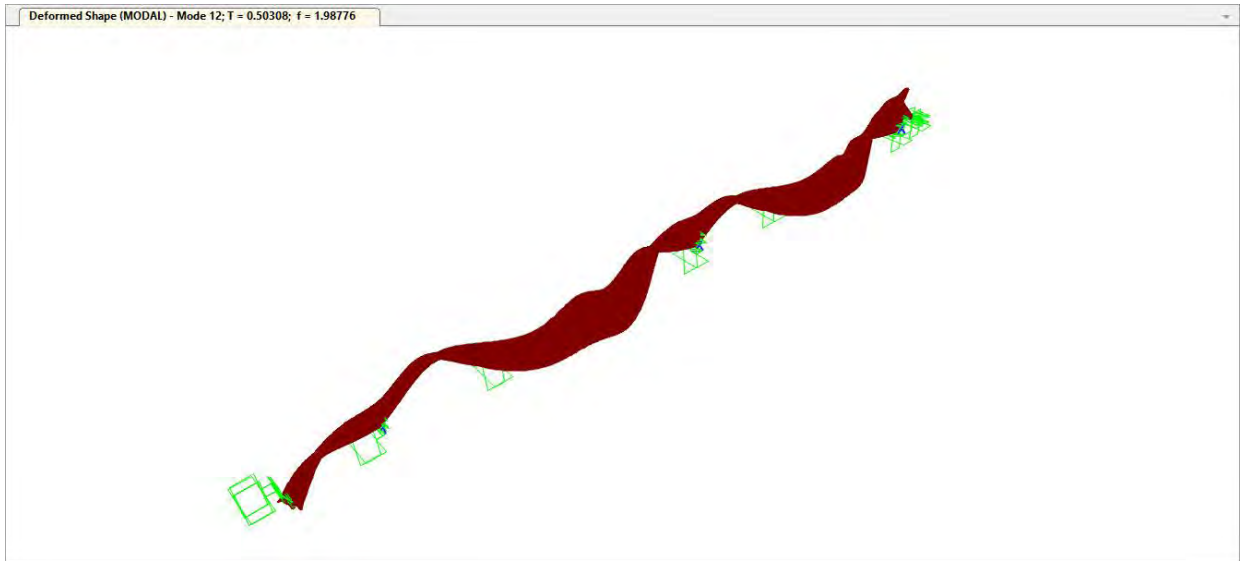


**Figure 4.82: 3D View of Mode Shape 12 for First Model (T=0.50)**



**Figure 4.83: 3D View of Mode Shape 1 for Second Model (T=1.36)**



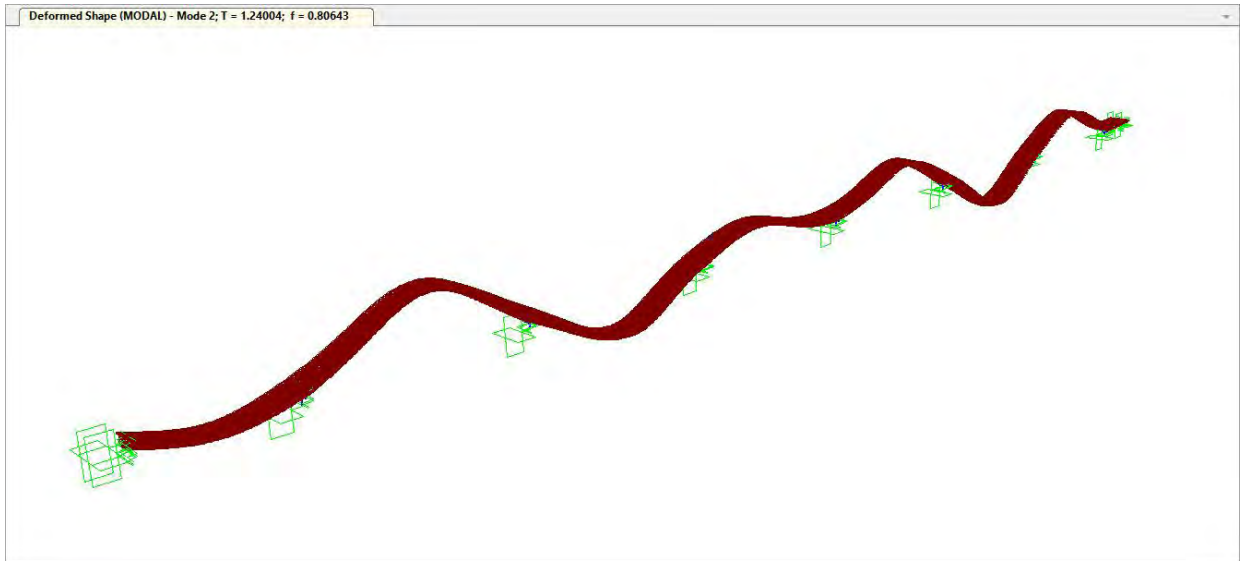


**Figure 4.84: 3D View of Mode Shape 2 for Second Model (T=1.24)**

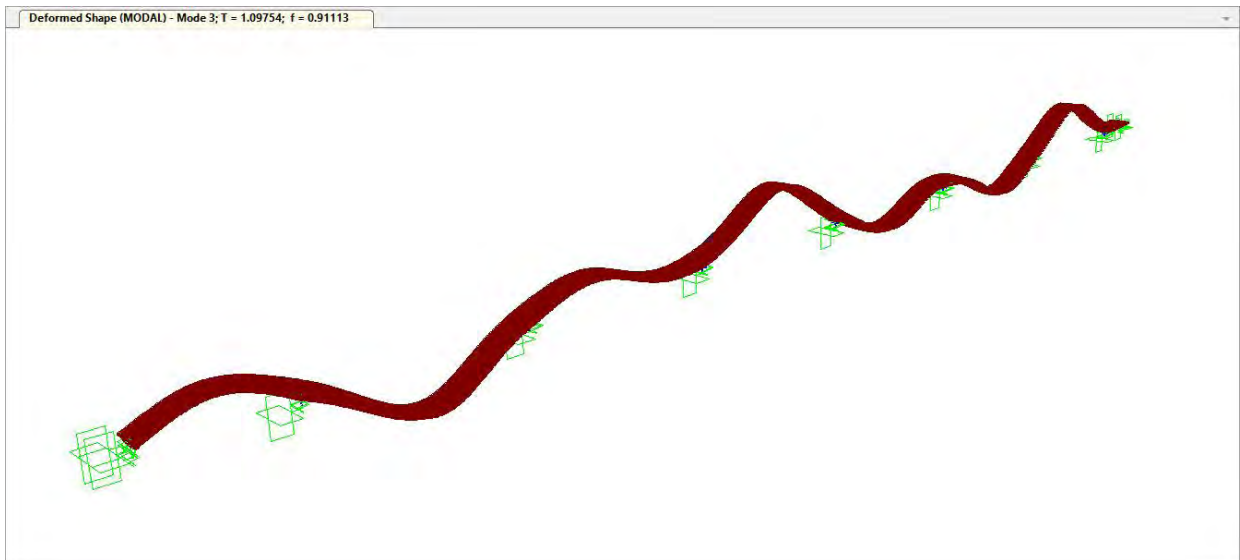


**Figure 4.85: 3D View of Mode Shape 3 for Second Model (T=1.10)**

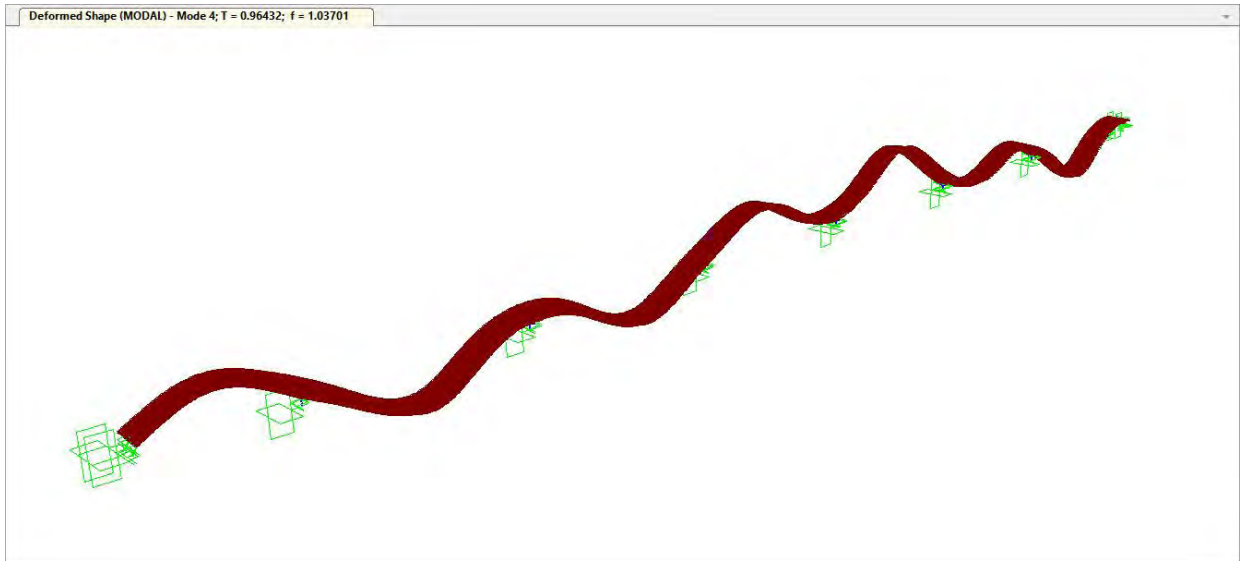


**Figure 4.86: 3D View of Mode Shape 4 for Second Model (T=0.96)**

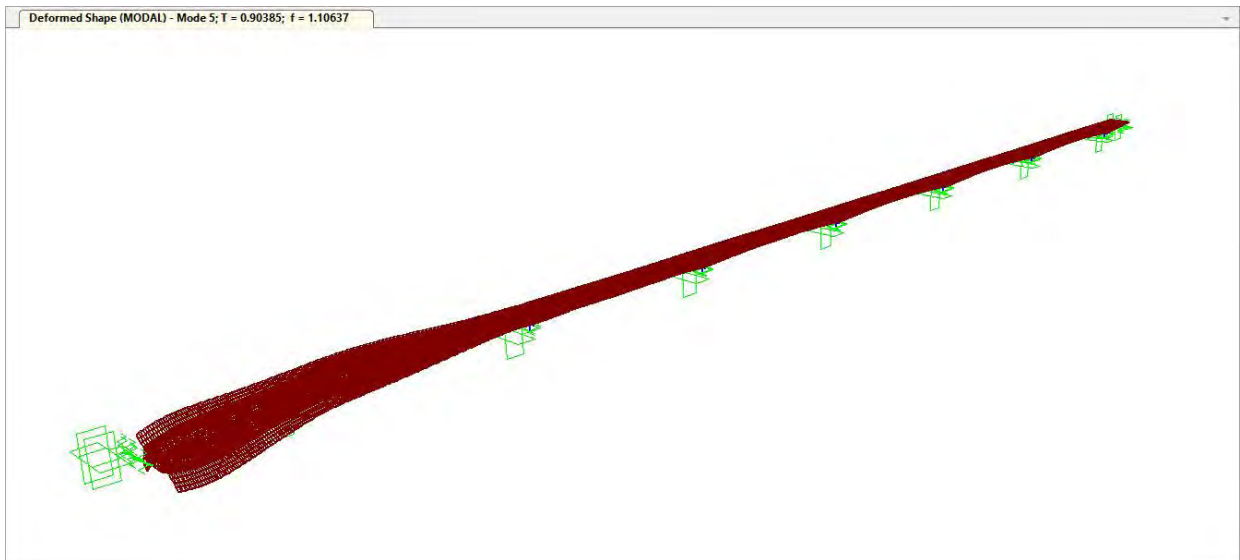


**Figure 4.87: 3D View of Mode Shape 5 for Second Model (T=0.90)**

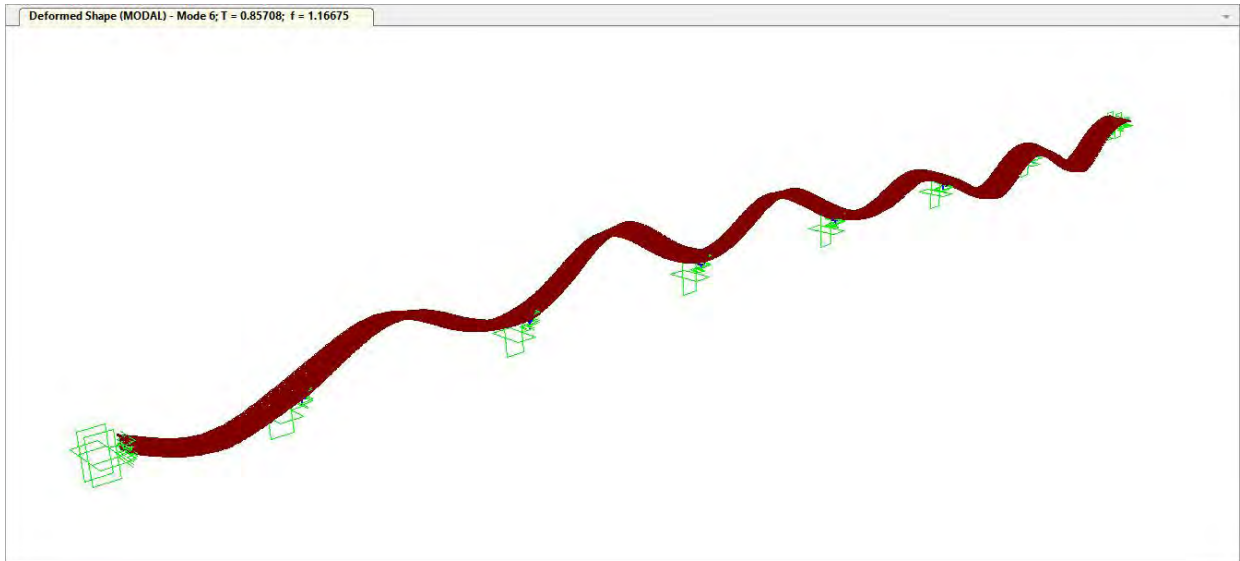


**Figure 4.88: 3D View of Mode Shape 6 for Second Model (T=0.86)**

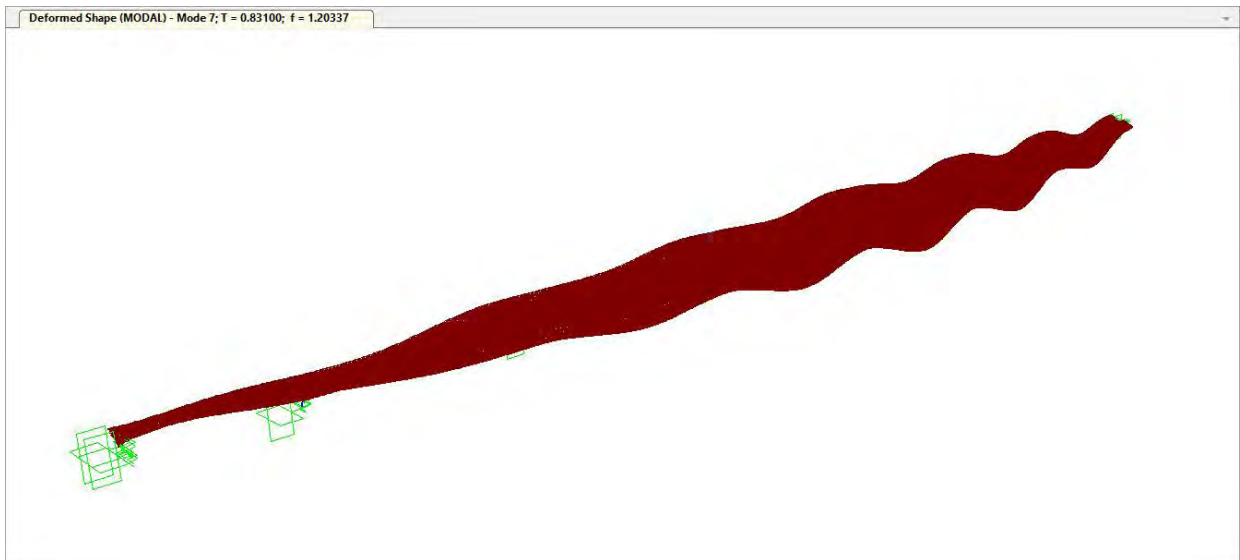


**Figure 4.89: 3D View of Mode Shape 7 for Second Model (T=0.83)**

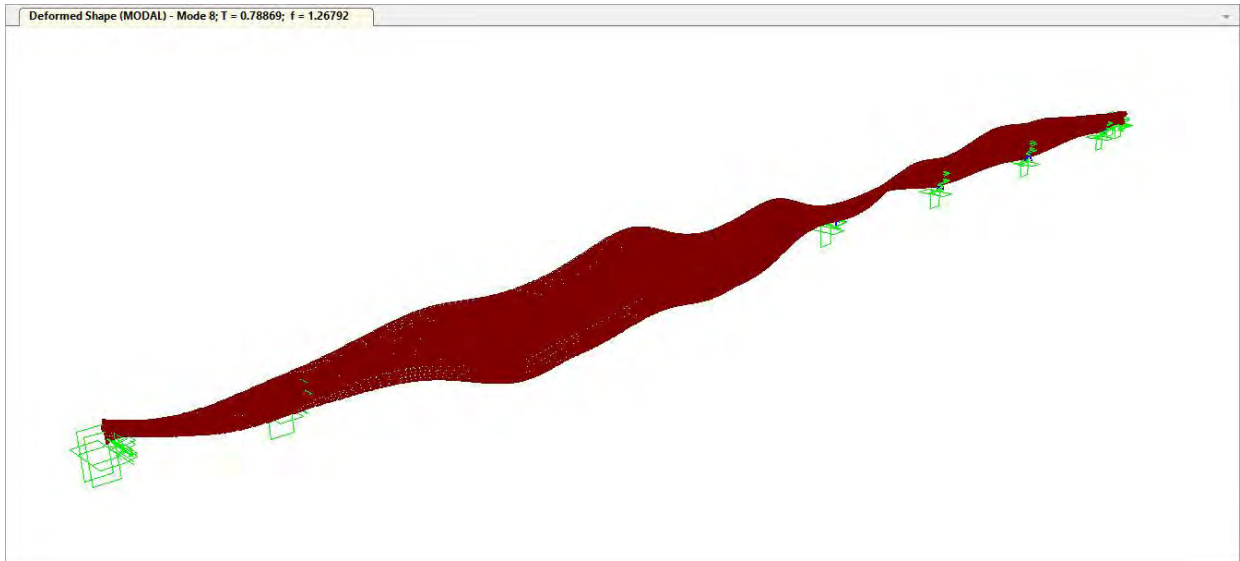


**Figure 4.90: 3D View of Mode Shape 8 for Second Model (T=0.79)**

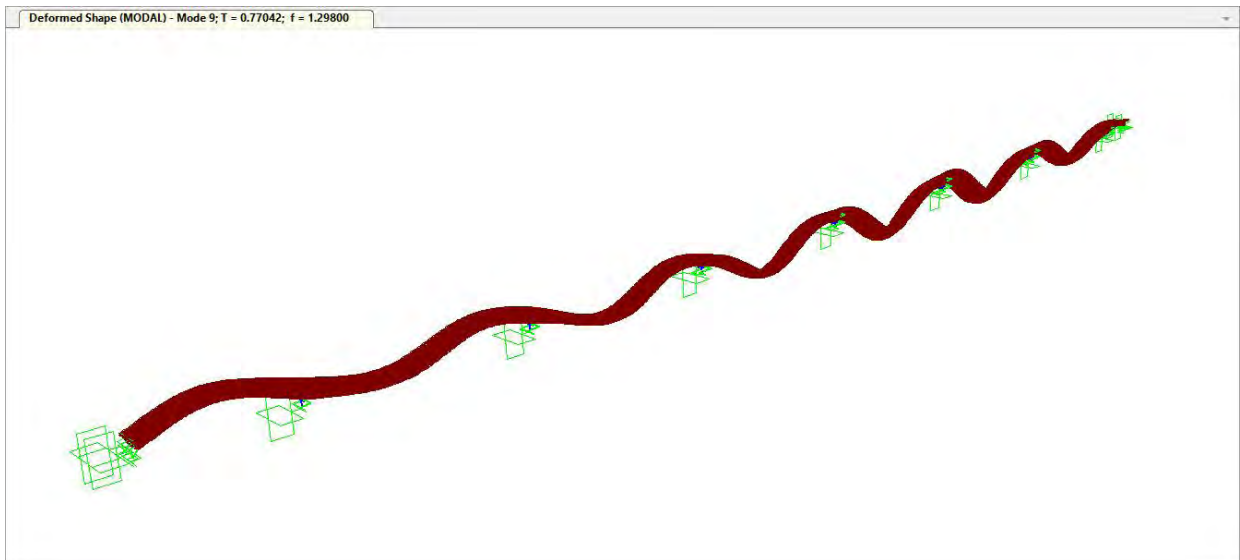


**Figure 4.91: 3D View of Mode Shape 9 for Second Model (T=0.77)**

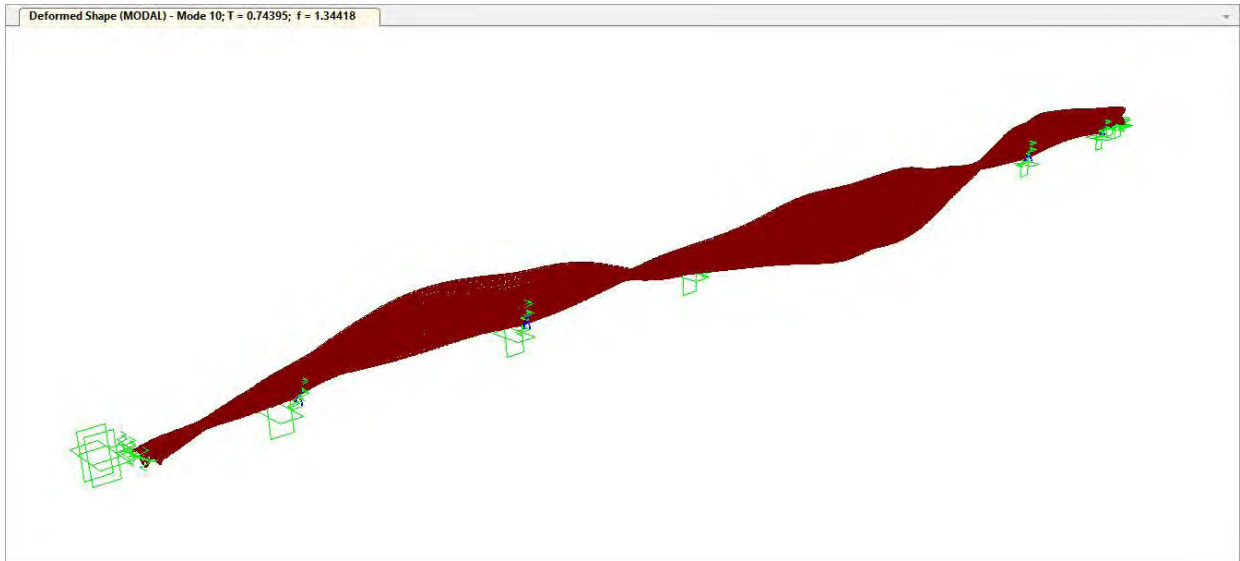


**Figure 4.92: 3D View of Mode Shape 10 for Second Model (T=0.74)**

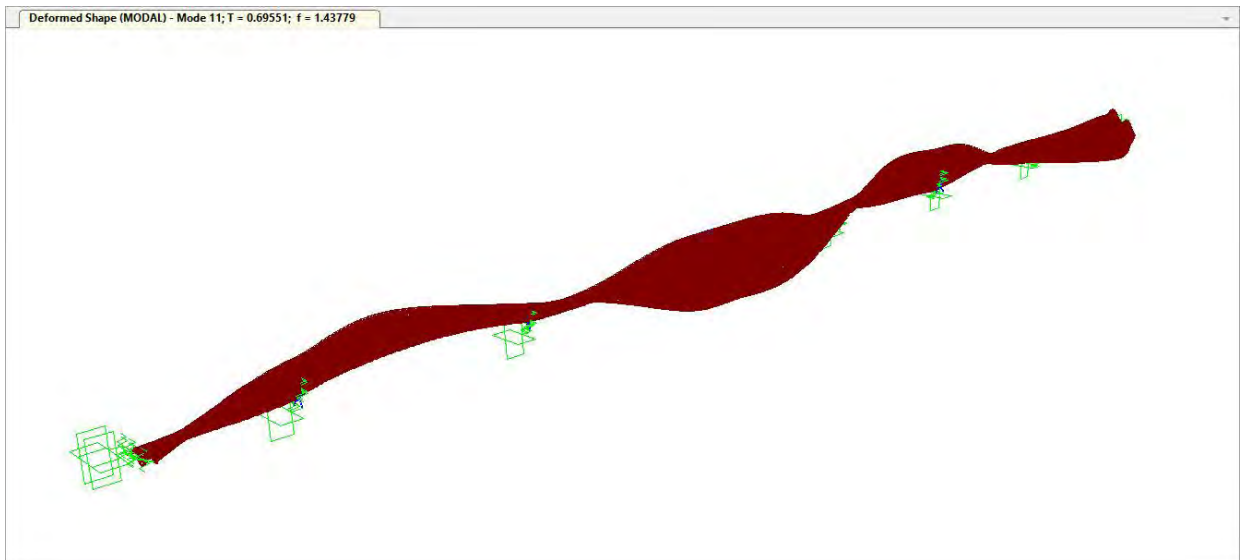


**Figure 4.93: 3D View of Mode Shape 11 for Second Model (T=0.70)**

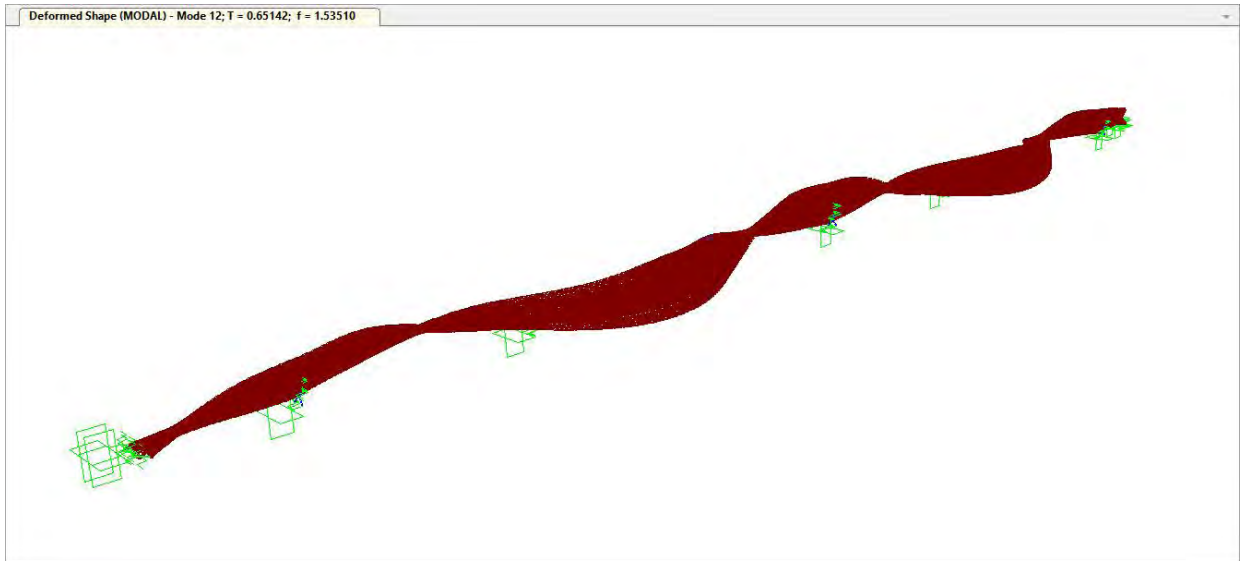


**Figure 4.94: 3D View of Mode Shape 12 for Second Model (T=0.65)**

## CHAPTER 5

### 5. CONCLUSIONS AND RECOMMENDATIONS

---

#### 5.1 GENERAL

The main objectives of the present study are to study the response of box girder bridges due to time differences in dynamic motions at different piers and to study the response of box girder bridges to variations of soil conditions at different piers.

Outline of methodology are to develop Finite Element Models for the analysis of bridges with varying span. Then time differences in the start time of earthquake motions at different piers have been applied in two bridges. Besides, different input motions caused by different soil conditions under bridge piers of long span bridges for the same motion at the base rock have been applied in models. In addition to that synchronous load in the piers of all bridges have been applied. Then time history analysis for different input motions has been performed. Comparison of results found from synchronous effect, asynchronous effect with time lag & asynchronous soil effect has been carried out.

Two models have been prepared with varying span (100 metre span and 125 metre span). Cantilever tendons are assigned in the models. Seven type of load cases due to earthquake are assigned in model-

- a) Synchronous Motion
- b) Asynchronous Motion with 0.01 sec time lag
- c) Asynchronous Motion with 0.1 sec time lag
- d) Asynchronous Motion with 0.1 sec time lag and 45 degree angle
- e) Asynchronous Motion with 0.01 sec time lag and 90 degree angle
- f) Asynchronous Motion with 0.5 sec time lag
- g) Asynchronous Motion due to soil effect

Earthquake data have been changed by using MATLAB due to soil properties. In Asynchronous-Soil load case, new earthquake data have been assigned from fourth pier to end abutment and old earthquake data from start abutment to fourth pier.

## 5.2 CONCLUSIONS

Findings of the study as presented in the previous chapters are summarized below:

- Considering a time lag of 0.01 second from one pier to another pier, displacement of box girder system has been found more than 10 times of synchronous motion along the long direction (along length), 5-6 times of synchronous motion in lateral direction (along width) and 22 times of synchronous motion in vertical direction.
- Considering a time lag of 0.1 second from one pier to another pier, displacement can be more than 18 times of synchronous motion along the long direction (along length), 15 times of synchronous motion in lateral direction (along width) and 45 times of synchronous motion in vertical direction.
- The asynchronous effect in box girder system of 125m span bridge has been found 8-10 times of 100m span bridges in lateral & vertical direction.
- From first two mentioned findings, it has been found that displacement of box girder system varies significantly from Synchronous motion to Asynchronous motion due to augmentation of the time lag. If span of bridge increases, then time lag will be larger and asynchronous effect will be larger as confirmed from above mentioned third findings.
- Considering soil effect of asynchronous motion from one pier to another pier, displacement of box girder system has been found 10-15 times of synchronous motion along the long direction (along length), 2-5 times of synchronous motion in lateral direction (along width) and more than 10 times of synchronous motion in vertical direction.
- In this box girder bridge the finite element analysis with synchronous earthquake is acceptable for overall design. But finite element analysis with asynchronous earthquake is required for designing some local member such as slab, girder at particular section in the bridges.

## 5.3 FUTURE RECOMMENDATIONS

- In the study only two locations were selected for comparison. Other locations can also be selected.
- In the study, the design is only for straight concrete box Girder Bridge. Other bridges such as Figured Bridge can be used for future study.
- Response can be studied for same bridge with different parameters.
- Response can be also studied for another type of bridges.
- Non-linear behaviour of the material can be used for further study.
- In future study superimposed dead load and moving load for vehicle may be applied and static analysis can be done for staged construction for this with this model.
- In this study, scour depths have not been considered here. Actual scouring depths may be considered in future study.



## REFERENCES

Konagai, K & Ahsan, R 2002, 'Simulation of nonlinear soil-structure interaction on a shaking table' *Journal of Earthquake Engineering*, vol 6, no. 1, pp. 31-51

Bodganoff, J.L., Goldberg, J.E. and Schiff, A.J. (1965), "The Effect of Ground Transmission Time on the Response of Long Structures", *Bull. Of Seismological Soc. of Am.*, 55, 627-640.

Burdette, N. J. and Elnashai, A. S., Lupoi, A. and Sextos, A. G. (2008). "Effect of Asynchronous Earthquake Motion on Complex Bridges. I: Methodology and Input Motion," *ASCE*, 1084-0702, Vol.13 (2).

Burdette, N. J. and Elnashai (2008). "Effect of Asynchronous Earthquake Motion on Complex Bridges. II: Results and Implications on Assessment," *ASCE*, 1084-0702, Vol.13 (2).

Der Kiureghian, A. and Neuenhofer, A. (1992), "Response Spectrum Method for Multiple Support Seismic Excitations", *J. Earthquake Eng. & Struct. Dyn.* 21: 713-740.

Dumanoglu, A.A. and Severn, R.T. (1987), "Seismic Response of Modern Suspension Bridges to Asynchronous Vertical Ground Motion", *Proc. Instn Civ. Engrs*, Part 2: 83, 701-730.

Dumanoglu, A.A. and Severn, R.T. (1987), "Seismic Response of Modern Suspension Bridges to Asynchronous Longitudinal and Lateral Ground Motion", *Proc. Instn Civ. Engrs*, Part 2: 87, 73 86.

Elnashai, A.S., Bommer, J.J., Baron, C.I., Lee, D., and Salama, A.I. (1995), "Selected engineering seismology and structural engineering studies of the Hyogo-Ken Nanbu (Great Hanshin) earthquake of 17 January 1995", *ESEE Research Report, No. 95-2*, Imperial College of Science, Technology, and Medicine.

Elnashai, A.S., Borzi, B., and Vlachos, S. (1999), "Deformation-Based Vulnerability Functions for RC Bridges", *J. Struct. Eng. and Mechanics*, 17(2): 215-244.

Leger, P., Ide, I.M., and Paultre, P. (1990), "Multiple-Support Seismic Analysis of Large Structures", *Computers and Structures*, 36(6): 1153-1158.

Luco, J.E. and Wong, H.L. (1986), "Response of a Rigid Foundation to a Spatially Random Ground Motion", *J. Earthquake Eng. & Struct. Dyn.*, 14: 891-908.

Lupoi, A., Franchin, P., Pinto, P. E., and Monti, G. (2005), "Seismic design of bridges accounting for spatial variability of ground motion", *J. Earthquake Eng & Struct. Dyn.* 34, 327–348.

Monti, G., Nuti, C., and Pinto, P.E. (1996), "Nonlinear Response of Bridges Under Multisupport Excitation", *J. Struct. Eng. ASCE*, 122(10): 1147-1159.

Oliveira, C.S., Hao, H., and Penzien, J. (1991), "Ground Motion Modeling for Multiple-Input Structural Analysis", *Structural Safety*, 10: 79-93.

Romanelli, F., Panza, G.F. and Vaccari F. (2004) "Realistic Modelling of the Effects of Asynchronous Motion at the Base of Bridge Piers," *JSEE*, Vol. 6(2), pp. 19-28.

Sextos, A.G., Ptilakis, K.D., and Kappos, A.J. (2003a), "Inelastic Dynamic Analysis of RC Bridges Accounting for Spatial Variability of Ground Motion, Site Effects and Soil-Structure Interaction Phenomena. Part 1: Methodology and Analytical Tools", *J. Earthquake Eng. & Struct. Dyn.* 32: 607-627.

Sextos, A.G., Kappos, A.J. and Ptilakis, K.D. (2003b), "Inelastic Dynamic Analysis of RC Bridges Accounting for Spatial Variability of Ground Motion, Site Effects and Soil-Structure Interaction Phenomena. Part 2: Parametric Study", *J. Earthquake Eng. & Struct. Dyn.* 32: 629 652.

Sextos, A. G., Kappos, A. J., and Mergos, P. (2004), "Effect of soil structure interaction and spatial variability of ground motion on irregular bridges: The case of the Krystallopigi Bridge.", *13<sup>th</sup> World Conf. on Earthquake Eng.*, Paper No. 2298.

Tzanetos, N., Elnashai, A.S., Hamdan, F.H., and Antoniou, S. (2000), "Inelastic Dynamic Response of RC Bridges subjected to Spatial Non-Synchronous Earthquake Motion", *Adv. In Struct. Eng.*, 3(3): 191-214.

Wang, J., Carr, A. Cooke, N. and Moss P. (2004) "Inelastic Responses of Long Bridges to Asynchronous Seismic Inputs," *13th World Conference on Earthquake Engineering, Vancouver*, August, paper no. 638.

Zerva, A. (1990), "Response of Multi-Span Beams to Spatially Incoherent Seismic Ground Motions", *J. Earthquake Eng. & Struct. Dyn.* 19: 819-832.

## APPENDIX A

### FINITE ELEMENT MODELING OF THE BRIDGE

---

#### BRIDGE LAYOUT LINE

The bridge has one module and it is straight. The first step of modelling using the CSiBridge2015 is initiated by bridge layout line data, the form shown in Figure A.1 will be displayed. The end section is selected 695.625 m as design data for first bridge and 845.625 m for second bridge.

Bridge Layout Line Data

Bridge Layout Line Name: BLL1

Coordinate System: GLOBAL

Shift Layout Line: Modify Layout Line Stations...

Units: KN, mm, C

Coordinates of Initial Station

Global X	0.
Global Y	0.
Global Z	0.

Initial and End Station Data

Initial Station (mm)	0.
Initial Bearing	N900000E
Initial Grade in Percent	0.
End Station (mm)	695.625.

Horizontal Layout Data

Define Horizontal Layout Data... Quick Start...

Define Layout Data

Define Vertical Layout Data... Quick Start...

Refresh Plot

OK Cancel

Figure A.1: Bridge Layout Line Form

#### DECK SECTION AND MATERIAL PROPERTIES

Then concrete box girder bridge section data is assigned for two models. Then the form shown in Figure A.2 will be displayed.

**Section Data**

Item	Value
<b>General Data</b>	
Bridge Section Name	BSEC1
Material Property	4000Psi
Number of Interior Girders	0
Total Width	18500.
Total Depth	6500.
Left Exterior Girder Bottom Offset (L3)	2340.
Right Exterior Girder Bottom Offset (L4)	2340.
Keep Girders Vertical When Superelevate? (Area & Solid Models)	No
<b>Slab and Girder Thickness</b>	
Top Slab Thickness (t1)	280.
Bottom Slab Thickness (t2)	850.
Exterior Girder Thickness (t3)	500.
<b>Fillet Horizontal Dimension Data</b>	
f1 Horizontal Dimension	460.
f2 Horizontal Dimension	460.
f3 Horizontal Dimension	460.
f4 Horizontal Dimension	460.

**Figure A.2: Deck Section Data Form**

The properties of the materials (concrete, rebar, steel) used in two bridges are shown in Figure A.3, Figure A.4, Figure A.5 respectively.

**Material Property Data**

**General Data**

Material Name and Display Color: 4000Psi

Material Type: Concrete

Material Notes:

**Weight and Mass**

Weight per Unit Volume: 2.356E-08

Mass per Unit Volume: 2.403E-12

Units: KN, mm, C

**Isotropic Property Data**

Modulus of Elasticity, E: 24.8556

Poisson: 0.2

Coefficient of Thermal Expansion, A: 9.900E-06

Shear Modulus, G: 10.3565

**Other Properties for Concrete Materials**

Specified Concrete Compressive Strength,  $f_c$ : 0.0276

Lightweight Concrete

Shear Strength Reduction Factor:

Switch To Advanced Property Display

**Figure A.3: Concrete Property**

**Material Property Data**

**General Data**

Material Name and Display Color: A615Gr60

Material Type: Rebar

Material Notes:

---

**Weight and Mass**

Weight per Unit Volume:

Mass per Unit Volume:

Units:

---

**Uniaxial Property Data**

Modulus of Elasticity, E:

Poisson:

Coefficient of Thermal Expansion, A:

Shear Modulus, G:

---

**Other Properties for Rebar Materials**

Minimum Yield Stress, Fy:

Minimum Tensile Stress, Fu:

Expected Yield Stress, Fye:

Expected Tensile Stress, Fue:

---

Switch To Advanced Property Display

**Figure A.4: Rebar Property**



**Figure A.5: Steel Property**

## **DIAPHRAGM, PIER**

There are seven piers in each bridge. Solid type diaphragm is used in this bridge and thickness of diaphragm is 2 m and diaphragm depth is 1 m shown in Figure A.6.



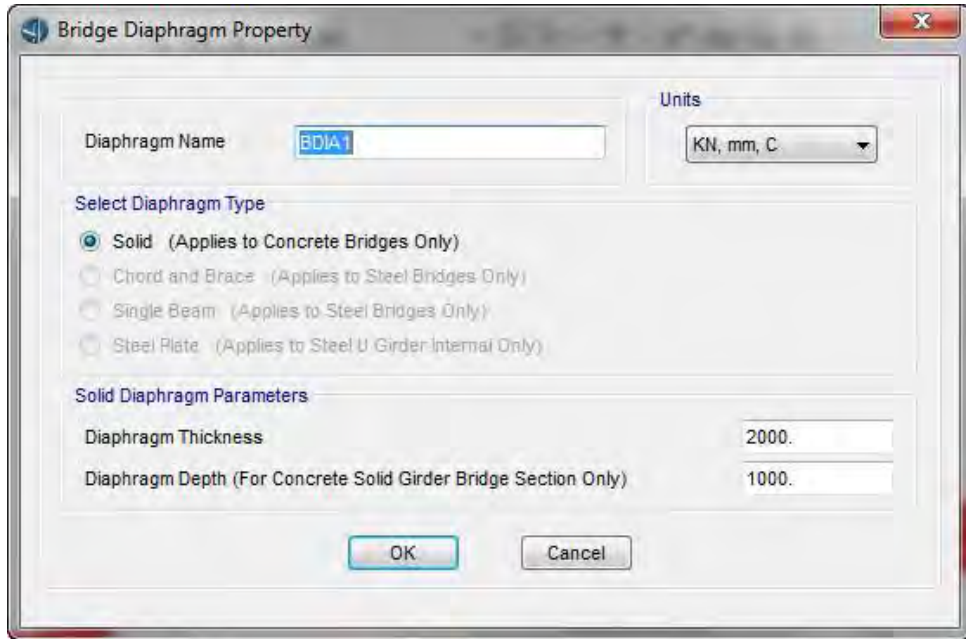


**Figure A.6: Diaphragm Property**

## BEARING, ABUTMENT AND BENT

Bearing properties of the bridge are defined in two bridges and filling out the form shown in Figure A.7.

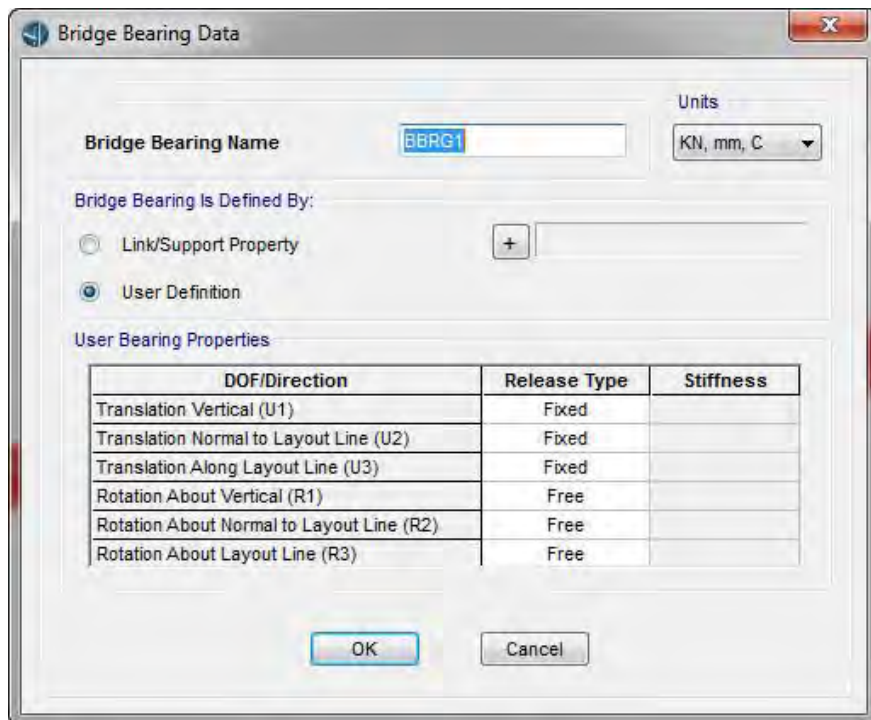


**Figure A.7: Bearing Properties**



Abutment properties of the bridge are defined in two bridges and filling out the form shown in Figure A.8.

Bridge Abutment Data

Bridge Abutment Name: BAPT1

Units: KN, mm, C

Girder Support Condition:

- Integral
- Connect to Girder Bottom Only

Substructure Type:

- Foundation Spring
- Continuous Beam (Continuously Supported)

Section Property: + [ ]

Beam Length: [ ]

Foundation Spring:

Foundation Spring Property: + Fixed

Note: When substructure type is grade beam, foundation spring property represents a line spring.

OK Cancel

**Figure A.8: Abutment Properties**

Bent properties of the bridge are defined in two bridges and filling out the form shown in Figure A.9.

Bridge Bent Data

Bridge Bent Name: BENT1

Units: KN, mm, C

Girder Support Condition:

- Integral
- Connect to Girder Bottom Only

Bent Data:

Cap Beam Length: 6400

Number of Columns: 1

Cap Beam Section: + BEAM

Modify/Show Column Data...

Bent Type:

- Single Bearing Line (Continuous Superstructure)
- Double Bearing Line (Discontinuous Superstructure)

OK Cancel

**Figure A.9: Bent Properties**

## BRIDGE OBJECTS AND UPDATING BRIDGE STRUCTURAL MODEL

Bridge object is selected for designing spans of the bridge in CSIBridge2015. There are eight spans for each bridge. Then the form segmental bridge object data shown in Figure A.10 will be displayed for first bridge.

**Segmental Bridge Object Data**

Bridge Object Name: BOBJ1    Layout Line Name: BLL1    Coordinate System: GLOBAL    Units: KN, mm, C

Define Segmental Bridge Spans

Span Label	Start Station mm	Length mm	End Station mm	Start Support	End Support
01-SA-P01	0.	73050.	73050.	BABT1	BENT1
02-P01-P02	73050.	99375.	172425.	BENT1	BENT1
03-P02-P03	172425.	99375.	271800.	BENT1	BENT1
04-P03-P04	271800.	99375.	371175.	BENT1	BENT1
05-P04-P05	371175.	99375.	470550.	BENT1	BENT1
06-P05-P06	470550.	99375.	569925.	BENT1	BENT1
07-P06-P07	569925.	99375.	669300.	BENT1	BENT1
08-P07-P08	669300.	26325.	695625.	BENT1	BABT1

Note: 1. Bridge object location is based on bridge section insertion point following specified layout line.

Bridge Object Plan View (X-Y Projection)

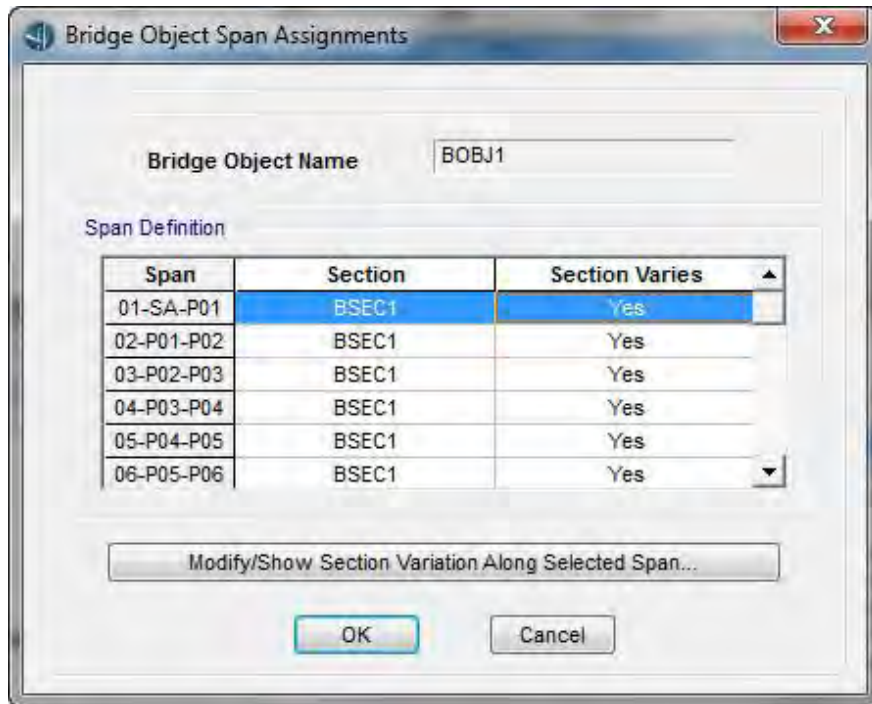
Modify/Show Assignments

- Spans
- User Discretization Points
- Abutments
- Bents
- In-Span Hinges (Expansion Jts)
- In-Span Cross Diaphragms
- Superelevation
- Prestress Tendons
- Girder Rebar
- Staged Construction Groups
- Point Load Assigns
- Line Load Assigns

Lock to Prevent Updating the Linked Model

**Figure A.10: Bridge Object Form**

Bridge object span assignment and bridge object discretization point's assignments are defined as per Figure A.11 and Figure A.12 respectively.



Bridge Object Name: BOBJ1

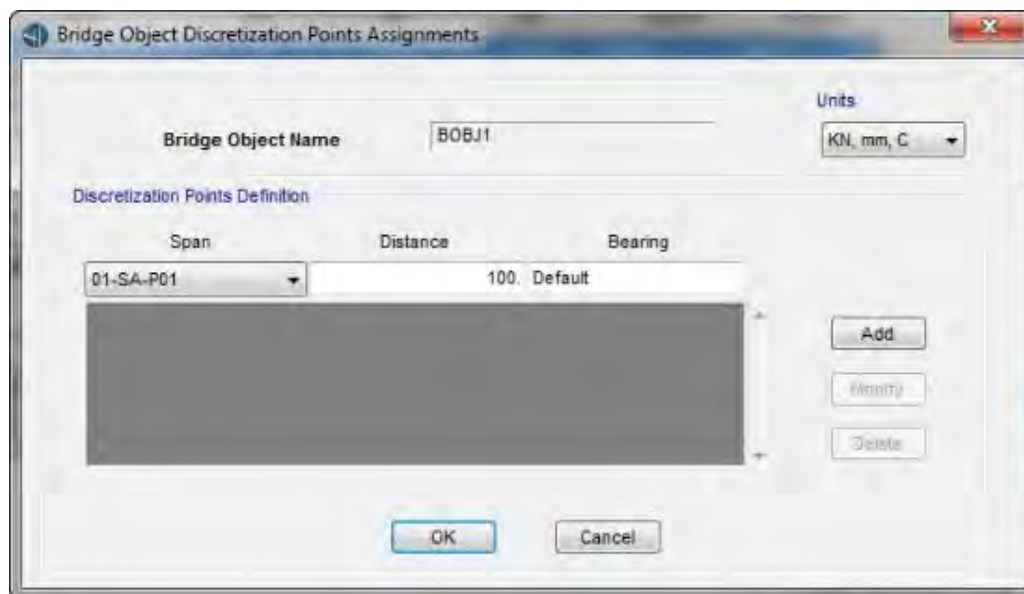
Span Definition

Span	Section	Section Varies
01-SA-P01	BSEC1	Yes
02-P01-P02	BSEC1	Yes
03-P02-P03	BSEC1	Yes
04-P03-P04	BSEC1	Yes
05-P04-P05	BSEC1	Yes
06-P05-P06	BSEC1	Yes

Modify/Show Section Variation Along Selected Span...

OK Cancel

**Figure A.11: Bridge Object Span Assignment Form**



Bridge Object Name: BOBJ1

Units: KN, mm, C

Discretization Points Definition

Span	Distance	Bearing
01-SA-P01	100	Default

Add  
Empty  
Delete

OK Cancel

**Figure A.12: Bridge Object Discretization Points Assignments Form**

Bridge object abutment assignment, bridge object bent assignments, cross diaphragm assignments and bridge construction group definition are defined as per below Figure A.13, Figure A.14, Figure A.15 & Figure A.16 respectively.

Bridge Object Name: BOBJ1  
Units: KN, mm, C

Start Abutment: | End Abutment: |

**Start Abutment**

Superstructure Assignment  
Support Name: SA  
Abutment Direction (Bearing Angle): Default  
Diaphragm Property: + None

Substructure Assignment  
 None  
 Abutment Property: + BABT1  
 Bent Property: +

Substructure Location  
Elevation (Global Z): -2438.4  
Horizontal Offset: 0.  
Note: Horizontal offset is from layout line to midlength of abutment.

**Bearing Assignment**  
 Girder-by-Girder  
 General  
Bearing Property: + BBRG1  
Restrainer Property at Bearing: + None  
Elevation at Layout Line (Global Z): -6500.  
Rotation Angle from Bridge Default: 0.

**Girder-by-Girder Overwrites**  
Modify/Show Overwrites... No Overwrites Exist

OK Cancel

**Figure A.13: Bridge Object Abutment Assignment Form**

Bridge Object Name: BOBJ1  
Units: KN, mm, C

Specify Bent Considered  
Bent is At the End of This Span: 01-SA-P01  
Bent is At This Station: 73050.  
Support Name: 01-SA-P01

Superstructure Assignment  
Superstructure Continuity Condition: Continuous  
Mesh Superstructure to Match Bent Bearing: Yes  
Diaphragm Property: + BDIA1  
Steel I-Girder Diaphragm: + None

Bent Assignment  
Bent Property: + BENT1  
Bent Direction (Bearing Angle): Default

Bent Location  
Elevation (Global Z): -6368.5  
Horizontal Offset: 0.  
Note: Horizontal offset is from bridge layout line to midlength of cap beam.

**Bearing Assignment**  
 Girder-by-Girder  
 General  
Bearing Property: + BBRG1  
Restrainer Property at Bearing: + None  
Elevation (At Layout Line, Global Z): -6068.5  
Rotation Angle from Bridge Default: 0.  
Number of Bearings for Bridge Section: 2  
Uniform Spacing: 5970.  
Offset from Section Ref. Point to Bearing Center: 0.

**Bearing-by-Bearing Bearing Overwrites**  
Modify/Show Overwrites... No Overwrites Exist

OK Cancel

**Figure A.14: Bridge Object Bent Assignments Form**



Bridge Object In-Span Cross-Diaphragm Assignments

Bridge Object Name: BOBJ1

Units: KN, mm, C

In-Span Cross-Diaphragm Definition

Span	Diaphragm Property	Location	Bearing	Distance	Ref Line
01-SA-P01	BDIA1	All Spaces	Default	100	Layout Line

Buttons: Add, Modify, Delete, OK, Cancel

**Figure A.15: Bridge Object Cross Diaphragm Assignments Assignment Form**

Bridge Construction Group Definition

Bridge Group Name: 01-SA-P01

Bridge Group Type: Section

Bridge Object: BOBJ1

Units: KN, mm, C

Group Ranges

Position	Start Span	Start Distance	End Span	End Distance
Entire Section	01-SA-P01	0.	08-P07-P08	26325.
Entire Section	01-SA-P01	0.	01-SA-P01	73050.

Note 1. Distance contains the location of User Points, In-span Hinges, Diaphragms and Span Ends.  
 2. Distance is measured along the layout line.

Buttons: Add, Modify, Delete, OK, Cancel

**Figure A.16: Bridge Construction Group Definition Form**

Parametric variations for first bridge are defined as per below Figure A.17 & Figure A.18.

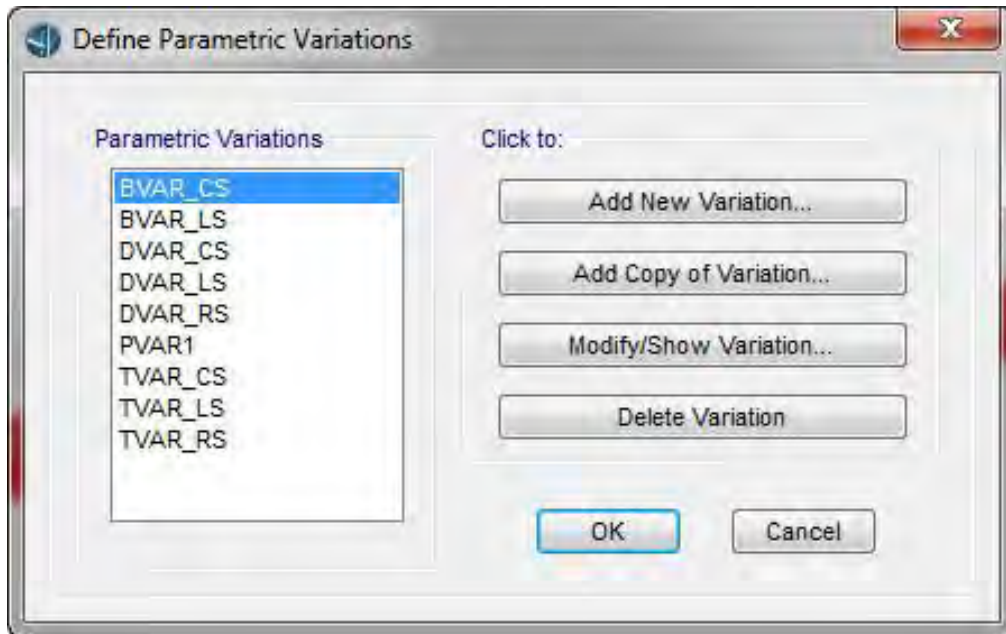


**Figure A.17: Bridge Parametric Variations Definition Form**

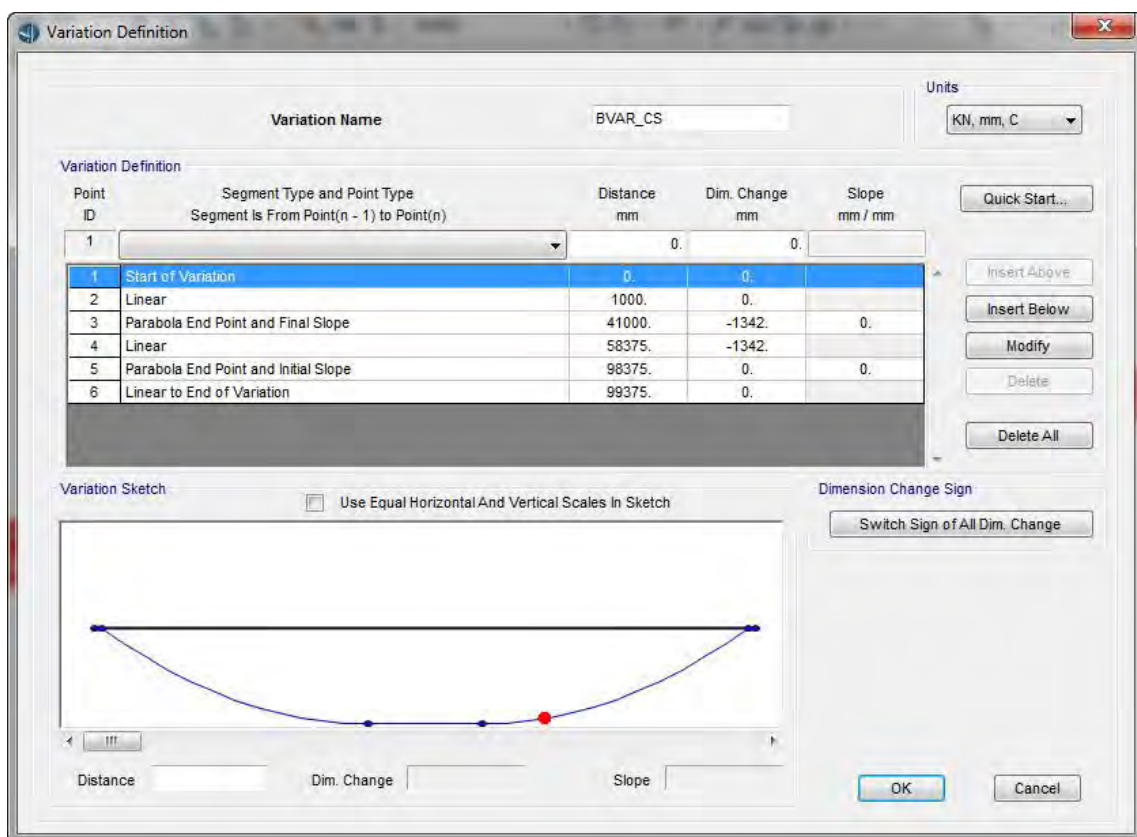


**Figure A.18: Bridge Parametric Variations Definition Form\_2**

In each bridge, cantilever tendons are used. Tendon layout plan and tendon details for first bridge are shown in Figure A.19. Then this tendon is assigned at CSIBridge2015 model as below Figure A.20. All this tendons are assigned for second bridge at proportionate way.

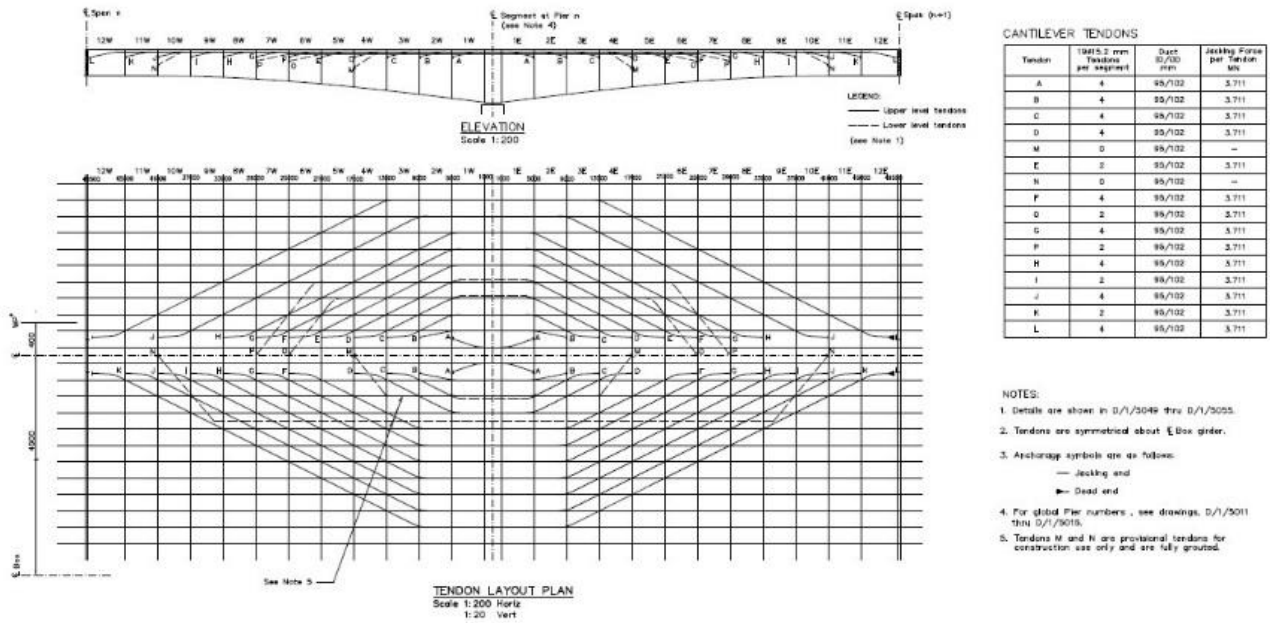


**Figure A.19: Tendon Layout Plan and Tendon Details for First Bridge**

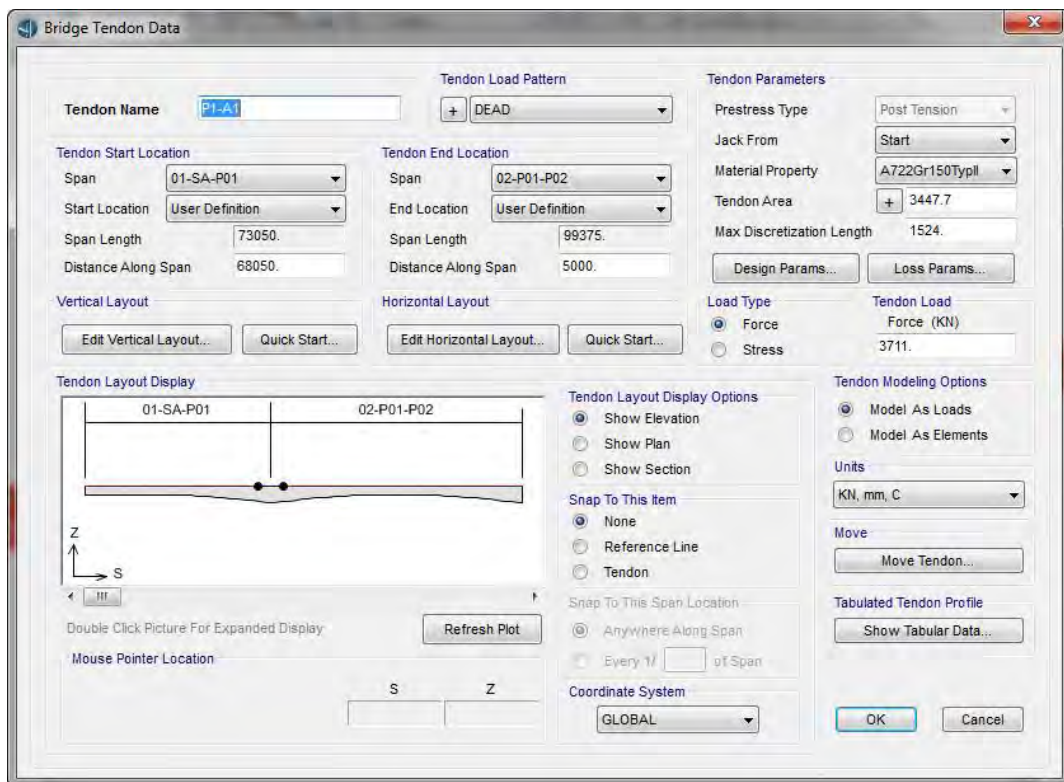


**Figure A.20: Bridge Tendon Assignment**

## DEFINING LOAD PATTERNS

Static load patterns such as dead load, live load, synchronous, asynchronous load cases are defined which will create a form similar to the one shown in Figure A.21.

Load Pattern Name	Type	Self Weight Multiplier	Auto Lateral Load Pattern
DEAD	DEAD	1	
DEAD	DEAD	0	
Prestress	PRESTRESS	0	
ST-ABUT	QUAKE	0	None
PIER-1	QUAKE	0	None
PIER-2	QUAKE	0	None
PIER-3	QUAKE	0	None
PIER-4	QUAKE	0	None
PIER-5	QUAKE	0	None
PIER-6	QUAKE	0	None
PIER-7	QUAKE	0	None

Click To:

- Add New Load Pattern
- Modify Load Pattern
- Modify Lateral Load Pattern...
- Delete Load Pattern
- Show Load Pattern Notes...

OK Cancel

Figure A.21: Static Load Pattern Definition Form

## SOIL EFFECT DUE TO ASYNCHRONOUS MOTION

In this study, we have used acceleration, velocity and displacement data recorded on the Jamuna Multi-Purpose bridge pile cap (horizontal direction) on June 16, 2004.

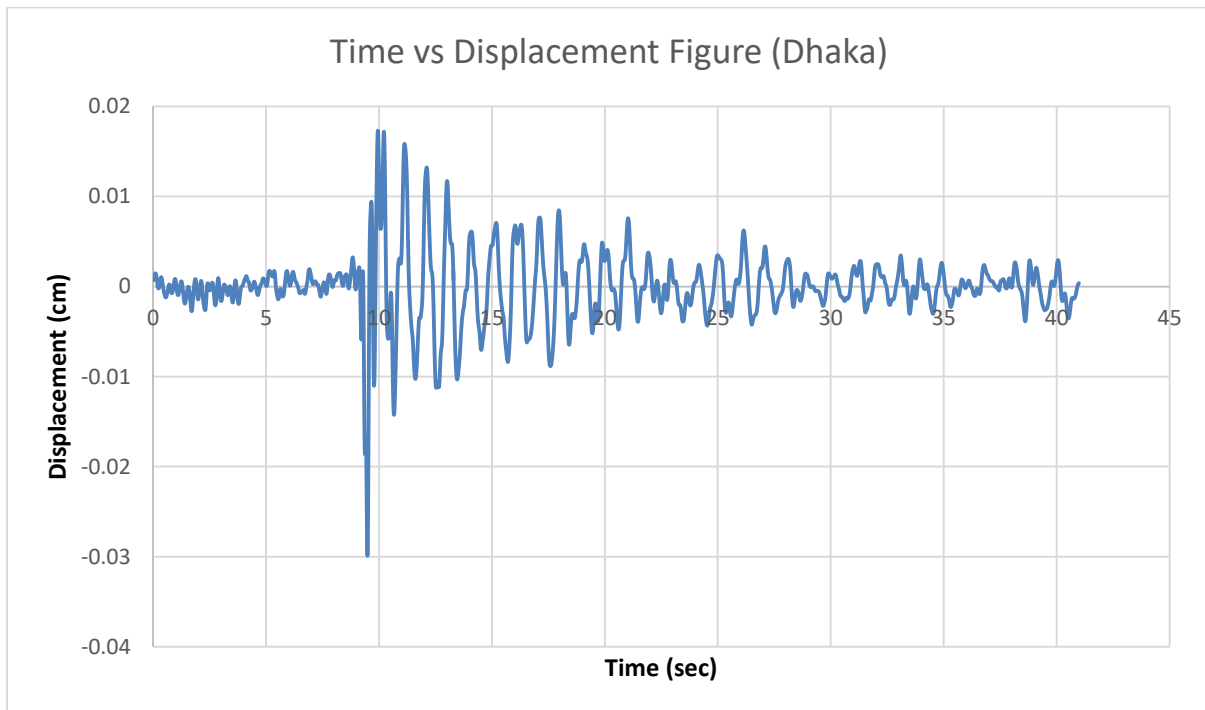


Figure A.22: Time vs Displacement Figure (Dhaka)



## DEFINING LOAD CASES

Seven type of load cases due to earthquake are assigned in model which will create a form similar to the one shown in Figure A.23.

1. Synchronous Motion
2. Asynchronous Motion with 0.01 sec time lag
3. Asynchronous Motion with 0.1 sec time lag
4. Asynchronous Motion with 0.1 sec time lag and 45 degree angle
5. Asynchronous Motion with 0.01 sec time lag and 90 degree angle
6. Asynchronous Motion with 0.5 sec time lag
7. Asynchronous Motion due to soil effect

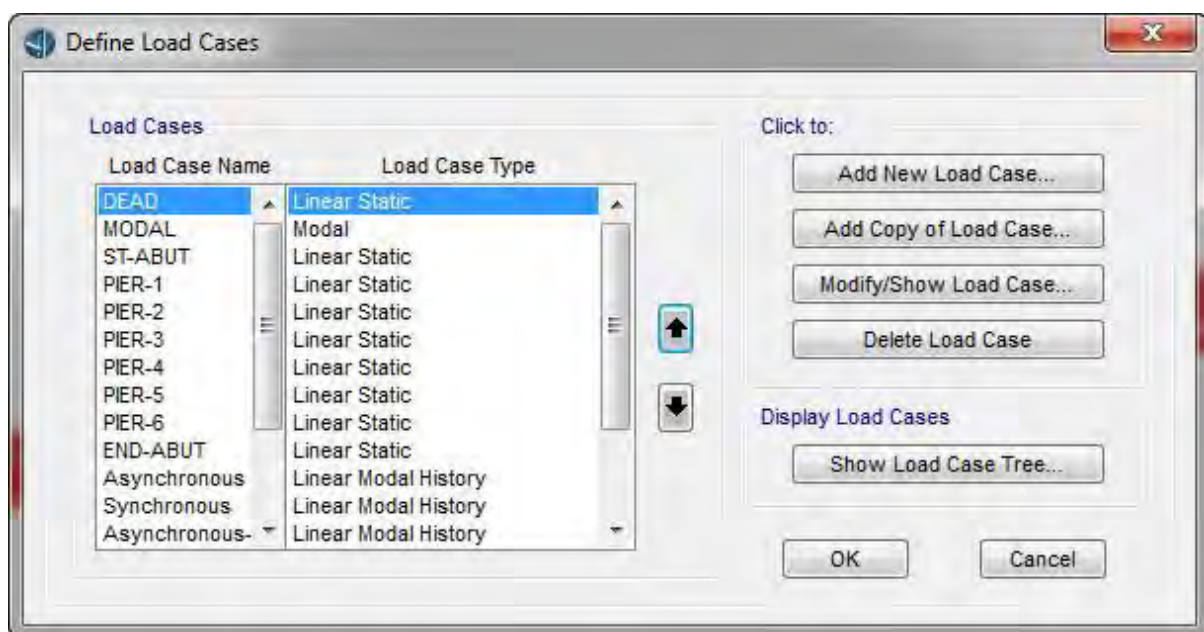


**Figure A.23: Static Load Case Definition Form**

Assignment of this seven criteria are shown in Figure A.24 to Figure A.30 respectively for two bridges.

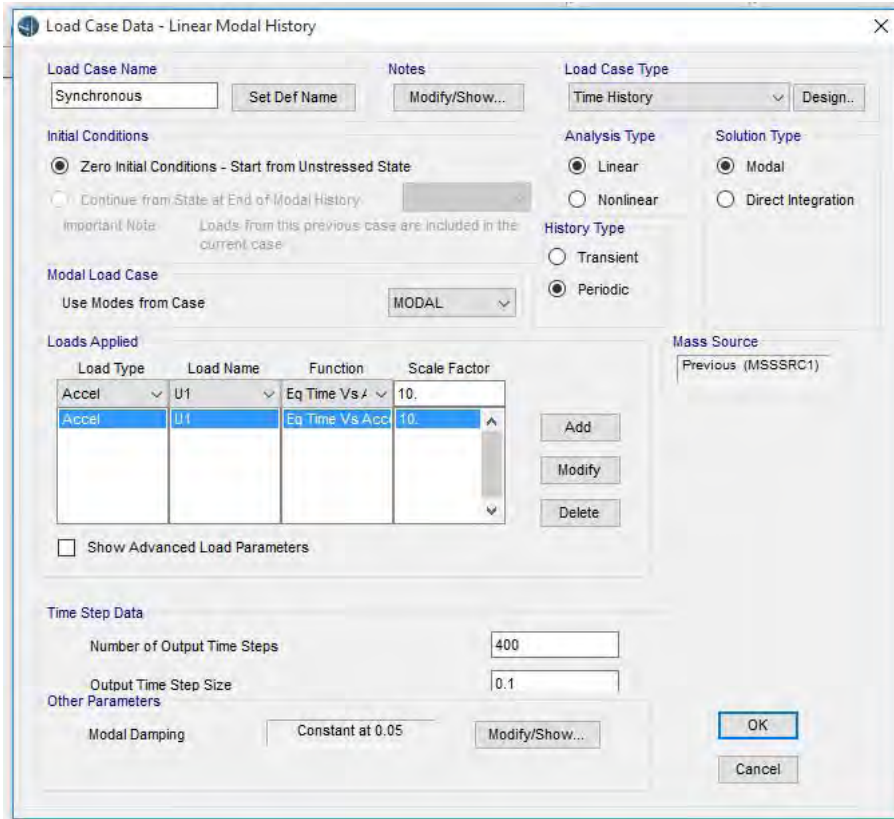


**Figure A.24: Load Case Assignment-Synchronous**

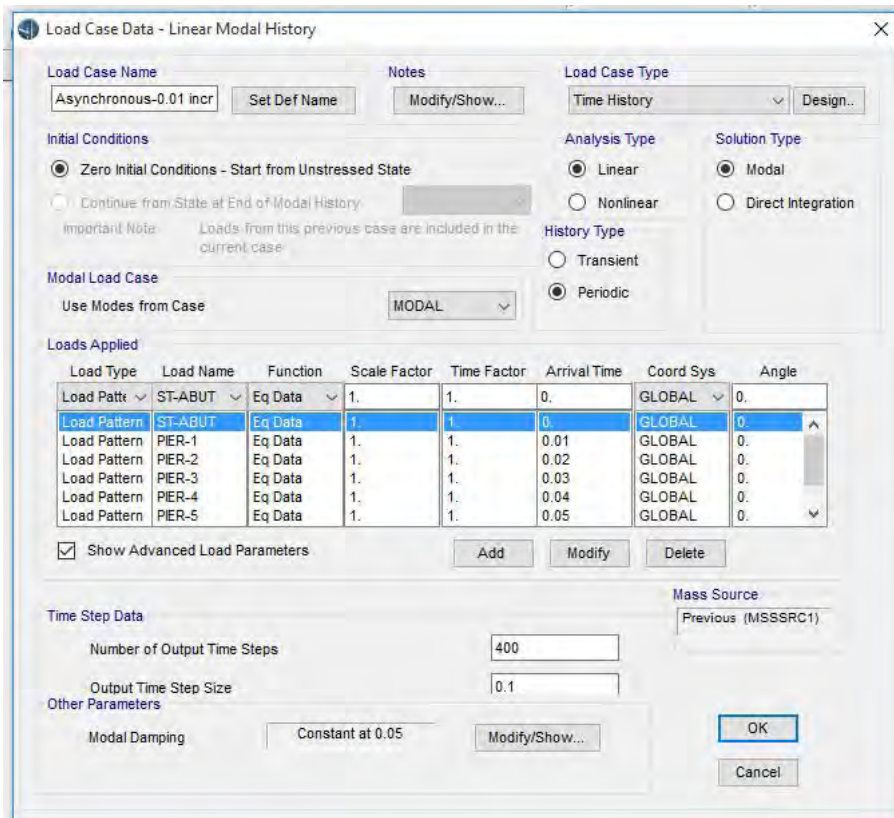


**Figure A.25: Load Case Assignment-Asynchronous with 0.01 sec time lag**

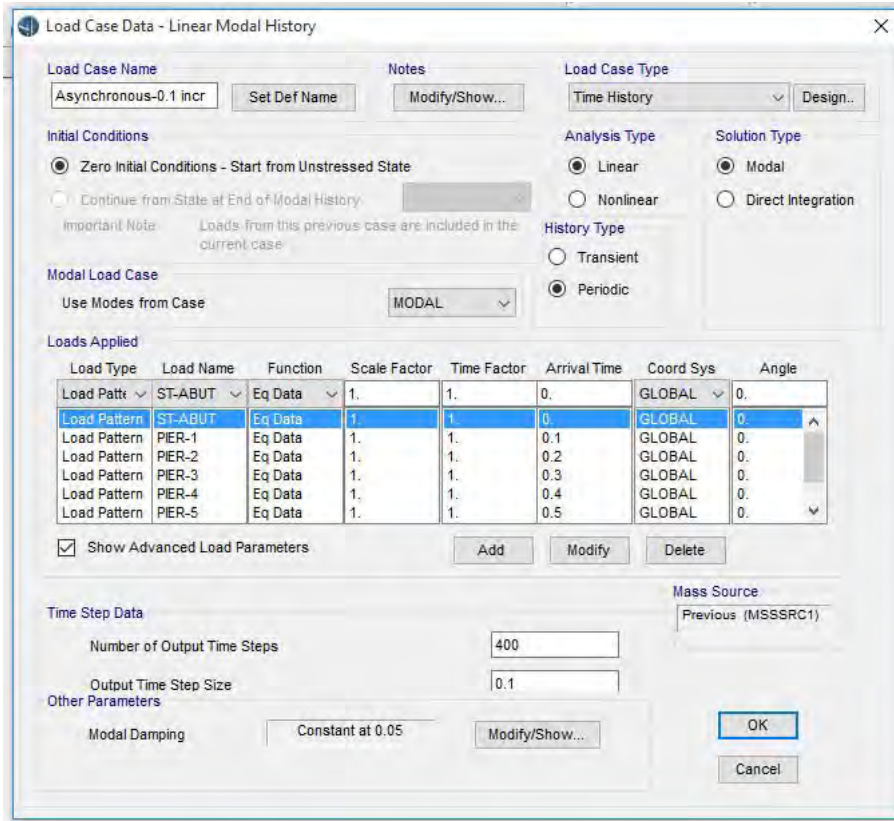


**Figure A.26: Load Case Assignment-Asynchronous with 0.1 sec time lag**

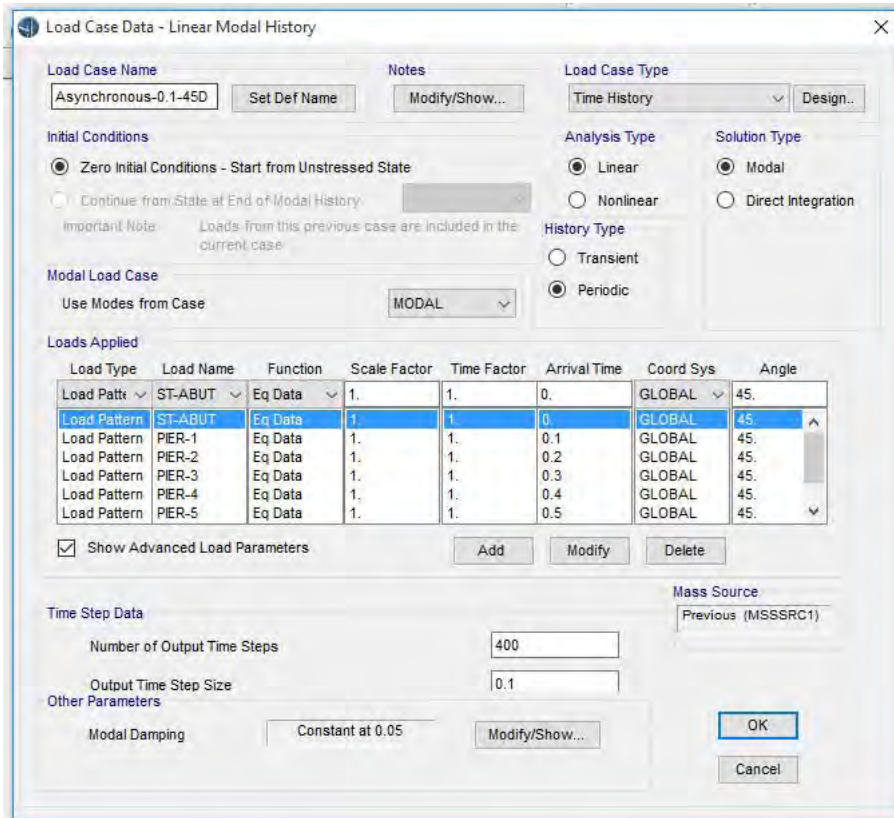


**Figure A.27: Load Case Assignment-Asynchronous with 0.1 sec time lag (45 degree)**



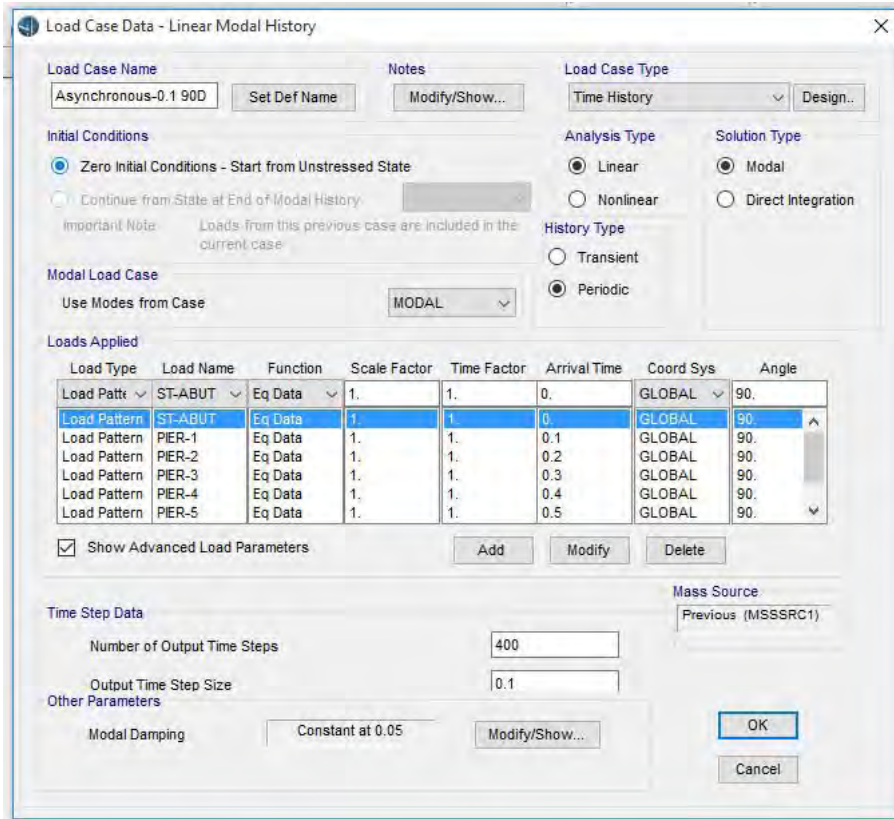


Figure A.28: Load Case Assignment-Asynchronous with 0.1 sec time lag (90 degree)

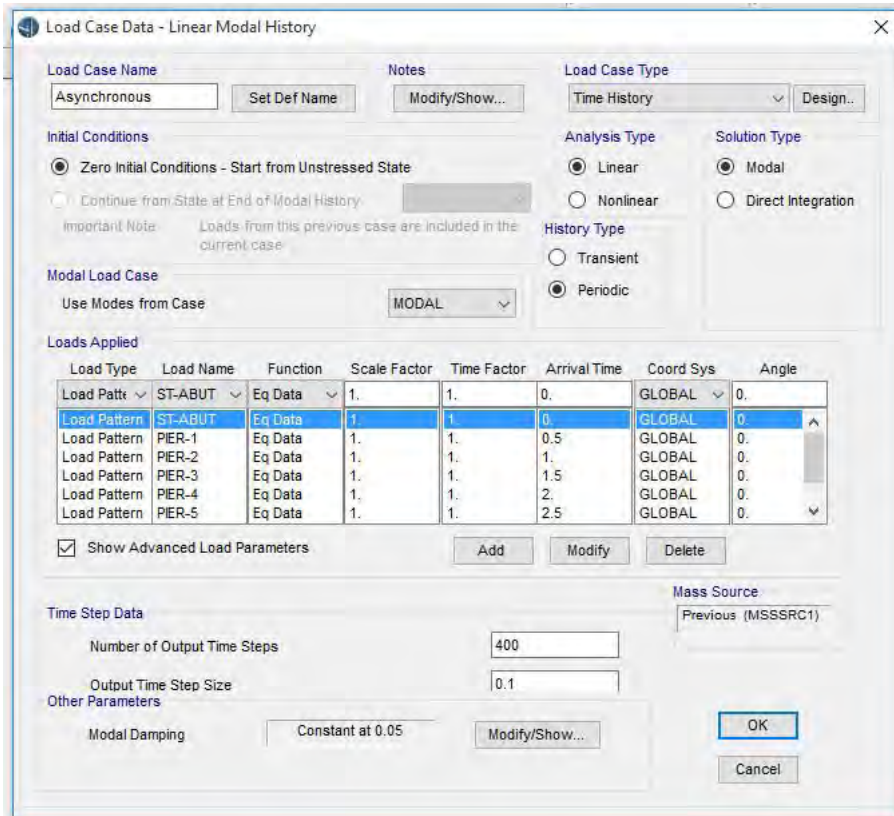
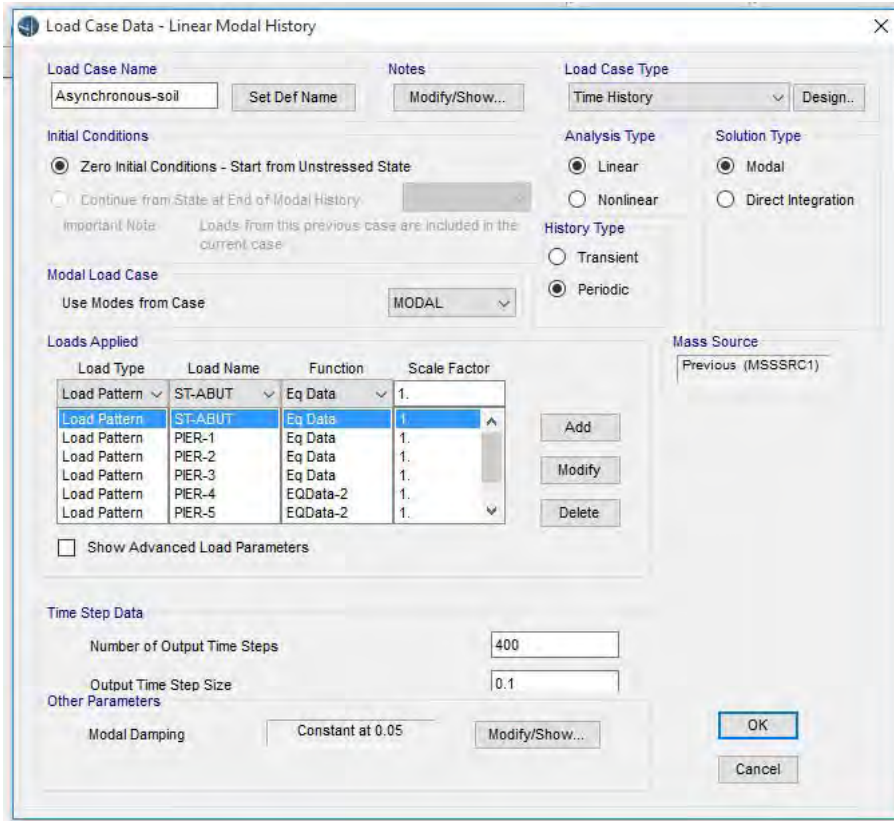


Figure A.29: Load Case Assignment-Asynchronous with 0.5 sec time lag



**Figure A.30: Load Case Assignment-Asynchronous with Soil Variation**

## DEFINING STRUCTURAL LOADS

A unit displacement 10 mm is applied at every pier including start and end abutment for two bridges.

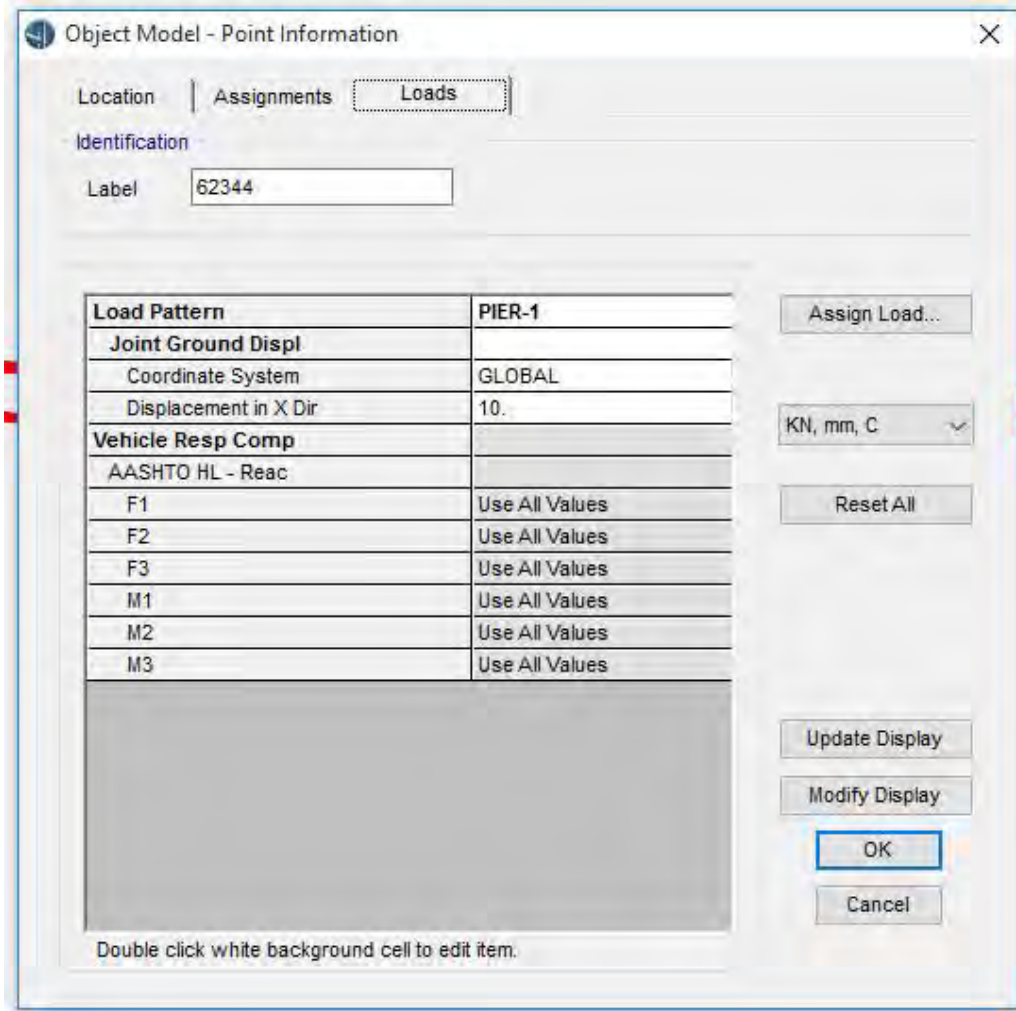


Figure A.31: Load Assignment at Pier

3D view of final two models are shown in Figure A.32 and Figure A.33.



**Figure A.32: 3D View of First Model (each span 100 metre)**



**Figure A.33: 3D View of Second Model (each span 125 metre)**

## APPENDIX B

### MATLAB PROGRAM FOR ESTIMATION SURFACE DISPLACEMENT FROM THE INPUT ACCELERATION

---

A Matlab program has been prepared for estimation surface displacement from the input acceleration (Konagai, K & Ahsan, R 2002, 'Simulation of nonlinear soil-structure interaction on a shaking table' Journal of Earthquake Engineering, vol 6, no. 1, pp. 31-51). Detail Matlab program is shown below.

```
% wavedamp.m
% This M-file analyzes the earthquake response of
% horizontally layered soil-profile, possessing
% non-linear stress-strain relationship, by solving
% one dimensional wave equation.

dampin % input-script

initdamp % initializes matrices
%
% loop for each time-step starting from the second
%

for isec = indelt+deltat:deltat:totime

    % counter for the loop, writes it in the console 'stime' no. of times
    if mod(isec,(totime/stime))==0
        k = k + 1
    else
        k = k + 1;
    end

    % nodal force component from the lower element

    force1 = -0.5*[[globmass(1,nelem)-
    [[eleprop(:,1).*elength]./[elength.*eleprop(:,1)]].*globmass(nelem,nele
m)]*gainter(k)]-[[globstif(1,nelem)-
    [[eleprop(:,1).*elength]./[elength.*eleprop(:,1)]].*globstif(nelem,nele
m)]*Def(k)]];
    force1 = [ force1];
    % calculation of total nodal force by adding contribution from the
    higher element
    for ielem = 2:nelem-1
        force1(ielem) = force1(ielem) - 0.5*[[[globmass(ielem,nelem)-
    [[eleprop(ielem,1).*elength(ielem)]./[elength(nelem).*eleprop(nelem,1)
]].*globmass(nelem,nelem)]*gainter(k)]-[[globstif(ielem,nelem)-
    [[eleprop(ielem,1).*elength(ielem)]./[elength(nelem).*eleprop(nelem,1)
]].*globstif(nelem,nelem)]*Def(k)]];
    end
    force1 = gainter(k);
    delf = force1 - force; % delta f
```



```

    %delu1 = Mhat\(Khat*delu-Chat*delu_1+delf); % additional displacement
for delta f
    b1 = Khat*delu-Chat*delu_1+delf;
    delu1 = pinv(Mhat) *b1;

    Uk1 = Uk1 + delu1; % total displacement

    constidamp % script that calculates stress, strain and modulus and
changes the stiffness matrix
    if mod(isec,indelt)==0
        l = l + 1;
        uksur(l) = Uk1(11); % deformation vector of the surface element
    end

    % saves the values of the present time step to that of the previous
time step for the calculations of the next time step
    delu_1 = delu;
    delu = delu1;
    force = forcel;

end
saver % saves the variables needed to be plotted
%clear all % clears all the variables
%loader % loads the variables to be plotted
crout % Outputs stress-strain Figure.

% constidamp.m
% updates the stiffness matrix

%Uknode = zeros(nelem+1,1); % initializes nodal deformation vector
Uknode = Uk1;

% stores the nodal deformations
%for inode=2:nelem+1
%    Uknode(inode) = Uk1(inode-1);
%end

%
% calculates strain
%
for ielem =1:nelem-1
    difdisp(ielem) = Uknode(ielem+1)-Uknode(ielem);
end
for ielem = 1:nelem-1
    elength1(ielem)= elength(ielem) ;
end
strain(:,k) = difdisp./elength1';

%rehystress1 % calculates stress and inst. shear modulus
effihyster
%bb
    mul=[mu; eleprop(nelem,2)];
globstif = kasdamp(nelem,elength,mul); % modifies global stiffness matrix

```

```

Khat = ((-1)*globstif) + ((2/(deltat*deltat))*globmass); % modifies
coefficient matrix of Uk

%contodis.m
t = [0 1.5 3.5 6.5 8.5 10.5];
b1 = [40 1.2 2.0 2.8 4.0 6.8];
b2 = [560 2.4 28.0 50.4 78.0 146];
c1 = [20400 400 450 980 1432 2660];
c2 = [2120000 13600 18000 58800 8e4 2e5];
c3 = [5.6e7 53600 4e5 1360000 2.08e6 5.36e6];
ti = [0:10.5:0.5];
blin =interp1(t,b1,ti, 'linear');
b2in =interp1(t,b2,ti, 'linear');
c1in =interp1(t,c1,ti, 'linear');
c2in =interp1(t,c2,ti, 'linear');
c3in =interp1(t,c3,ti, 'linear');
k = 0;
for time = 0:10.5:0.5
    k = k + 1;
    num = [0 0 blin(k) b2in(k)];
    den = [1.0 c1in(k) c2in(k) c3in(k)];
    [dn dd] = c2dm[num,den,inv(1024), 'tustin'];
    dnum = [dnum; dn];
    dden = [dden; dd];
end
tm = 0:10.5:0.5;
plot(t,dnum(:,1))
plot(t,dnum(:,2))
plot(t,dnum(:,3))
plot(t,dnum(:,4))
plot(t,dden(:,1))
plot(t,dden(:,2))
plot(t,dden(:,3))
plot(t,dden(:,4))

% crout.m
% output script for the program waveinter

%
% plots stress-strain history
%
for ielem = 1:nelem-1
    ielcr = find(elecr==ielem); % finds for which elements stress-strain
Figure is to be plotted
    if isempty(ielcr)
        ielcr=[];
    else
        ksec = 0;
        for jsec = 1:ptime/deltat:nstep
            ksec = ksec +1;
            xstrain(ksec) = strain(ielem,jsec);
            ystress(ksec) = sigma(ielem,jsec);
        end
        figure
        plot(xstrain,ystress)
        selem = int2str(ielem);

```

```

        heading = ['Dynamic stress-strain behaviour in element ', selem];
        xlabel('strain')
        ylabel('stress, kN/m^2')
        title(heading)
    end
end

%
% Displacement-time history plot for the surfac element
%
time = 0:indelt:totime;
figure
plot(time,uksur)
xlabel('time, second')
ylabel('displacement, m')
title('Displacement history at layer 11')
%
% Input ground acceleration plot
%
anydat = [0; anydat];
figure
plot(time,anydat)
xlabel('time, second')
ylabel('surface acceleration, m/s^2')
title('input surface acceleration history')
%
% Output of secant modulus
%
for ielem = 1:nelem-1
    figure
    i = find(reverse(:,1,ielem));
    mx = max(i);
    plot(reverse(1:mx,1,ielem),reverse(1:mx,2,ielem))
    xlabel('time, second')
    ylabel('secant modulus, kN/m^2')
    selem = int2str(ielem);
    heading = ['Change of secant modulus with time at layer ',selem];
    title(heading)
end
size(Mhat)
size(Khat)
size(Chat)
size(globmass)
size(globstif)
size(globdamp)
det(globmass)
det(globstif)
det(globdamp)
det(Mhat)
det(Chat)
det(Khat)

% dampin.m
% creates input data for the program wavedamp

%
% Element information
%
nelem = 14; % number of elements

```

```

% elements are numbered from rigid base to surface %

%length = [2; 2; 2; 2; 2; 2; 2; 2; 2; 2; 2; 2; 2; 2; 2; 2; 2; 2; 2];
% length of elements
length = [3.0; 3.0; 5.0; 2.875; 2.875; 2.875; 2.875; 0.9; 3.05; 3.05;
3.05; 3.05; 3.6; 3.8];
% element properties [ density, initial shear modulus and ref. strain ]
eleprop = [0.194 6867 0.002; 0.194 6867 0.002; 0.194 5026 0.0018; 0.143
3634 0.003; ...
0.143 3634 0.003; 0.143 3634 0.003; 0.143 3634 0.003; 0.194
5816 0.0012; ...
0.143 3648 0.002; 0.143 3648 0.002; 0.143 3648 0.002; 0.143
3648 0.002; ...
0.194 3241 0.0005; 1.6 40000 .001];
% 1.6 40000 0.001; 1.6 40000 0.001; 1.6 40000 0.001; 1.6 40000
0.001; ...
% 1.6 40000 0.001; 1.6 40000 0.001; 1.6 40000 0.001; 1.6 40000
0.001; ...
% 1.6 40000 0.001; 1.6 40000 0.001; 1.6 40000 0.001; 1.6 40000
0.001];

%
% Properties of the rigid bed rock [density, shear modulus]
%
bedprop = [0.255 63750];

%
% Initial condition
%
inicon = [];
% initial condition [ deformation and velocity ]

%
% Base acceleration history
%
deltat = 0.001; % time step for computation
indelt = 0.02; % time step of the acceleration input

load dhaka_eq.dat; % base acceleration: user specified .dat file/ user
should
% change the file name of this line and two lines
following this
anydat = dhaka_eq; % instead of user specified file name variable anydat
will be
% used for subsequent calculations

clear dhaka_eq;
load Def.dat;

%%%%%loading an impulse at 0.5 sec
%preced = zeros((0.5/indelt)-1,1);
%trail = zeros(9.5/indelt,1);
%anydat = [preced; 100; trail];
%clear preced;
%clear trail;

totime = (length(anydat)*indelt); % total duration of the input

inptime = indelt:indelt:totime;

```

```

intertime = indelt:deltat:totime;

% nstep = fix(totime/deltat); % number of calculation steps
interstep = fix(indelt/deltat); % number of interpolations needed between
two
                                % input data
% gainter = zeros(nstep,1); % initializing the final base acceleration
variable

gainter = interp1(inptime,anydat,intertime);

%% replacing the input data into final base acceleration variable
% for inpstep = 1:length(anydat)
%   gainter(interstep*inpstep) = anydat(inpstep);
% end

%
nhyper =2; % value of n in hyperbolic model

%
% Output control
%
stime = 10; % number of times the value of the time-loop execution be
shown in the monitor
% resint = 10; % Time interval for plotting ground response
% elecr = [ 1:nelem ]; % elements for which stress-strain graph is plotted
% ptime = 0.02; % time interval for plotting

% effihyster.m
% calculates stress according to the hyperbolic constitutive model

%
% loop for each element
%
for ielem = 1:nelem-1
    tau_f = eleprop(ielem,2)*eleprop(ielem,3); % asymptotic stress
    %
    % for the first time step
    %
    if k == 1
        slope1(ielem) = sign(strain(ielem,k)); % if it is in the positive
or negative quadrant
        sigma(ielem,k) = tau_f*(1-1/(1+(nhyper-
1)*abs(strain(ielem,k)/eleprop(ielem,3))) ...
        ^ (1/(nhyper-1))) * sign(strain(ielem,k)); % back-bone stress
        mu(ielem) = eleprop(ielem,2)*(1-abs(sigma(ielem,k)/tau_f))^nhyper;
% back-bone slope
    %
    % for all other time steps
    %
    else
        slope2(ielem) = sign(strain(ielem,k) - strain(ielem,k-1)); % if
strain is increasing or decreasing
    %
    % checks if reversal
    %
    if slope1(ielem)*slope2(ielem)<0

```

```

        slope1(ielem) = slope2(ielem); % updates slope1 after stress
reversal
        govcount(ielem) = govcount(ielem) + 1; % increases the counter
of reversal
        govstore(govcount(ielem),:,ielem) = [sigma(ielem,k-1)
strain(ielem,k-1)];
        % stores the reversal stress and strain
        prevtau(ielem) = revtau(ielem); % stores the immediately
previous reversal stress
        prevgama(ielem) = revgama(ielem); % stores the immediately
previous reversal strain
        revtau(ielem) = sigma(ielem,k-1); % stores the value of stress
when reversal occurred
        revgama(ielem) = strain(ielem,k-1); % stores the value of strain
when reversal occurred
        revcount(ielem) = revcount(ielem) + 1; % keeps count of number
of reversals
        reverse(revcount(ielem),:,ielem) = [isec ((revtau(ielem) -
prevtau(ielem)) ...
        / (revgama(ielem) - prevgama(ielem))]); % for each reversal
stores the secant shear modulus
        elseif slope1(ielem) == 0 % if strain is initially 0
            slope1(ielem) = slope2(ielem); % for the check of slope when it
becomes nonzero
        end
        %
        % depending on the order of loop, stress is calculated
        %
        switch govcount(ielem)
        %
        % if it is on the back-bone Figure
        %
        case 1
            sigma(ielem,k) = tau_f*(1-1/(1+(nhyper-
1)*abs(strain(ielem,k)/eleprop(ielem,3)))) ...
            ^ (1/(nhyper-1))*sign(strain(ielem,k)); % back-bone stress
            mu(ielem) = eleprop(ielem,2)*(1-
abs(sigma(ielem,k)/tau_f))^nhyper; % back-bone slope
            %
            % if it is the first reversal from the back-bone Figure
            %
            case 2
                if abs(strain(ielem,k)) < abs(govstore(2,2,ielem)) % if it
doesn't intersect back-bone Figure
                    sigma(ielem,k) = 2*tau_f*(1-1/(1+(nhyper-
1)*abs((strain(ielem,k)-govstore(2,2,ielem))/ ...
                    (2*eleprop(ielem,3)))) ^ (1/(nhyper-
1)))*sign(strain(ielem,k)-govstore(2,2,ielem)) ...
                    + govstore(2,1,ielem); % stress on the reversal path
                    mu(ielem) = eleprop(ielem,2)*(1-abs((sigma(ielem,k)-
govstore(2,1,ielem)) ...
                    / (2*tau_f))^nhyper; % slope on the reversal path
                else % if it intersects back-bone Figure
                    sigma(ielem,k) = tau_f*(1-1/(1+(nhyper-
1)*abs(strain(ielem,k)/eleprop(ielem,3)))) ...
                    ^ (1/(nhyper-1))*sign(strain(ielem,k)); % back-bone
stress
                    mu(ielem) = eleprop(ielem,2)*(1-
abs(sigma(ielem,k)/tau_f))^nhyper; % back-bone slope
                    govcount(ielem) = 1; % reestablishes on the back-bone

```

```

end
%
% if it is the second reversal from the back-bone Figure
%
case 3
sigma(ielem,k) = 2*tau_f*(1-1/(1+(nhyper-
1)*abs((strain(ielem,k)-govstore(3,2,ielem))/ ...
(2*eleprop(ielem,3))))^(1/(nhyper-
1))) * sign(strain(ielem,k)-govstore(3,2,ielem)) ...
+ govstore(3,1,ielem); % stress on the reversal path
mu(ielem) = eleprop(ielem,2)*(1-abs((sigma(ielem,k)-
govstore(3,1,ielem)) ...
/(2*tau_f)))^nhyper; % slope on the reversal path
if slope2(ielem)*strain(ielem,k)>0 % quadrants of the back-bone
Figure
bsigma1 = tau_f*(1-1/(1+(nhyper-
1)*abs(strain(ielem,k)/eleprop(ielem,3)))) ...
^(1/(nhyper-1)) * sign(strain(ielem,k)); % back-bone
stress
bsigma2 = tau_f*(1-1/(1+(nhyper-1)*abs(strain(ielem,k-
1)/eleprop(ielem,3)))) ...
^(1/(nhyper-1)) * sign(strain(ielem,k-1));
% stress for the strain of the previous time-step if it were
on the back-bone Figure
%
% if it intersects with the back-bone Figure
%
if ((sigma(ielem,k-1)>bsigma2 & sigma(ielem,k)<=bsigma1) |
...
(sigma(ielem,k-1)<bsigma2 & sigma(ielem,k)>=bsigma1))
sigma(ielem,k) = bsigma1; % stress assigned as back-bone
stress
mu(ielem) = eleprop(ielem,2)*(1-
abs(sigma(ielem,k)/tau_f))^nhyper;
% back-bone slope
govcount(ielem) = 1; % reestablishes on the back-bone
end
end
%
% if the order of loop is greater than three
%
otherwise
sigma(ielem,k) = 2*tau_f*(1-1/(1+(nhyper-
1)*abs((strain(ielem,k)-govstore(govcount(ielem),2,ielem)) ...
/(2*eleprop(ielem,3))))^(1/(nhyper-
1))) * sign(strain(ielem,k)-govstore(govcount(ielem),2,ielem)) ...
+ govstore(govcount(ielem),1,ielem); % stress in the current
loop
mu(ielem) = eleprop(ielem,2)*(1-abs((sigma(ielem,k)-
govstore(govcount(ielem),1,ielem))/(2*tau_f)))^nhyper;
% slope in the current loop
govpt = govcount(ielem) -2; % identifier of the reversal point
of the previous loop
ensigma1 = 2*tau_f*(1-1/(1+(nhyper-1)*abs((strain(ielem,k-1)-
govstore(govpt,2,ielem))/ ...
(2*eleprop(ielem,3))))^(1/(nhyper-1))) * sign(strain(ielem,k-
1)-govstore(govpt,2,ielem)) ...
+ govstore(govpt,1,ielem); % stress on the Figure of the
previous loop for the strain of the
% last time step

```

```

        ensigma2 = 2*tau_f*(1-1/(1+(nhyper-1)*abs((strain(ielem,k)-
govstore(govpt,2,ielem))/ ...
        (2*eleprop(ielem,3))))^(1/(nhyper-
1))) * sign(strain(ielem,k)-govstore(govpt,2,ielem)) ...
        + govstore(govpt,1,ielem); % stress on the Figure of the
previous loop for the present strain
        %
        % check if the current loop intersects the previous one at the
present strain
        %
        if (sigma(ielem,k-1)>=ensigma1 & sigma(ielem,k)<=ensigma2) |
...
            (sigma(ielem,k-1)<=ensigma1 & sigma(ielem,k)>=ensigma2)
            govcount(ielem) = govpt; % establishes the path in the
previous loop
            sigma(ielem,k) = ensigma2; % assigns stress of the previous
loop
            mu(ielem) = eleprop(ielem,2)*(1-abs((sigma(ielem,k)-
govstore(govcount(ielem),1,ielem))/(2*tau_f)))^nhyper;
            % slope of the previous loop
        end
    end
end
end
end

```

```

function mass = elemass(cofactor)
% ELEMASS Element mass matrix
% ELEMASS(ielem,ilength, idensity) provides element mass matrix
% for linear elements.

```

```

mass = (1/6*cofactor)*[2 1; 1 2];

```

```

function stiff = elestif(cofactor)
% ELESTIF Element stiffness matrix
% ELESTIF(ielem,ilength,imodulus) provides element stiffness
% matrix for linear elements.

```

```

stiff = cofactor*[1 -1; -1 1];

```

```

% initdamp.m
% initializes global matrices for subsequent calculation

```

```

globmass = masdamp(nelem,elength,eleprop(:,1)); %global mass matrix
globstif = kasdamp(nelem,elength,eleprop(:,2)); %global stiffness matrix
globdamp = zeros(nelem,nelem);
%globdamp(1,1) = sqrt(bedprop(1)*bedprop(2));
Mhat = (1/(deltat*deltat))*globmass + (1/(2*deltat))*globdamp;
Khat = ((-1)*globstif) + ((2/(deltat*deltat))*globmass);
Chat = (1/(deltat*deltat))*globmass - (1/(2*deltat))*globdamp;

```

```

%
% initialization of displacement vector of one time-step behind
%

```

```

if isempty(inicon)
    Uk = zeros(nelem,1);

```



```

    Uk_1 = Uk;
else
    Uk = inicon(:,1);
    Vk = inicon(:,2);
    Ak = (-1)*(globmass\(globstif*Uk));
    Uk_1 = Uk-deltat*Vk+(deltat*deltat/2)*Ak;
end
revtau = zeros(nelem-1,1); % initializes a vector to store reversal
stresses
revgama = zeros(nelem-1,1); % initializes a vector to store reversal
strains
revcount = ones(nelem-1,1); % initializes a vector to keep count of the
reversals
reverse(1,1:2,1:nelem-1) = zeros(2,nelem-1); % initializes a matrix to
store the secant shear modulus
govcount = ones(nelem-1,1); % initializes a vector to keep count of the
points to be used in the Masing rule
onstrain = zeros(nelem-1,1); % initializes a vector to store the reversal
strain on the back-bone
onbbone = ones(nelem-1,1); % logical variable if stress-strain point is
on the back-bone
gammamax = zeros(nelem-1,1); % initializes maximum strain vector
experienced
difdisp = zeros(nelem-1,1); % initializes a vector to store the difference
of deformation between two nodes of an element
nstep = floor((totime-indelt)/deltat) + 1; % total number of time-steps
sigma = zeros(nelem-1,nstep); % initializes stress vector
strain = zeros(nelem-1,nstep); % initializes strain vector
mu = zeros(nelem-1,1); % initializes modulus vector
uksur = zeros(length(anydat)+1,1); % initializes a vector to store the
displacement time history of the surface element
uksur(1) = Uk(1); % stores the value of surface deformation at 0th time
l = 1;

%
% calculations of the first time step
%
k =1

% nodal force component from the lower element

force = -0.5*[[[globmass(1,nelem)-
[[[eleprop(:,1).*elength]./[elength.*eleprop(:,1)]].*globmass(nelem,nele
m)]*gainter(1)]-[[[globstif(1,nelem)-
[[[eleprop(:,1).*elength]./[elength.*eleprop(:,1)]].*globstif(nelem,nele
m)]*Def(1)]]];
%force = [ force];
% calculation of total nodal force by adding contribution from the higher
element
for ielem = 2:nelem-1
    force(ielem) = force(ielem) - 0.5*[[[globmass(ielem,nelem)-
[[[eleprop(ielem,1).*elength(ielem)]]./[elength(nelem).*eleprop(ielem,1)]]
].*globmass(nelem,nelem)]*gainter(1)]-[[[globstif(ielem,nelem)-
[[[eleprop(ielem,1).*elength(ielem)]]./[elength(nelem).*eleprop(nelem,1)]]
].*globstif(nelem,nelem)]*Def(1)]];
end
force(1)= gainter(1);
%Uk1 = Mhat\(Khat*Uk-Chat*Uk_1+force); % displacement at the first time
step

```

```

b = Khat*Uk-Chat*Uk_1+force;
Uk1 = pinv(Mhat) *b;
if mod(deltat,indelt)==0
    l = l + 1;
    uksur(l) = Uk1(11); % surface deformation at the first time step
end
constidamp % script that calculates stress, strain and modulus and changes
the stiffness matrix

delu = Uk1 - Uk; % delta u
delu_1 = Uk - Uk_1; % delta u_1

function k = kasdamp(n,length,prop)

% KASDAMP global stiffness matrix
% KASDAMP assembles global stiffness matrix
% for 2-node elements connected in series

mubyl = prop./length;
nnode = n+1; % number of nodes
k1 = zeros(nnode,nnode); % initializes the global stiffness matrix
for ielem = 1:n
    elestif = (1/6*mubyl(ielem))*[1 -1; -1 1]; % element stiffness matrix
    for inode = 1:2
        for jnode = 1:2
            % assembled global stiffness matrix
            k1(ielem+inode-1,ielem+jnode-1) = k1(ielem+inode-1,ielem+jnode-
1) + elestif(inode,jnode);
        end
    end
end
for inode = 2:n
    k1 (1,inode)= 0 ;
end

    k1 (1,inode)= 1 ;

for jnode = 2:n
    k1(jnode,1)= 0 ;
end
% elimination of the first row and column of the global stiffness matrix,
since the first node is fixed
%for inode = 1:nnode-1
% for jnode = 1:nnode-1
%     k(inode,jnode) = k1(inode+1,jnode+1);
% end
%end

k = zeros(nnode-1,nnode-1);
for inode= 1:n-1
    for jnode= 1:n-1
        k(inode,jnode)=k1(inode,jnode)-
[[length(inode) .*prop(inode,1) ]./[length(n) .*prop(n,1) ]].*k1(n,jnode);
    end
end
% MASDAMP global mass matrix

```

```

% MASDAMP assembles global mass matrix
% for 2-node elements connected in series

lxden = length.*prop;
nnode = n+1; %number of nodes
m1 = zeros(nnode,nnode); % initializes the global mass matrix
for ielem = 1:n
    elemass = (1/6*lxden(ielem))*[2 1; 1 2]; % element mass matrix
    for inode = 1:2
        for jnode = 1:2
            % assembled global mass matrix
            m1(ielem+inode-1,ielem+jnode-1) = m1(ielem+inode-1,ielem+jnode-
1) + elemass(inode,jnode);
        end
    end
end
for inode = 1:n
    m1(1,inode)= 0 ;
end
for jnode = 1:n
    m1(jnode,1)= 0 ;
end
% elimination of the first row and column of the global mass matrix,
since the first node is fixed
%for inode = 1:nnode-1
% for jnode = 1:nnode-1
%     m(inode,jnode) = m1(inode+1,jnode+1);
% end
%end
m = zeros(nnode-1,nnode-1);
for inode = 1:n-1
    for jnode = 1:n-1
        m(inode,jnode) = m1(inode,jnode) -
[[length(inode).*prop(inode,1)]./[length(n).*prop(n,1)]].*m1(n,jnode);
    end
end

% saver.m
% saves only the variables needed for plotting

%save nelem
%save elecr
%save ptime
%save deltat
%save nstep
%save strain
ksec = 0;
for jsec = 1:ptime/deltat:nstep
    ksec = ksec +1;
    xstrain(ksec) = strain(nelem-1,jsec);
    ystress(ksec) = sigma(nelem-1,jsec);
end
x = xstrain';
clear xstrain
save strain.dat -ascii x
y = ystress';
clear ystress
save sigma
save stress.dat -ascii y

```

```

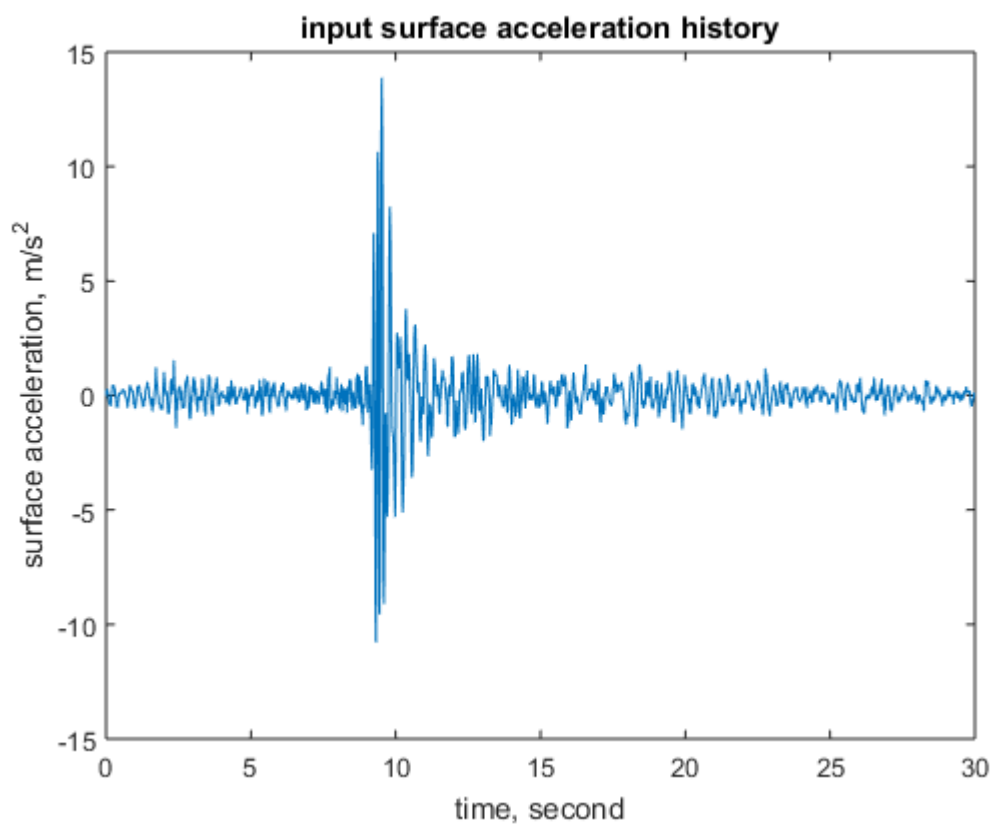
%save indelt
%save totime
%save uksur
save surdisp.dat -ascii uksur
%save anydat
%save reverse
for ielem = 1:nelem-1
    retime = reverse(:,1,ielem);
    selem = int2str(ielem);
    fname = ['save isec',selem,'.dat -ascii retime;'];
    eval(fname);
    secmod = reverse(:,2,ielem);
    fname = ['save gsec',selem,'.dat -ascii secmod;'];
    eval(fname);
end

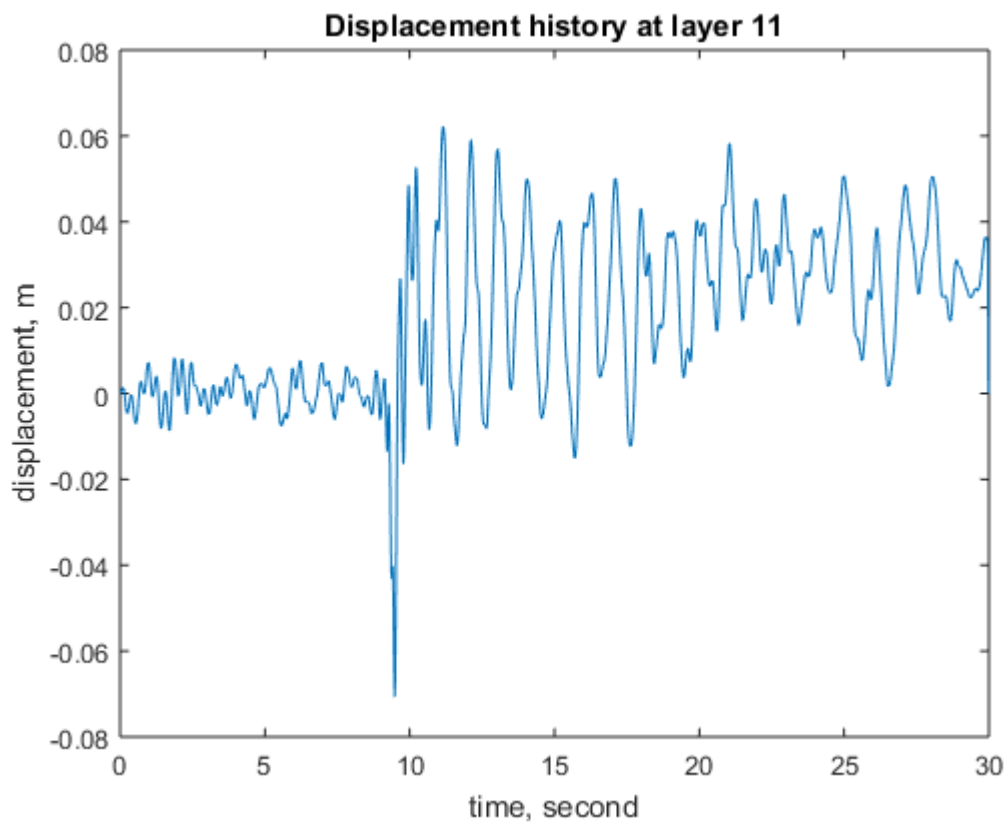
% calculates stress according to the hyperbolic constitutive model with
any value of n
bsigma = 0;
for ielem = 1:nelem
    tau_f = eleprop(ielem,2)*eleprop(ielem,3); % asymptotic stress
    %          bsigma = tau_f*(1-1/(1+(nhyper-
1)*abs(strain(ielem,k)/eleprop(ielem,3)))) ...
    %          ^ (1/(nhyper-1))*sign(strain(ielem,k)); % back-bone stress
    if strain(ielem,k)==0
        bsigma = 0;
        bmu = eleprop(ielem,2);
    else
        romodb = [50 0 1 abs(strain(ielem,k)/eleprop(ielem,3))];
        rb = roots(romodb);
        rindexb = find(imag(rb)==0);
        rrootb = rb(rindexb);
        prootb = find(rrootb>=0);
        if isempty(prootb)
            bsigma =0;
        else
            bsigma = rrootb(prootb)*tau_f*sign(strain(ielem,k));
        end
    %    bmu = eleprop(ielem,2)*(1-abs(bsigma/tau_f))^nhyper; % back-bone
shear modulus
        bmu = eleprop(ielem,2)./(150*(bsigma./tau_f)^2 + 1);
    end
    if onbbone(ielem)==1 % checks if previously it was on the back-bone
Figure
        if abs(strain(ielem,k)) >= abs(gammax(ielem)) % checks if max. strain
is exceeded
            sigma(ielem,k) = bsigma; % stress is equal to back-bone stress
            gammax(ielem) = strain(ielem,k); % updates max. strain
            taumax (ielem)= sigma(ielem,k); % updates max. stress
            mu(ielem) = bmu; % shear modulus is equal to back-bone modulus
        else
            onbbone(ielem) = 0; % stress reversal
            revtau(ielem) = taumax(ielem); % stores the value of stress when
reversal occurred
            revgama(ielem) = gammax(ielem); % stores the value of strain
when reversal occurred
            % checks if strain is decreasing or increasing
            if gammax(ielem)>0
                slopel(ielem) = -1; % strain is decreasing

```

```
else
    slope1(ielem) = 1; % strain is increasing
end
end
end
```

```
load react_Vz.dat;
y = react_Vz;
x = 1:10:621;
z = y(x,:);
save toprot_stiff.dat -ascii z
```





## APPENDIX C

### DISPLACEMENT VARIATION FOR SYNCHRONOUS AND ASYNCHRONOUS EARTHQUAKE

---

#### DISPLACEMENT VARIATION FOR 125 M MODEL

Displacements due to different earthquake data for second bridge (125 m span) along X-axis (along length of the bridge), along Y-axis (along width of the bridge) & along Z-axis (along vertical direction of the bridge) are shown in below.

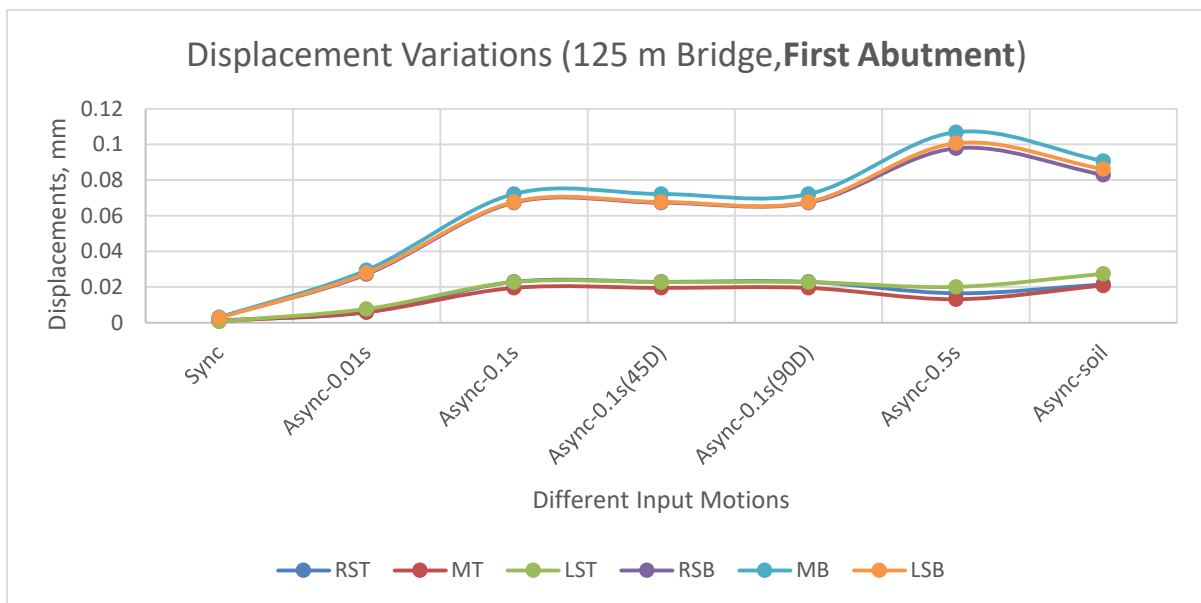


**Figure C.1: Displacement Variation at First Abutment along X-axis**

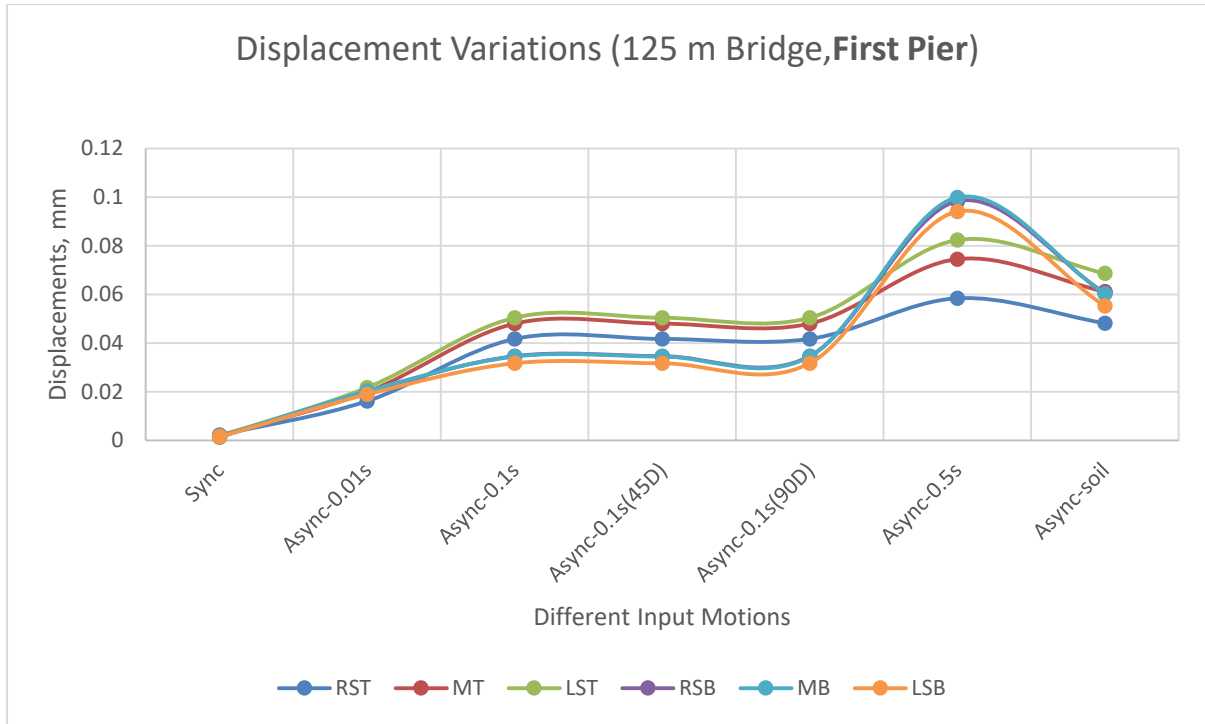


**Figure C.2: Displacement Variation at First Pier along X-axis**

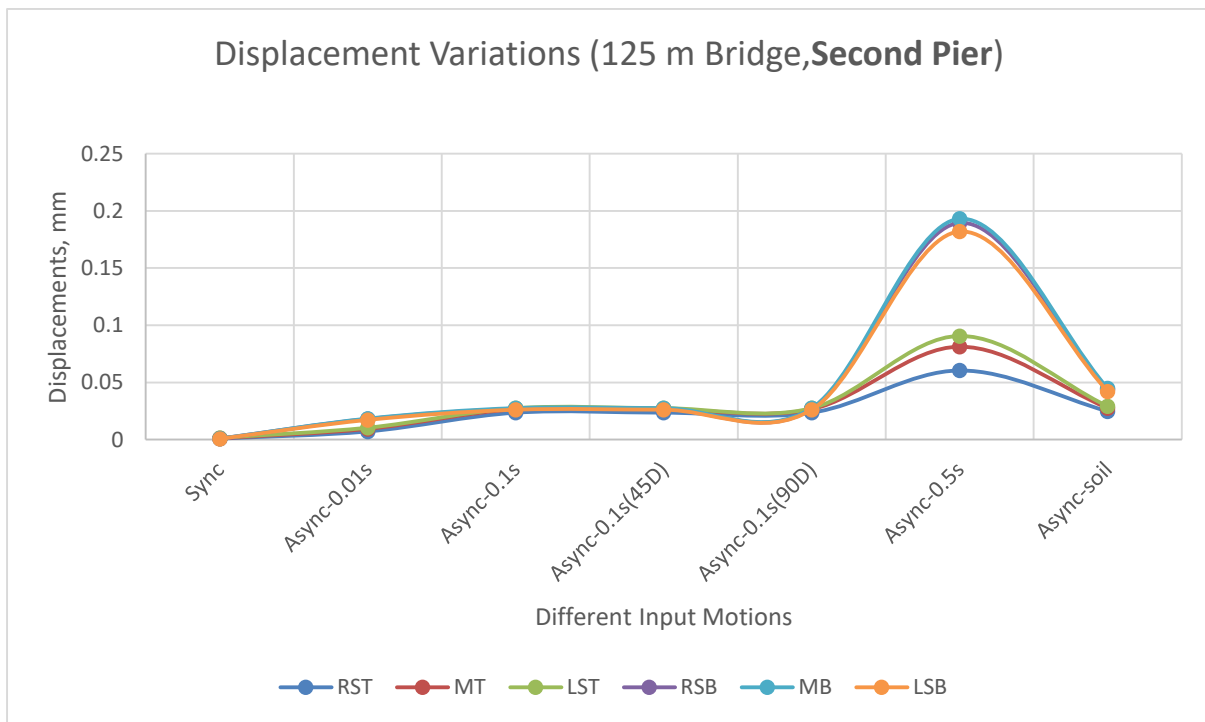


**Figure C.3: Displacement Variation at Second Pier along X-axis**



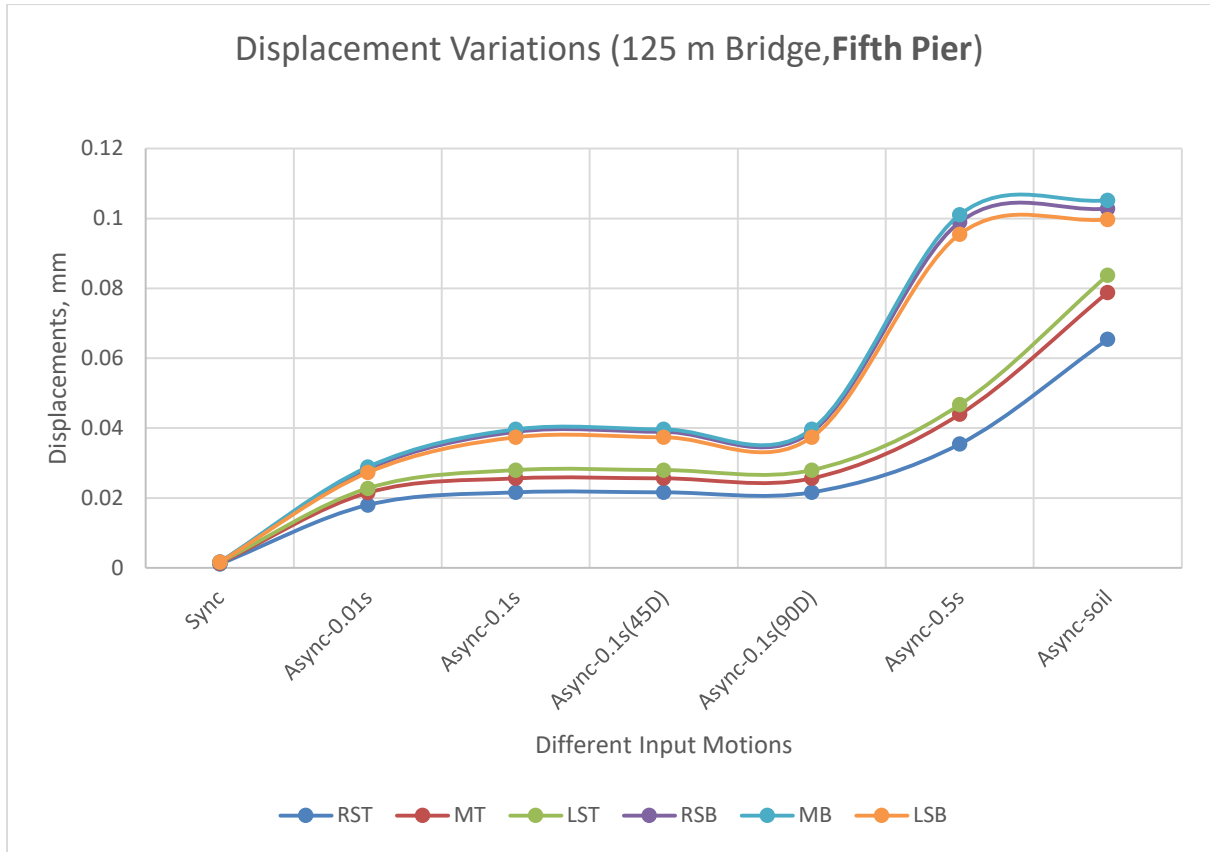


**Figure C.4: Displacement Variation at Fifth Pier along X-axis**

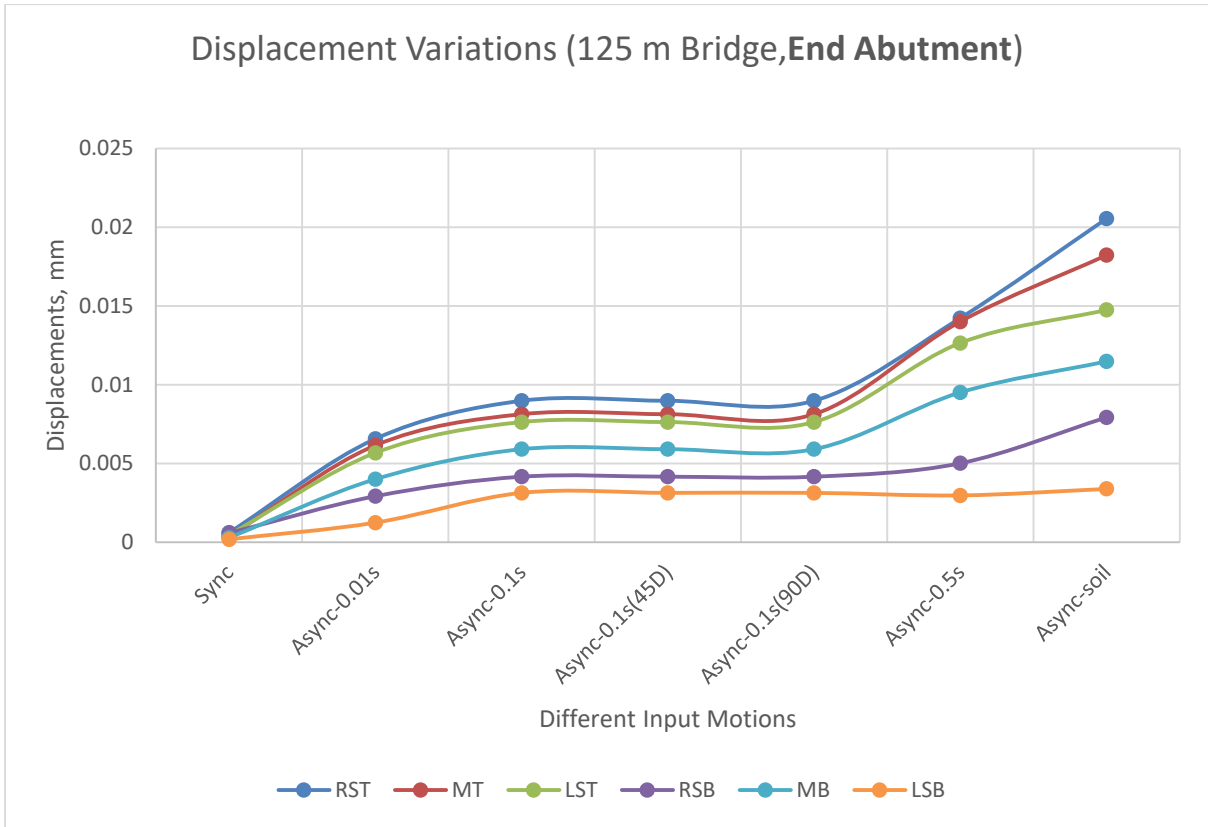


**Figure C.5: Displacement Variation at End Abutment along X-axis**

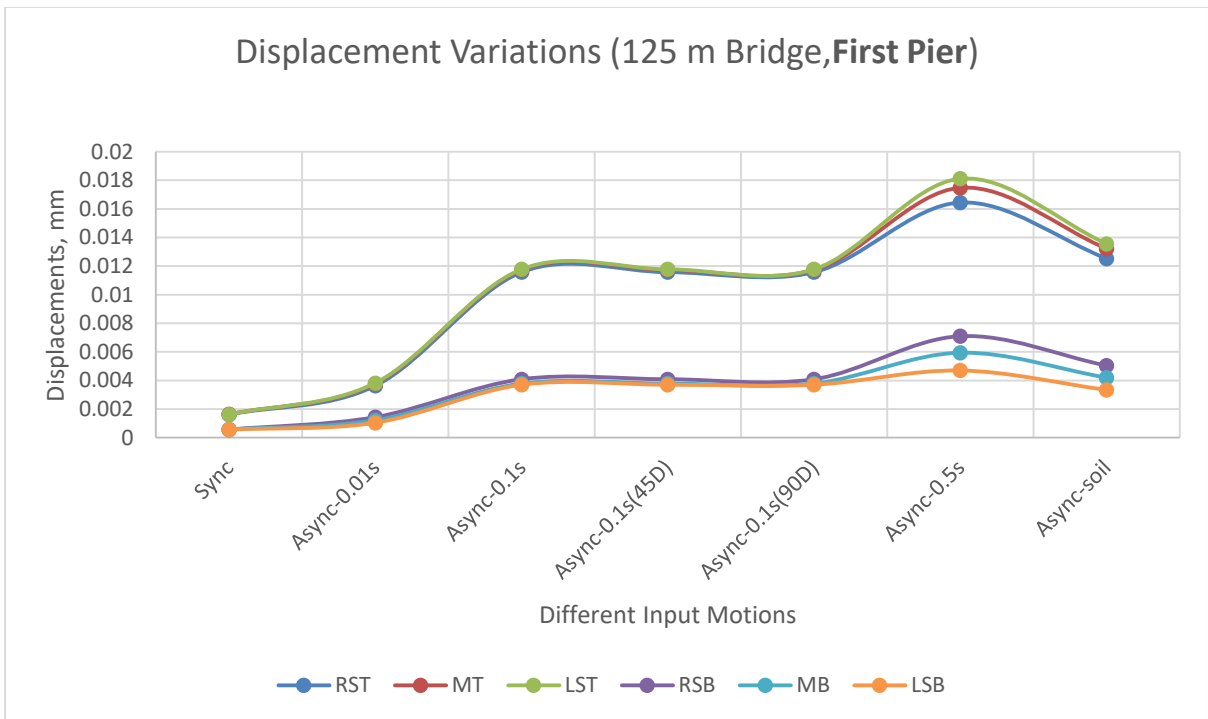


**Figure C.6: Displacement Variation at First Pier along Y-axis**

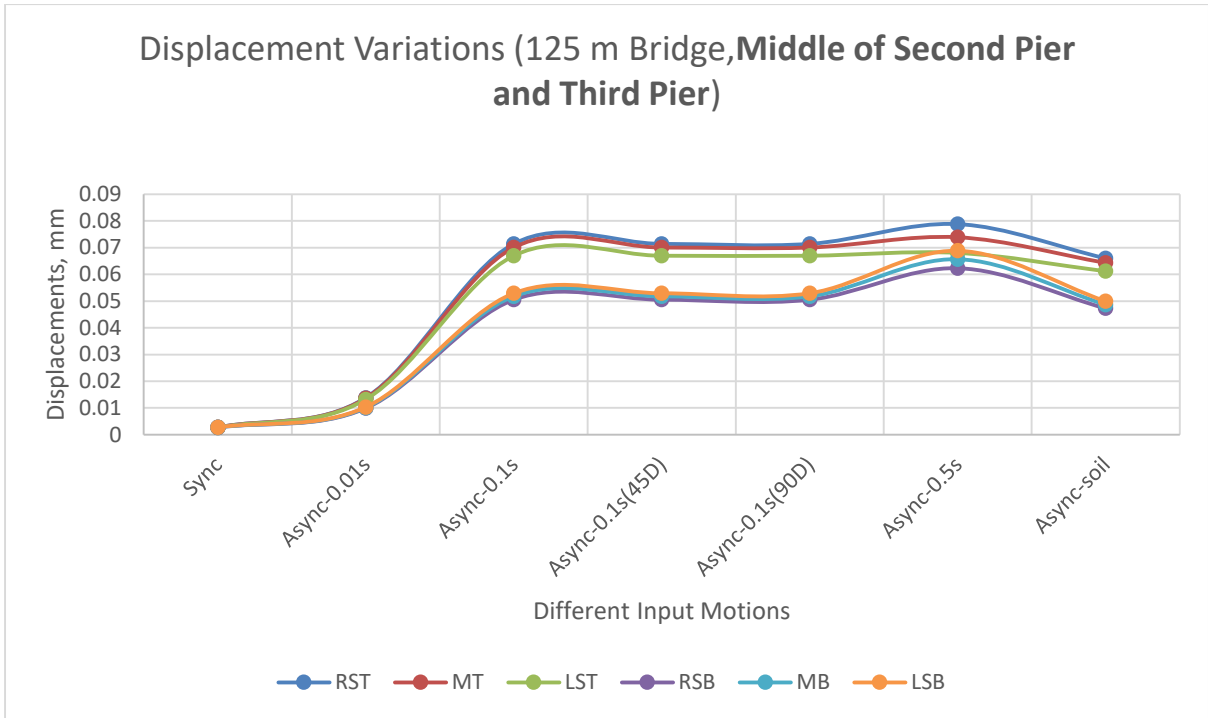


**Figure C.7: Displacement Variation at Middle of Second Pier and Third Pier along Y-axis**

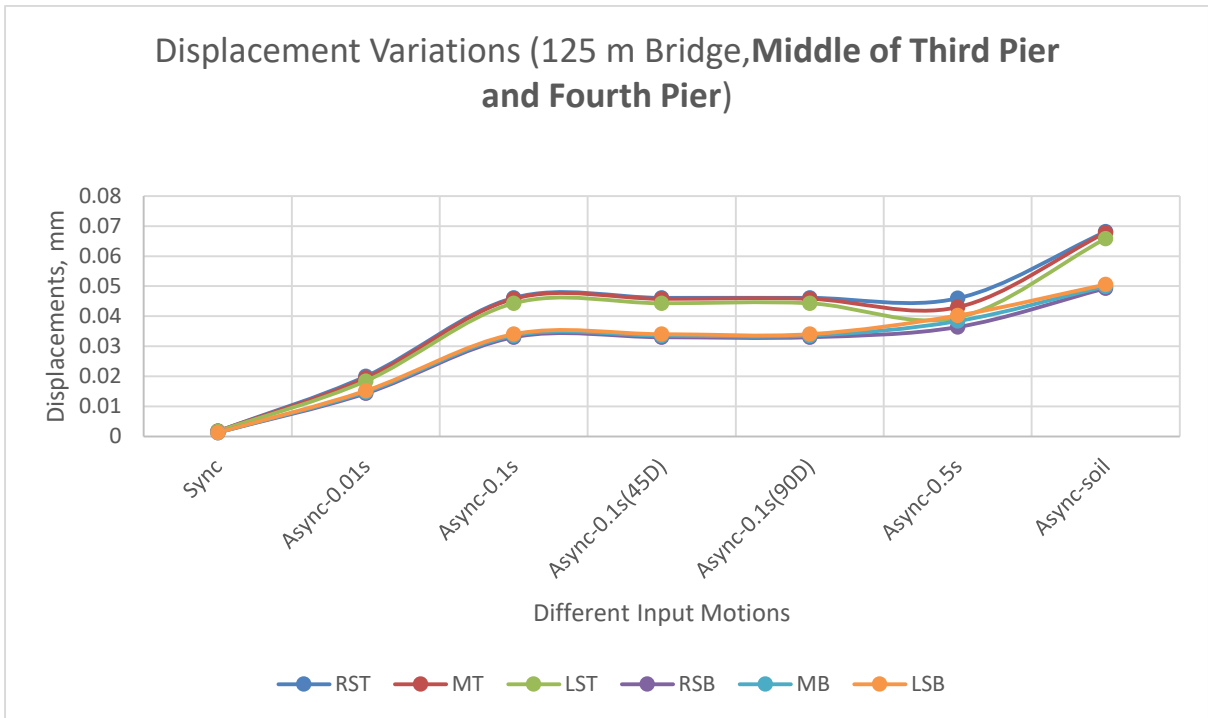


**Figure C.8: Displacement Variation at Middle of Third Pier and Fourth Pier along Y-axis**

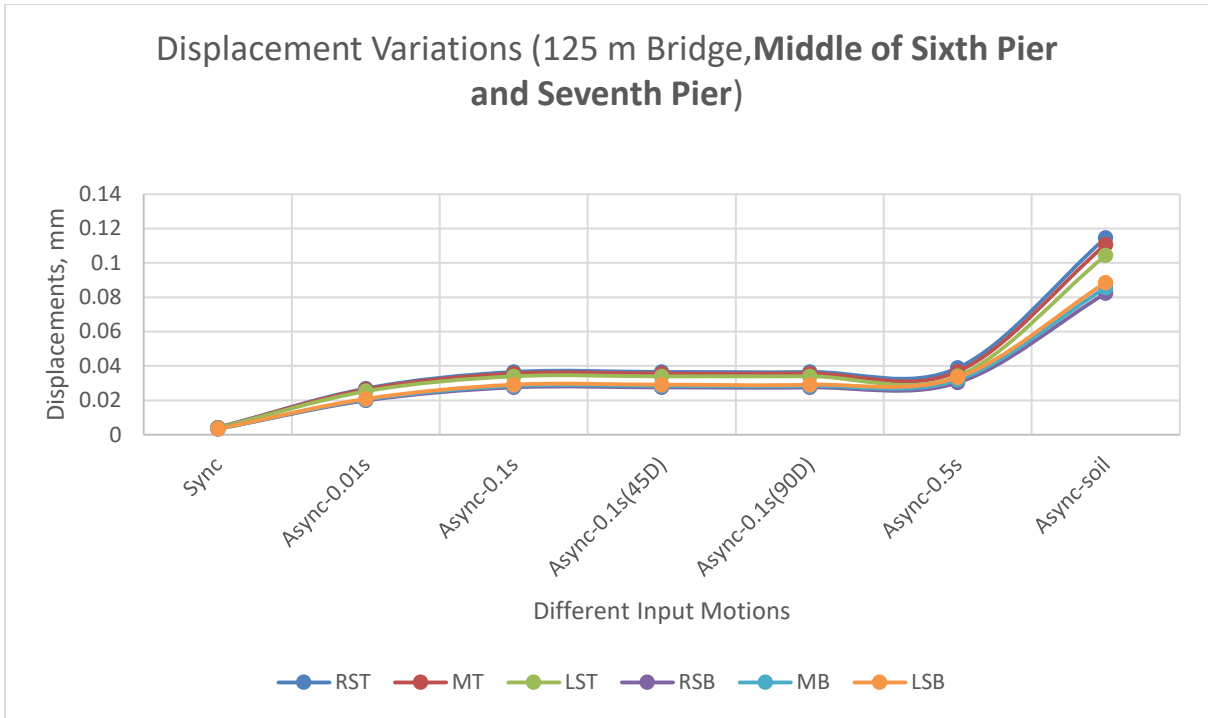


**Figure C.9: Displacement Variation at Middle of Sixth Pier and Seventh Pier along Y-axis**

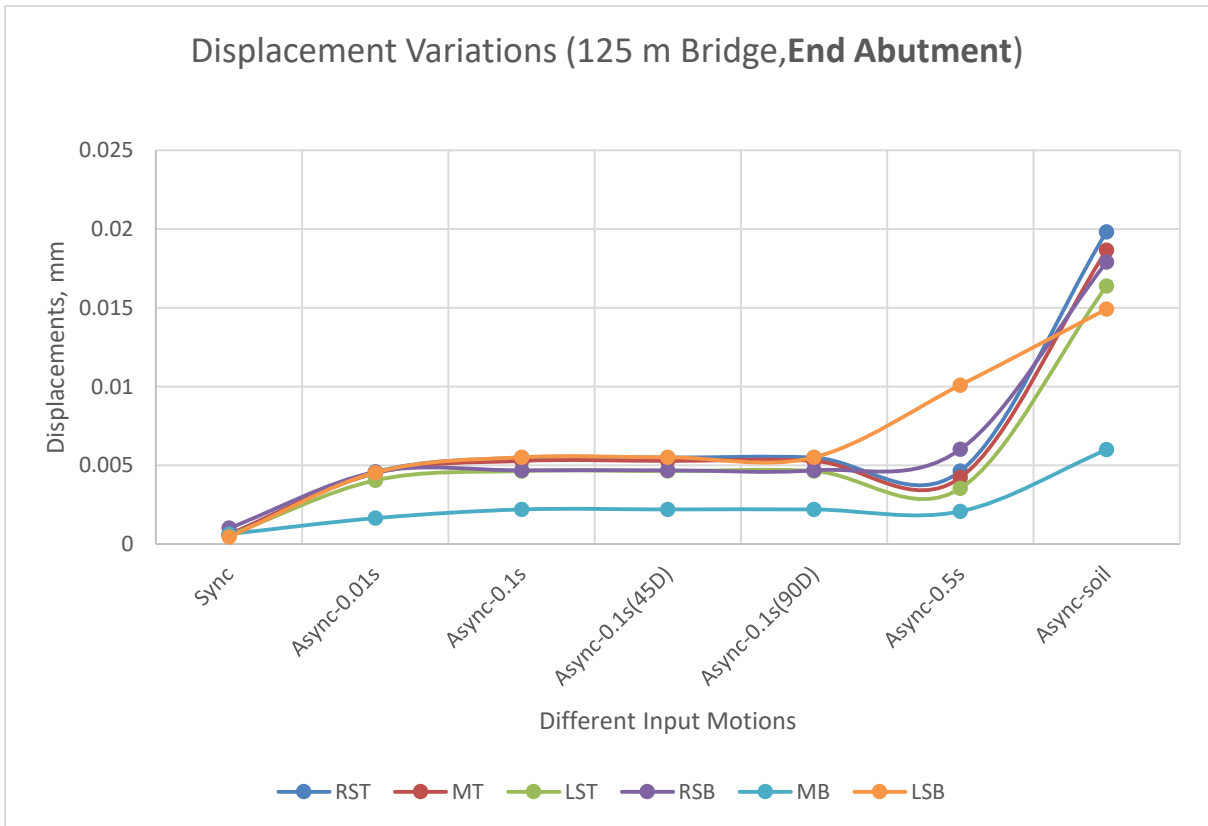


**Figure C.10: Displacement Variation at End Abutment along Y-axis**

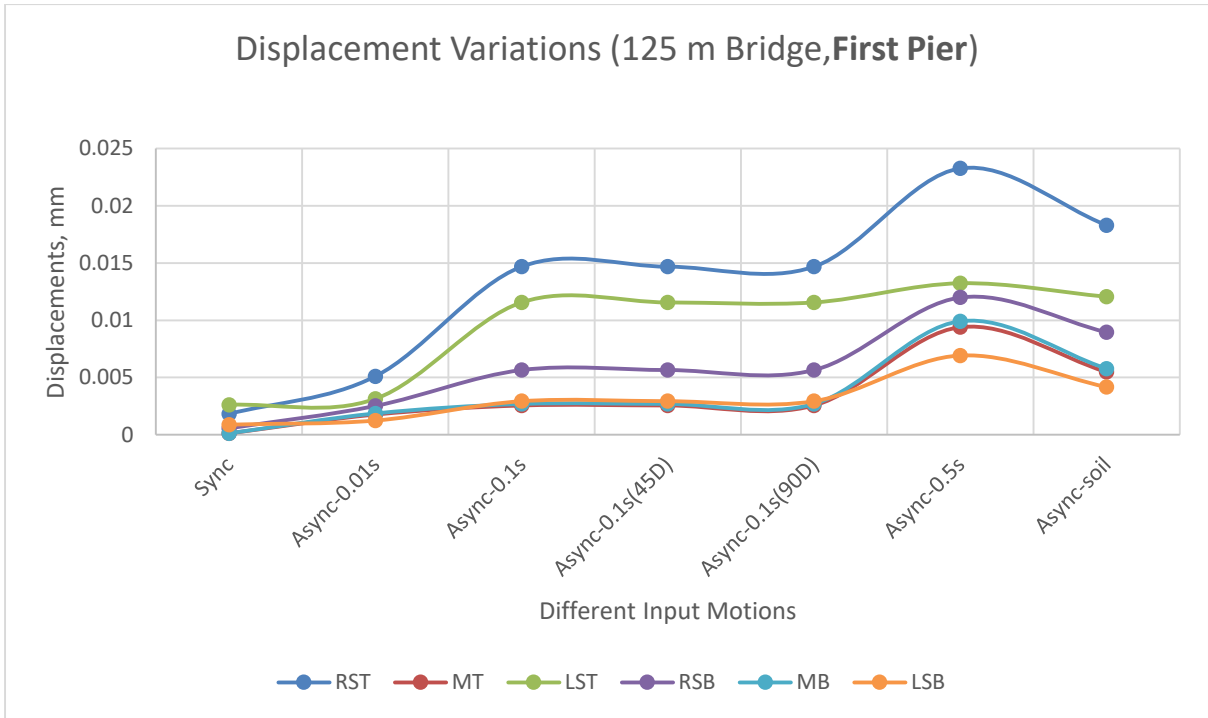


**Figure C.11: Displacement Variation at First Pier along Z-axis**

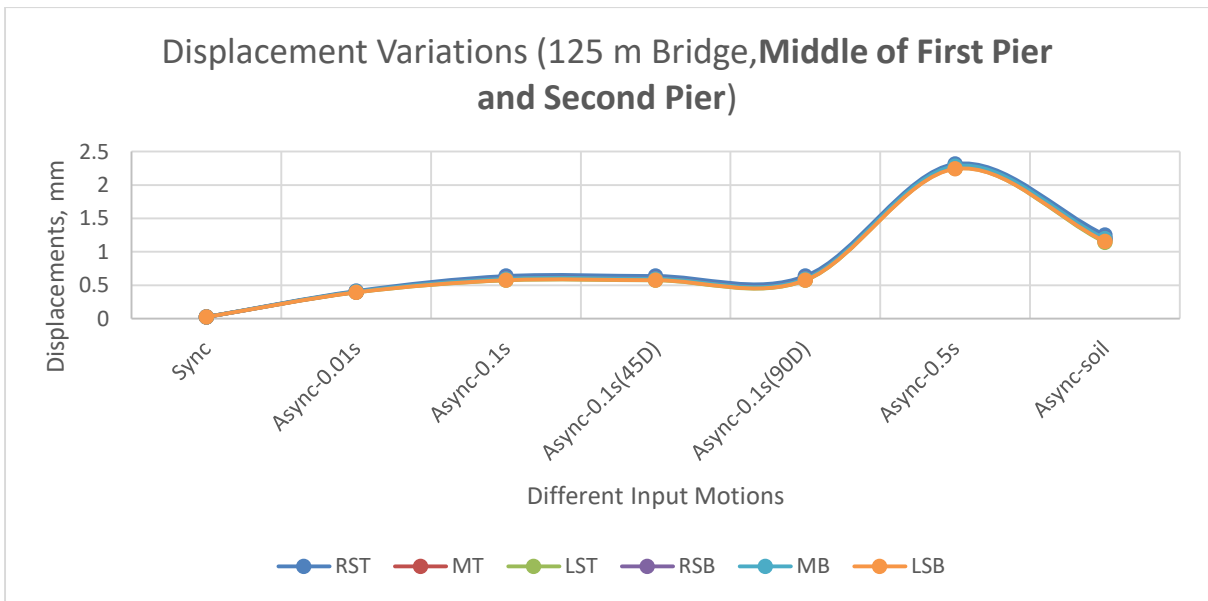


**Figure C.12: Displacement Variation at Middle of First Pier and Second Pier along Z-axis**

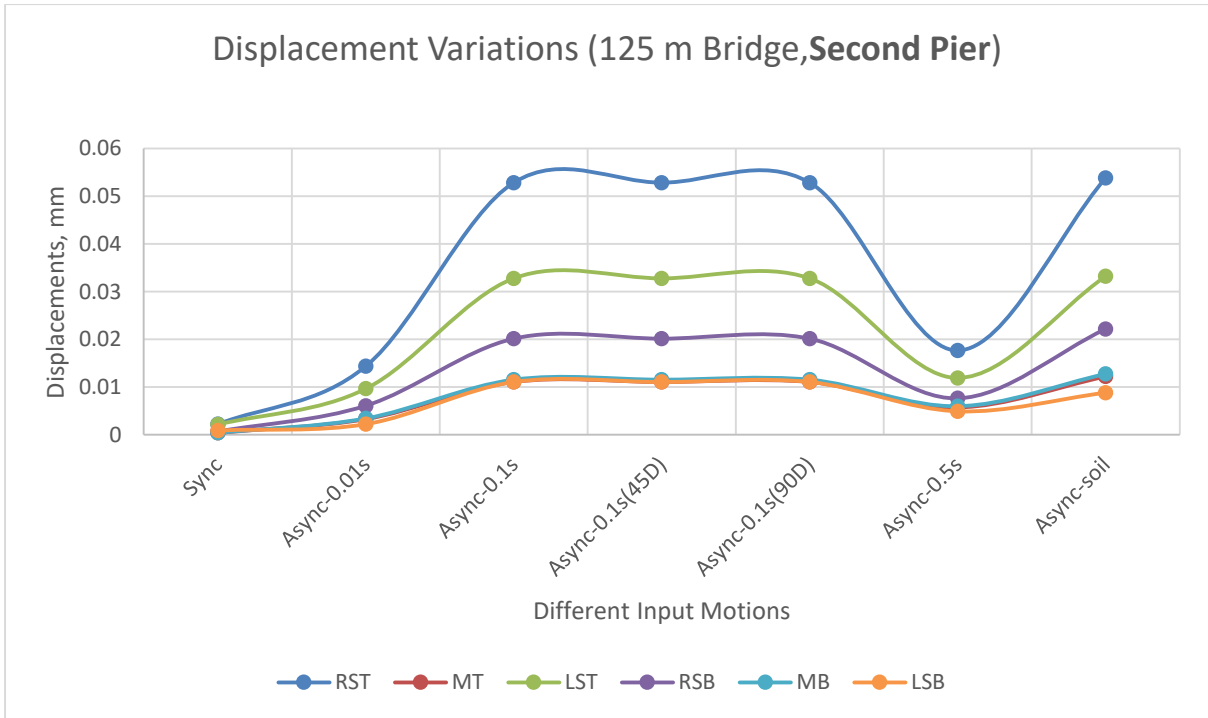


**Figure C.13: Displacement Variation at Second Pier along Z-axis**

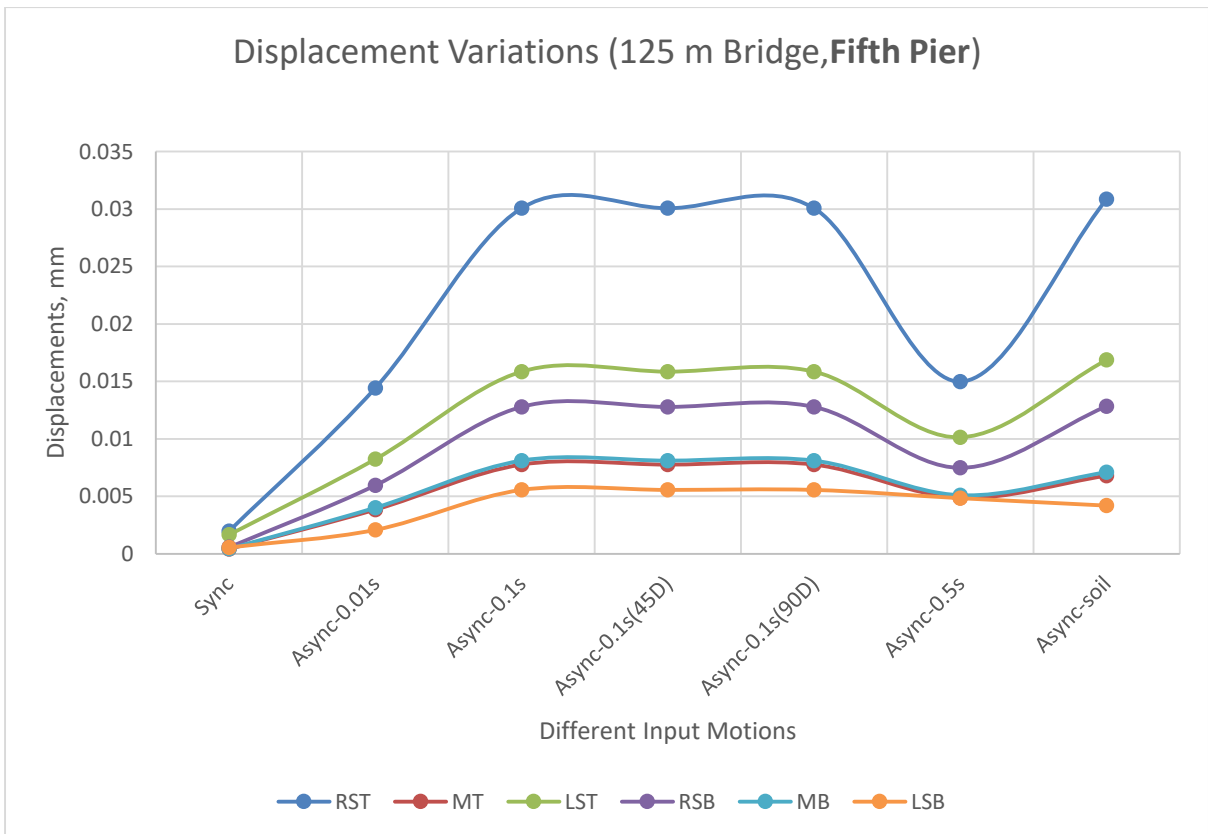


**Figure C.14: Displacement Variation at Fifth Pier along Z-axis**

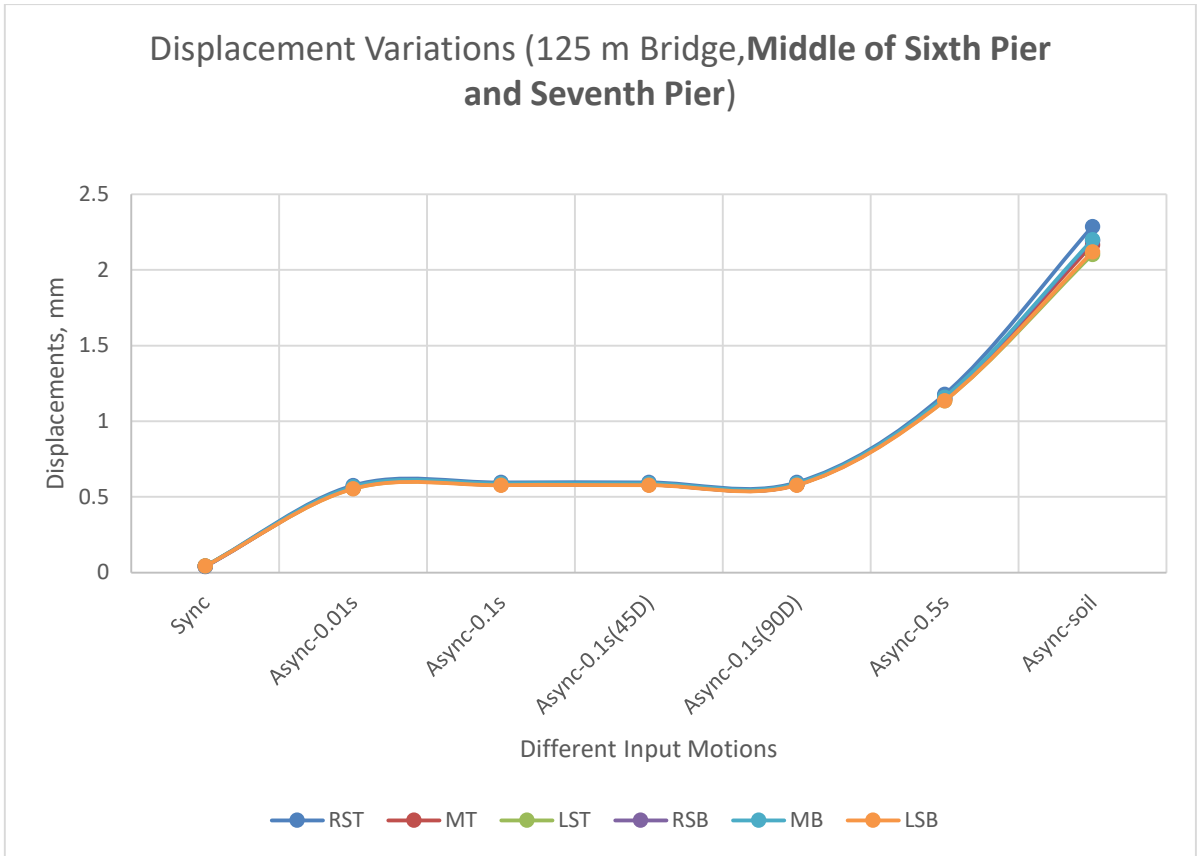


**Figure C.15: Displacement Variation at Middle of Sixth Pier and Seventh Pier along Z-axis**

**SYNCHRONOUS AND ASYNCHRONOUS EFFECT FOR 100 M MODEL ALONG X-AXIS (ALONG LENGTH OF THE BRIDGE)**

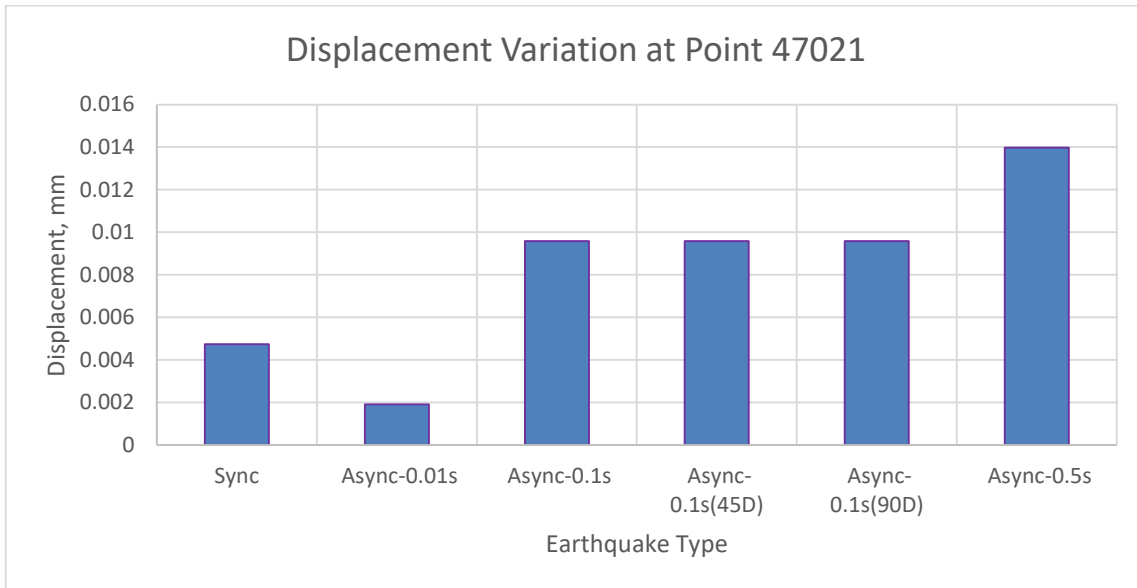


**Figure C.16: Displacement Variation at right side top of middle of second & third pier along X-axis**

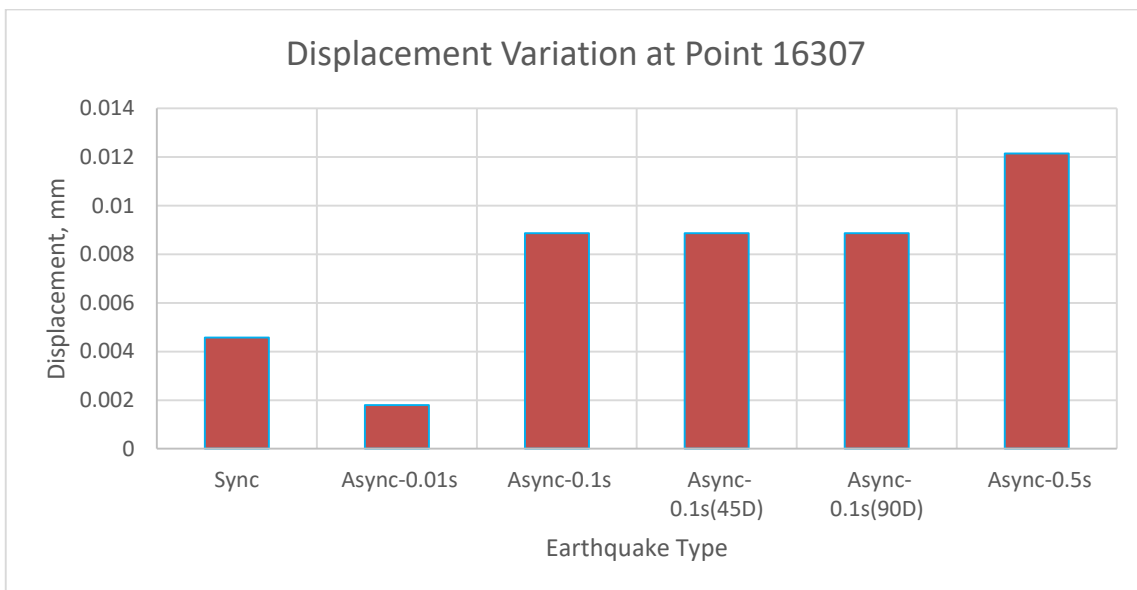


**Figure C.17: Displacement Variation at middle top of middle of second & third pier along X-axis**



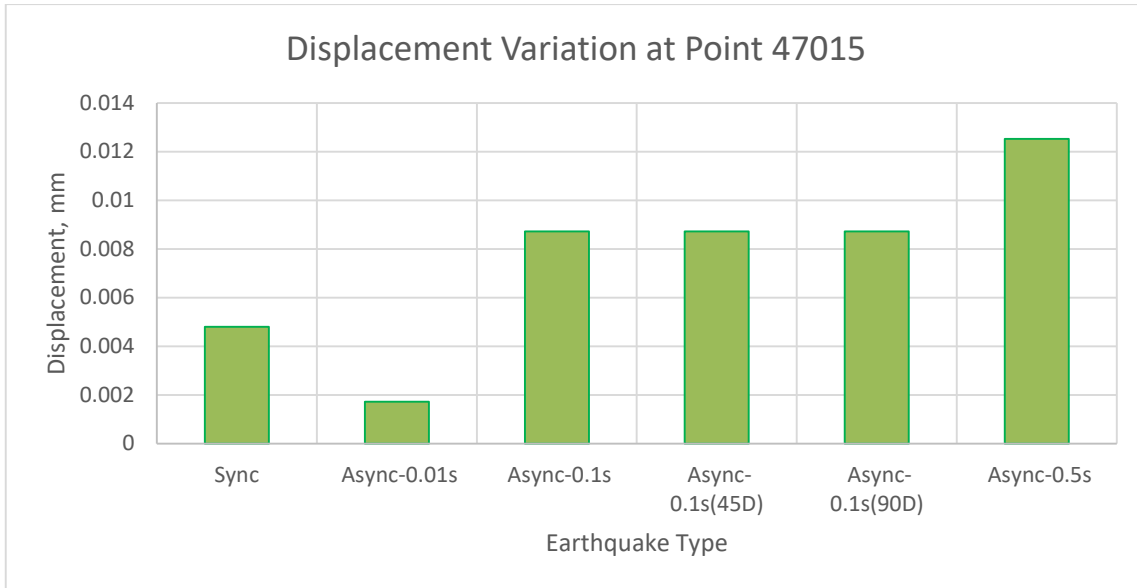


**Figure C.18: Displacement Variation at left side top of middle of second & third pier along X-axis**

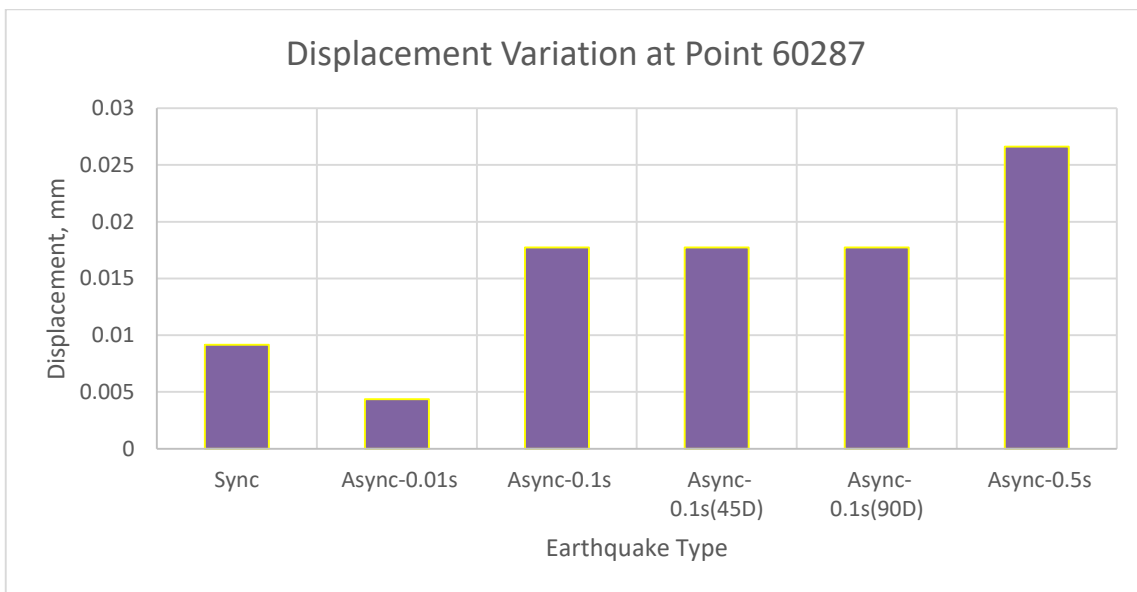


**Figure C.19: Displacement Variation at right side bottom of middle of second & third pier along X-axis**

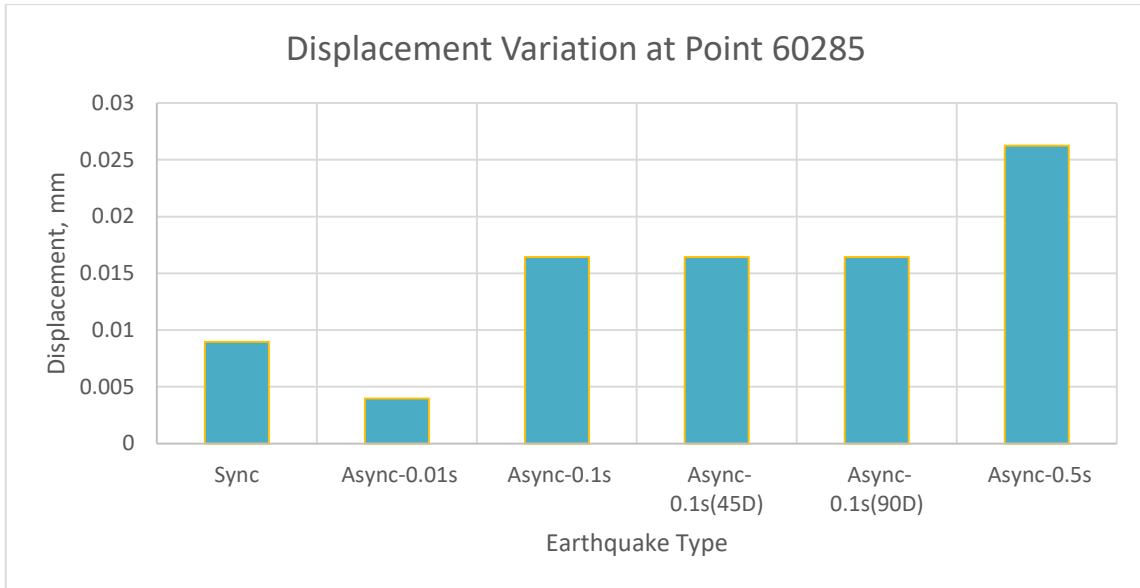


**Figure C.20: Displacement Variation at middle bottom of middle of second & third pier along X-axis**

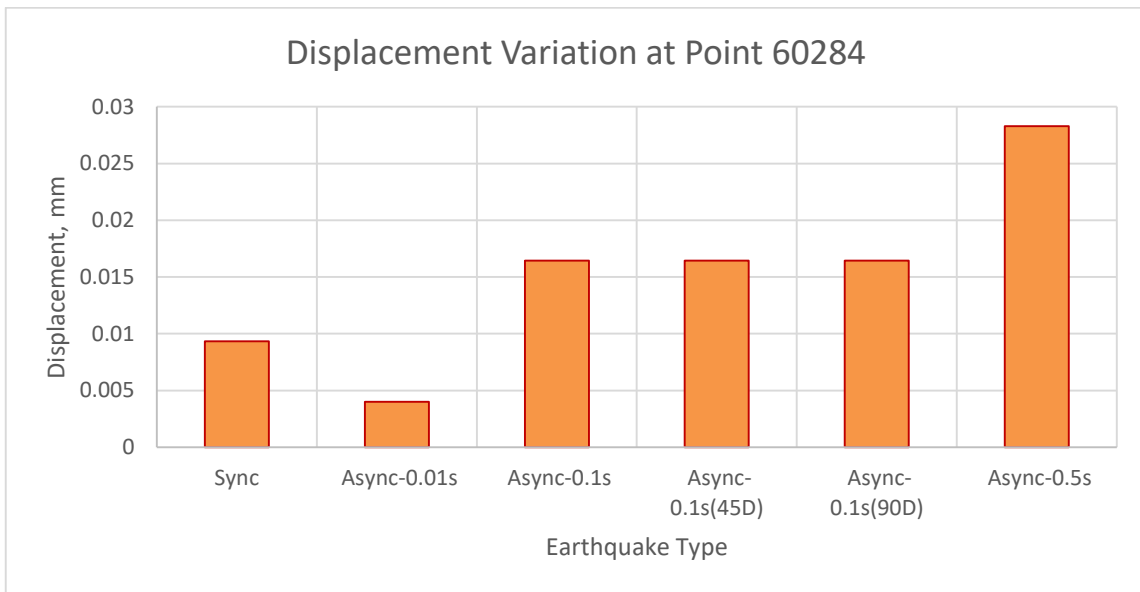


**Figure C.21: Displacement Variation at left side bottom of middle of second & third pier along X-axis**

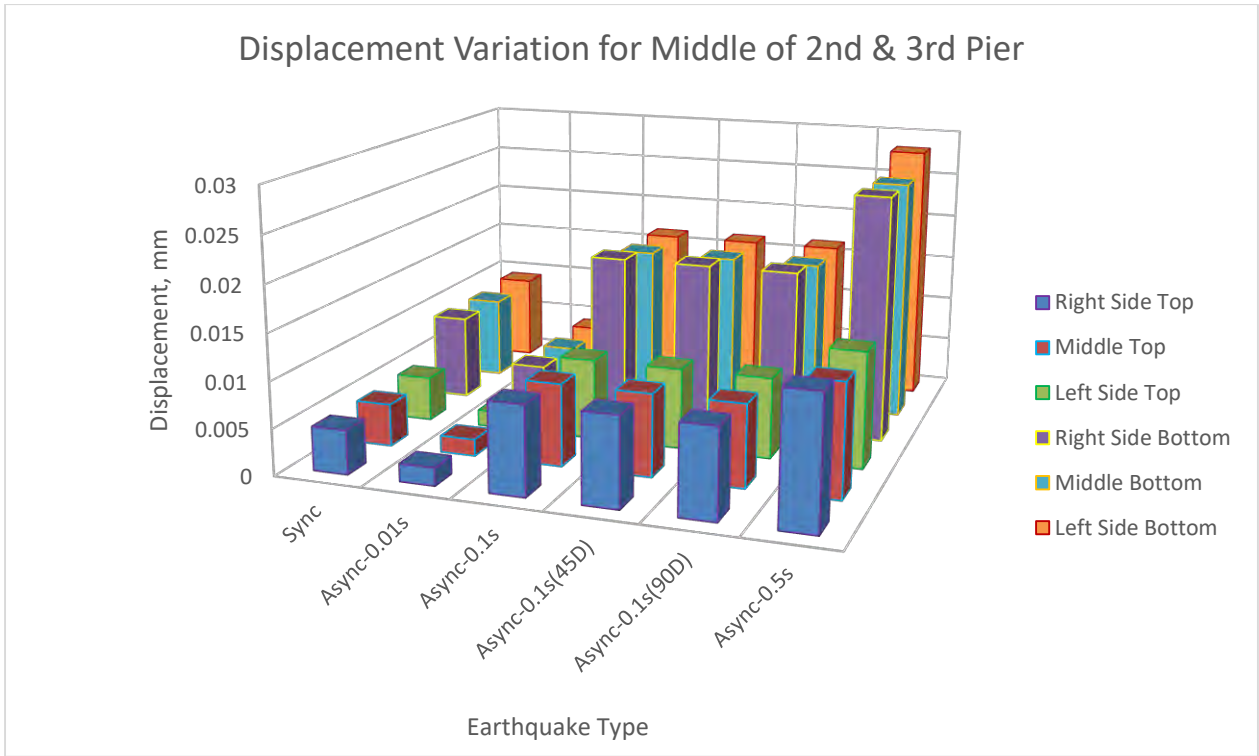


**Figure C.22: Displacement Variation for middle of second & third pier along X-axis**

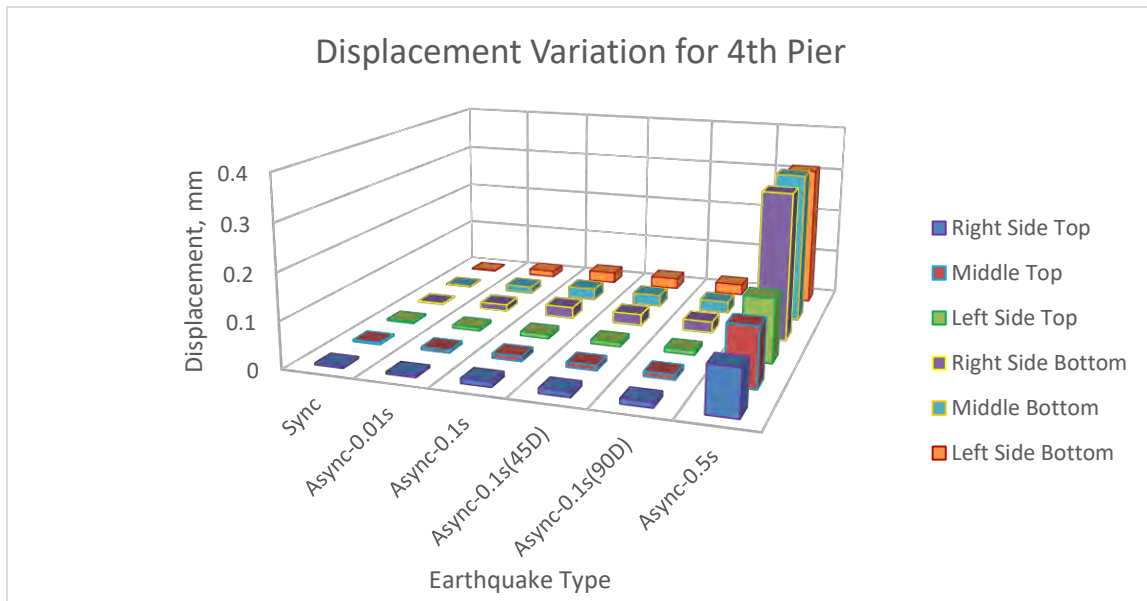


**Figure C.23: Displacement Variation for Fourth Pier along X-axis**

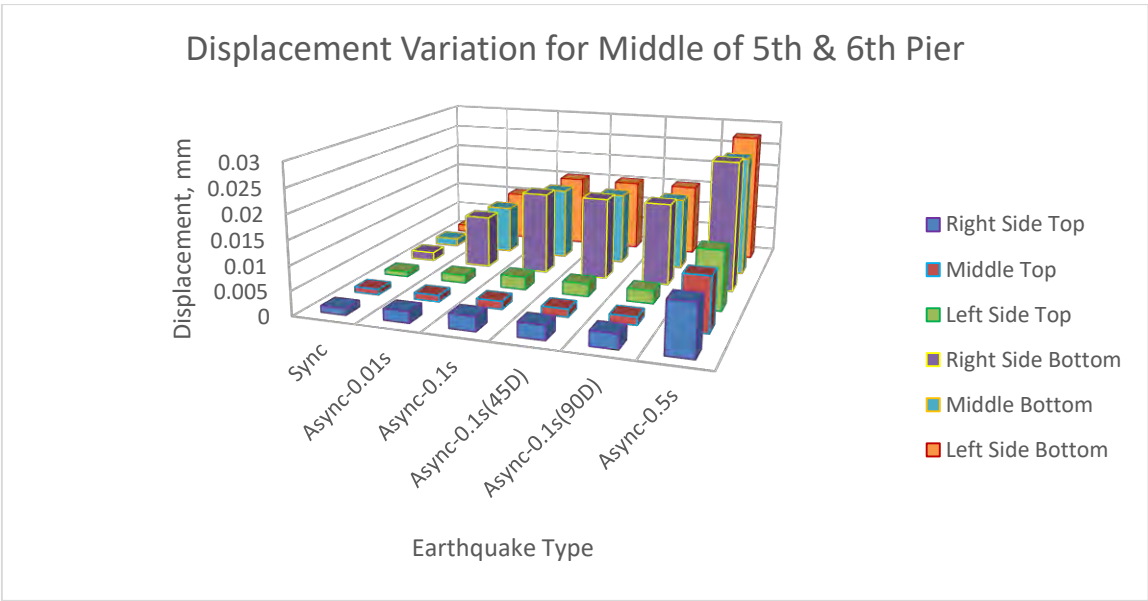


**Figure C.24: Displacement Variation for middle of fifth & sixth pier along X-axis**

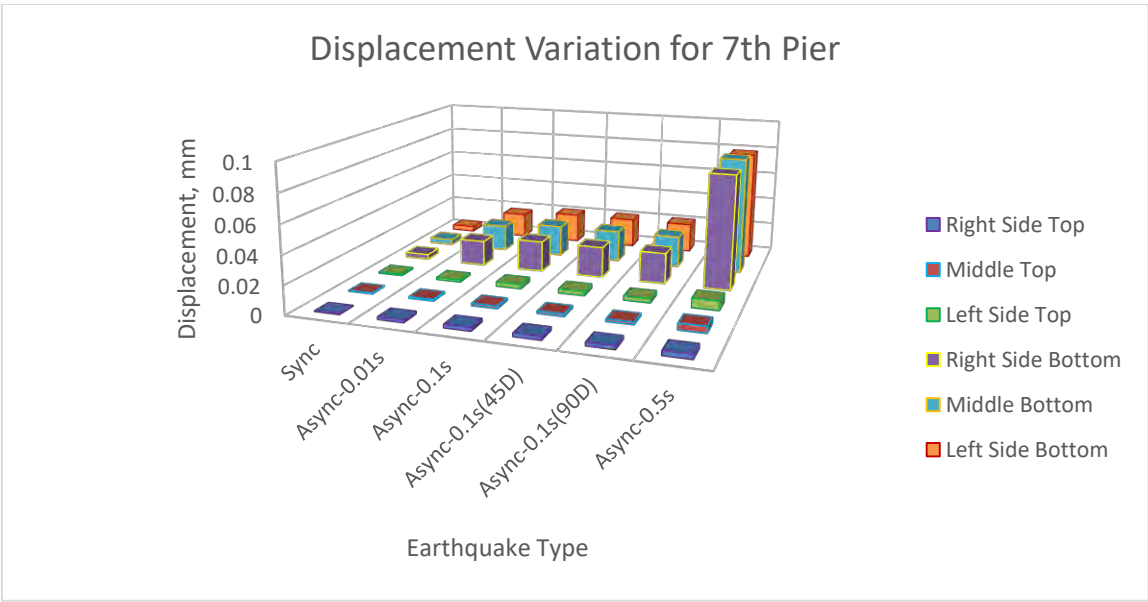


**Figure C.25: Displacement Variation for Seventh Pier along X-axis**

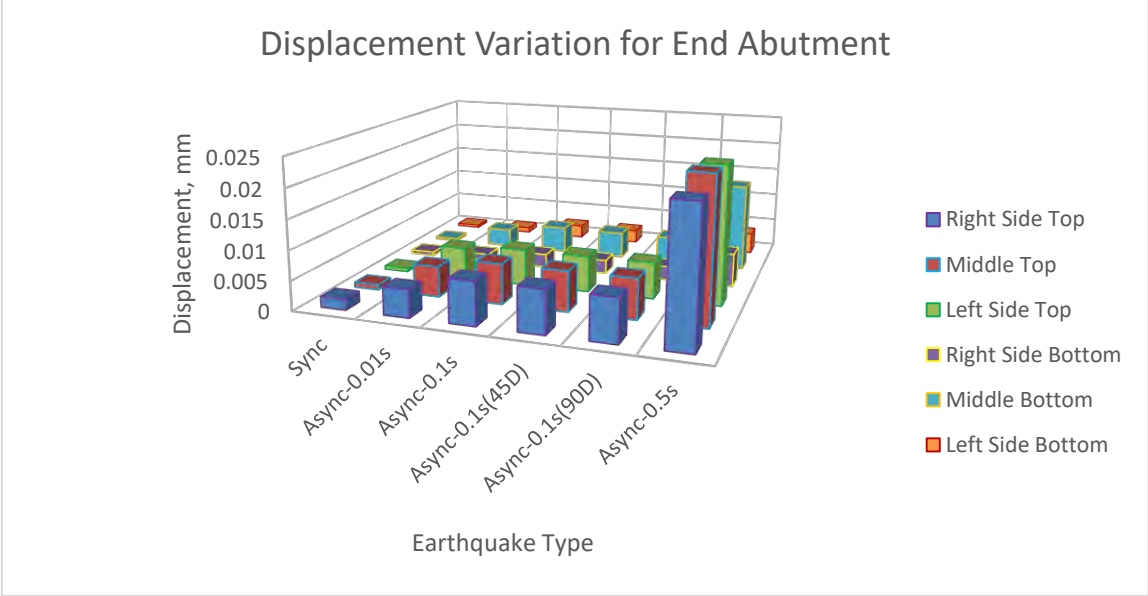


**Figure C.26: Displacement Variation for end abutment along X-axis**

**SYNCHRONOUS AND ASYNCHRONOUS EFFECT FOR 100 M MODEL ALONG Y-AXIS (ALONG WIDTH OF THE BRIDGE)**

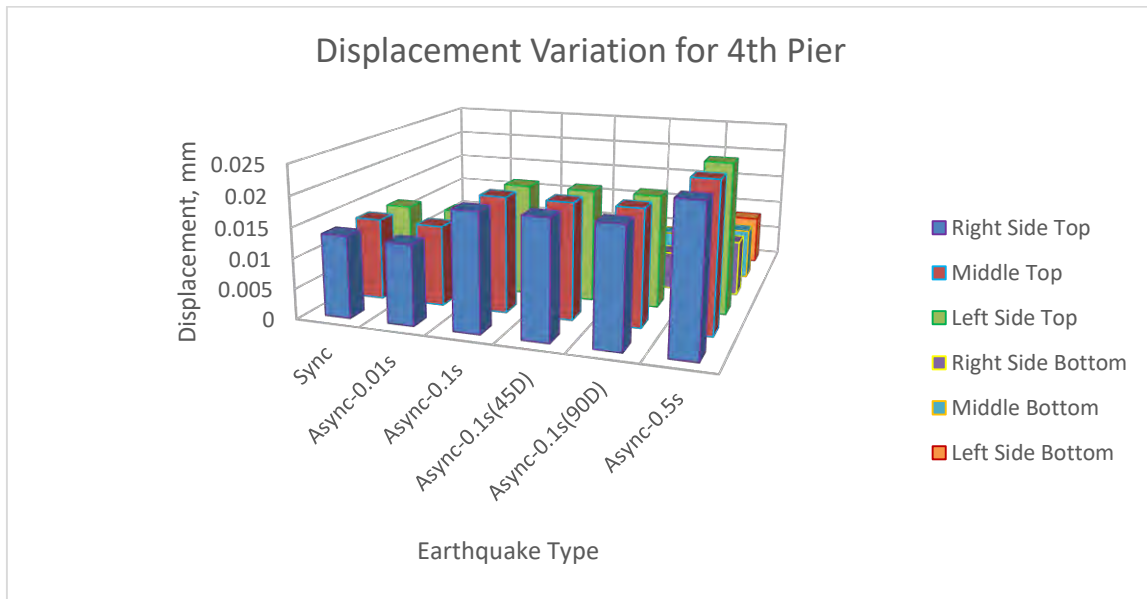


**Figure C.27: Displacement Variation for Fourth Pier along Y-axis**

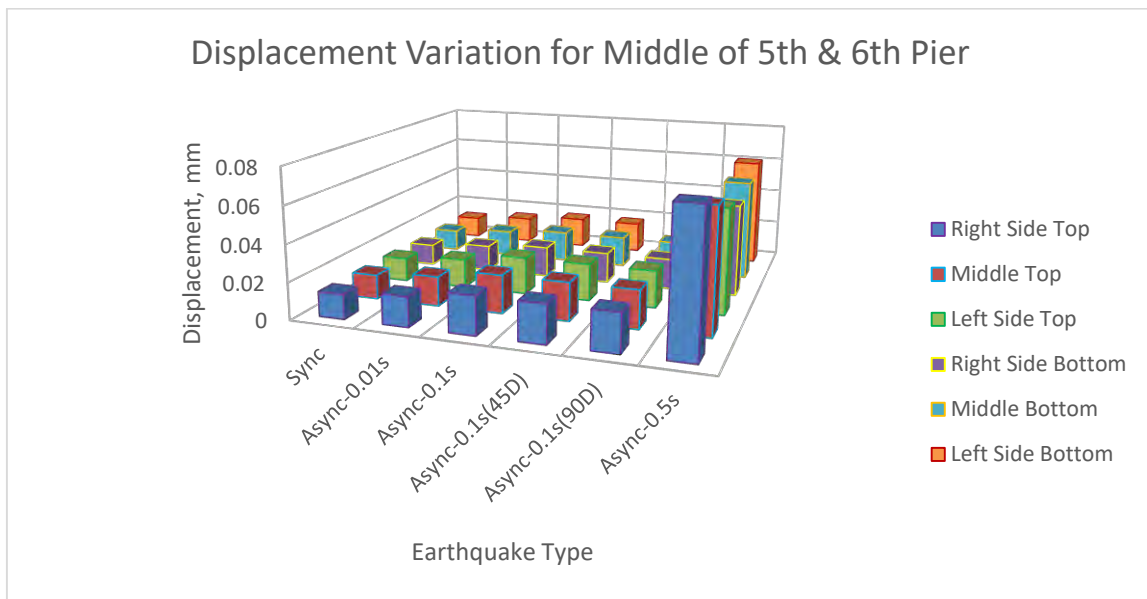


**Figure C.28: Displacement Variation for middle of fifth & sixth pier along Y-axis**

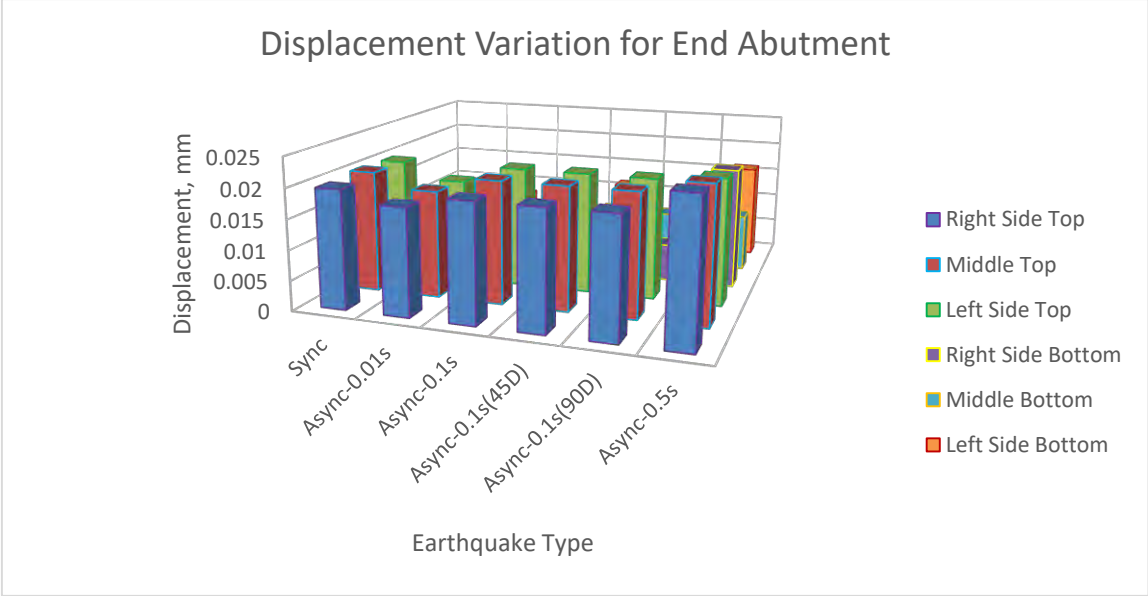


**Figure C.29: Displacement Variation for end abutment along Y-axis**

**SYNCHRONOUS AND ASYNCHRONOUS EFFECT FOR 100 M MODEL ALONG Z-AXIS (ALONG VERTICAL DIRECTION OF THE BRIDGE)**

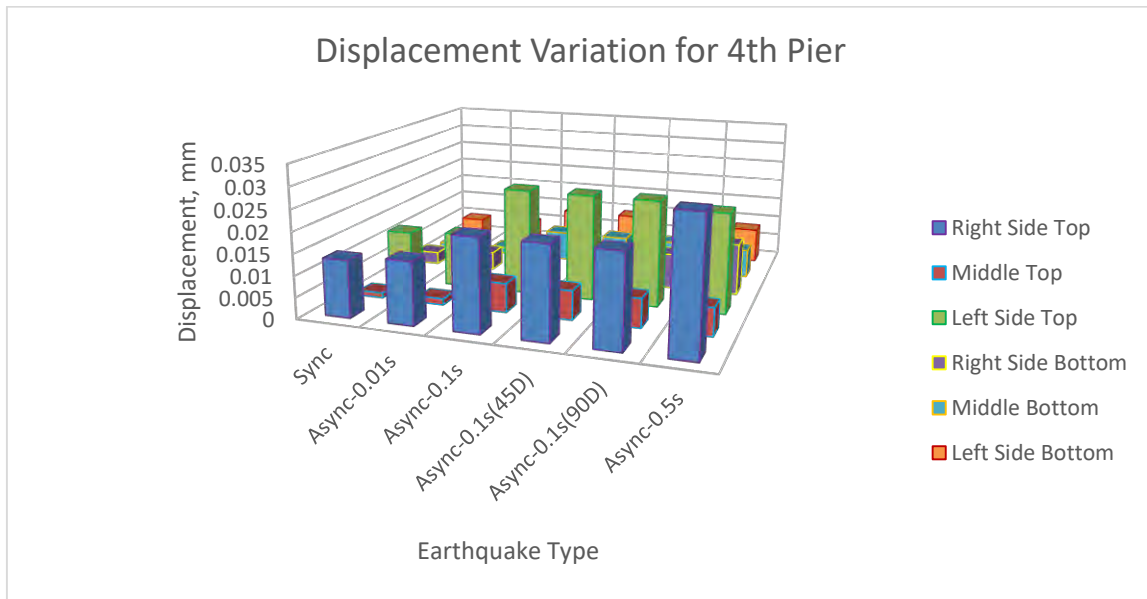


**Figure C.30: Displacement Variation for Fourth Pier along Z-axis**

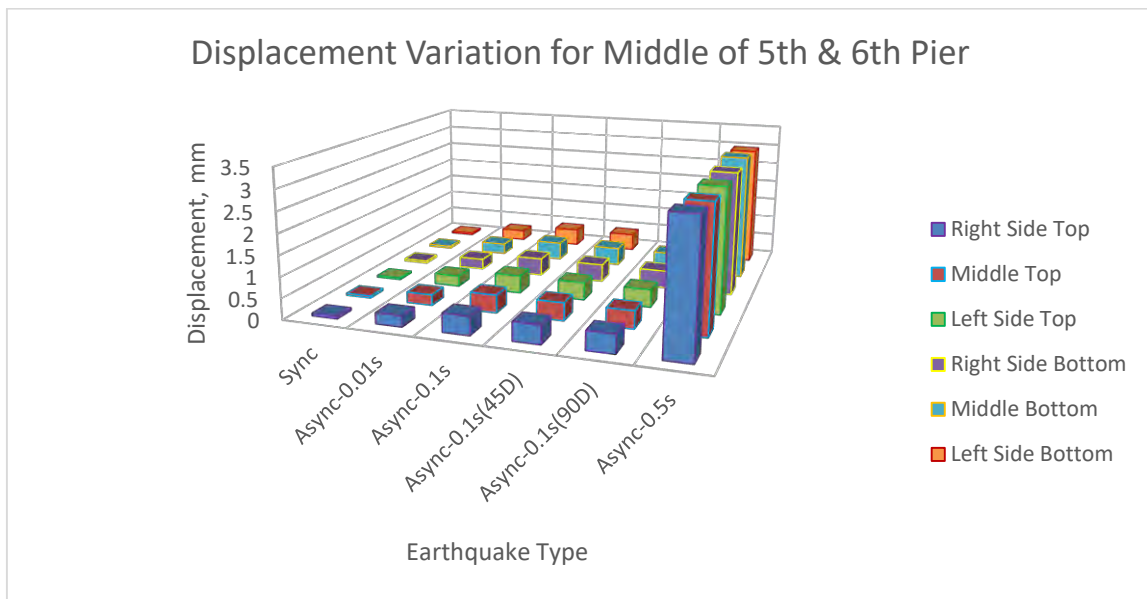


**Figure C.31: Displacement Variation for middle of fifth & sixth pier along Z-axis**



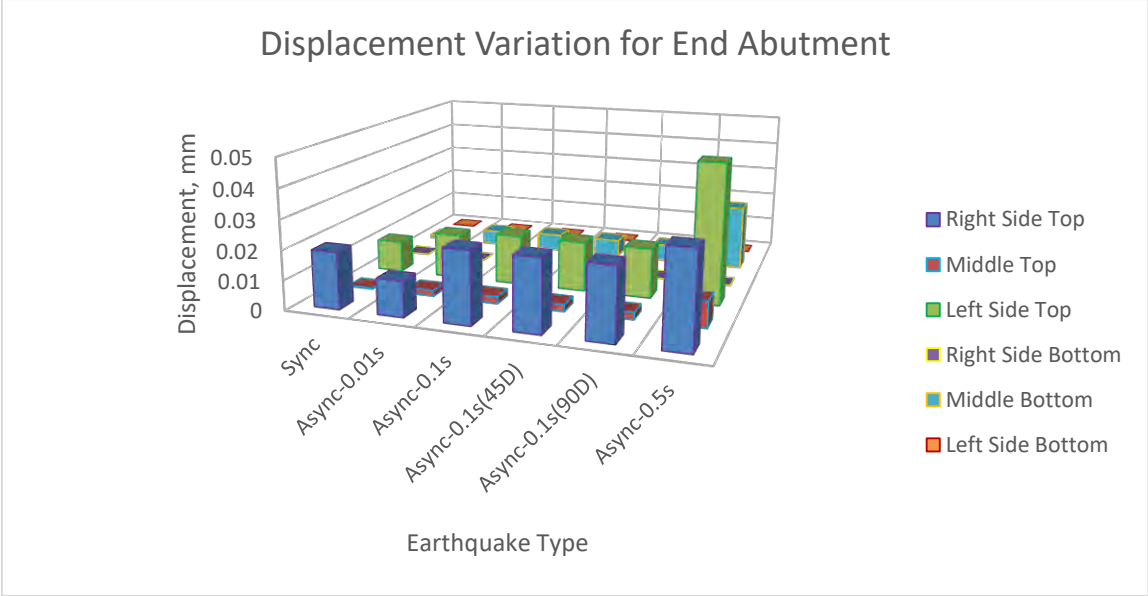


**Figure C.32: Displacement Variation for end abutment along Z-axis**

**SYNCHRONOUS AND ASYNCHRONOUS EFFECT FOR 125 M MODEL ALONG X-AXIS (ALONG LENGTH OF THE BRIDGE)**

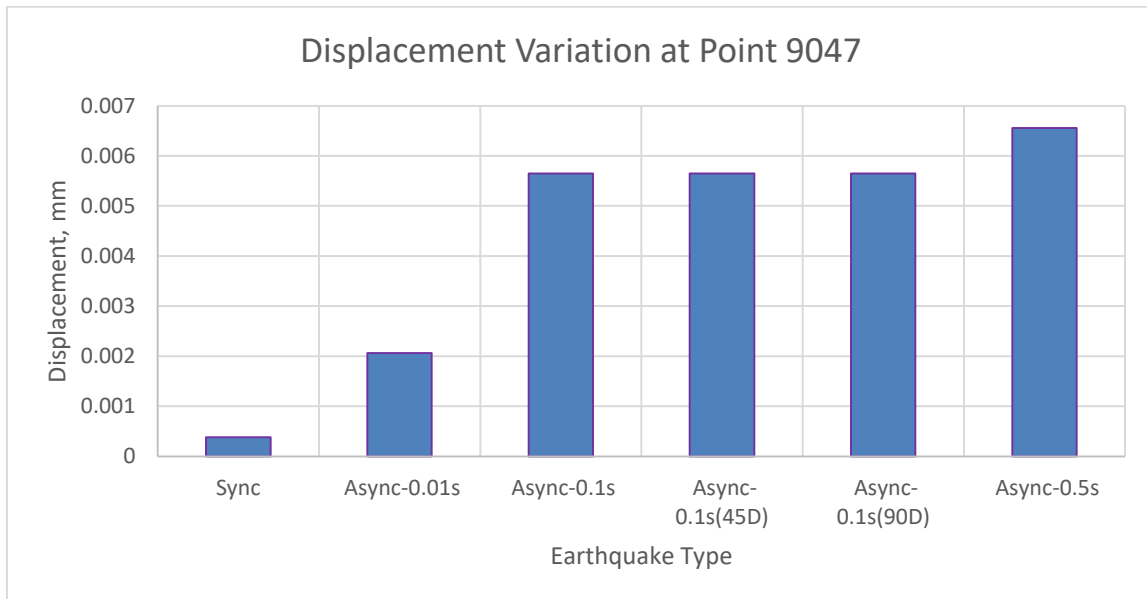


**Figure C.33: Displacement Variation at right side top of middle of second & third pier along X-axis**

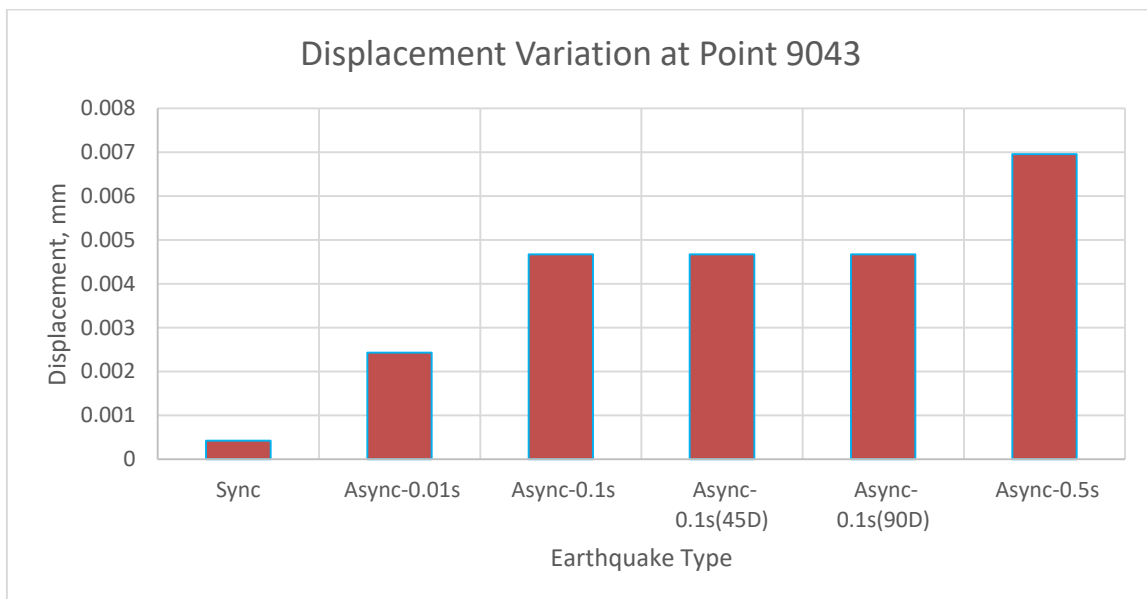


**Figure C.34: Displacement Variation at middle top of middle of second & third pier along X-axis**

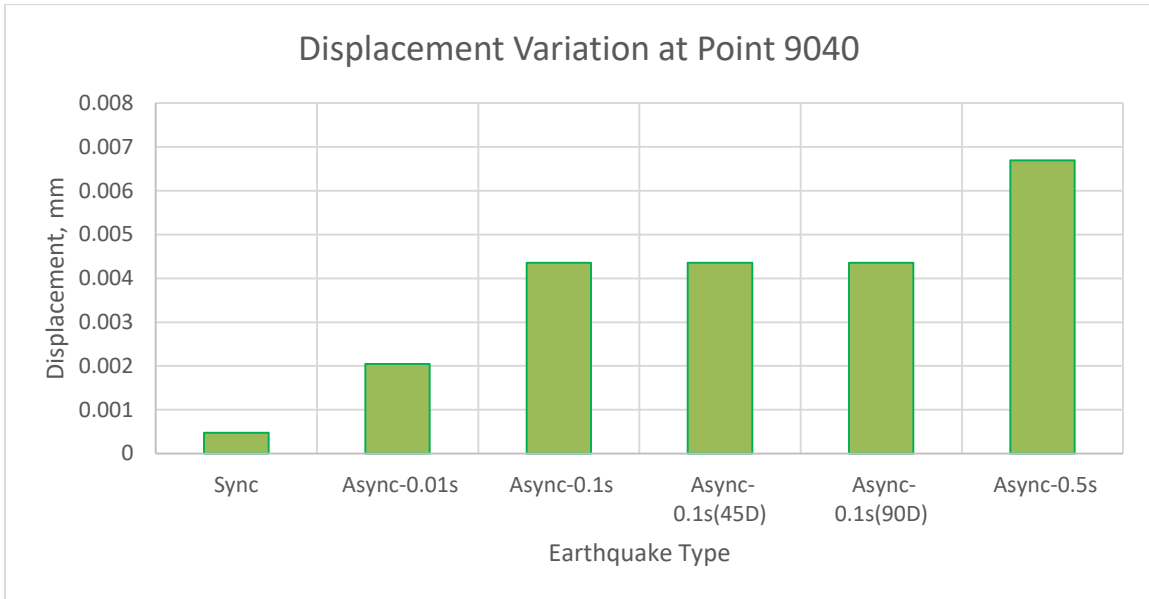


**Figure C.35: Displacement Variation at left side top of middle of second & third pier along X-axis**

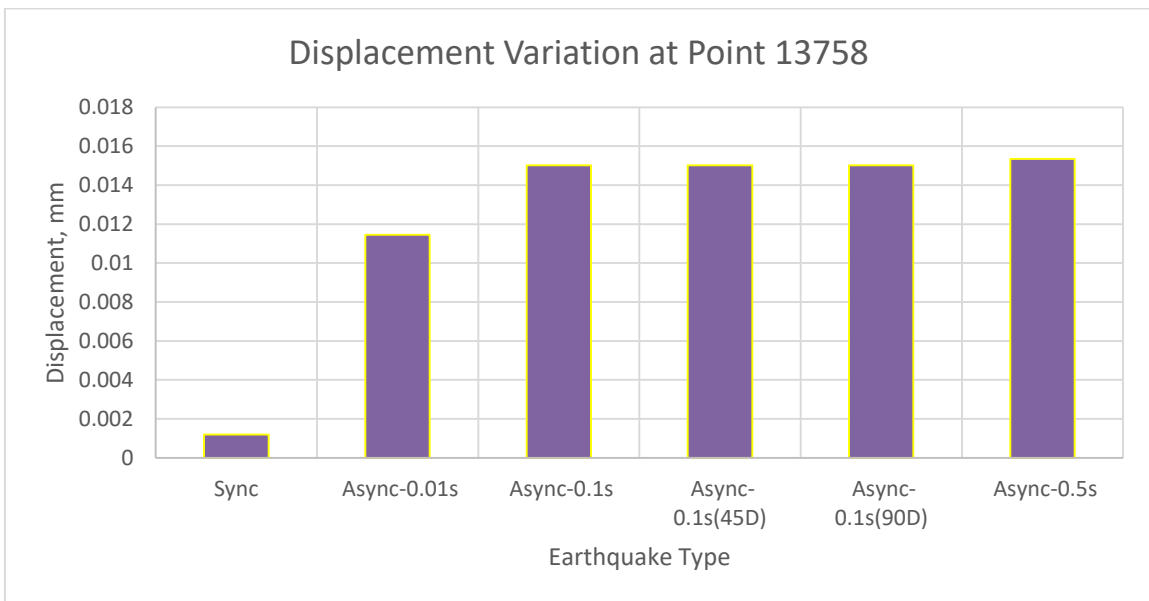


**Figure C.36: Displacement Variation at right side bottom of middle of second & third pier along X-axis**

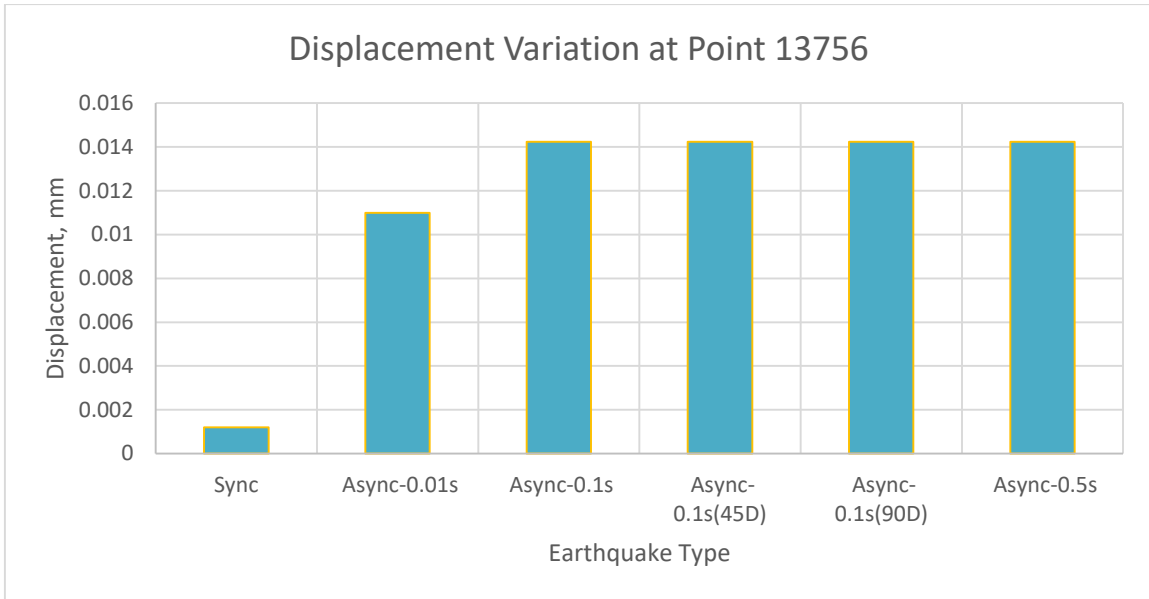


**Figure C.37: Displacement Variation at middle bottom of middle of second & third pier along X-axis**

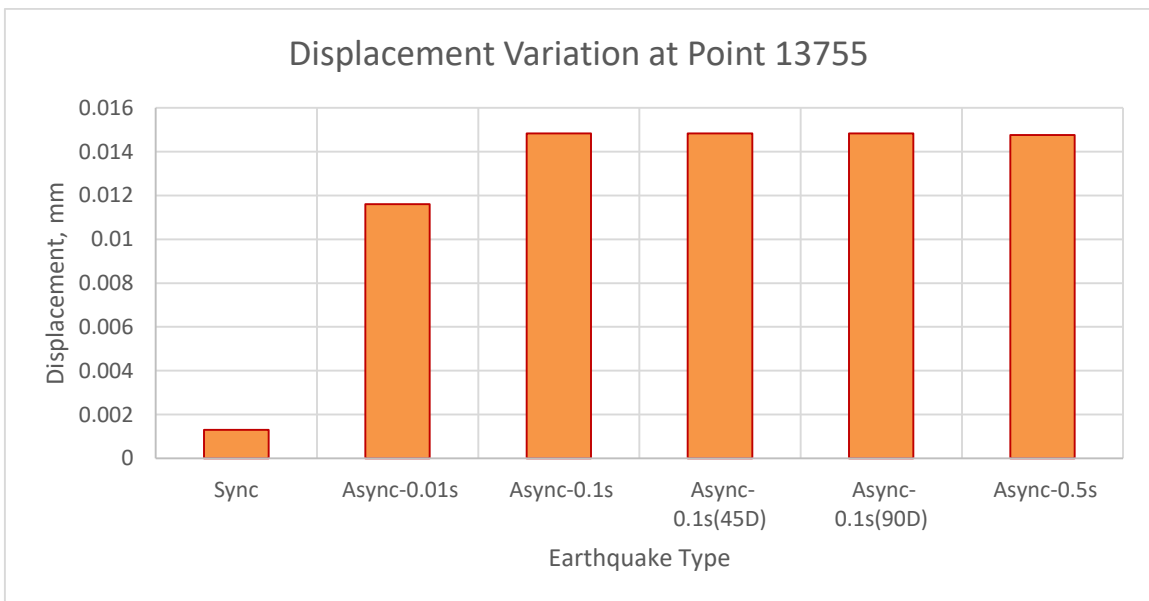


**Figure C.38: Displacement Variation at left side bottom of middle of second & third pier along X-axis**

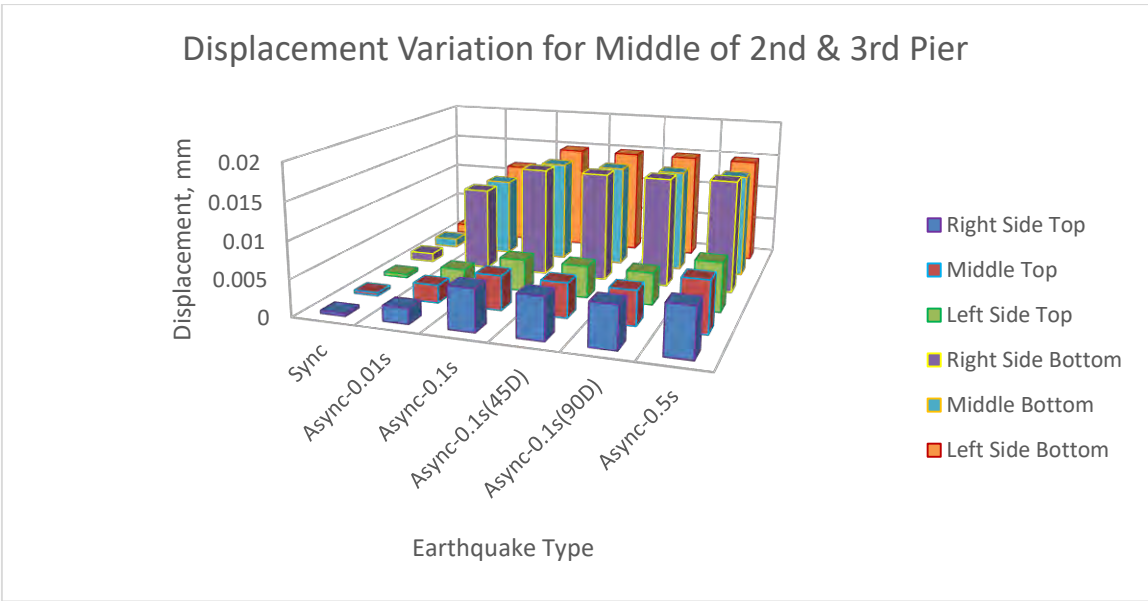


**Figure C.39: Displacement Variation for middle of second & third pier along X-axis**

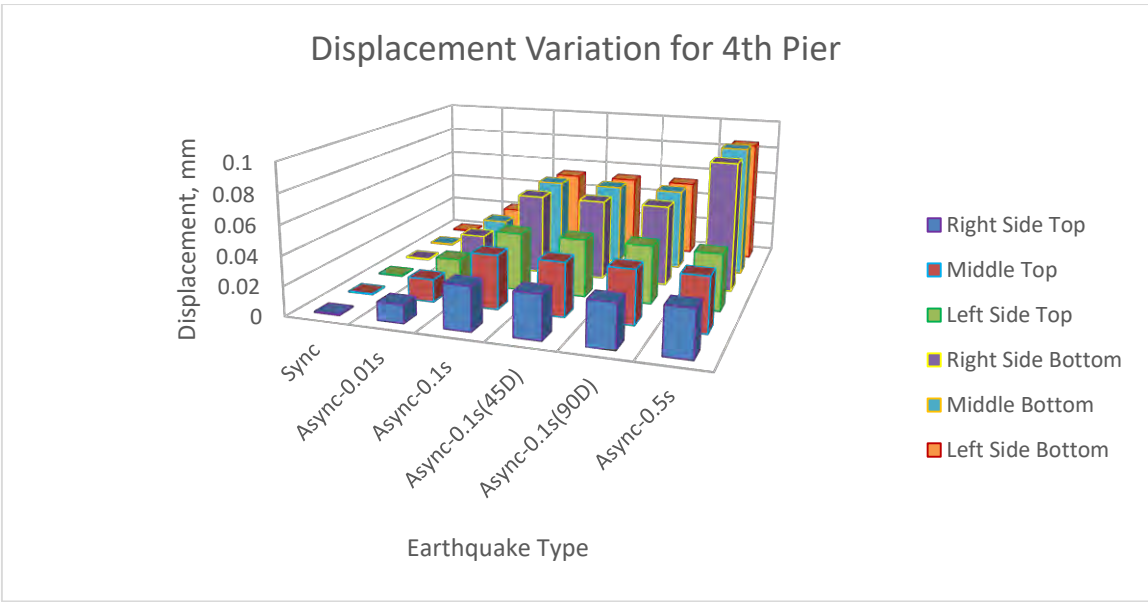


**Figure C.40: Displacement Variation for Fourth Pier along X-axis**

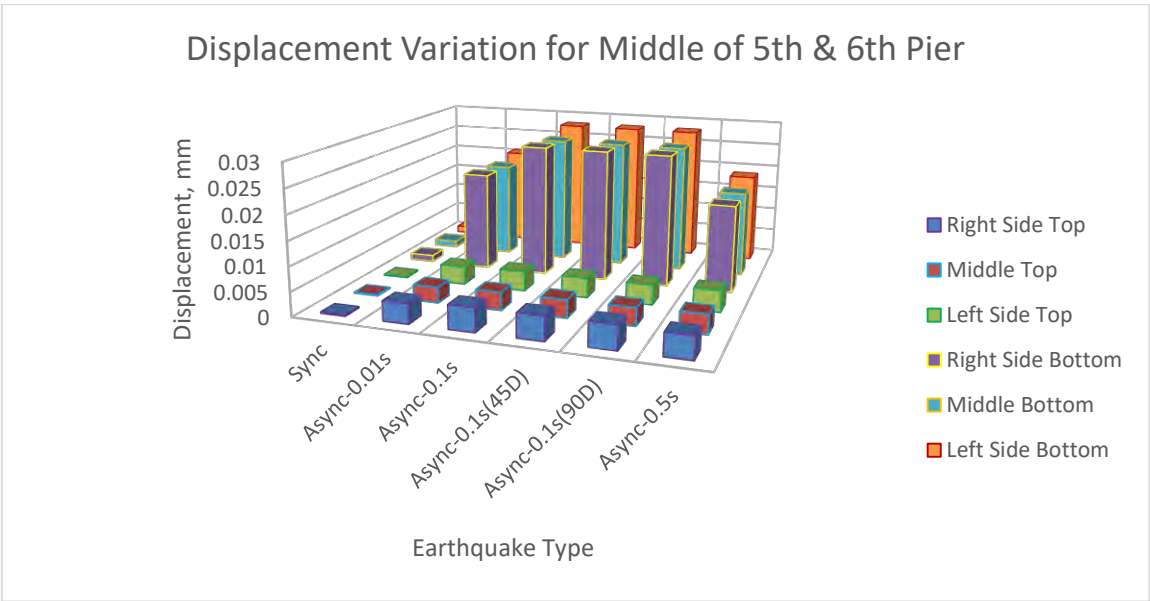


**Figure C.41: Displacement Variation for middle of fifth & sixth pier along X-axis**

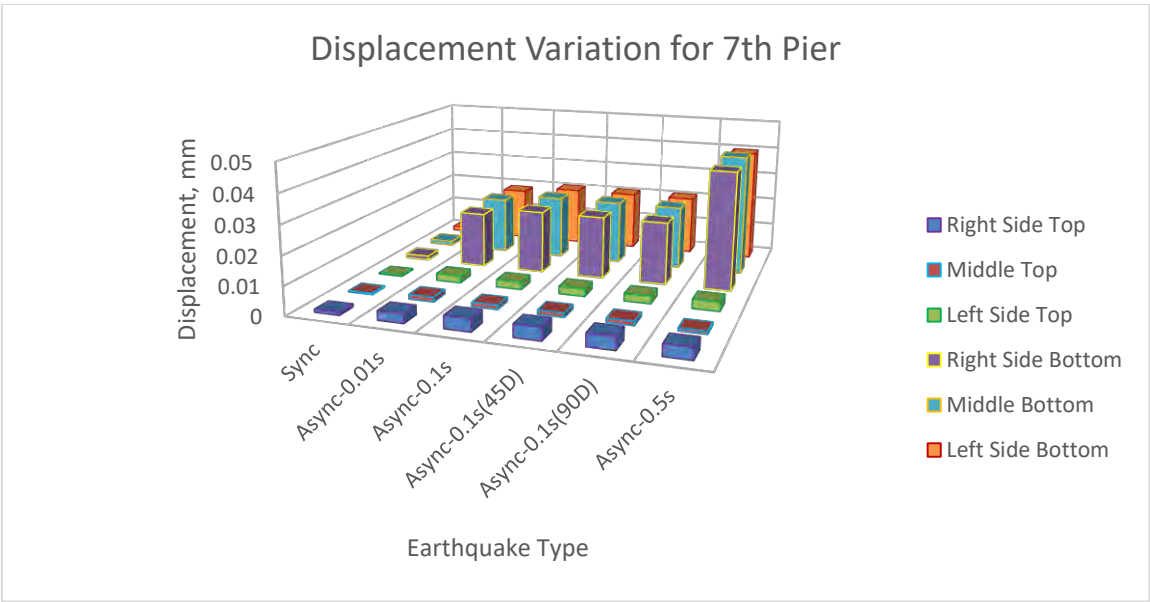


**Figure C.42: Displacement Variation for Seventh Pier along X-axis**

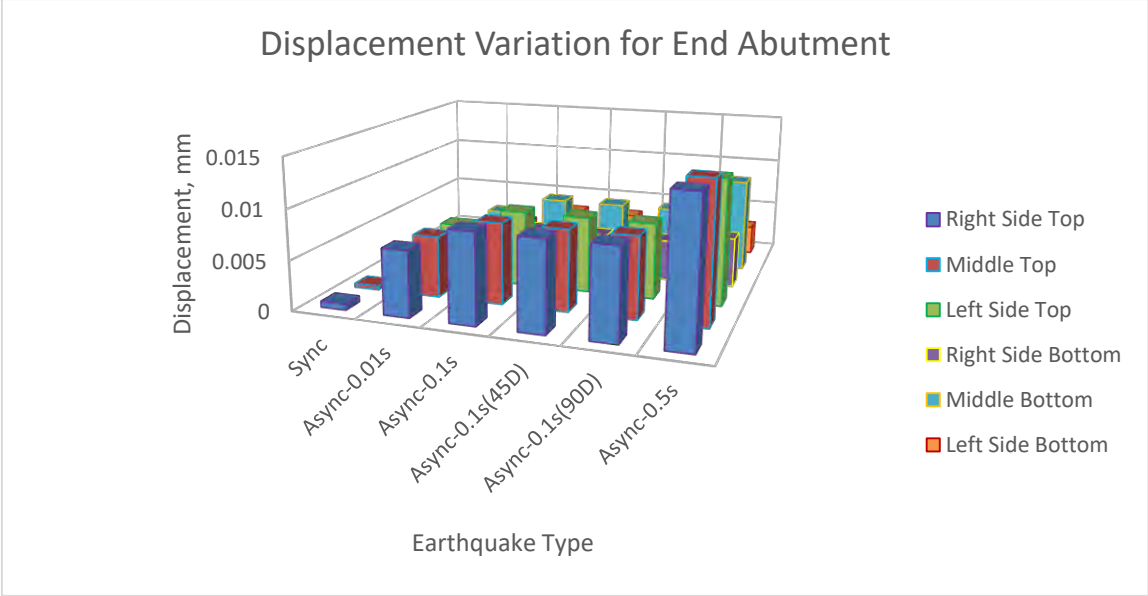


**Figure C.43: Displacement Variation for end abutment along X-axis**

**SYNCHRONOUS AND ASYNCHRONOUS EFFECT FOR 125 M MODEL ALONG Y-AXIS (ALONG WIDTH OF THE BRIDGE)**

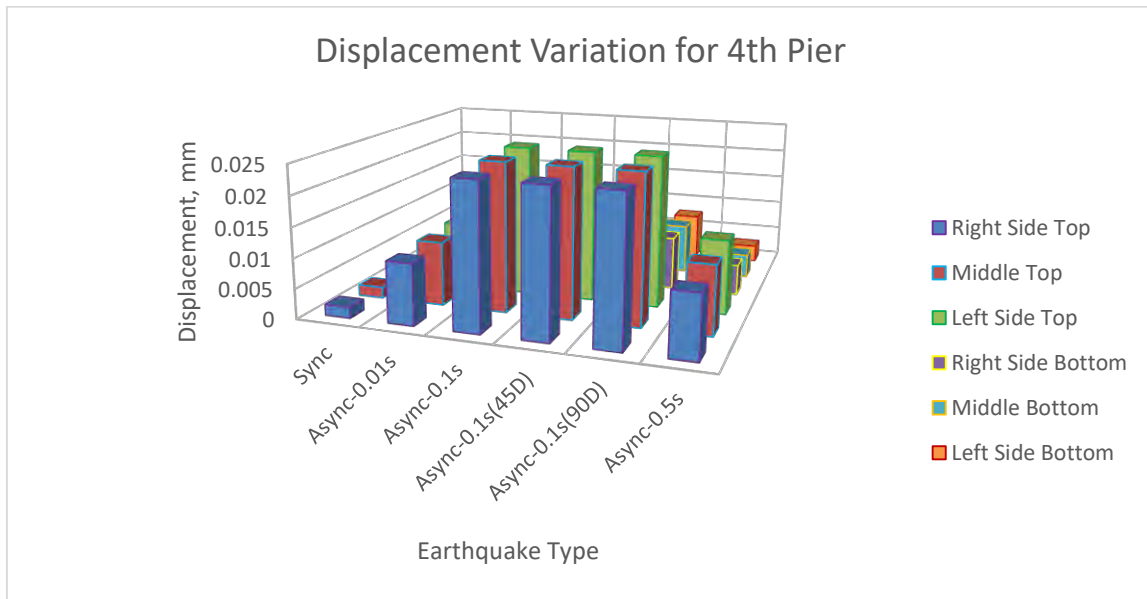


**Figure C.44: Displacement Variation for Fourth Pier along Y-axis**

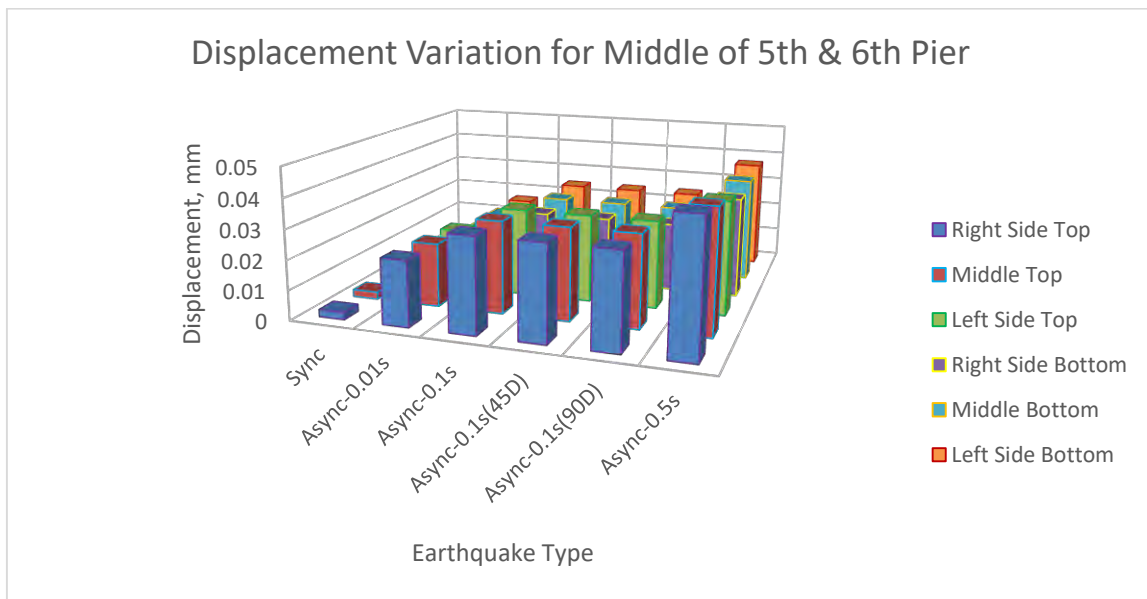


**Figure C.45: Displacement Variation for middle of fifth & sixth pier along Y-axis**



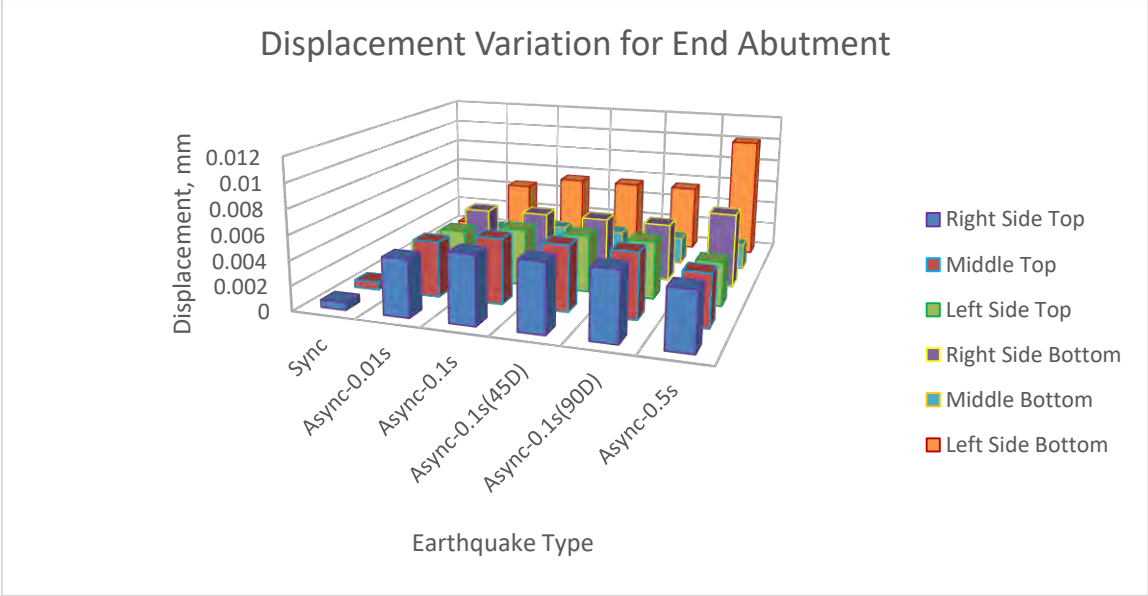


**Figure C.46: Displacement Variation for end abutment along Y-axis**

**SYNCHRONOUS AND ASYNCHRONOUS EFFECT FOR 125 M MODEL ALONG Z-AXIS (ALONG VERTICAL DIRECTION OF THE BRIDGE)**

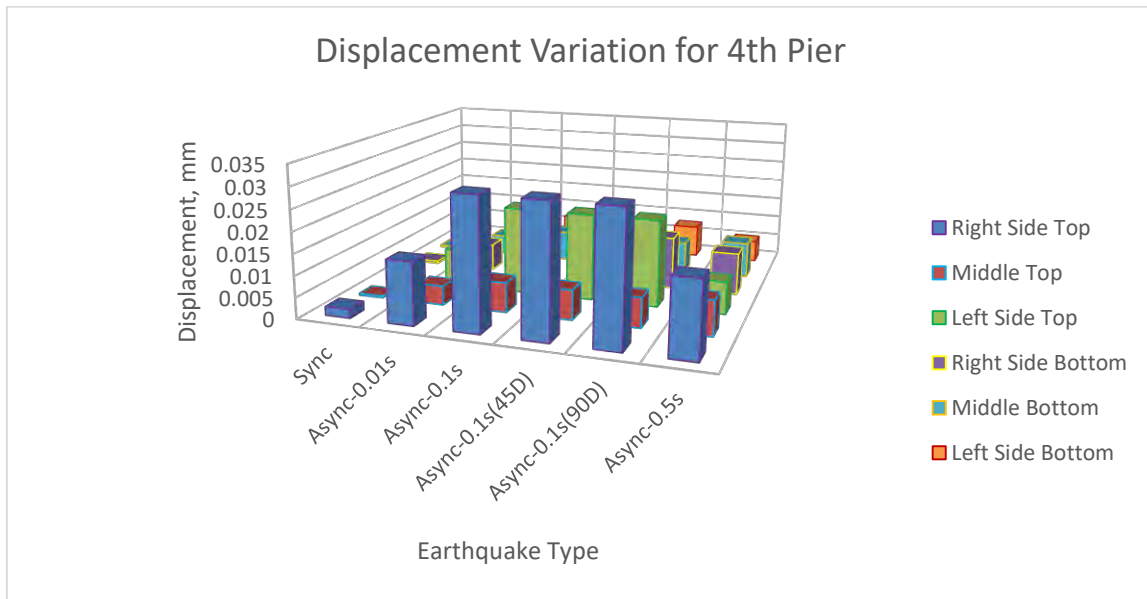


**Figure C.47: Displacement Variation for Fourth Pier along Z-axis**

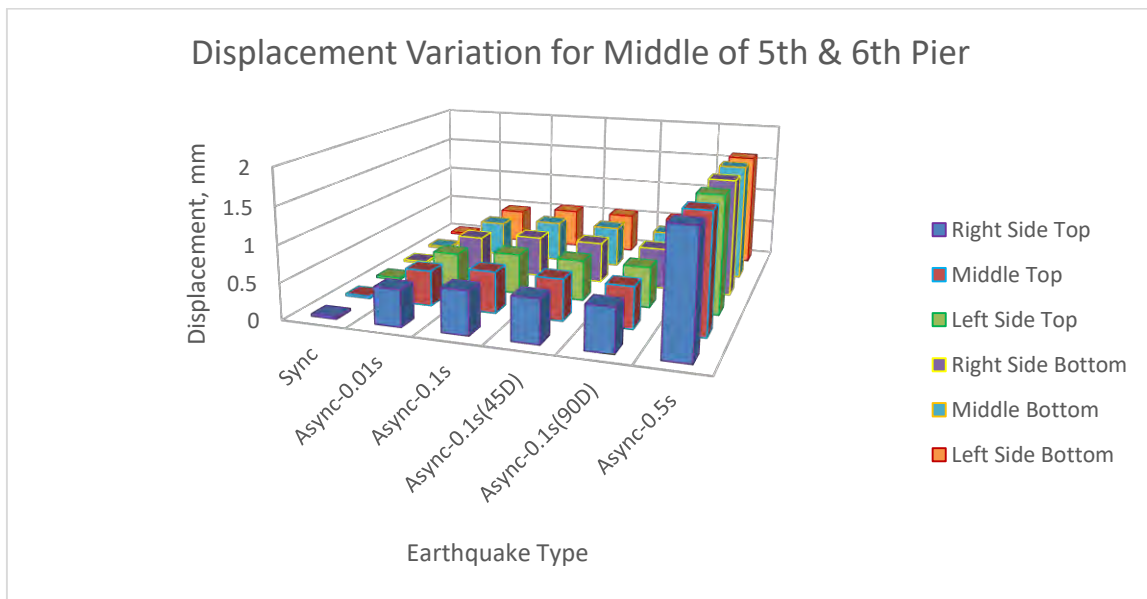


**Figure C.48: Displacement Variation for middle of fifth & sixth pier along Z-axis**

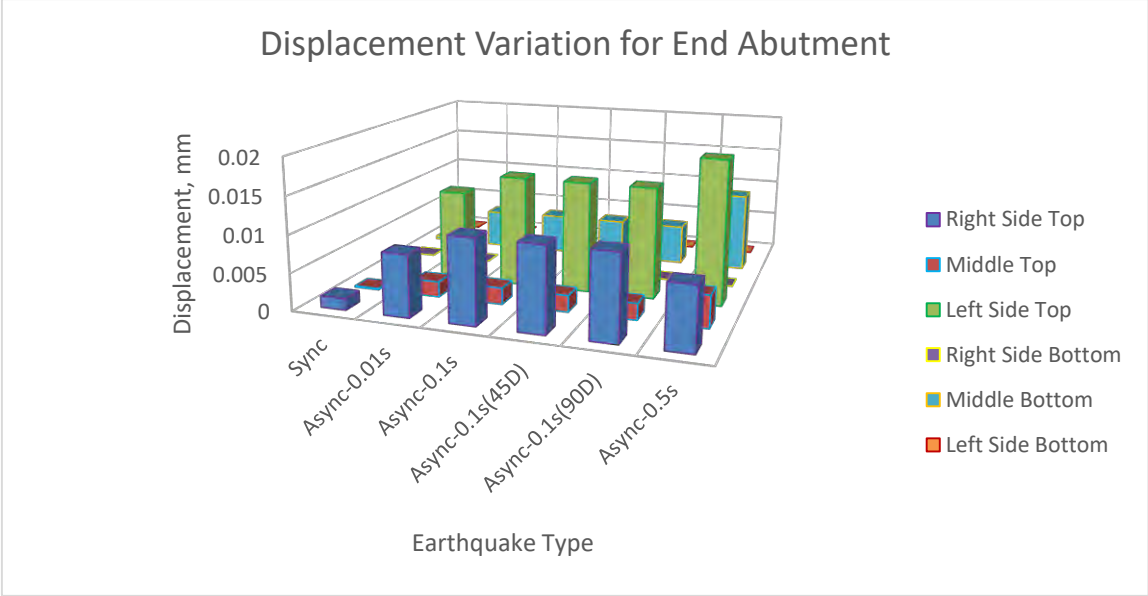


**Figure C.49: Displacement Variation for end abutment along Z-axis**

## APPENDIX D

### SOIL EFFECT ON TWO BRIDGES

---

#### SOIL EFFECT FOR 100 M MODEL ALONG X-AXIS (ALONG LENGTH OF THE BRIDGE)

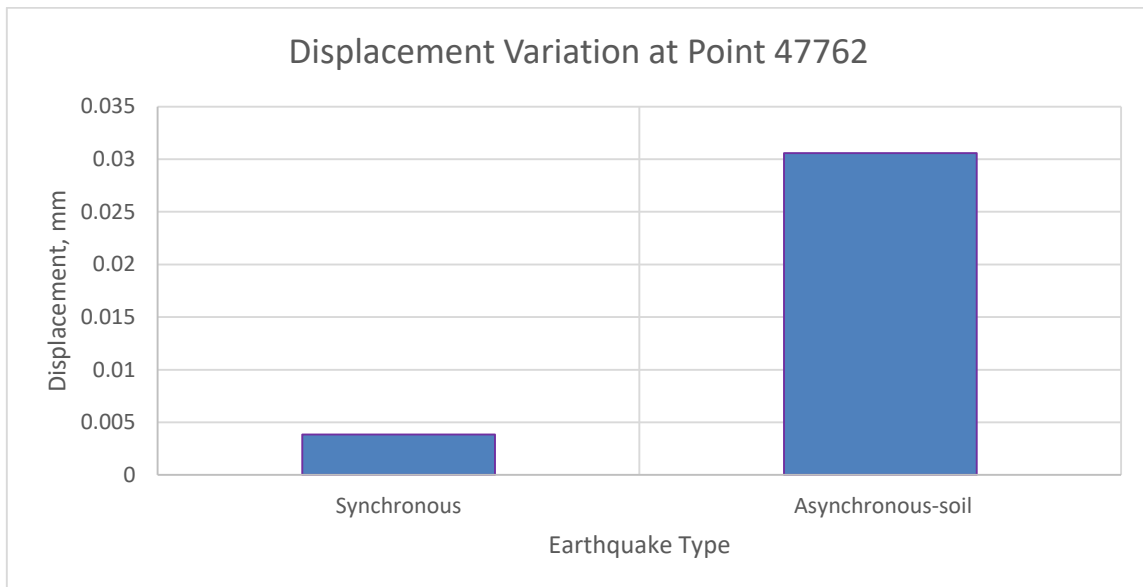


**Figure D.1: Displacement Variation at right side top of fourth pier along X-axis**

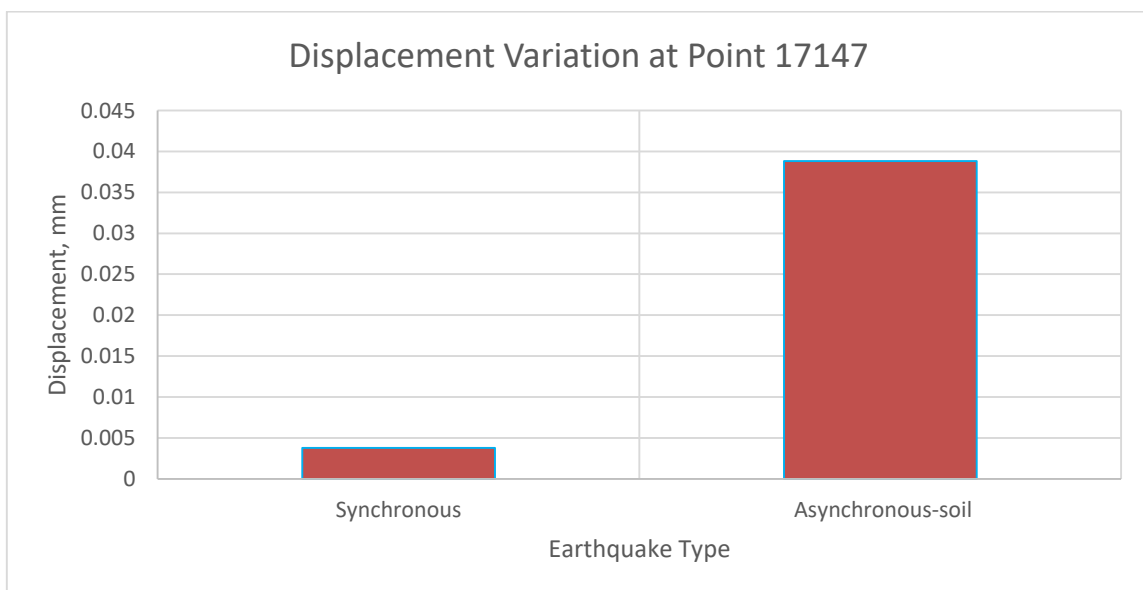


**Figure D.2: Displacement Variation at middle top of fourth pier along X-axis**

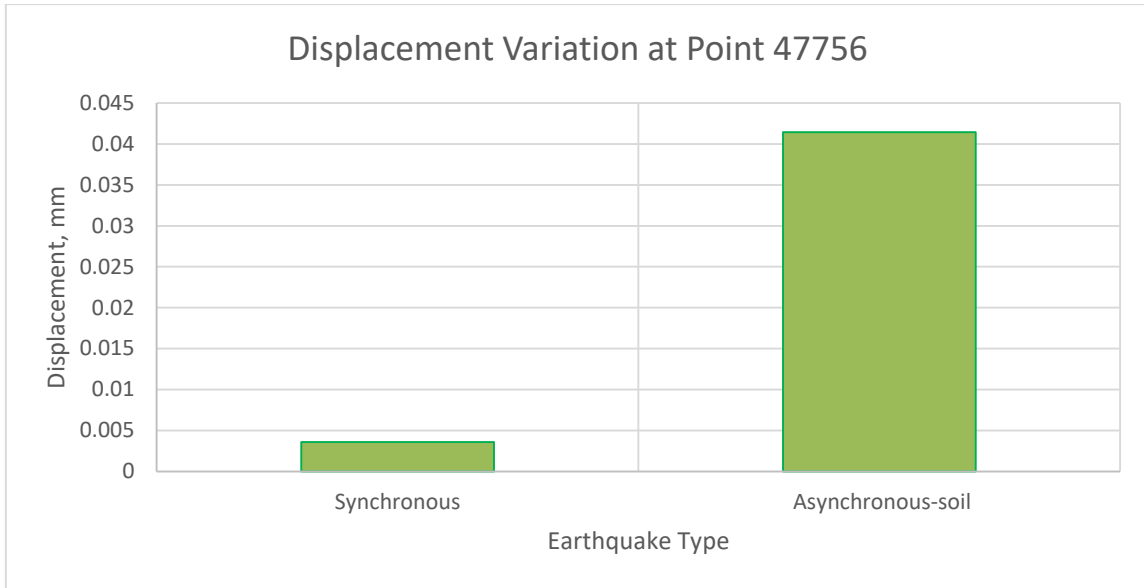


**Figure D.3: Displacement Variation at left side top of fourth pier along X-axis**

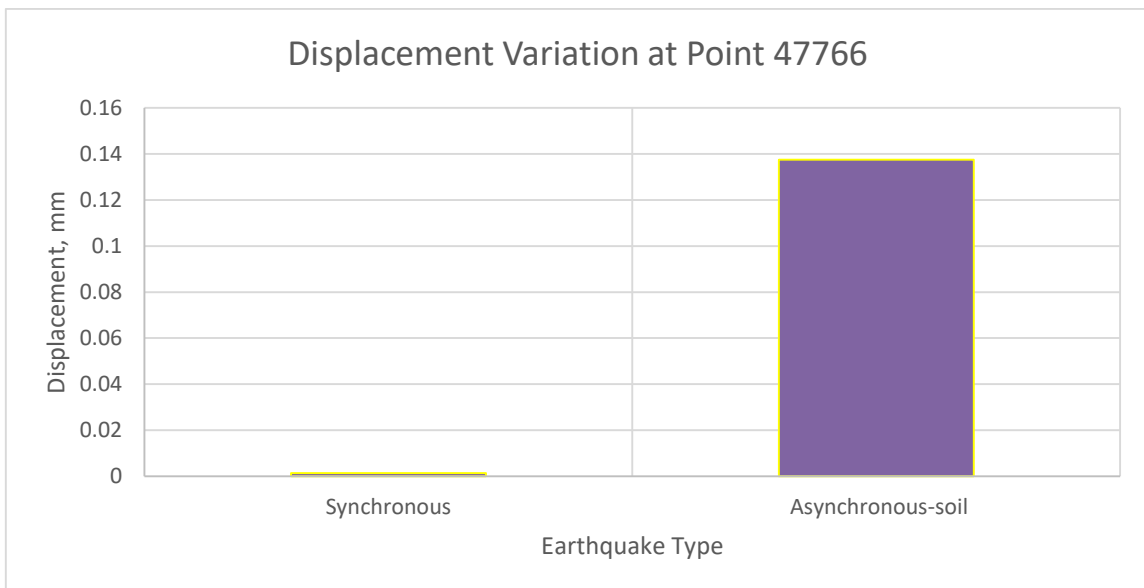


**Figure D.4: Displacement Variation at right side bottom of fourth pier along X-axis**

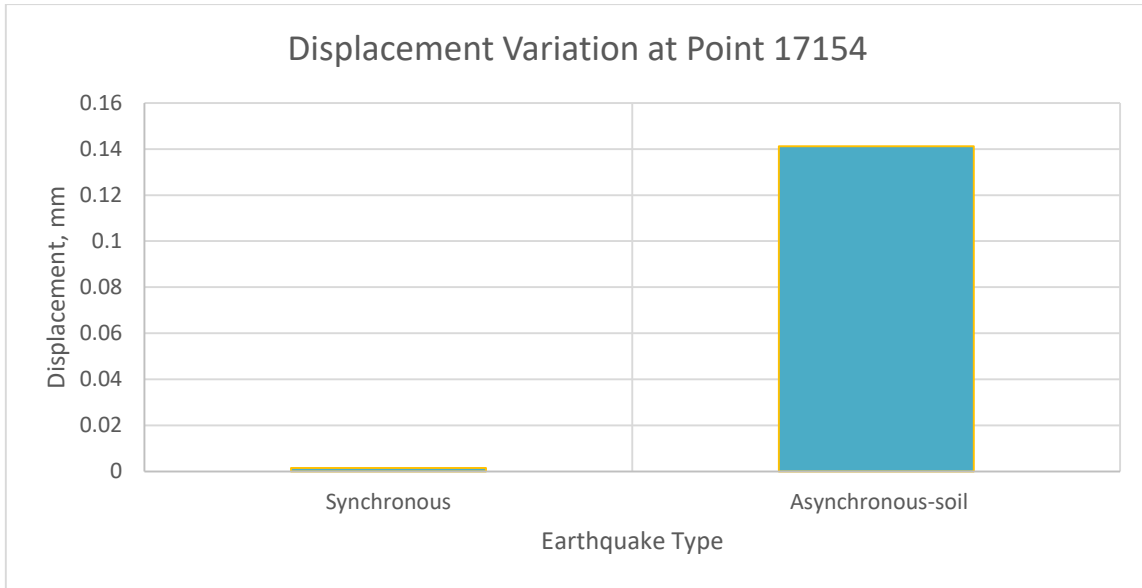


**Figure D.5: Displacement Variation at middle bottom of fourth pier along X-axis**

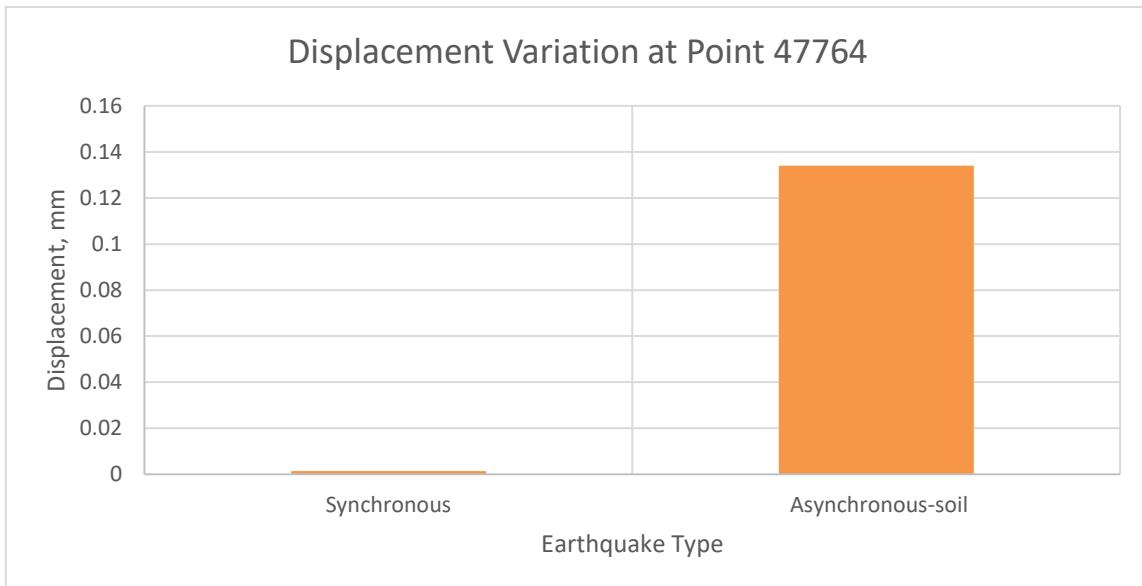


**Figure D.6: Displacement Variation at left side bottom of fourth pier along X-axis**

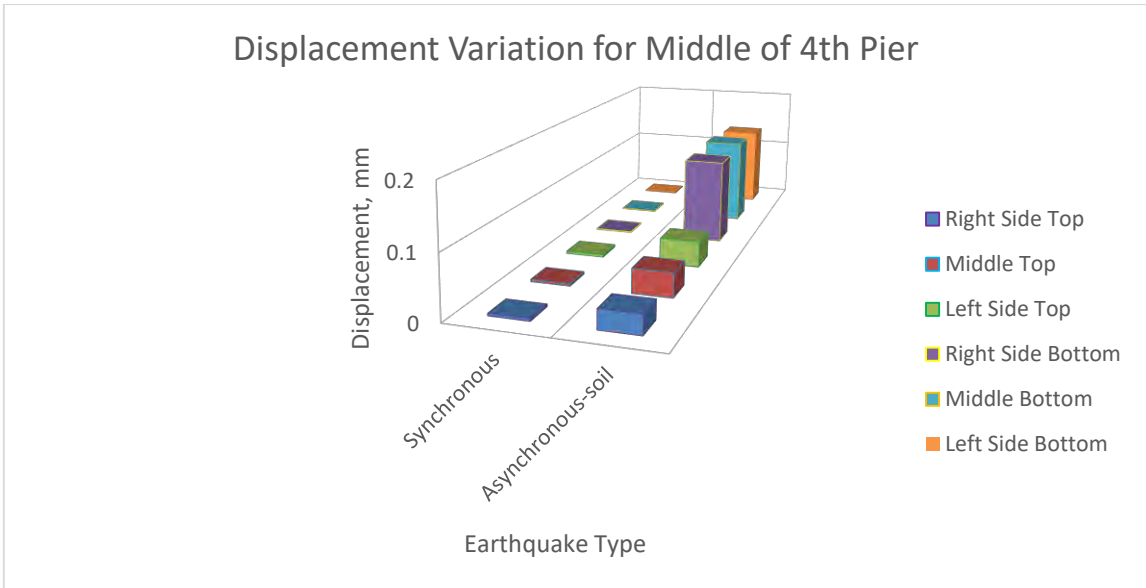


**Figure D.7: Displacement Variation for Fourth Pier along X-axis**

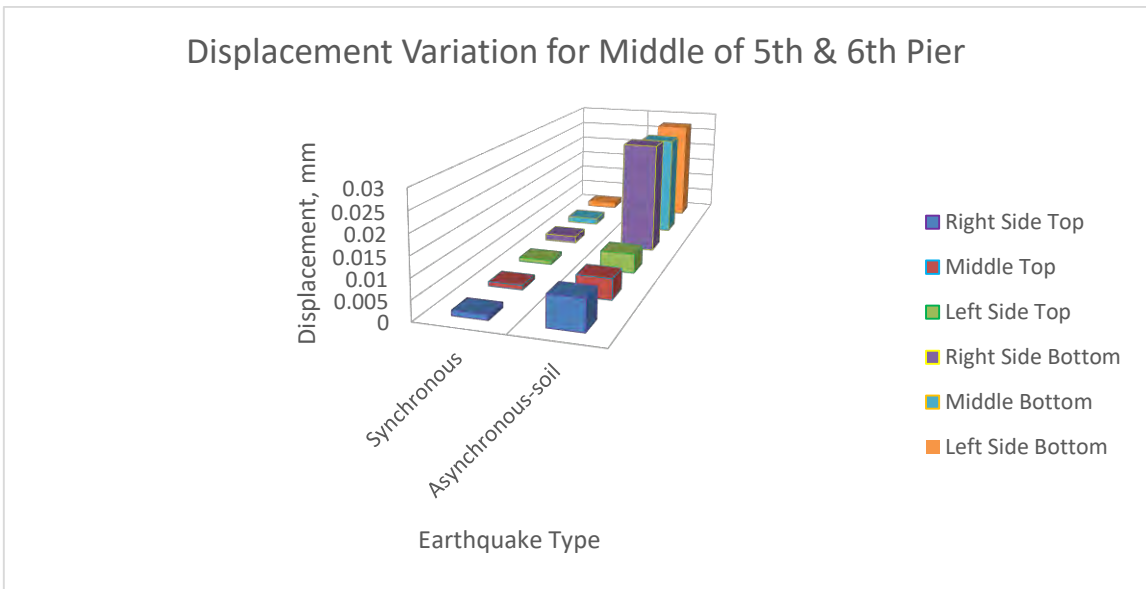


**Figure D.8: Displacement Variation for middle of fifth & sixth pier along X-axis**

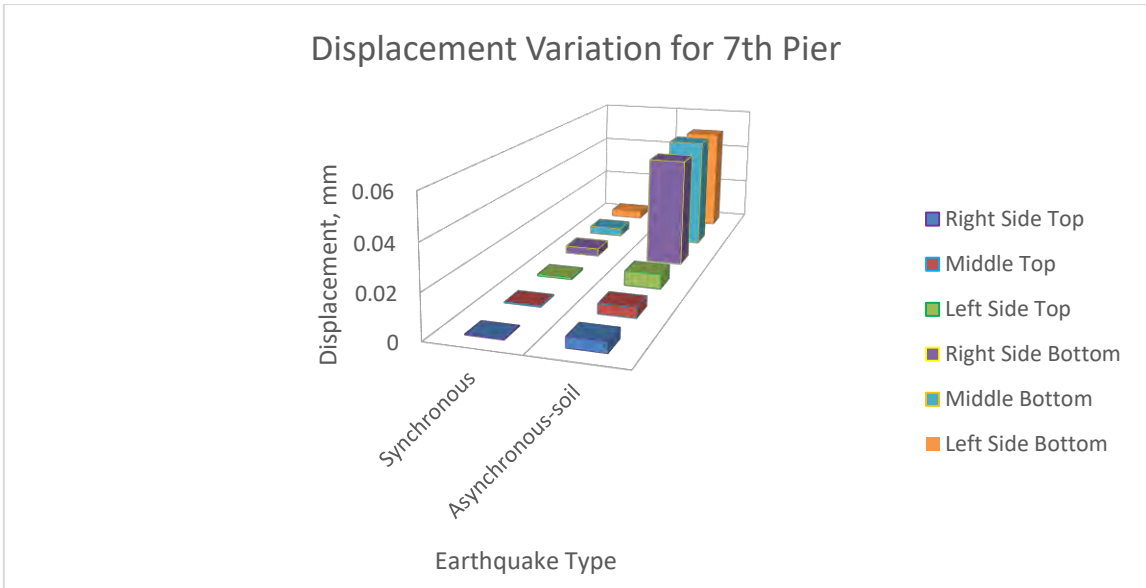


**Figure D.9: Displacement Variation for Seventh Pier along X-axis**

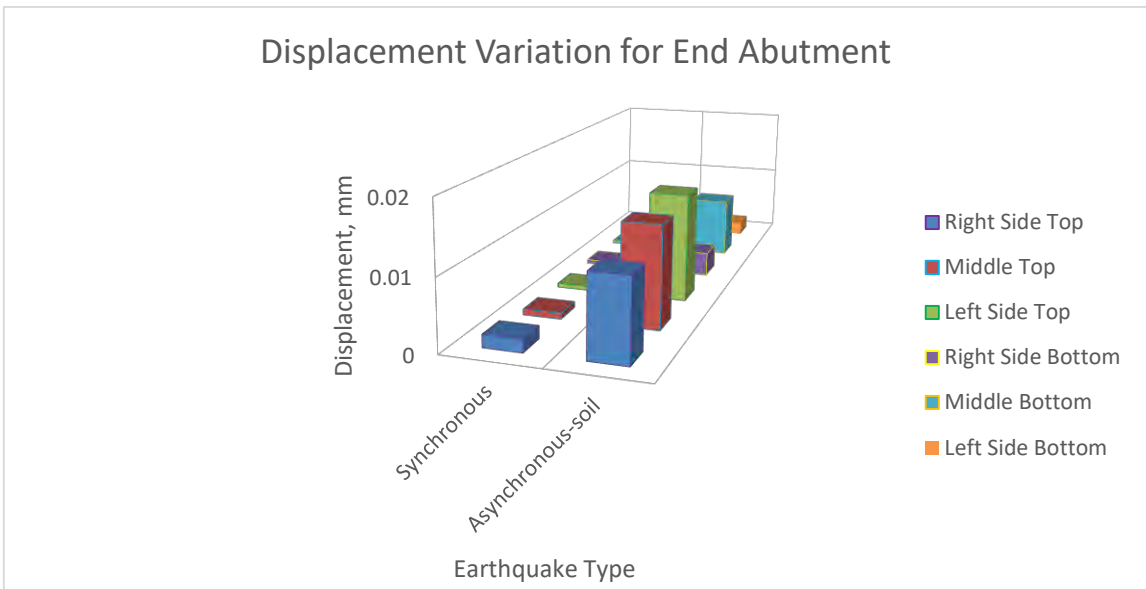


**Figure D.10: Displacement Variation for end abutment along X-axis**



**SOIL EFFECT FOR 100 M MODEL ALONG Y-AXIS (ALONG WIDTH OF THE BRIDGE)**

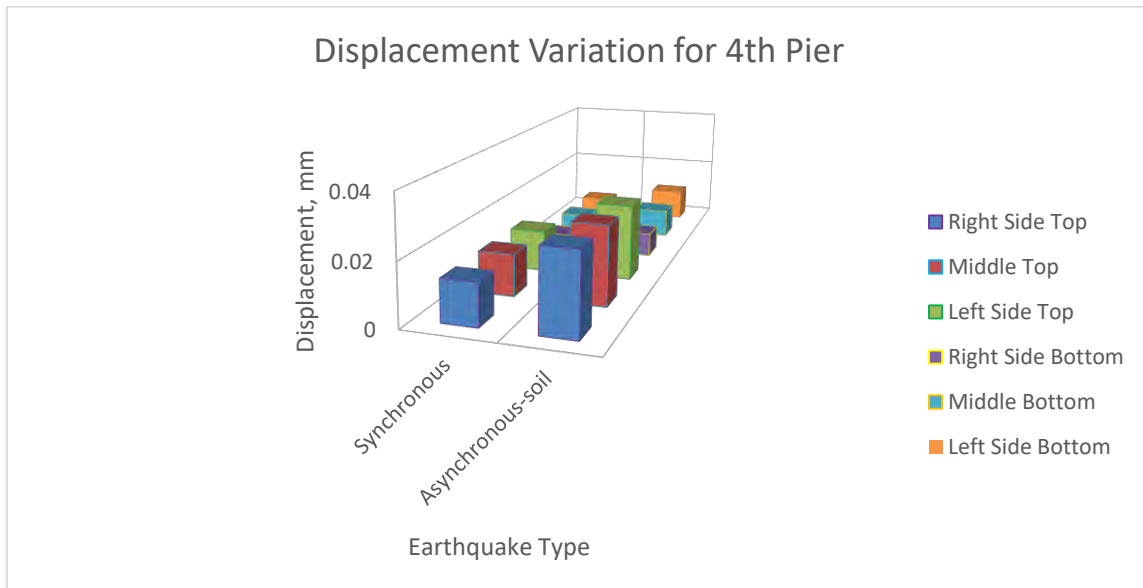


**Figure D.11: Displacement Variation for Fourth Pier along Y-axis**

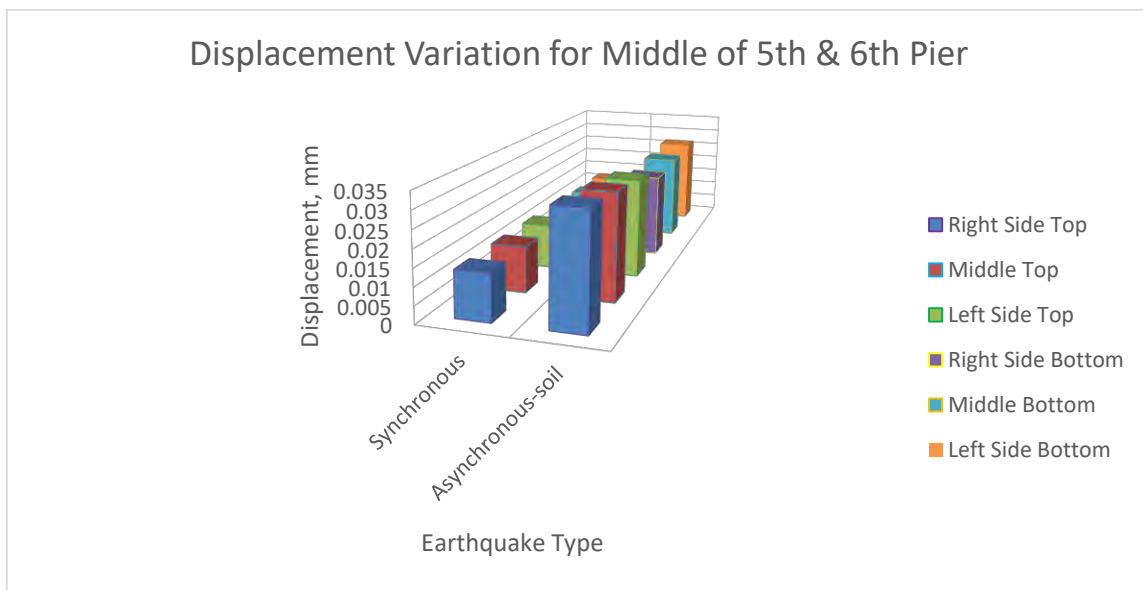


**Figure D.12: Displacement Variation for middle of fifth & sixth pier along Y-axis**

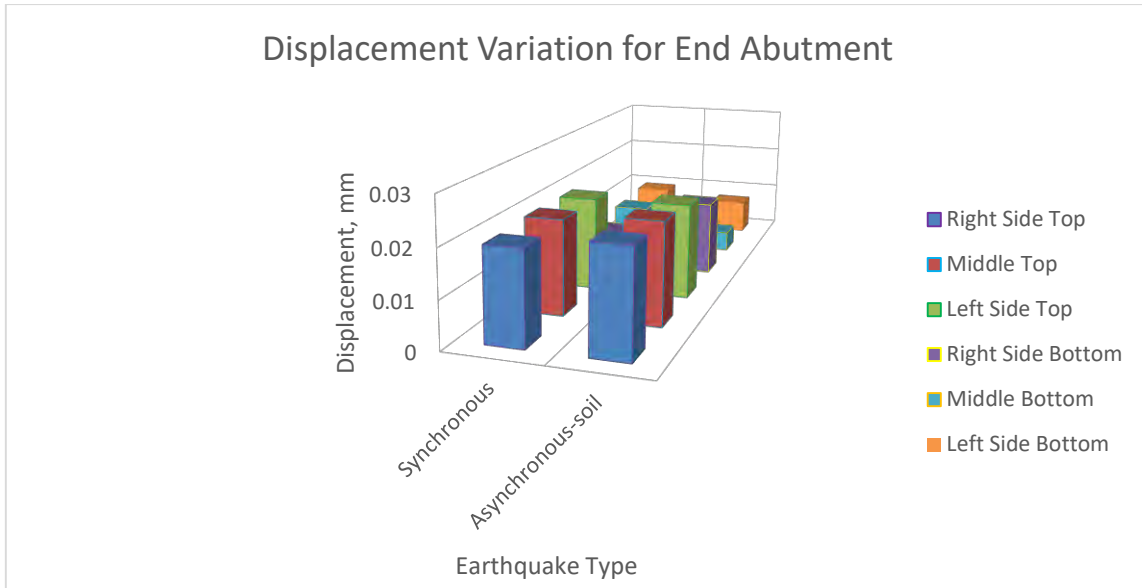


**Figure D.13: Displacement Variation for end abutment along Y-axis**

**SOIL EFFECT FOR 100 M MODEL ALONG Z-AXIS (ALONG VERTICAL DIRECTION OF THE BRIDGE)**

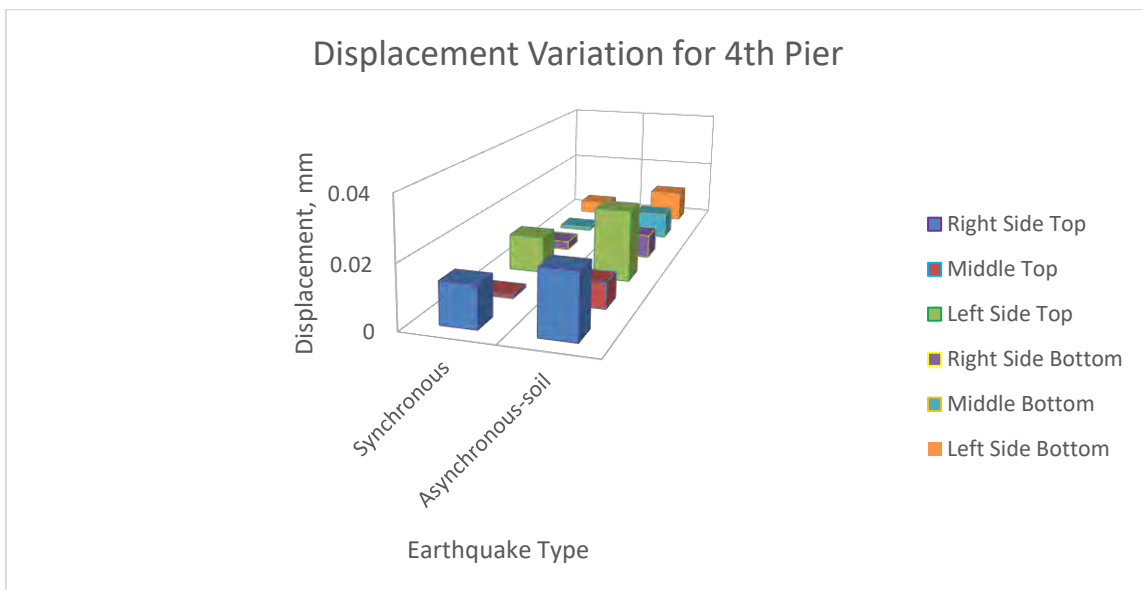


**Figure D.14: Displacement Variation for Fourth Pier along Z-axis**

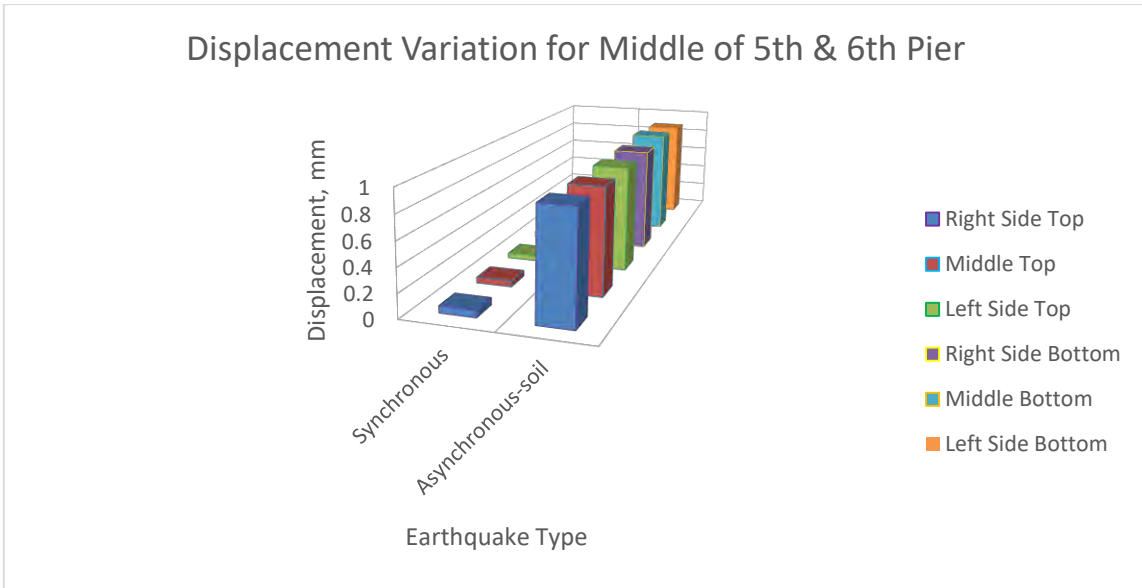


**Figure D.15: Displacement Variation for middle of fifth & sixth pier along Z-axis**

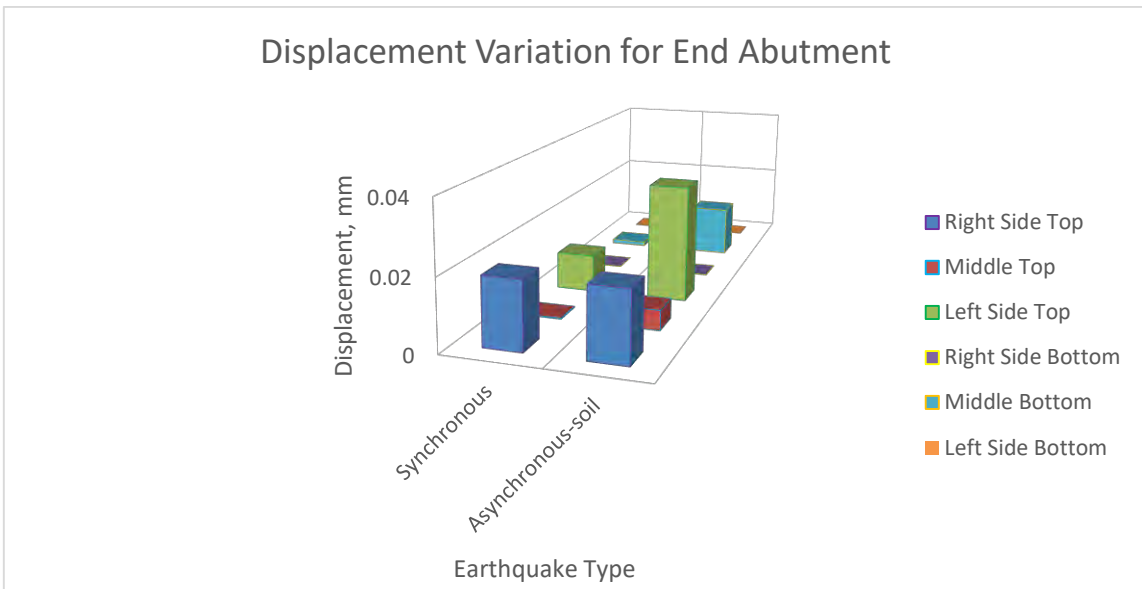


**Figure D.16: Displacement Variation for end abutment along Z-axis**

**SOIL EFFECT FOR 125 M MODEL ALONG X-AXIS (ALONG LENGTH OF THE BRIDGE)**

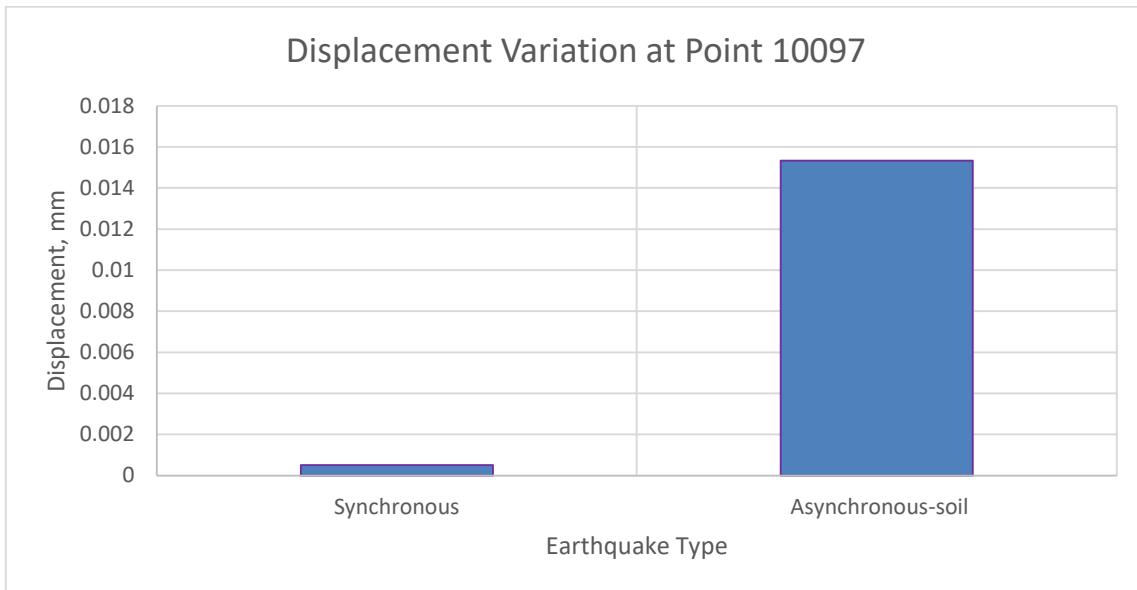


**Figure D.17: Displacement Variation at right side top of fourth pier along X-axis**

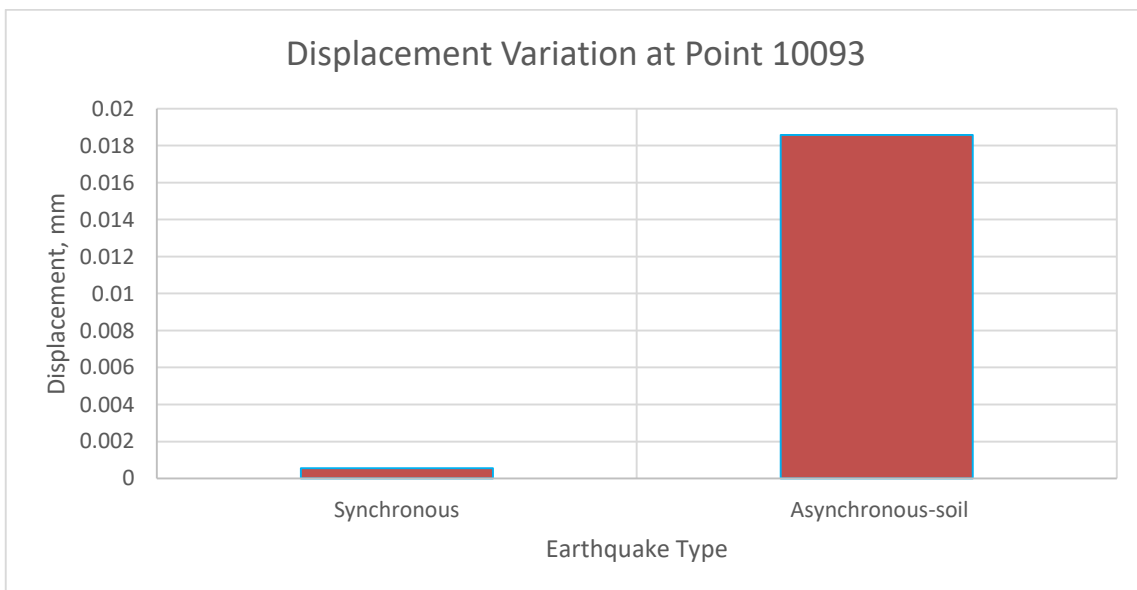


**Figure D.18: Displacement Variation at middle top of fourth pier along X-axis**

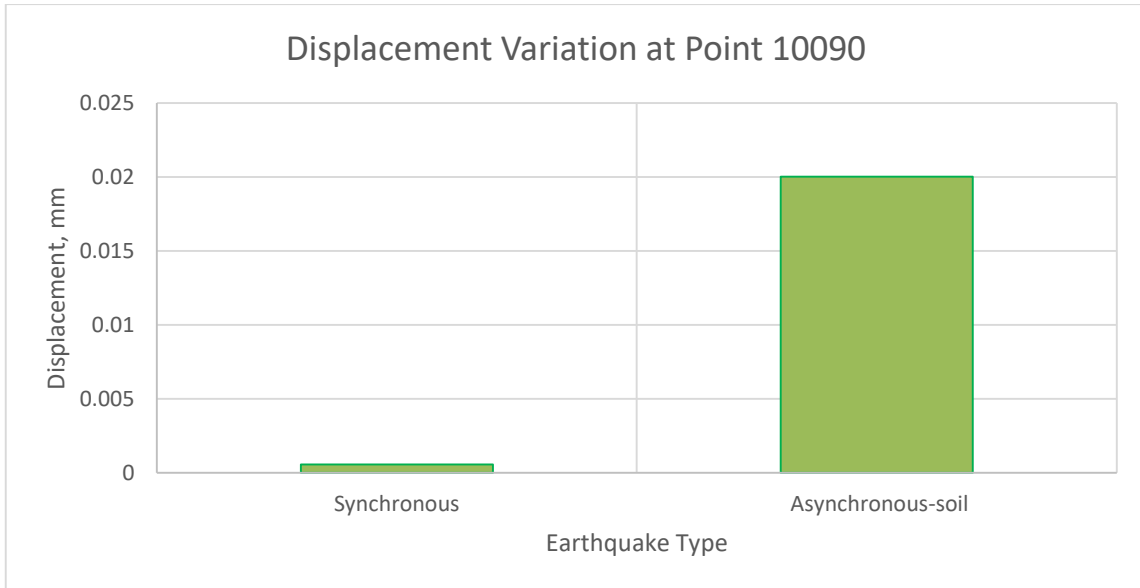


**Figure D.19: Displacement Variation at left side top of fourth pier along X-axis**

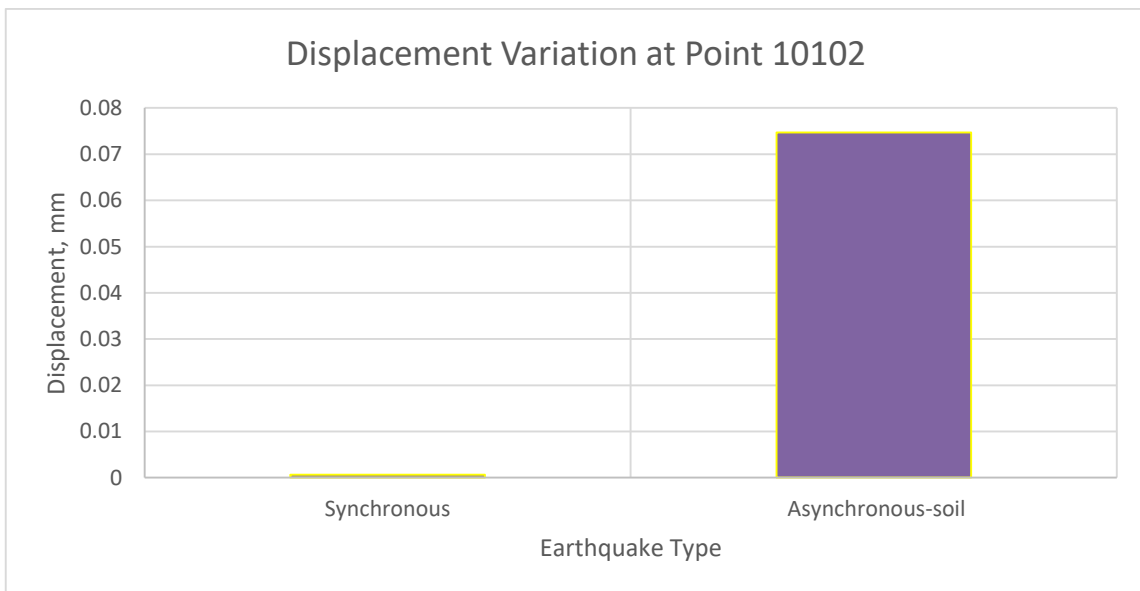


**Figure D.20: Displacement Variation at right side bottom of fourth pier along X-axis**

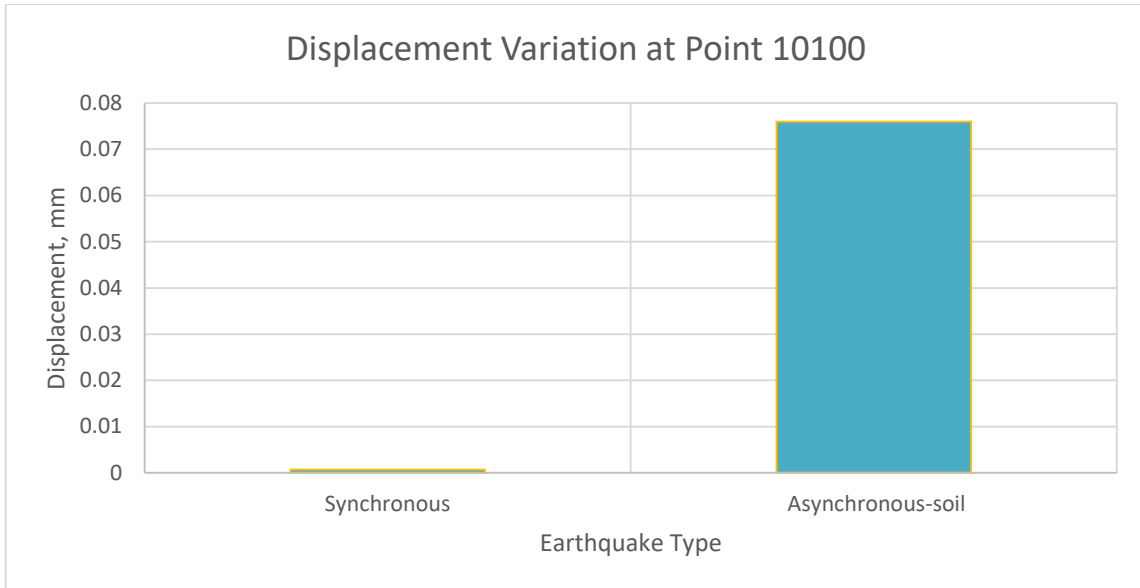


**Figure D.21: Displacement Variation at middle bottom of fourth pier along X-axis**

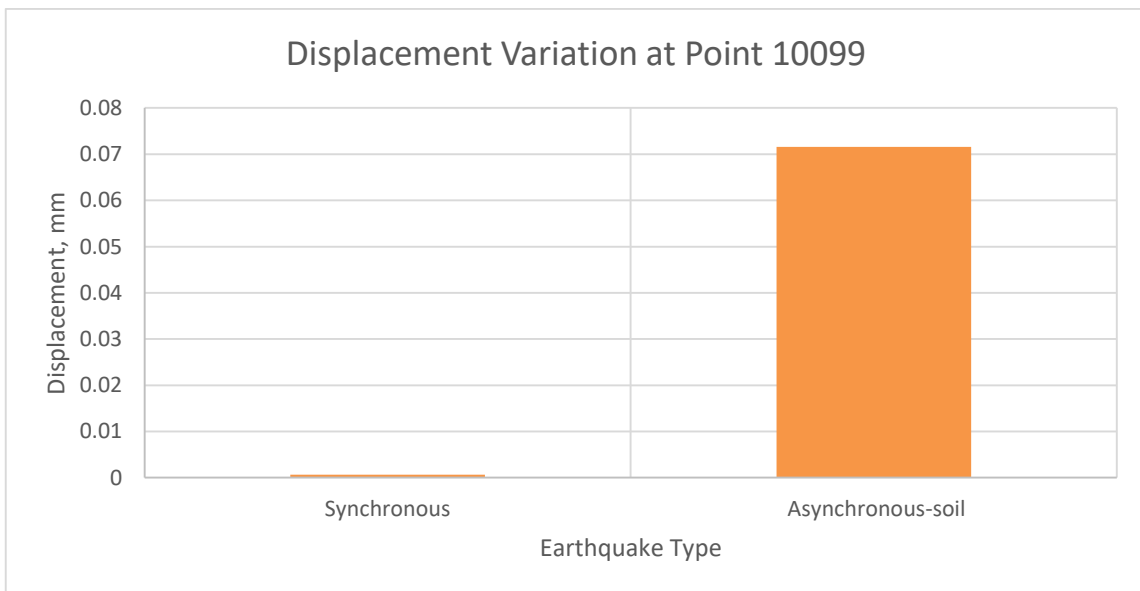


**Figure D.22: Displacement Variation at left side bottom of fourth pier along X-axis**

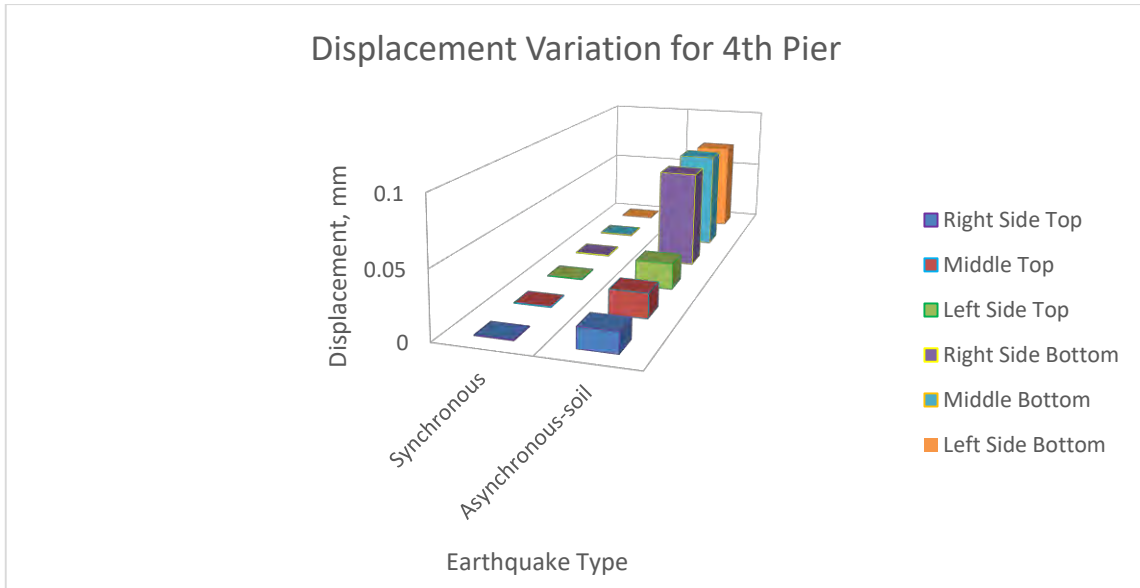


**Figure D.23: Displacement Variation for Fourth Pier along X-axis**

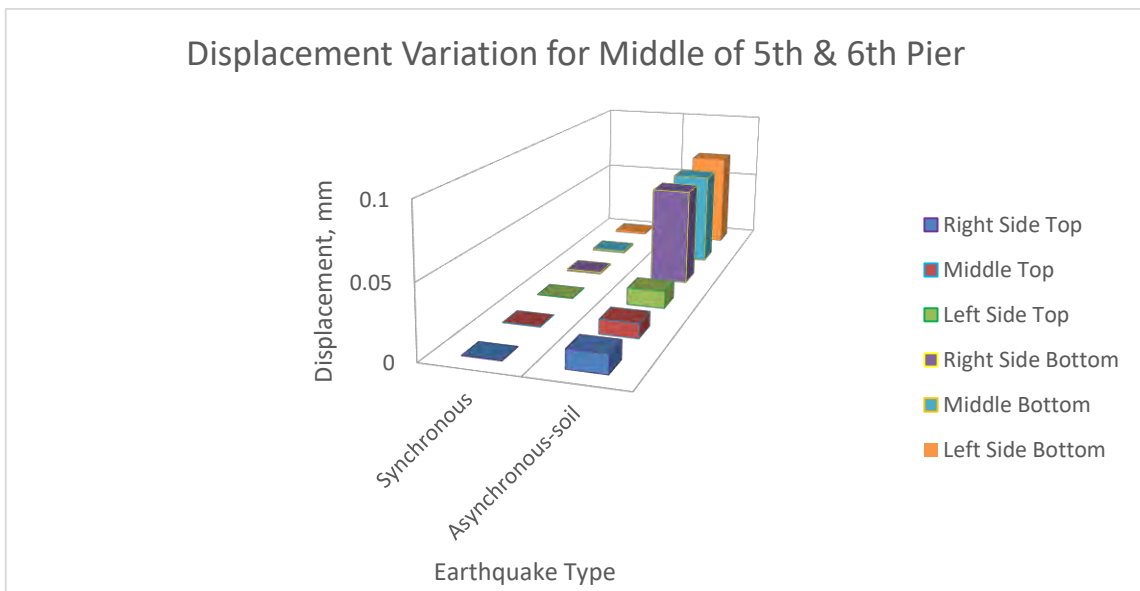


**Figure D.24: Displacement Variation for middle of fifth & sixth pier along X-axis**

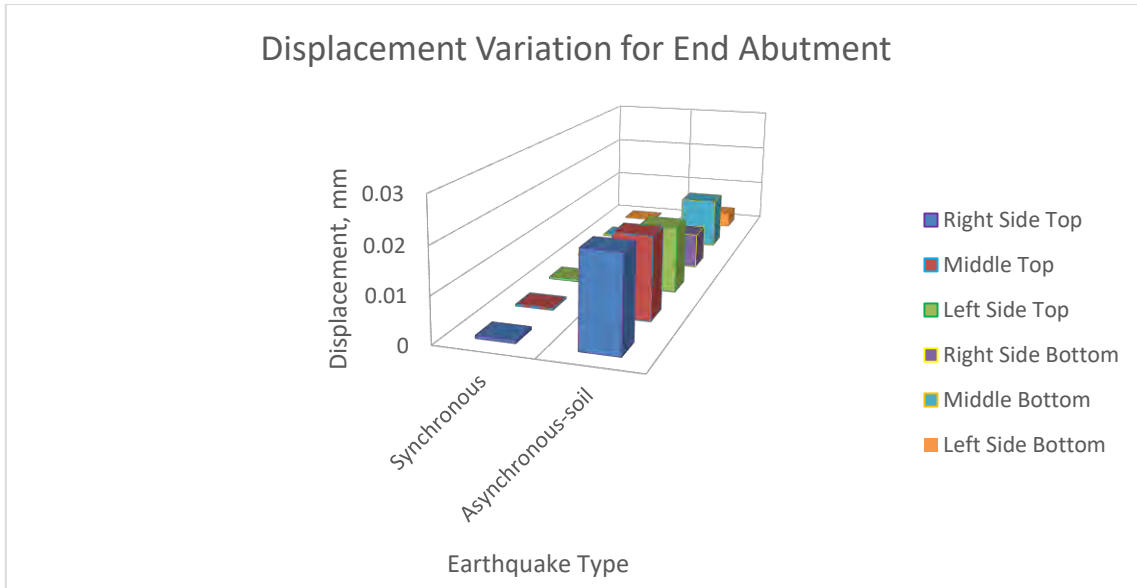


**Figure D.25: Displacement Variation for end abutment along X-axis**

**SOIL EFFECT FOR 125 M MODEL ALONG Y-AXIS (ALONG WIDTH OF THE BRIDGE)**

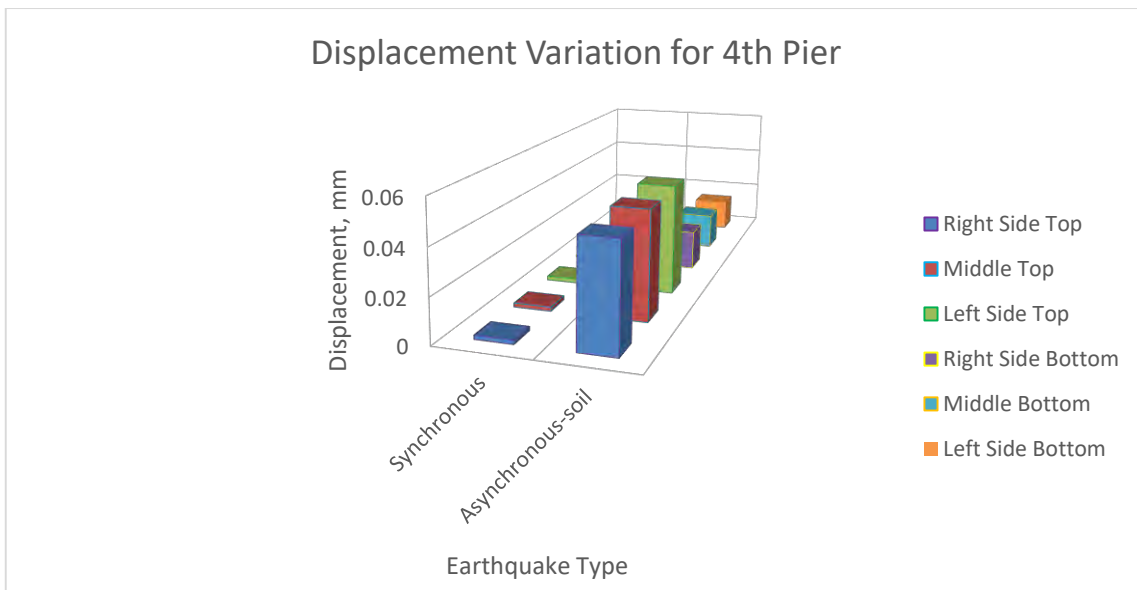


**Figure D.26: Displacement Variation for Fourth Pier along Y-axis**



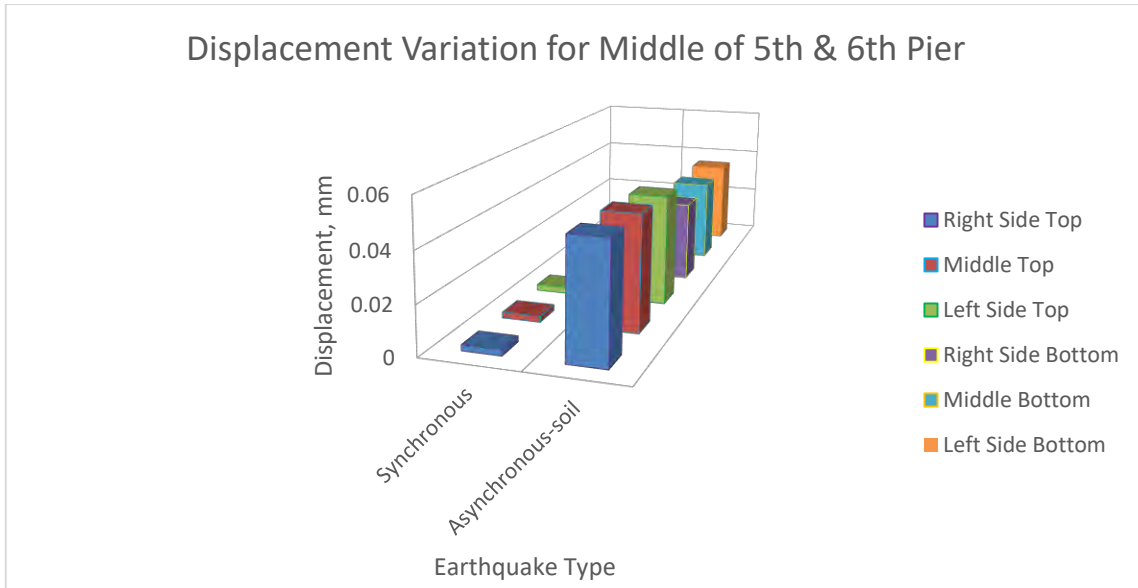


**Figure D.27: Displacement Variation for middle of fifth & sixth pier along Y-axis**

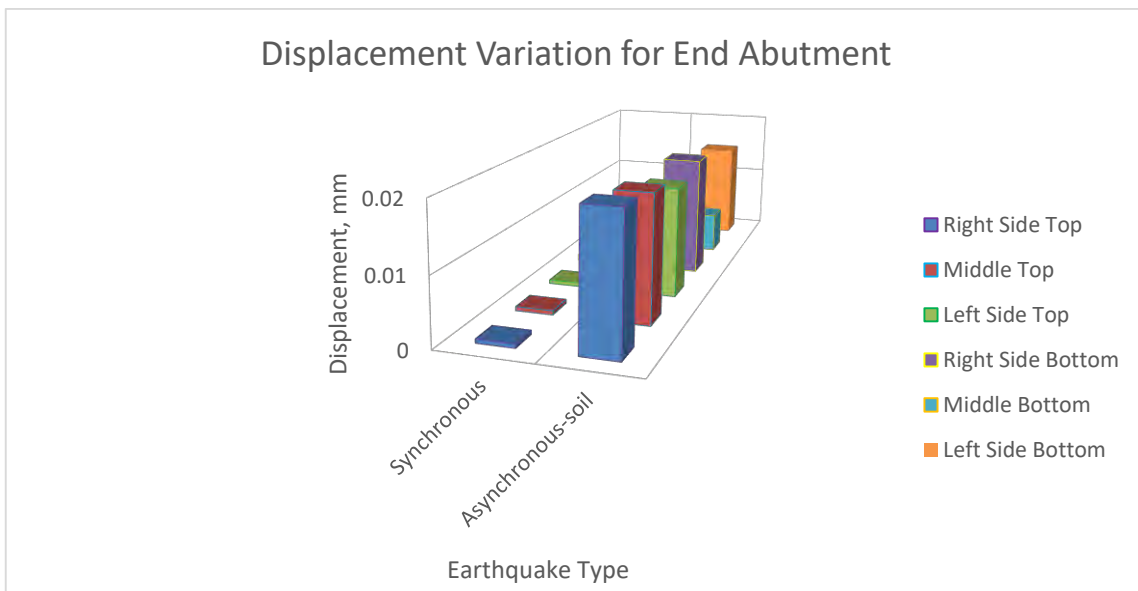


**Figure D.28: Displacement Variation for end abutment along Y-axis**

**SOIL EFFECT FOR 125 M MODEL ALONG Z-AXIS (ALONG VERTICAL DIRECTION OF THE BRIDGE)**

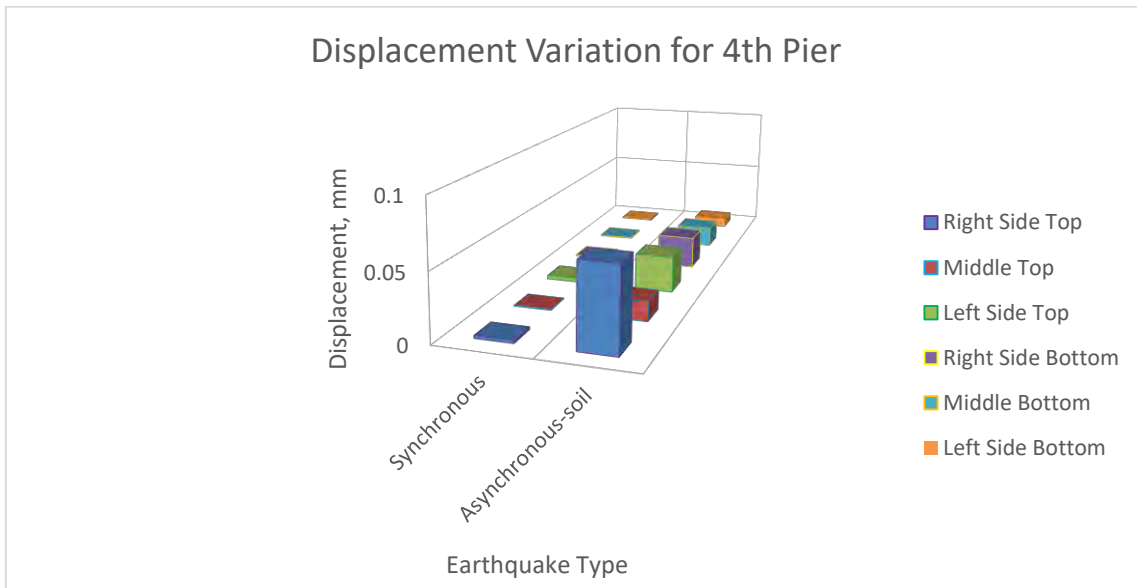


**Figure D.29: Displacement Variation for Fourth Pier along Z-axis**

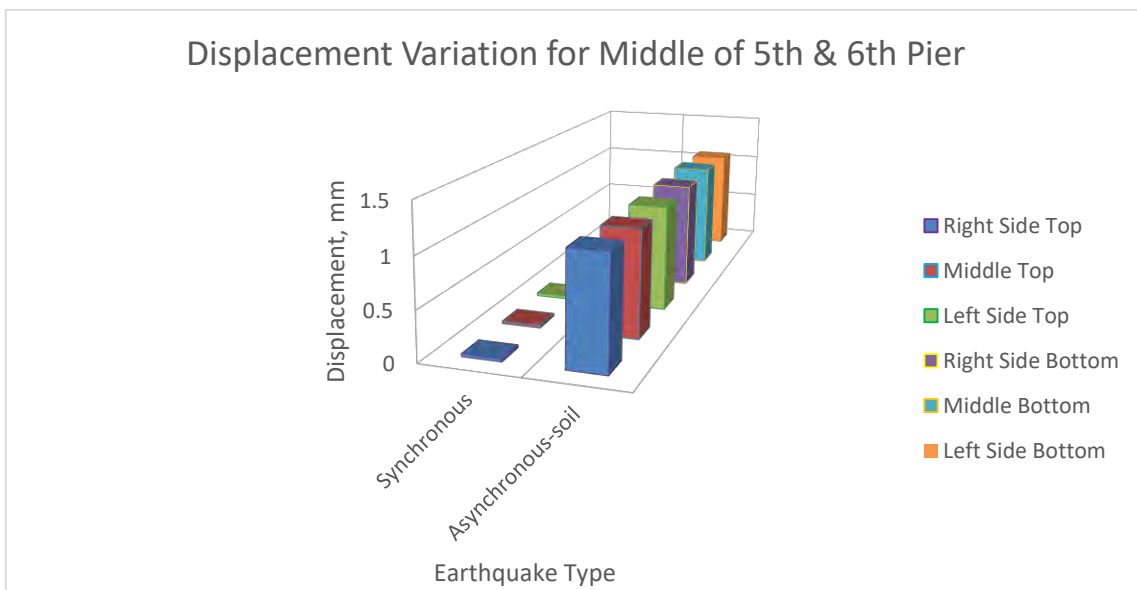


**Figure D.30: Displacement Variation for middle of fifth & sixth pier along Z-axis**

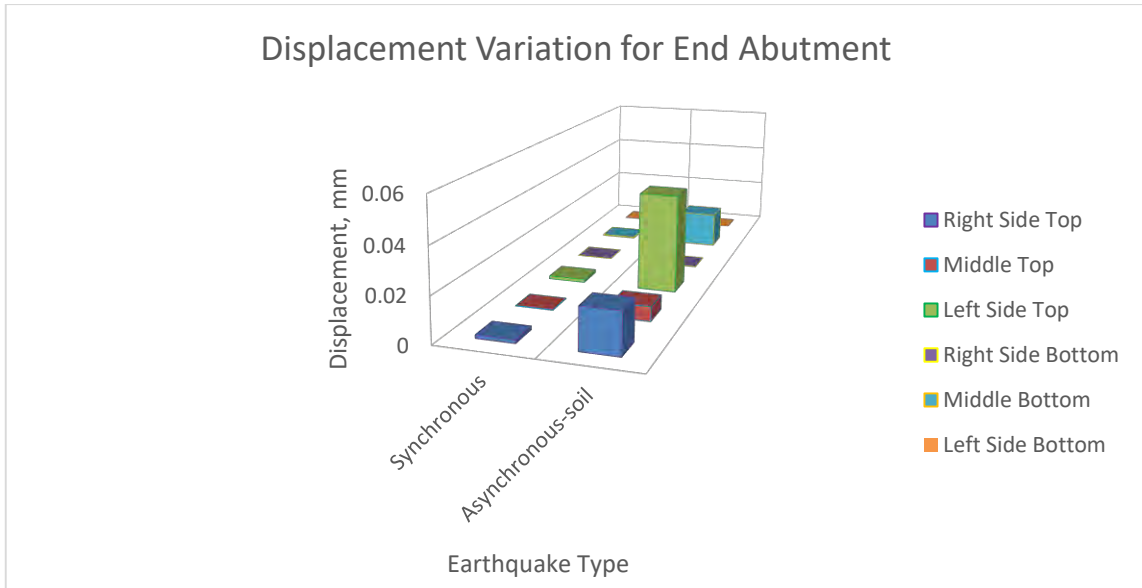


**Figure D.31: Displacement Variation for end abutment along Z-axis**